Development and application of dual fluorescent reporting systems for HIF-1α and other transcription factor pathways

Timothy Patrick Allen
B.Sc. (Biomedical Science), Honours (Biochemistry)

A thesis submitted in fulfilment of the requirements
for the degree of Doctor of Philosophy

Discipline of Molecular and Cellular Biology
School of Biological Sciences
University of Adelaide, Australia
2023

Table of Contents

Declaration

I certify that this work contains no material which has been accepted for the award of any other degree or diploma in my name, in any university or other tertiary institution and, to the best of my knowledge and belief, contains no material previously published or written by another person, except where due reference has been made in the text. In addition, I certify that no part of this work will, in the future, be used in a submission in my name, for any other degree or diploma in any university or other tertiary institution without the prior approval of the University of Adelaide and where applicable, any partner institution responsible for the joint award of this degree.

The author acknowledges that copyright of published works contained within the thesis resides with the copyright holder(s) of those works. I give permission for the digital version of my thesis to be made available on the web, via the University's digital research repository, the Library Search and also through web search engines, unless permission has been granted by the University to restrict access for a period of time. I acknowledge the support I have received for my research through the provision of an Australian Government Research Training Program Scholarship.

Timothy Allen
December 2023

Abstract

The ability to detect and quantify transcription factor (TF) activity has a broad range of utilities when probing for molecular interactions that intersect with their respective pathways or physiological function. This thesis describes the creation, optimisation, and application of the dFLASH (dual FLuorescent transcription factor Activity Sensor for Histone integrated reporting) system used to target a range of different TF pathways in a robust and sensitive manner with a focus on Hypoxia Inducible Factor 1 alpha (HIF-1α). HIF-1α is major regulator of the low oxygen response and is tightly regulated by a canonical post-translation pathway that, when inhibited, facilitates stabilisation of HIF-1α. Activation of its gene program drives processes such as erythropoiesis and vascularisation, and this has led to interest in targeting HIF-1α with small molecule regulators. Correspondingly, HIF-1α dysregulation has been implicated as a promoter of tumorigenesis and cell survival in hypoxic tumour microenvironments, although to date no small molecule inhibitor against HIF-1α has been successful in clinical trials. Conversely, pharmacological stabilisation of HIF-1α has been demonstrated to be beneficial in chronic anaemia. As a result, we established a dFLASH reporter for HIF-1α that was applicable in a high throughput context, utilising high content imaging and flow cytometry to demonstrate detection of HIF-1α activation at scale. We then leveraged dFLASH to perform a pilot screen utilising a library of ~1600 compounds in a live-cell bimodal arrangement, allowing detection of novel activator and inhibitor compounds, with efforts made to validate their mode of action. We further utilised an 800-compound library to refine our high-throughput screening approach, with an interest in combining the dFLASH HIF-1α-specific readout with phenotypic measurements of the live cells that contain the reporter. Specifically, we combined nuclear morphology scoring with dFLASH reporting to refine our lead selection process. Finally, we utilised dFLASH to probe for interactions between the microbial metabolome and the HIF-1α pathway in two distinct disease contexts, diabetic foot ulcers and Inflammatory Bowel Disease (IBD). HIF-1α has been implicated as a protective factor in both cases, and in both disease cases, changes in the bacterial species present in the local environment have been observed. Given there are a number of described physiological and metabolite-mediated interactions with the HIF-1α pathway, we therefore probed both individual bacterial species and complex co-cultures for activation and inhibition of the pathway. As a result, we described a novel downregulatory event with the HIF-1α dFLASH system by an IBD microbiome culture. As a result, we developed and undertook an exploratory pipeline that further utilised dFLASH, 16s sequencing, and metabolomics in an effort identify the causative agent.

Acknowledgements

Word on a page cannot convey how thankful I am to the great many people who helped me throughout the years, for celebrating the highs and helping me through the lows.

Firstly, I'd like the thank my supervisors for all the help, mentorship, and feedback over the years. Murray, you've always been a bedrock of support, sharp-eyed insight, and guidance. I couldn't have imagined doing a PhD with anyone else. Dave, you've always been a guiding star, expecting the best, providing a level of expertise and knowledge to strive for. Dan, thank you for your patience and your level of calmness is unparalleled, even in the face of my outlandish ideas. I am deeply indebted to the other members of the Whitelaw and Peet groups. Emily, Ice, Alexis, Cam, Josh, and Joe for providing me with a wonderful working environment when I was a fresh-faced honours student through to a fledgling PhD student. In particular Emily for coping with my drafts, Cam for coping with me in the office and Joe for being messier in the lab so I look better by comparison. Dave Hansman, it's been a blast, even though Cam taught you to cut out rat eyes right across from my desk. Ali, it's been really awesome to see you learn and grow from a terrified (?) undergraduate to a hard-bitten, veteran PhD student carrying things forward. I am eternally grateful that my support network extends beyond my lab to the wider MLS community both old and new, including Fiona, Ornella and the Beard, Bell, Bruning, Sherwin and Pitman groups. Lynn, without your love of biochemistry, I wouldn't be here today, I hope I've made you proud. I'd like to thank Michael, Kylie, Byron, Brooke & Xavier, for letting me collaborate, sometimes listening to me, more often sassing me and their support over the years. Stephen, thanks for your dry humour, occasional eyerolls, and chemistry input. Ornella for getting coffee with a side of gossip as needed. Thanks as well to Mel, for letting me use your office, being on board with expanding lab meeting, sharing your vision for your lab and occasional teaching work. Kat, what do I know? I'm just a guy. Ruth and Miguel, for being my biochem peeps for so many years now. Also, a special mention to Joel, for being the friend you need when you need that friend. The last MLS group to mention are the people I started honours, and then PhDs, with years ago and are now finishing up and moving on. Dan and Emily, it's been such a pleasure to share this journey with you. I'd also like to say thank you to the variety of collaborators that made this possible. Jane and Agatha, thanks for your patience, hard work and help with keeping the ArrayScan running. Andy, for your help and cool variety of bacteria. The CSIRO team at Adelaide for the various fun IBD cultures. Ron Quinn and his group at UQ for letting me test a bunch of fun and rare compounds and their advice and assistance pursuing interesting leads. Rodgers group at Flinders for getting the sequencing done and AWRI for the metabolomics data. Additionally, I'd like to thank the people behind the George Rogers AO Supplementary Scholarship for their generosity. Finally, I have to thank my family and friends for their love, support, and polite listening faces. I love you all dearly. My family have always been a bedrock of support, comfort, and constant cups of coffee even if I did drive them a little crazy. Thanks to my Grandparents for their enduring support and interest. Mum, thank you for your nagging (not really) and for knowing when we needed a long walk through the forest to talk things through. Dad, please read the abstract so you stop telling people I work with zebrafish. Eve, thanks for providing a distraction. Claudia, I carry your advice close to my heart. I am taking a breath, I have taken my time, caffeinated, eaten lunch and now I am finishing my damn PhD.

I couldn't have done it without you all. ~Tim

Publications

Publications:

This thesis is based on the following publication, that comprises part of a results chapter:

dFLASH; dual FLuorescent transcription factor Activity Sensor for Histone integrated live-cell reporting and high-content screening

Timothy P. Allen, Alison E. Roennfeldt, Moganalaxmi Reckdharajkumar, Miaomiao Liu, Ronald J. Quinn, Darryl L. Russell, Daniel J. Peet, Murray L. Whitelaw & David C. Bersten

Biorivx

doi: https://doi.org/10.1101/2023.11.21.568191

Additional Publications:

NanoFIRE: A NanoLuciferase and Fluorescent Integrated Reporter Element for Robust and Sensitive Investigation of HIF and Other Signalling Pathways

Authors: Alison E. Roennfeldt, Timothy Allen, Brooke N. Trowbridge, Michael R. Beard, Murray L. Whitelaw, Darryl L. Russell, David C. Bersten, Daniel J. Peet.

Biomolecules

doi: https://doi.org/10.3390/biom13101545

The utility of CRISPR activation as a platform to identify interferon stimulated genes with anti-viral function

Authors: Emily N. Kirby, Xavier B. Montin, Timothy Allen, Jaslan Densumite, Brooke N. Trowbridge, Michael R. Beard.

Biorivx

doi: https://doi.org/10.1101/2023.08.28.555046

Conference Presentations

Australian Society for Medical Research, 2021, Oral Presentation.

A Chemical Screening Platform for Hypoxia Inducible Factor 1 alpha: Investigating Microbiota and HIF crosstalk within Inflammatory Bowel Disease

Timothy Allen, David Bersten, Jo Hawkes, Michael Conlon, Dan Peet, Murray Whitelaw

ComBio, 2022, Oral Presentation

Application of a Novel Transcription Factor Screening platform for discovery of HIF-1α modulators

Timothy Allen, Alison Roennfeldt, Miaomiao Liu, Ronald Quinn, Dan Peet, David Bersten & Murray Whitelaw

Keystone Symposia: Hypoxia, 2023, Oral & Poster Presentation

Development and application of a dual fluorescent HIF sensor for small molecule discovery and genetic screening

Timothy Allen, Alison Roennfeldt, Miaomiao Liu, Ronald Quinn, Dan Peet, David Bersten & Murray Whitelaw

Chapter 1: Introduction

The PAS domain implicates bHLH-PAS family proteins as ligand binding

The basic Helix-Loop-Helix Per ARNT SIM (bHLH-PAS) transcription factors (TFs) form functional heterodimers between a role-specific Class I member and a more ubiquitously expressed Class II member[1] (**Figure 1.1**). The Class I factors therefore are used as mammalian physiological sensors that control a diverse range of gene expression profiles. These factors contain repeated Per-ARNT-SIM (PAS) domains known as PAS-A and PAS-B that are approximately 100 residues in length and structurally form anti-parallel five-stranded β-sheets[2], which form an outer surface that acts as a dimerisation surface between the Class I and the Class II monomers, and can mediate other protein-protein interactions[3-5]. These PAS domains are found commonly within prokaryotes where they mediate diverse signalling functions through coactivator or small molecule interactions as they contain internal cavities that are amenable to ligand binding. This signalling capacity is due to described structural plasticity of the PAS domain, as they can be diverse in sequence and change shape upon ligand binding. This means that identification of a PAS domain doesn't indicate binding of a discrete class of substrates[6].

The PAS domain has been co-opted in the mammalian system to facilitate sensing to a variety of environmental cues, such as regulation by small molecules. This is most classically shown by the Aryl Hydrocarbon Receptor (AhR) which senses a diverse range of ligands such as indole and tryptophan metabolites but also xenobiotics. Upon a ligand binding to AhR intracellularly, it undergoes conformation changes that expose a nuclear translocation signal and AhR transitions to the nucleus where it heterodimerises with its Class II factor, the Aryl Hydrocarbon Nuclear Translocator (ARNT). As dimerisation with ARNT occurs, it causes AhR to dissociate from its cytosolic latent complex which comprises of Heat Shock Factor 90 (HSP90), X associated protein 2 (XAP2) and co-chaperone p23[7]. ARNT acts as a general binding factor for most mammalian Class I factors, and in turn facilitates binding to conserved E-box-like enhancer sequences to mediate transcriptional upregulation[8]. Recent Cryo-EM structures of AhR, which is more structurally divergent from other bHLH-PAS members, show that agonists can bind stably into PAS-B domains but also that the

AhR PAS-B domain has a larger, less constrained cavity that may facilitate the plasticity seen in AhR ligand binding[9].

Importantly, the presence of the PAS-A domain is what confers DNA binding specificity, and therefore functional diversity, to dimerised bHLH-PAS transcriptional units[3]. The intracellular cavities within PAS domains found in bacteria has been suggested to also exist within the mammalian bHLH-PAS factors[10]. As no full length TF structures have been crystallised, partial structures of the mammalian TFs by the Rastinejad group showed that there were two conserved hydrophobic cavities within the PAS domains of the HIF-α subunits[11] and Neuronal PAS Factors 1 and 3 (NPAS1 and NPAS3)[10]. These pockets were described as between 100-600 Å^3 which, while small, are like reported ligand binding pockets in other proteins[12]. Modelling of the uncrystallised bHLH-PAS Single Minded (SIM) factors based on their prior data allowed the Rastinejad group to speculate that they too contain these ligand binding pockets. Wu, et al. [11] also report that plasticity of the PAS pockets, previously described in bacterial PAS domains, also occurs in the mammalian bHLH-PAS proteins with 0X3, a HIF-2α specific PAS-B binding inhibitor, increasing the size of the ligand binding pocket from 370 Å^3 to 560 Å^3. This has led them to suggest that members of the bHLH-PAS family have the capacity to bind small molecules to regulate their function.

There have been prior efforts to target these PAS domains for ligand discovery. HIF-1α[13,14], ARNT[15] and HIF-2α[16-18] have all had synthetic ligands reported that negatively regulate protein function through binding their PAS-B. Targeting the PAS-B region for drug discovery has been successful in developing therapies against HIF-2α[17]. While no endogenous ligands have been found for those factors, a HIF-3α isoform has been shown to bind endogenously derived oleoylethanolamide, a lipid that binds PPAR-α and is produced as part of the satiety response in the intestine, in its PAS-B domain[19]. This, coupled with the emerging structural data, suggest that there may be further undiscovered levels of control of bHLH-PAS factors mediated through these PAS domains which may inform their response and biology. As a result, we gained an interest in creating tools that would facilitate expanded screening of bHLH-PAS

factors, such as the HIFs, to probe for endogenous ligands or for small molecule discovery efforts.

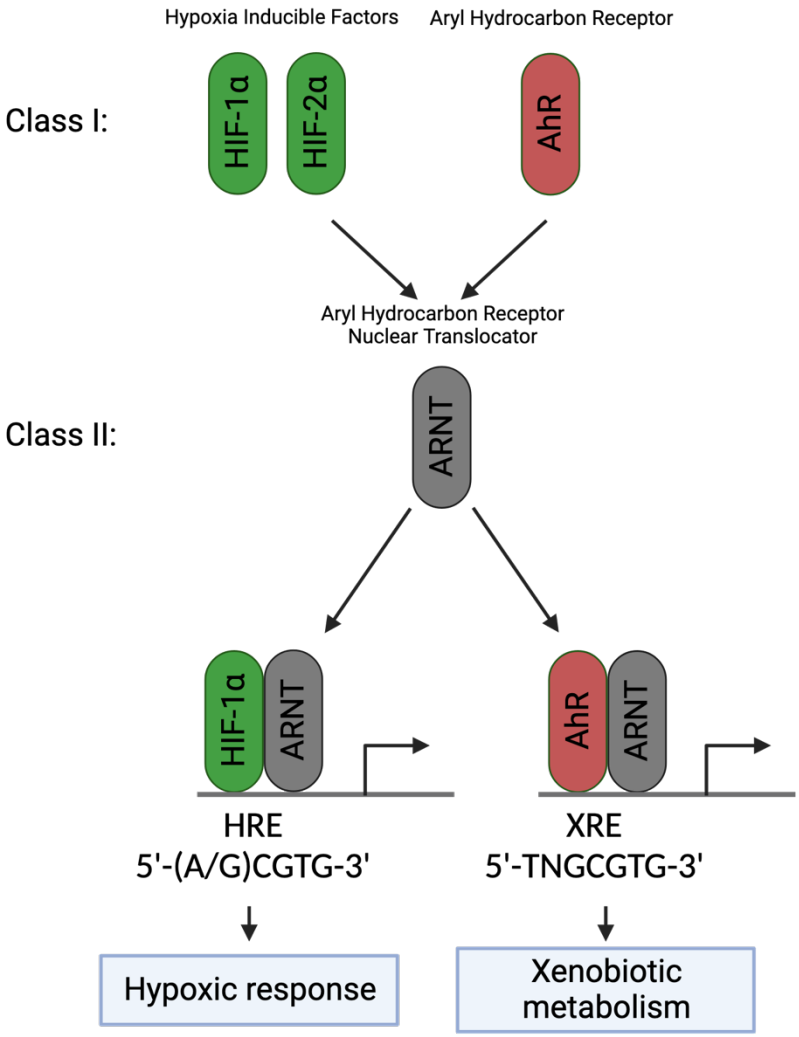

Figure 1.1 bHLH-PAS family members share Class II binding partners for diverse responses
Role-specific Class I factors such as the Hypoxia Inducible Factors (HIF-1α/HIF-2α) and the Aryl hydrocarbon Receptor (AhR) respond to different environmental stimuli. However, once activated they heterodimerise with the same Class II factor, the Aryl Hydrocarbon Receptor Nuclear Translocator (ARNT), forming active transcriptional complexes. Each active complex can then move to the nucleus where it binds to different DNA response elements and initiates different transcriptional programs, despite the same central partner.

Expression and Regulation of the Hypoxia Inducible Factors

The mammalian Hypoxia Inducible Factors (HIFs) are members of the bHLH-PAS family that act as physiological sensors and control cellular response to low oxygen. The active transcriptional complex comprises of an alpha subunit (HIF-α) that is stabilised under low oxygen conditions that dimerises with the partner protein Aryl Hydrocarbon Nuclear Translocator (ARNT). This HIF complex then binds to conserved Hypoxic Response Elements (HRE, 5'-(A/G)CGTG-3') and drives a battery of genes to promote cellular survival including promotion of glycolytic flux and Lactose Dehydrogenase A *(LDHA)* for anaerobic metabolism, promotion of angiogenesis through Vascular Endothelial Growth Factor *(VEGF)* expression and upregulation of erythropoiesis via erythropoietin *(EPO)* upregulation[20]. There are three mammalian HIF-α homologs. HIF-1α which is the most ubiquitously expressed, HIF-2α is closely related to HIF-1α although has a more tissue-restricted expression pattern and the more distantly related HIF-3α that can produce a HIF-α antagonist in certain splice variants. HIF-1α and HIF-2α however are the masters of the mammalian hypoxic response. These isoforms have different functions during a hypoxic response, with HIF-1α and HIF-2α sharing expression of angiogenic processes but a distinct preference for HIF-1α in driving glycolytic responses[21] while HIF-2α is thought to drive erythropoiesis[22]. Additionally, it's has been reported that there are some differences in isoform stabilisation at different oxygen levels. HIF-2α detection has been reported at 5% O_2 while HIF-1α required 1% O_2[23]. As a result, any discussion of hypoxic responses needs to consider both isoforms.

HIF-1α and HIF-2α are co-expressed in several cell types yet these isoforms have been shown to regulate distinct gene expression patterns, largely split between HIF-1α responsive genes and HIF-1α and HIF-2α responsive[21], with a degree of redundancy[24], despite binding to identical HRE sequences, even when co-expressed[25]. This selectivity was shown to be mediated through the N-terminal transactivation domain of HIF-1α and HIF-2α, by domain swapping experiments[26,27]. Additionally, a model whereby HIF-1α acts as the controller of acute hypoxic responses whereas HIF-2α is activated under longer hypoxic exposure has been proposed[28]. Despite binding the same HRE element the Mole group have shown,

through a series of Chromatin Immunoprecipitation (ChIP) and ChIP-seq experiments in MCF-7 cells, that HIF-1α and HIF-2α do not compete for binding sites even under longer hypoxic exposure and that HIF-1α binds within 5kb of regulated promoters while HIF-2α binds >5kb away[29,30]. These data suggests that the epigenetic environment around HIF binding sites were the determining factor to the observed differential gene expression as no differences between the DNA sequences bound by HIF-1α and HIF-2α were observed[29,31], confirmed independently in DNA binding experiments[32]. These differences contribute to our understanding of how diverse HIF-dependent responses in tumorigenesis and other disease states that feature elevated HIF signalling[33] contribute to overall disease progression.

HIF-1α and HIF-2α are tightly controlled at a post-translational level by a canonical regulatory pathway that confers their hypoxic dependent activity (**Figure 1.2**). They are constitutively expressed but are hydroxylated at conserved proline residues within the C-terminal Oxygen Dependent Degradation Domain (ODDD). This is mediated by the Prolyl-Hydroxylation Domain (PHD) containing enzymes 1, 2 and 3 (PHD 1-3), members of the 2-oxoglutarate (2-OG) dioxygenase family, which utilise Fe(II), oxygen, and 2-OG as part of their reaction mechanism. Hirsilä, et al. [34] demonstrated that the K_m of O_2 for the PHDs (230-250μM) was close to that for the concentration of dissolved O_2 in the air (200μM), therefore it is the PHDs that act as the cellular sensors for oxygen and small decreases in cellular pO_2 will influence their activity. Knockdown of these factors by siRNAs indicates isoform preference within the PHD family, with PHD2 considered a primary regulator of HIF-1α while PHD3 has more influence over HIF-2α than HIF-1α[35]. These hydroxylation events catalyse increased recruitment of the Von Hipple Lindau (pVHL) complex which leads to ubiquitination of the HIF-α isoforms and targeting for 26s proteasomal degradation. An additional layer of control is Factor Inhibiting HIF (FIH), another 2-OG dioxygenase that catalyses asparagine hydroxylation in the C-terminal transactivation domain of the HIFα subunits which sterically inhibits co-activator CBP/p300 recruitment to the mature HIF complex[36,37].

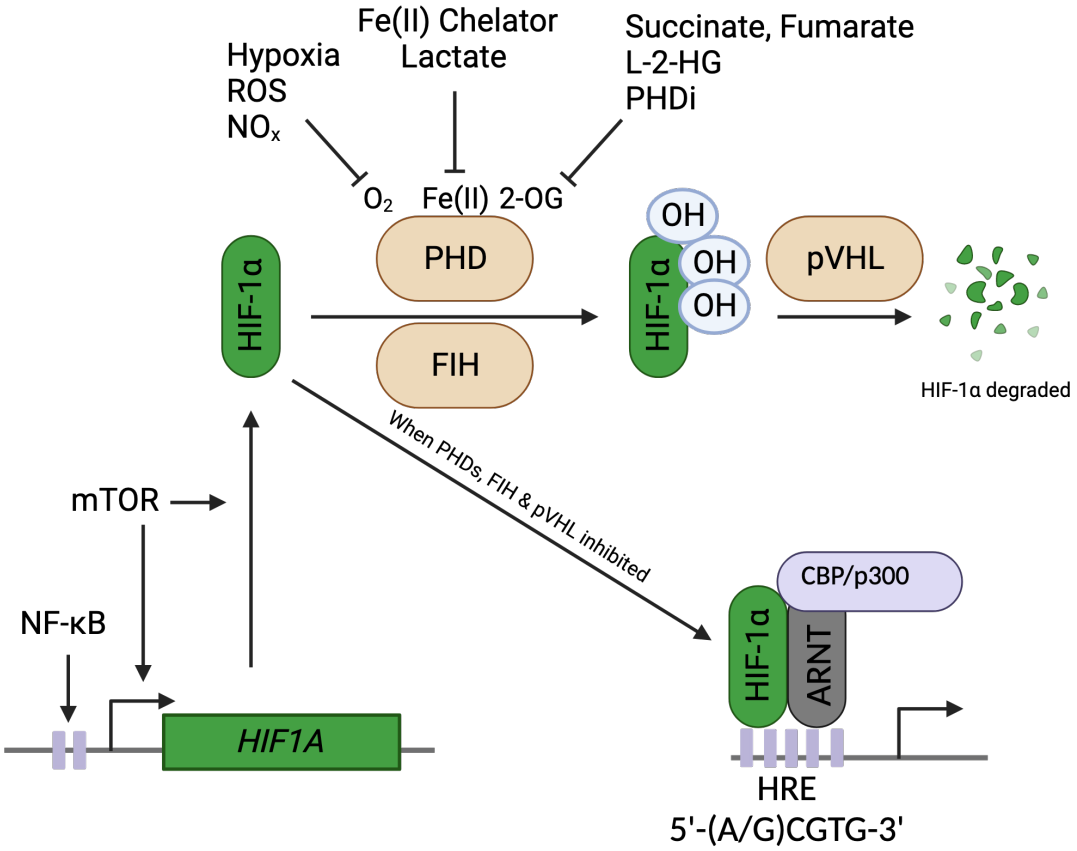

Figure 1.2 HIF-1α is tightly post-translationally regulated however has multiple environmental signals that activate its signalling.
HIF-1α is constitutively transcribed from the *HIF1A* locus however has multiple points of regulation. At 21% oxygen, HIF-1α is hydroxylated at conserved proline residues by the PHD enzymes. It is also hydroxylated at a conserved asparagine by FIH. These enzymes require oxygen, iron (Fe(II)), and 2-OG to function. The PHD-mediated hydroxylation recruits the pVHL complex, which targets the HIF-1α subunit for 26s proteasomal degradation. The PHD enzymes can be inhibited by several conditions, such as limiting oxygen (Hypoxia), reactive oxygen species (ROS), iron chelators, mitochondrial intermediates (succinate, fumarate, L-2-HG). Other conditions, such as NF-κB signaling or mTOR can upregulate HIF-1α transcription (NF-κB, mTOR) or translationally (mTOR). This allows for stabilisation of the HIF-1α subunit which heterodimerizes with ARNT, moves to the nucleus, binds to conserved hypoxic response elements (HREs) and drives the hypoxic response gene program.

The PHD/FIH axis of HIF regulation allows for HIF stability in contexts other than low oxygen availability. This plays a crucial role into understanding both points of intervention against the HIFs and how they can be dysregulated in disease states to contribute to pathogenesis. Iron chelators are well established activators of the HIF pathway and HIF stabilisation upregulates the iron transporter transferrin, stimulates erythropoiesis that suppresses hepcidin, a hormone that promotes iron sequestration, and encourages mobilisation of iron through the body. It has been suggested that low cellular iron stabilises HIF through the PHDs, positioning the PHDs as a cellular iron sensor[38]. The other major co-factor for the PHDs hydroxylation of HIF regulation is 2-OG, a citric acid cycle intermediate. Additionally, further work has demonstrated the connection between HIF signalling and mitochondrial products. Citric acid cycle intermediates succinate (350-460μM) and fumarate (50-80μM) were identified as mitochondrial substrates that could inhibit the PHD enzymes and mediate HIF stabilisation *in cellulo*[39]. This observation is backed by mutations in succinate dehydrogenase A and fumarate hydratase that stabilise HIF-1α in tumour-derived cell lines[40]. 2-OG can also be interconverted into 2-hydroxyglutarate (2-HG), in either L- (L-2HG) or D- (D-2HG) enantiomer forms that have a complex relationship with HIF signalling. 2-HG is a known oncometabolite that has been observed at high levels in gliomas, arising from mutations in isocitrate dehydrogenase (IDH) enzymes *IDH1* and *IDH2,* with cancer associated mutants favouring production of D-2HG[41]. D-2HG and L-2HG have been demonstrated to competitively inhibit several members of the 2-oxoglutarate dioxygenase family including the PHDs and the closely related collagen prolyl hydroxylase[42], although L-2HG has a much higher affinity for the PHDs than D-2HG and D-2HG was deemed unlikely to be inhibitory *in vivo*[43]. Koivunen, et al. [44] demonstrated that increased D-2HG was an activator of the PHDs and that the *IDH* mutants were anti-HIF and pro-tumorigenic because HIF-1α in certain cancer contexts can be anti-tumorigenic. However, L-2HG, which is not the favoured isoform in the cancer-associated mutations of IDH, has been shown to be promoted in acidic and hypoxic conditions leading to stabilisation of HIF-1α *in vitro*[45]. In the activation of $CD8^+$ T cells, it was reported that L-2HG was stabilised in response to HIF-1α signalling and can accumulate to millimolar levels, further promoting HIF-1α stability and affecting population persistence and anti-tumour capacity[46].

To further support the role of L-2HG in stabilising HIF-1α, mutations to oxoglutarate dehydrogenase (OGDH), which converts 2-OG to succinyl-CoA, lead to accumulation of L-2HG and aerobic stabilisation of HIF-1α in HeLa cells[45]. As a result, 2-HG signalling into the HIF pathway is likely niche-dependent but suggests another avenue of intersection between mitochondria and HIF. Another mechanistic association is that reactive oxygen species (O_2^-) generated from mitochondrial oxidation have also been shown to stabilise HIF-1α[47], predicted to do so through complexing with the non-heme Fe(II) converting it to Fe(III) and preventing hydroxylation of the HIF ODD[48] and therefore regulation by pVHL. High levels of lactate can also lead to stabilisation of HIF-1α[49]. Lactic acid forms a stable complex with Fe(III), driving an increase in the Fenton reaction that leads to an increase in cellular H_2O_2 which promotes an increase in oxygen radical formation, which in turn interacts with the non-haem Fe(II) in the PHDs[50].

Beyond the canonical pathway, there have been other, non-oxygen-associated pathways that have been implicated in control or expression of the HIF signalling pathway. The Mammalian Target of Rapamycin (mTOR) is linked with HIF-1α stability and expression. mTOR signalling has been shown to upregulate HIF-1α transcriptionally and translationally through upregulation of 4E-BP1 and S6K1[51]. In murine prostate epithelial cells, Majumder, et al. [52] reported that blocking mTOR prevented epithelial cell neoplasia and decreased HIF-1α target gene expression downstream of a PTEN mutation and constitutive Akt signalling. This highlights that the Akt/mTOR/HIF-1α axis is a potential cancer driver. An additional layer of control and inflammatory-dependent cross-talk of *HIF1A* transcription is data pointing toward NF-κB upregulating HIF-1α transcriptionally. NF-κB activation leads to normoxic stabilisation of HIF-1α in HEK293 cells and Glucose Transporter 1 *(GLUT1)* expression through conserved binding sites upstream of the HIF-1α promoter[53].

The HIFα subunits are known to associate with Heat Shock Protein 90 (HSP90) which can facilitate normoxic stabilisation through an interaction with the PAS-A domain, a similar mechanism to ligand-activated AhR[54]. Receptor of Activated Protein Kinase C (RACK1) competes with HSP90 for HIF-1α PAS-A and mediates O_2-independent HIF-

1α degradation[55]. Non-pVHL mediated degradation of HIFα subunits are implicated in the HIFα isoform transition that occurs under conditions of prolonged hypoxia. There has been a repeated observation that under periods of extended hypoxia, HIF-1α expression declines while HIF-2α expression increases. HIF-1α is selectively targeted by two mechanisms, firstly by Heat Shock Protein 70 (HSP70) and Carboxyl-terminus of Hsc70-Interacting Protein (CHIP)[56] and secondly by hypoxia-associated factor (HAF)[57]. Both HAF and HSP70/CHIP mediate pVHL-independent ubiquitination of HIF-1α and are suggested to mediate the isoform switch under prolonged hypoxia. This isoform switch is also thought to be mediated in part by hypoxia-mediated miRNA expression. A number of miRNAs are expressed in response to hypoxia[58] and have been suggested to contribute to the HIF isoform transition in some cell types through selective targeting of *HIF1A* mRNA[59]. For instance, miR-155 was shown to, in Caco2 intestinal epithelial cells, be upregulated under hypoxia due to 5' HRE elements and decreases *HIF1A* transcripts. This was not the case with *EPAS1* (HIF-2α), suggesting miR-155 forms part of a negative feedback loop that decreases HIF-1α protein expression under extended hypoxia[60]. Jaskiewicz, et al. [59] tested 23 predicted miRNAs, 18 of which were hypoxically induced, for regulation of *EPAS1* transcript levels and showed none were functional *in vitro*. This led to them suggesting HIF-2α expression is resistant to miRNA-mediated downregulation. These modes of regulation are important to delineate, as they provide alternate therapeutic entry points that can be captured by unbiased, whole pathway screening approaches. Beyond that, they also point to how mechanistically the hypoxic pathways can be co-opted in disease.

The Hypoxia Inducible Factors in human disease:

As the HIFs respond to a crucial physiological signal, oxygen, they have been implicated in multiple disease states. While abnormal upregulation of these factors is often a central process in tumorigenesis, they also act as important factors in homeostatic and repair mechanisms. This has resulted in significant interest in positive and negative regulation of HIFs in various therapies. This section provides an overview of several disease states that the HIFs are known to be involved in: cancer

development, inflammatory bowel disease including HIF activity in inflammation, and HIFs role in wound healing in the context of diabetes and ischemic disease.

HIFs as cancer drivers:

Many cancers contain regions of intratumoural hypoxia, with elevated tumour hypoxia being correlated with increased metastasis and malignant progression[61]. These regions are characterised by sharp oxygen gradients within tumours that exist between anoxic, necrotic regions to highly vascularised regions of the tumour[62]. Correspondingly, there are numerous cancer types that see correlation between HIF-1α or HIF-2α and decreased patient prognosis[62]. For example, Yamamoto, et al. [63] analysed 171 cases of breast cancer, detecting HIF-1α in 63 of them and found a correlation between HIF-1α detection with increased metastasis and decreased patient survival. The HIF factors have also been linked experimentally with the promotion of tumorigenesis. For instance, in embryonic stem (ES) cell driven teratocarcinomas, HIF-1α knockouts prevented formation of solid tumours and downregulated *VEGF* that promotes tumour vascularisation[64,65]. Murine knockout models also support that both HIF-1α and HIF-2α promote tumorigenesis. Liao, et al. [66] generated a conditional HIF-1α KO in a spontaneous breast cancer murine model that, with HIF-1α not present, had decreased vascularisation and metastasis. They conclude that HIF-1α does not initiate cancer formation, but significantly promotes tumour formation and spread.

The HIFs play a role in cancer cell reprogramming that contributes to tumour burden and the molecular mechanisms at play are increasingly well characterised. In particular HIF-1α plays a core role in cancer metabolism. HIF-1α upregulates pyruvate dehydrogenase kinase 1 (PDK1), LDHA and mitophagy-regulator BNIP3[20,67]. These all promote a shift from oxidative metabolism toward anaerobic glycolysis, decreasing reactive oxygen species generated, promoting glucose and glutamine dependency that is observed in many cancer cells[68], and rewiring of citric acid cycle intermediates toward processes that maintain and fuel proliferation[69]. HIF signalling also promotes angiogenesis through regulation of *VEGF* by both isoforms[64] and a battery of other

angiogenic factors such as Stromal Derived Factor 1α (SDF1α)[70]. These processes stimulate growth, migration, permeability and survival of endothelial cells, leading to tumour vascularisation[71]. The multi-factorial contribution of HIF to angiogenesis has been blamed for the resistance that is seen in VEGF-mediated therapies to downregulate angiogenesis[70,71]. HIF is also considered a promoter of metastasis, as it has been linked with hypoxic-dependent promotion of lysyl oxidases that modulate collagen and stimulate integrins for increased cell-matrix adhesion, promoting tumour cell invasion of other tissues[72,73].

There are also differing roles for HIF-1α and HIF-2α in these models and in certain cancers HIF-2α, not HIF-1α, is seen as a major driver. The clearest example is in clear cell Renal Cell Carcinoma (ccRCC), that is commonly pVHL-defective[27]. Raval, et al. [25] overexpressed HIF-1α and HIF-2α in 786-O cells, a renal cell carcinoma (RCC) cell line and observed that, in xenographs, HIF-2α accelerated tumour burden whilst HIF-1α was suppressive. This was supported by their observations that, in RCC cell lines, HIF-1α or HIF-2α overexpression suppresses the alternate isoform. This, coupled with the development of a HIF-2α antagonist, has led to targeting of HIF-2α specifically in RCC models. Chen, et al. [74] demonstrated that *ex vivo* RCC tumourgraft models were suppressed by antagonist treatments. This body of research has led to approval for a HIF-2α inhibitor, Belzutifan, for VHL-driven cancers[75].

The roles of HIFs in cancer are what has driven an interest in development of HIF-specific antagonists soon after its discovery[76]. However, targeting the HIFs in cancer also points toward the importance for development of isoform-specific inhibitors of HIF for greater therapeutic control depending on cancer type. For example, there is data pointing toward suppression of HIF-1α by cancer associated IDH mutants acting as an oncometabolite-mediated cancer driver[44]. Additionally, HIF-1 is a well-established cancer driver in metastatic breast cancer[63,77] and HIF-2α, not HIF-1α, is the primary driver in ccRCC[74,78,79]. Furthermore, expression of HIF-1a has been suggested to act as a tumour suppressor in ccRCC, in direct contrast to HIF-2α's pro-oncogenic role[25,80]. As a result, there have been multiple attempts to develop inhibitors against

these factors to facilitate specificity for targeting HIF in cancer and HIF-1 may be an active driver in specific cancer types, rather than a universal factor.

HIF in ischemia, anaemia and diabetic wound healing

Therapeutically targeting HIF is not limited to inhibition of the pathway, as there are clear examples where upregulation of HIF is beneficial. PHD inhibitors (PHDi) were first clinically approved for treatment of renal anaemia arising from chronic kidney disease[81], due to the ability of HIF stabilisation to promote erythropoiesis through upregulation of *EPO* and mobilisation of iron. This facilitates an increase in red blood cell counts in anaemic patients[82]. As a result, there have been a number of clinical trials, with a range of different PHDi compounds, that support the idea that HIF stabilisation as a result of PHDi treatment increases patient haemoglobin in renal anemia[83-88]. These treatments are just as effective as existing treatments, with largely mild side effect profiles[89]. However, given the involvement of the HIFs with a number of pro-tumorigenic, pro-vascularisation pathways, Li, et al. [82] raise the issue that clinical data is lacking for long-term PHDi treatment given the potentially pleiotropic effects of HIF signalling. This is compounded by the shared active site target, although different binding modes and PHD-selectivity, of the clinically trialled PHDi compounds[90].

The same processes that drive tumour survival in a cancer context also contribute to HIF-α signalling promoting cell survival in conditions of low oxygen delivery (ischemia) or in wound healing. Ischemic events in the heart are a common event in coronary heart disease, which can act as precursor events to myocardial infarction, whereby myocytes die as a result of oxygen deprivation[91]. It was originally observed in animal models, such as mice and pigs, that controlled bursts of ischemia, known as remote ischemic preconditioning (RIPC) confers wider protection to various organs including the heart to infarction[92]. This molecular mechanism of protection has been shown to be HIF-1α dependent. Cai, et al. [91] demonstrated that heterozygous knockouts of HIF-1α had decreased RIPC due to a decrease in IL-10 production. This effect was replicated by Olenchock, et al. [93] whom showed that PHDi FG-4497 was sufficient to

confer cardiac protection against future, more severe ischemic events. Therefore, PHDi compounds may be beneficial in treatment of ischemic disease[94].

Wound healing is a dynamic, well-regulated process. Hypoxic events occur at wound boundaries from damaged vasculature or can be caused by wound-associated inflammation. The requirement to promote angiogenesis as part of the wound healing process all emphasise the role of HIF-1 within the wound-repair signalling cascade[95]. In diabetic patients, there is often impaired wound healing which can lead to diabetic foot ulcers forming chronic wounds, with a high rate of infection resulting from abnormal wound healing responses[96]. Disrupted HIF signalling within wounds has been reported within murine diabetes models[97,98] and under conditions of hyperglycemia, destabilised HIF has been reported[99] although the mechanism remains opaque. One potential mechanism was the upregulation of methylglyoxal which has been suggested to dysregulate HIF though the CHIP/HSP70 axis[100] or blocking HIF and p300 coactivator binding[101]. This has been suggested to be an incomplete mechanism, as greater than physiological levels of methylglyoxal is required to stabilise HIF[100,102]. As there are big fluctuations in cellular metabolism[96,103] and the commensal microbiome[104] during diabetic wound healing, HIF inhibition in this model requires further investigation. From an intervention perspective however, there have been several reported models whereby treatment of diabetic wounds with HIF-activating PHDi or iron chelating compounds result in promotion of wound healing[98,105,106]. This has resulted in a Phase 2 clinical trial whereby topical application of a HIF-stabilising iron chelator is being investigated as a potential intervention within patients with chronic diabetic foot ulcers[103], despite lingering questions over the molecular mechanisms that underpin the original dysregulation.

Intestines, Inflammation, Inflammatory Bowel Disease & HIF:

There are also physiologically hypoxic niches within the human body. These locations are oxygen privileged and as a result, hypoxic signalling within these tissues is a crucial homeostatic control mechanism. One of these niches is the gastrointestinal (GI) tract that has a sharp oxygen gradient between a well-oxygenated vascular layer

adjacent to the anaerobic lumen, which acts as the signalling interface between the host and the gut microbiome. This gradient is steep and subject to periodic fluctuations based on feeding-fasting cycles that see dramatic changes in blood volume and hence, pO_2 gradient. The presence of physiological hypoxia at this surface is visible in nitroimidazole staining of healthy murine gut models, a sharp gradient across the epithelial cells lining the gut lumen[107]. This has led to corresponding adaptions in the cell populations present[108] and co-opting the HIF pathway for essential processes. In addition to the oxygen gradient, there exists a resting state of regulated mucosal inflammation[107]. This is a product of the juxtaposition between the intestinal epithelial cells, that form and promote the mechanical mucosal barrier, and the commensal microbiota that inhabit the lumen which produce a constant stream of antigens. Therefore, both nutrient absorption through the gut barrier and the homeostatic mechanisms that maintain a healthy gut barrier are regulated tightly by oxygen[109].

Unsurprisingly the HIFs, in particular HIF-1α, is linked with homeostatic control mechanisms within the GI tract[110] (**Figure 1.3**). HIF-1α has a well characterised role in the maintenance of the intestinal epithelial barrier. Saeedi, et al. [111] knocked down ARNT in T84 intestinal epithelial cells and observed a loss of barrier function as a result. They went on to define the HIFs as being essential for promotion of Claudin-1, a tight junction regulatory protein, as a HIF target gene. Claudin-1 promotes tight junction formation and helps respond to mucosal layer damage. HIF also regulates several complexes involved in the formation of the innate mucosal layer that prevents direct contact between commensal bacteria and the intestinal cell layer. The mucosal layer also harbours antimicrobial peptides, is comprised of glycosylated mucin proteins, and has a large resident myeloid cell population as part of the homeostatic inflammatory response within this environment. Mucin 3, a glycoprotein that forms part of the mucosal barrier, and intestinal trefoil factor, which promotes epithelial barrier function and mucosal barrier repair, are known HIF targets in intestinal epithelia[112,113]. Additionally, Kelly, et al. [114] report that HIF-1α, and not HIF-2α, is essential for homeostatic expression of the human anti-microbial peptide β-defensin 1 that is constitutively produced, instead of in response to pathogens, establishing HIF as a key regulator for maintenance of a healthy gut epithelium and immune environment.

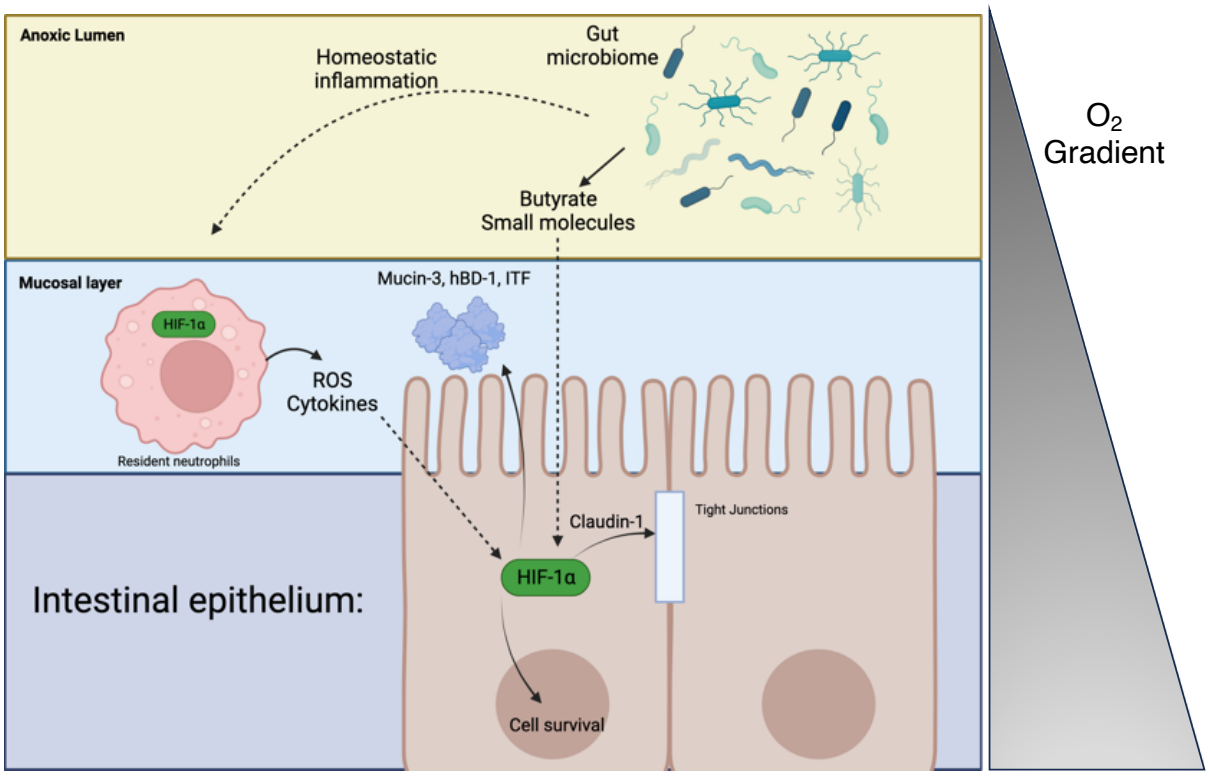

Figure 1.3 HIF-1α is a key regulator of homeostasis in the intestinal environment.
There exists a sharp O_2 gradient between the anoxic lumen and vascularized host sub-mucosa that creates a hypoxic niche within the intestine that stabilises HIF-1. HIF-1 is also stabilised in part by the resting inflammatory environment, that produces cytokines, immunometabolites and ROS which can stabilise HIF-1. HIF-1 promotes cellular survival under these conditions for both intestinal epithelial cells and resident neutrophils. HIF-1 also acts to promote the innate immune function, regulating several components of the protective mucosal layer (Mucin-3, hBD-1 and ITF) as well as promoting tight junctions, essential for the intestinal epithelial mechanical barrier, through regulation of Claudin-1. Furthermore, the resident gut microbiota, that produces a bevy of signalling molecules, can also potentially regulate HIF-1. Butyrate has been shown to stabilise HIF-1 and is a product of those microbial species.

HIF is also important for regulatory pathways within immune cell, which informs its role in the intestinal immunological niche. Macrophages and neutrophils rely on HIFα for survival during inflammation, as regions of inflammation can be characterised as forming highly hypoxic foci, with elevated local ROS that can feed into stabilisation of HIFα. Cramer, et al. [115] knocked out HIF-1α and VHL in myeloid lineages within murine models. They found that macrophages were significantly less aggressive and had impaired motility, invasion, and ability to kill bacteria resulting from defective glycolysis. This was supported by their later study, where HIF-1α null macrophages had decreased anti-bacterial effects *in vitro* and the HIF-1α myeloid lineage deletion model resulted in more aggressive infections[116]. Additionally, inflammation can result in an upregulation of several immunometabolites[117]. Most notably for HIF-1α, succinate can accumulate in macrophages in response to lipopolysaccharide (LPS) exposure which in turn can stabilise HIF-1α under normoxic conditions and drive interleukin 1β (IL-1β) expression in a HIF-dependent manner[118]. NF-κB is a key immune regulatory component, driving inflammatory mediators such as tumour necrosis factor α (TNF-α) or interleukin 1 (IL-1)[119]. NF-κB also forms part of the immune response under hypoxia, and is activated under low oxygen tension[120] and has been shown to drive HIF-1α transcription[53]. There has been some reported crosstalk between the two transcription factor pathways which may contribute to immunological outcomes, with stabilisation of HIF reported to repress NF-κB immune responses, acting as a brake to the pro-inflammatory response[121]. HIF is also important in TH_{17}/T_{reg} cell balance, although the exact role is still unclear given conflicting reports. HIF in TH_{17} cells has been reported to downregulate Forkhead Box P3 (FOXP3) and promote RAR-related Orphan Receptor (ROR)γt[122] however Clambey, et al. [123] reported HIF signalling as promoting T_{reg} cell formation through FOXP3 promotion, likely indicating a more complex molecular or context-dependent mechanism as a core determinant of HIF-dependent T-cell fate[124]. Therefore, there are multiple avenues by which HIF contributes to inflammation or is activated as a response to inflammatory stimuli.

Inflammatory Bowel Disease (IBD) is a term that encompasses two distinct sub-types with similar symptoms, Crohns Disease (CD) and Ulcerative colitis (UC). IBD is

characterised by chronic relapsing inflammation in the lower gastrointestinal tract. IBD has an unknown aetiology however is considered to be a result of interplay between genetic, microbial, or environmental and inflammatory factors[125-128]. This results in impaired intestinal barrier function, a dysregulated mucosal immune response and dramatic shifts in the commensal microbiome. At the tissue level, IBD is the abnormal triggering of the innate immune response within the patient, causing tissue damage to the intestinal epithelium and a loss of barrier homeostasis and dybiosis of the GI microbiome. Histology notes this occurs with an influx of neutrophils and abscess formation as well as mucosal ulceration, with depletion of the mucosal layer and a loss of epithelial barrier function[128].

As a result, there is a heavily disrupted oxygen environment within the gut and there have efforts to profile the role of HIF within the IBD environment. Giatromanolaki, et al. [129] found elevated expression of both HIF-1α and HIF-2α in colonic sections from IBD patients, with tissue staining highlighting upregulated HIFα isoforms in intestinal epithelial cells and immune cells, pointing toward a role for HIF signalling within IBD. The assertion that HIF is important within the gut microenvironment is backed by experimental evidence. Karhausen, et al. [130] conditionally deleted and overexpressed HIF-1α in a TNBS model of murine colitis, mirroring IBD. The HIF-1α null mouse had more severe symptoms in response to TNBS whereas the HIF-1α overexpression had a near complete rescue of the IBD phenotype in the same model. This is supported by several other studies such as Cummins, et al. [131] whom treated a dextran sodium sulfate (DSS) induced colitis murine model with 2-OG dioxygenase inhibitor DMOG and observed a protective effect with decreased tissue damage and inflammatory cytokines within the colonic samples. This all fits with the presented model of HIF in the gut, in that it promotes molecular homeostatic effects and maintenance of the epithelium that gets heavily damaged during IBD. This has led to the proposal that targeting IBD with prolyl hydroxylase inhibitors may present a potential supportive therapy[124]. This in turn has been trialled in murine models, with specific PHD inhibitors (PHDi), which specifically activate HIFα, supporting repression of colitis in Trinitrobenzene Sulfonic Acid (TNBS) models through promotion of innate immune pathways[132-134]. The data from the above mouse models points towards HIF-α as a

protective factor. There are some cell-specific HIF-α reports that add more complexity to HIF's function in the gut. HIF-1α knockouts in myeloid cells in inflammatory bowel disease models have a milder inflammation than wild type mice[135,136]. This fits with the established model that myeloid-derived macrophage are heavily dependent on HIF-1α for function[115]. Yet systemic HIF-α upregulation with PHDi and DMOG present as anti-inflammatory in colitis[130-134]. It is important to note however, that current data suggests HIF is already stabilised in this environment, both as a result of homeostasis or as a result of inflammation. It remains an open question as to whether or not HIF-α signalling is disrupted within an IBD gut environment, as this is predicted to promote disease progression. It is essential to understand these complexities fully prior to targeting HIF for therapeutic intervention in IBD.

HIF and the microbiome:

Beyond the immune environment, the gut microbiome is a rich source of signalling molecules that have extensive host-signalling capacity and is dramatically affected in IBD patients. Indeed, the gut microbiome and its products are reported to have a dramatic influence on metabolism, of which HIF is a central player, in colonic tissue[137]. The most commonly reported example of crosstalk between the host gut microbiome and HIF-1α is through butyrate. Kelly, et al. [138] reported that microbially-derived short chain fatty acids (SCFAs) promoted barrier function in cell culture models, proposing a mechanism whereby HIF-1α was stabilised as a consequence of enhanced O_2 consumption by mitochondria. However, this mechanism was incomplete. The same group have since suggested that butyrate also acts as a non-competitive inhibitor of the prolyl hydroxylases[139]. Butyrate administration to mouse models of *Clostridium difficile* infection was suggested to decrease inflammation in a HIF-1α-dependent mechanism[140]. These reports however do need to be considered in the wider context as butyrate is known to act as a histone deacetylase (HDAC) inhibitor[141], leading to general upregulation of transcription, and such HDAC inhibitory activity has been proposed to regulate intestinal macrophages[142]. Interestingly, butyrate-producing phyla are among those that are decreased in the dysbiotic microbiome population shifts that occur within IBD patients[143].

These periods of dysbiosis are commonly characterised by a narrowing of the species present and large swings in the microbial metabolome, which is the pool of host-signalling potential produced by the gut microbiome[144,145]. There are documented HIF-stabilising microbial interactions that could be predominant in the gut environment that are oxygen-independent. Lipopolysaccharide (LPS) has been shown to lead to accumulation of HIF-1α[146] through pathways such as NF-κB signalling[53,147,148]. Gut microbes also secrete iron-scavenging factors which in turn have been shown to facilitate normoxic stabilisation of HIF in co-culture models[149]. Interestingly, enriched within an IBD gut are bile acids and bile-acid metabolising species[144,150]. The O'Gara group have previously suggested that bile acids can act as destabilising compounds on HIF-1α in airway epithelial cells and cancer contexts[151,152]. Mechanistically, this was through increased PHD-mediated degradation, however they were able to show that increased levels of bile acids did repress the immune response to Pseudomonas *aeruginosa* (gram-negative species) infection. This same group has also reported that *P. aeruginosa* biofilm-promoting quorum signalling compounds can also act to destabilise HIF through promotion of proteasomal degradation in a non-PHD dependent manner[153]. Therefore, while interkingdom signalling between HIF and the microbiome points toward mechanistic upregulation of HIF, there have also been described mechanisms of microbial downregulation of HIF signalling. Thus, there is still an incomplete picture surrounding HIFs interaction with the gut microbiome, particularly through the lens of IBD which sees both disordered immune responses, an altered microbiome and elevated HIF signalling.

HIF-1α is an elusive druggable target

As there are multiple entry points and contexts for targeting of the HIF pathway in various diseases, there have correspondingly been targeted efforts to develop small molecule regulators. These efforts have resulted in development of a number of PHDi compounds and an isoform specific HIF-2α antagonist. A persistent gap is that there is no isoform selective HIF-1α antagonist, however a number of different mechanisms for non-selective HIF inhibition have been described.

The earliest pro-drug that targeted the HIF PHD enzymes was N-Oxaloglycine (NOG) and the cell permeable derivative dimethyl-oxalylglycine (DMOG)[154] these being immutably linked with the discovery of the HIF regulatory PHDs[155]. Mechanistically, it acted as a competitive inhibitor for 2-OG and Fe(II) binding, which occurs at the catalytic domain, and has since been exploited by a series of compounds that disrupt the catalytic site through active site chelation of the iron in PHDs[156]. Yet the issue that prevails with the current series of compounds is that this method is not selective as Yeh, et al. [90] demonstrated that all PHDi compounds interact with other prolyl hydroxylases. Certain inhibitors can bias selectivity for hydroxylation of the N-terminal or C-terminal oxygen dependent degradation site (NODD, CODD). As a result, this has led to a hypothesis that differential hydroxylation at these two sites may inform target gene activation and isoform-selectivity for next-generation PHD inhibitors[157,158]. As a result, there remains a persistent interest in the discovery of compounds that activate HIF-α.

In terms of inhibitor discovery however, HIF-2α and not HIF-1α has been the focus of small molecule development. While both HIF-1α and HIF-2α have the PAS-B pockets, HIF-2α's PAS-B pocket has been successfully targeted to develop a small molecule inhibitor[16-18,159-161]. These findings have led to approval of Belzutifan, a HIF-2α specific antagonist that has been approved with VHL-disease linked tumours[162]. This inhibitor was found through targeting of the purified PAS-B domain of HIF-2α with an NMR-based ligand-binding assay[160]. Structural optimisation of the scaffold was resolved into development of an isoform specific HIF-2α inhibitor that blocks heterodimer formation through conformational change[17,18]. Interestingly, binding to the PAS-B pocket has also been proposed to mediate allosteric promotion with specific activator compounds[163]. Importantly, these HIF-2α antagonists were shown, through use of purified protein, to be isoform specific. Given the differing roles in RCC for HIF-1α and HIF-2α[25] this has facilitated specific disease targeting in a clinical setting.

HIF-1α, the more ubiquitous isoform, has not seen a similar level of success. There have been a number of reported compounds and therapeutics that target HIF-1α in

the literature, however many lack distinct mechanistic information[164]. For example, PX-478 was an early reported HIF-1α inhibitor identified from luciferase screening[165]. It was shown to decrease HIF-1α transcription and stimulate non-proteasomal degradation of HIF-1α[166]. It was shown to be effective at reducing tumour burden within murine cancer models[167], supporting that small molecule downregulation of HIF-1α is valid cancer intervention. However the results of the Phase I clinical trial have not been fully disclosed[168]. Acriflavine was reported to be a pan-HIF inhibitor. It was proposed to function by preventing HIF-α and ARNT heterodimerisation and therefore function[169] although the original paper has since been retracted[170]. Additionally, acriflavine is known to trigger DNA damage and have pleotropic effects which prevent clinical usage. The same group have utilised the transcriptional signature of acriflavine-treated cells and reported development of a structurally unrelated compound that attenuated HCC xenograft growth, although again was pan-HIFα. There have also been non-small molecule approaches to targeting HIF-1. In a recent clinical trial setting however antisense mRNA against HIF-1α for hepatocellular carcinoma (HCC) patients, have been terminated twice with two different antisense RNAs for failing to inhibit sufficient levels of HIF-1α mRNA in tumour biopsies[171,172]. Peptide-based inhibitors targeting protein-protein interactions offer an alternate strategy to target the HIF pathway and such inhibitors have been developed to target HIF-1α. For example, the Tavassoli group report development of a intracellularly generated, membrane permeable cyclical peptide that blocked HIF-1α and ARNT heterodimerisation[14,173]. However, peptides are classically associated with a poor pharmacokinetic profile that has limited their clinical development[174]. The data surrounding small molecule HIF-1α inhibitors does illustrate issues with translating compound discovery to inhibitor development for HIF-1α however also reinforces that HIF-1α remains a key target.

Updating approaches: Push toward High Content

The HIFα pathway has been shown to be a clinically viable target, with the success of PHDi and HIF-2α antagonists, although there remains a persistent gap surrounding development of a potent HIF-1α antagonist. The prior screening campaigns relied on either *in vitro* purified protein approaches[13,169] or genetic reporters[175-178]. New opportunities are now present due to significant progress in the flexibility and robustness of genetic reporting elements, with a gulf between traditional genetic reporters, such as those used for prior HIF screens, and the next wave of small molecule screening approaches. The most obvious is the expansion of high throughput high content imaging approaches, previously the domain of pharmaceutical companies, into the academic sphere[179]. These approaches provide several distinct advantages over luciferase assay systems, which have been the most common method for HIF drug discovery. Luciferase assays are endpoint, provide low complexity readouts from the cell populations which can be confounded by cellular toxicity and interfering compounds[180,181]. In contrast, High content approaches, which are usually fluorescent and can capture multiple features regarding cellular appearance to isolate either specific phenotypes or be used in conjunction with capturing a target-specific signal[182] (**Figure 1.4**). Therefore, in a primary screening context, high content approaches enable combination of target-based drug discovery principles with cellular phenotyping for a more information-rich decision-making process.

Fluorescent reporters also offer other advantages beyond drug discovery. They facilitate labelling of single cells that are target-responsive and as a result FACS-based separation of fluorescent reporters have been increasingly applied to genomic screening as it allows isolation of high or lowly responsive cellular pools[183,184]. The current leading system for discovery of HIF regulators utilises a GFP-ODD genomic reporter that is HIF responsive and has been successful in defining several regulators of the HIF response[45,185,186]. This was used by Ortmann, et al. [185] whom delineated the role of SET1B, a histone methyltransferase, to active specific HIF target genes in a CRISPR knockout screen, indicating that these systems can be used to probe for

differential regulators of HIF target genes. However, this system is poorly suited to high content approaches and relies on a single transcriptional readout. Interestingly, there remain persistent gaps surrounding robust application of activity-dependent screens that can have cofounding effects[187,188]. Correspondingly, arrayed high content approaches are increasing in popularity and feasibility[189] as these approaches facilitate the isolation of individual guide-phenotype relationships and provide a higher-complexity readout on the impact of the genetic perturbation.

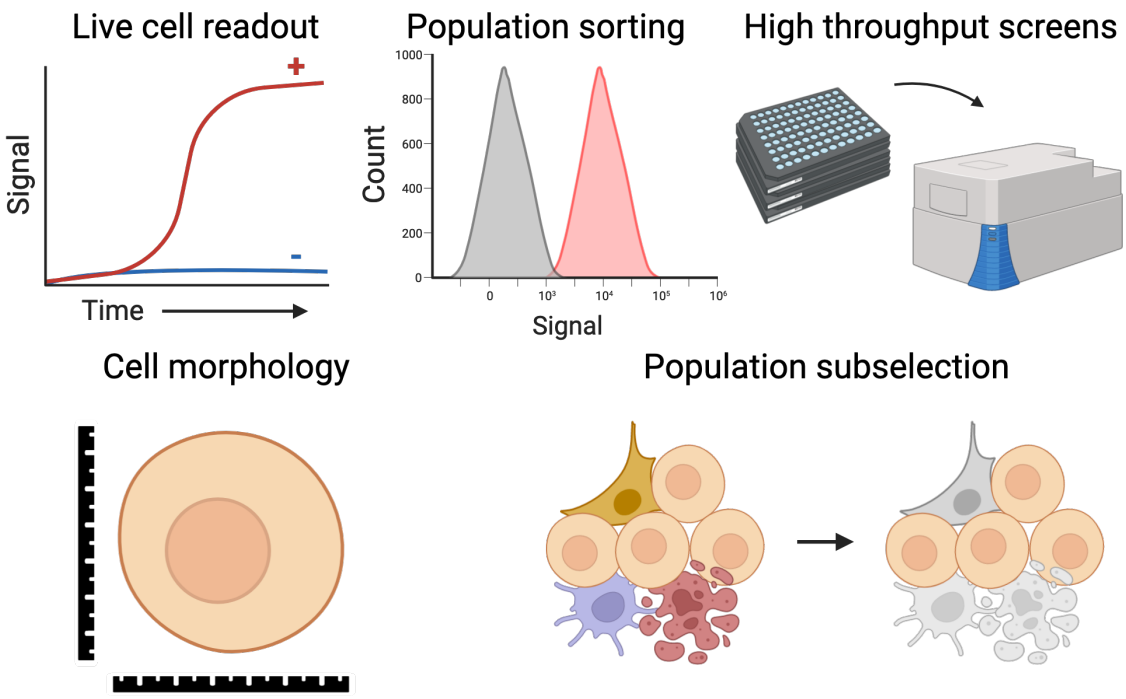

Figure 1.4 High content compatible genetic reporters offer flexible synthetic platforms for a range of applications.
Imaged-based capturing of reporter responses facilitate a wider range of reporting activity than traditional luciferase or bioassay-based reporters. They facilitate live cell readouts that can capture temporal reporter activity on the same population of cells over time or they can allow for sub-selection of the reporting population. They can be upscaled to a high throughput setting of a homogenous reporting population and reporter quantification, accurate measurements of cell morphology can also be taken, providing a higher complexity output than the reporter alone.

As a result of these trends and deficiencies in current genetic reporters, we designed a dual fluorescent, lentiviral compatible genetic reporter. In the following chapters we describe how we have developed this system for use in a high throughput context, demonstrating its robust nature. We show that we could use this system to target the HIF pathway as well as adapt it toward other transcriptional pathways and synthetic transcription factors. Because of the live cell nature of this system, we were able to demonstrate temporal responses and demonstrate how reporter activation facilitates formation of selectable pools due to the signal window created by target-pathway activation. To validate that this system is a valuable screening tool, we performed a pilot screen that identified a novel inhibitor and activator of the HIF pathway. We were able to exploit the live-cell nature of our systems reporter capacity in a bimodal screen design, providing activator and inhibitor screening in a single experimental workflow. We then describe how we have begun to integrate multiple parameters, specifically nuclear morphology, from the high content approach into refining our genetic reporter in a screening context. Finally, we describe how we have utilised this reporter to probe for HIF and microbiome interactions. Genetic reporter screening has been adopted as a robust method to delineate host microbiome signalling, specifically through the microbially derived metabolome[190-192]. As a result, we investigated if both individual strains and then complex microbiomes derived from IBD patients have the capacity to cross signal to HIF, probing these interactions with our genetic reporter and highlighting efforts to target other TF pathways, including other bHLH-PAS members. As a result, this thesis illustrates the design, performance, and broad application of a next-generation genetic reporter in a high content setting, utilising HIF as a proof-of-concept pathway given its complex regulation and role in human disease.

Project Aims:

The aim of this project was the establishment and application of a novel genetic reporter platform that could be used to readout for transcription factor activity in a high throughput manner, with a specific focus on HIF-1α regulation.

The overarching hypothesis for this work is that there exist ligands, either artificial or naturally occurring from sources such as the microbiome, which can bind and directly regulate HIF-1α through its PAS domains.

More specifically this project aimed to:

- Create and adapt an optimised genetic reporter that would allow sensing of a range of regulated transcription factor activities
- Demonstrate that this genetic reporter can be used for high throughput applications via drug library screening in a high content setting.
- Leverage the genetic reporter platform to probe for interactions between HIF-1α and microbial species from two distinct disease states, diabetic foot ulcers and inflammatory bowel disease.

Chapter 2. Methods and Materials

Table 2.1 Index of Solutions

Buffer/Solution	Ingredients
Luria Broth (LB)	1% (w/v) bacto-tryptone, 0.5% (w/v) yeat extract, 1% (w/v) NaCl (pH 7.0).
Solid agar	LB with 1.5% bacto-agar and 100mg/ml ampicillin
SOC	20mg/mL tryptone, 5mg/mL yeast extract, 10mM NaCl, 2.5mM KCl, 10mM $MgCl_2$, 10mM $MgSO_4$. 2% (v/v) glucose added after autoclaving.
BHI media (Oxoid)	12.5mg/mL Brain infusion solids, 5mg/mL Beef heart infusion solids, 10mg/mL proteose peptone, 2mg/mL glucose, 5mg/mL sodium chloride, 2.5 mg/mL disodium phosphate, pH 7.4.
CSIRO growth media (in 1L)	2g peptone, 2g yeast extract, 0.1g NaCl, 0.04g K_2HPO_3, 0.04g KH_2PO_4, 0.01g $MgSO_4$, 0.01g $CaCl_2$, 2g $NaHCO_3$, 0.05g Hemin, 0.5g L-Cysteine HCL, 0.5g Bile Salts, pH 6.8 1M Phosphoric acid. 10μL Vitamin K. 2g of either 1% Inulin, 0.2% galactose or 1% High Amylose Starch (HAMS).
FACS sort buffer	Ca^{2+}/Mg^{2+} free PBS, 2%FBS, 1mM EDTA, 25mM HEPES pH 7.0
DNA loading dye (5x)	50% (v/v) Glycerol, 0.1mM EDTA pH 8.0, 1% (w/v) Bromophenol blue
Agarose gel running buffer (20x)	21% (w/v) Trizma base, 10% (w/v) Boric Acid, 1% (w/v) EDTA, pH 8.3
PBS (1x)	130mM NaCl, 2.5mM KCL, 10mM Na_2HPO_4
PBST (1x)	PBS with 0.1% (v/v) Tween-20
Ponceau Stain	0.25g Ponceau, 1% (v/v) Glacial Acetic Acid, to 50mL MQ H_2O
SDS-PAGE running buffer	25mM Tris, 250mM Glycine, 0.1% SDS
SDS Loading Dye (5x)	40% Glycerol, 100mM Tris/HCL pH 6.8, 80uL 1% (w/v) Bromophenol Blue, 50mM DTT (fresh), 5% SDS
Urea Buffer	6.7M Urea, 10mM Tris-Cl (pH 6.8), 10% Glycerol, 1% SDS, 1mM DTT (fresh)
HPLC Buffer A	5% Methanol (v/v), 0.1% TFA (v/v), 95% H_2O
HPLC Buffer B	95% Methanol (v/v), 0.1% TFA (v/v), 5% H_2O

Table 2.2 Manufacturer Kits

Kit	Manufacturer
Plasmid Mini Kit	Qiagen
Plasmid Spin Mini Kit	Qiagen
Gel Extraction Kit	Qiagen
RNeasy Mini Kit	Qiagen

Table 2.3 Index of Enzymes

Enzyme	**Supplier**
CircLigase	Lucigen
Bst Polymerase	NEB
T4 DNA Ligase	NEB
Restriction Enzymes	NEB
Shrimp Alkyline Phosphotase (SAP)	NEB
Exonucleases	NEB
Proteinase K	Thermofisher Scientific
M-MLV Reverse Transcriptase	Promega
SYBER Green Master Mix	Thermofisher Scientific
DNase I	Qiagen

2.1 Plasmid and Bacteria general methodology

Table 2.4 List of plasmids used in this thesis

Plasmid	**Origin**
12xHRE-pLV-REPORT(PGK/CMV)	Whitelaw laboratory
12xHRE-LV-REPORT(EF1a)	Whitelaw laboratory
12xHRE-LV-REPORT(PGK)	Whitelaw laboratory
10xXRE-pLV-REPORT (CMV/PGK)	Whitelaw laboratory
psPAX2	Trono Laboratory
pMD2.G	Trono Laboratory

2.1.1 Plasmid DNA preparation

Plasmid DNA was propagated in DH5α cells in LB media or solid agar and purified using Qiagen Miniprep or Midiprep kits as per manufacturer instructions. For Midipreps, cultures were prepared via vacuum filtration. Plasmids for lentiviral preparation were prepared by Midiprep. DNA was stored at -20^{o}C.

2.1.2 Bacterial transformation

1-2μL of plasmid was combined with 50μL of DH5α and incubated for 30 min on ice. Mix was heat shocked for 45s before being placed on ice for 150s. 250μL of SOC was then added and outgrowth for 1hr at 37^{o}C prior to plating on solid agar with ampicillin selection. Individual colonies after overnight growth at 37^{o}C were selected for downstream applications.

2.1.3 DNA gel electrophoresis

1% or 1.5% agarose gels were stained with ethidium bromide (1μL per 20mL gel volume). Samples were combined with DNA loading dye prior to loading. Gels were run between 100-120V for 1hr depending on product size with markers and H_2O or

template-free controls. Gels were visualised by BioDoc-It Transilluminator or ChemicDoc MP Imager (Bio-Rad).

2.1.4 Restriction enzyme digests

1μg of plasmid DNA was digested with restriction enzymes for unique banding patterns (plasmid check digests) or for unique cut outs (e.g., ClaI/AvrII for pLV-REPORT enhancer cloning). Digestion mixtures were left at 37°C overnight and analysed by gel electrophoresis. For gel purification, DNA of appropriate size was cut out of gel and purified with the Qiagen gel purification kit as per manufacturer instructions.

2.1.5 Phenol chloroform clean-up

DNA samples were made to 100μL with MilliQ. 200μL of phenol:cholorform isoamylalchohol (Sigma) was added to samples. Samples were shaken and spun at 14,000 RPM at 4°C for 5 min. Supernatant was extracted and moved to a new vessel where 2 volumes of cold ethanol (EtOH, 100%) was added. Tubes were then placed at -80°C for two hours. DNA was pelleted by centrifugation at 14,000 RPM for 30 min and supernatant was removed. DNA pellet was washed with 500μL of EtOH, spun down at 14,000 RPM for 2 min and EtOH removed, followed by a second 14,000 RPM 5 min spin to remove excess EtOH. Pellet was briefly air dried and suspended in 30-40μL of MilliQ.

2.2 Enhancer Cloning methodology

Table 2.5 List of Plasmids generated for this thesis

Plasmid	**Purpose**
10xXRE-pLV-REPORT (CMV/PGK)	AhR-specific reporter with 10xCYP1A1 XRE repeats upstream of dual fluorescent reporter

Table 2.6 List of oligos for enhancer cloning

Plasmid	**Sequence (5' – 3')**
XRE Enhancer	CAGAGCCATGCCCAGGCGTTGCGTGAGAAGGACCGGAG GAAGGCTG
P1	ATATATCGATTCTGCAGCCTTC
P2	ATATCCTAGGGCTGCAGAGCCA
Sequencing primer	GGGTACAGTGCAGGGGAAAG

2.2.1 Enhancer concatemer creation

XRE enhancer oligo ssDNA with flanking sequences was ordered from Sigma, spun down and resuspended in milliQ at 100μM. Oligo was circularsied with CircLigase. 10pmol XRE enhancer was added to 1μL if 50mM $MnCl_2$, 4μL 5M Betaine, 0.5uL CircLigase (Lucigen), 1x CircLigase Buffer and H_2O. Mixture was incubated at 60°C for 2 hours, then 80°C for 1 hour. Reaction was then subjected to a phenol chloroform clean-up. Clean DNA was then exonuclease treated with 0.2 U/μg of DNA Exo VII, 5 U/μg DNA Exo III and 1x Exo III buffer at 37°C for 2 hours to digest non-circularised DNA followed by a second phenol chloroform clean-up. 1μL of XRE enhancer circDNA with 0.8μL of Bst polymerase (NEB, 8U/μL), 1x Bst Pol2 buffer (NEB), 3uL of DMSO and 1μL of 60μM stocks of P1 and P2 with H_2O and single primer negative controls. Reaction was run at 65°C for 90 min then 55°C for 120 min. DNA product was purified by phenol-chloroform clean up. Concatemers were digested with ClaI/AvrII double digest and purified on a PCR clean up column (Qiagen). Reaction was then run on a 1.5% agarose gel, concatemer formation confirmed and 10-15x concatemers (300-500bp) region was cut out and gel purified.

2.2.2 Enhancer cloning into pLV-REPORT backbone

1μg of pLV-REPORT(PGK/CMV) was digested with ClaI/AvrII overnight at 37°C, phosphatase (Shrimp Alkaline phosphatase, NEB) treated at 37°C for 30 min and inactivated at 65°C for 15 min. Cut backbone was gel purified with 1% agarose gel. 50ng of cut backbone was combined with concatemers at a 1:3 ratio with T4 ligase and incubated at room temperature for 2 hours. Ligated backbone was transformed into DH5α, colonies were picked and check digested for XRE insert with ClaI/AvrII and inserts were confirmed with sanger sequencing.

2.3 General Tissue Culture methodology

Table 2.7 List of cell lines utilised in this thesis:

Cell line	**Modification**	**Clonal (Y/N)**
HEK293T	Parental	N
HEPG2	Parental	N
HEK293T	12xHRE-LV-REPORT(EF1a)	N
HEK293T	12xHRE-LV-REPORT(PGK)	N
HEK293T	12xHRE-LV-REPORT(PGK/CMV)	N
HEK293T	12xHRE-LV-REPORT(PGK/CMV)	Y
HEK293T	VHL Knockout (C1C10)	Y
HEPG2	10xXRE-pLV-REPORT(PGK/CMV)	N

HEPG2	10xXRE-pLV-REPORT(PGK/CMV)	Y

2.3.1 Maintenance of cell lines

HEK293T and HEPG2 parental and stably-derived cell lines (**Table 2.7**) were cultured in DMEM with HEPES (pH 7.0) (Gibco) supplemented with 10% Foetal Bovine Serum (FBS, Corning), 1% Glutamax (Gibco) and 100ug/mL of Penicillin and Streptomycin. Cells were grown at 37^{o}C with 5% CO_2 in a humidified, UV sterilised incubator. Cells were passaged every 2-3 days or at 90% confluency. Cells were sub-cultured using 1xPBS and 0.5mL of trypsin/EDTA. Cells were resuspended in complete media prior to sub-cultivation, routinely at a 1:10 dilution in a 10cm dish or seeded as specified for assays 24 hours prior. To freeze cell lines, cells were trypsinised as above, pelleted at 1000-1200 RPM and resuspended in freezing media prior to controlled freezing in a cryo-freezing container at -80^{o}C prior to long-term storage in liquid nitrogen. For quantifying cell numbers prior to seeded, trypsinsied cells were mixed and diluted 1:2 with trypan blue and counted by haemocytometer or automated cell counter (Bio-Rad).

2.3.2 Monoclonal line derivation

For derivation of monoclonal lines, cells were seeded into 96 well trays at either 0.5 cell/well or 1 cell/well. Single colony formation was confirmed after a week's growth and after reaching 50% confluency were sub-cultured out into separate 96 well plates. Highly responsive clones were selected by high content imaging and underwent a second round of monoclonal derivation.

2.3.3 Lentiviral transduction and stable cell line creation.

Low passage HEK293T cells at 50-70% confluency was transfected with a 3:1 ratio of PEI and 12.5μg of lentiviral vector, 7.5μg of psPAX2 (Addgene #12260) and 3.75μg MD2.G (Addgene #12259). Media was changed after 18 hours and virus-containing media was harvested at 48 hours. Viral-containing media was 0.22μM filtered to ensure no cross-contamination of transfected cells and stably-derived lines. Virus was applied to 50% confluent dishes of requisite cell lines to obtain an MOI < 1 with 0.5mL of viral mediate diluted 1:20 in 10cm dishes. Cells were incubated with viral media for 48 hours prior to antibiotic selection. Standard concentrations were 1μg/mL Puromycin, 140μg/mL Hygromycin and 10μg/mL Blasticidin S. Cells were maintained under selection for 2 passages and were in quarantine for a minimum of 3 passages to ensure no viral contamination.

2.4 Protein isolation and western blotting

2.4.1 Cell lysis for HIF protein

For protein isolation cells were washed with 1mL of cold 1xPBS prior to addition of 50μL of urea extract buffer[25] to a 6cm dish at designated time point. Cells were scraped and lysate was collected. Lysate was incubated on ice for 30 min prior to sonication for 10 cycles of 30s on, 30s off. Lysates were then spun down at 14,000 RPM. Lysates were stored at -80°C but were not subjected to more than 1 freeze thaw cycle. Protein concentration was quantified by BCA assay (Pierce) with a BSA standard curve.

2.4.2 Western blotting

After BCA assay, equal amounts (in μg/μL) of each protein sample were added to a 1xSDS load buffer with 50mM DTT (added fresh) prior to loading. Samples were loaded onto a mini-PROTEAN TGX precast 12.5% SDS-PAGE gel (Bio-Rad) with Precision Plus pre-stained protein markers. Gel was run at 100-150V for 1-2 hours in 1x TGS running buffer. Gel was transferred to nitrocellulose membrane using TurboBlot Midi Kit (BioRad) for 7 minutes at 2.5V to ensure transfer of proteins between 200kDa – 20kDa. To confirm even transfer and equal protein loading, membrane was ponceau stained for 5 minutes at room temperature and then visualised. After ponceau staining, membrane was blocked for 1hr at room temperature with 10% skim milk and 1xPBST with gentle rocking. Membrane was incubated overnight with primary antibody at dilution specified in **Table 2.8** in 10mL of 2% milk and PBST at 4°C with gentle agitation. Membrane washes were three intervals of five minutes with PBST. The membrane was developed with Clarity ECL (BioRad) and visualised using the Chemidoc MP imaging system (BioRad). Multiple exposures were captured per development to ensure consistent interpretation between low exposure and high exposure. After developments, blots were then reprobed with different primary antibodies or wrapped, with PBST, for short term storage at 4°C.

Table 2.8 Antibodies utilised

Antibody (1°/ 2°)	**Manufacturer and species**	**Dilution**
α-HIF-1α (1°)	BD Transductions, Mouse	1:1000
α-GAPDH (1°)	Sigma, Mouse	1:10,000

α-Mouse-HRP (2°)	Pierce Biotechnologies, Goat	1:10,000

2.5 Cell imaging

2.5.1 High Content Imaging (HCI)

Cells were seeded at $1x10^4$ to $4x10^4$ cells per well within 96 well plates (Costar Cat#3603), 24 hours prior to treatment in complete media. Cell populations were imaged at 10x magnification using the ArrayScan™ XTI High Content Reader (ThermoFisher) using the inverted lens and while in complete media utilising the 560/25nm (Tomato) and 485/25nm (EGFP) excitation sources. Exposure times were selected based on 35% peak target range for each individual cell line using HCS Studio 3.0 and did not vary from treatment to treatment or across plates. 2000 individual nuclei per well were used for MFI calculations. Individual nuclei were delineated by EGFP expression followed by nuclear segmentation and isodata thresholding. Threshold values were derived against the vehicle control, excluding highly abnormal nuclei, cells on well edges and background objects. EGFP and Tomato intensity was then measured for each individual nucleus in the population and fluorescent protein intensity was not used to gate for cells, providing an unbiased population measurement of reporter cells. Imaging was done consistently from the centre of each well and imaged progressively outward in a consistent spiral fashion based on form factors that were defined for each plate batch and updated on a batch-to-batch basis. Quantification of the images utilised HCS Studio™ 3.0 Cell Analysis Software (ThermoFisher) and reporter quantification of Tomato/EGFP intensity was readout from raw data as MEAN_CircAvgIntensityRatioCh2Ch1, Tomato MFI was MEAN_CircAvgIntensityCh2 and EGFP MFI was MEAN_ObjectAvgIntensityCh1.

2.5.2 Widefield Fluorescent Imaging

AhR Reporter HEPG2 cells were seeded into 48-well plates at $2x10^4$ cells per well in required growth media (described above) overnight prior to incubation with requisite compounds to activate the indicated reporter constructs and relevant controls for 48 hours prior to imaging. Cells were imaged in media, in plates without fixation, in native media, with an inverted microscope (Nikon Ti) at 10x magnification with FITC and Cy3 filters for 1sec exposure times for EGFP and Tomato detection respectively. Images were background removed, mean grey values of image fields were recorded as

reporter output (mean fluorescent intensity) and false coloured using ImageJ[193]. Image brightness is uniformly increased by 40% from raw output for presentation.

2.6 qPCR for Reporter Expression

Table 2.9 List of qPCR primers utilised in this thesis:

Primer Set	Forward (5' – 3')	Reverse (5' – 3')
Polr2a	GCACCATCAAGAGAGTGCAG	GGGTATTTGATACCACCCTCT
nucTomato	TCCCCGATTACAAGAAGCTG	CCCATGGTCTTCTTCTGCAT
nucEGFP	AGAAGAACGGCATCAAGGTG	GAACTCCAGCAGGACCATGT

2.6.1 RNA extraction

Cell lines were seeded in 6 well trays dishes at $1x10^5$ cells dish and incubated overnight before treatment for 48 hours with 1mM DMOG or 0.1% DMSO.

Cells were in resuspended in Trizol (Invitrogen) and RNA was purified with the RNAEasy Kit and DNaseI treated. RNA quality was checked by 1% agarose gel to confirm no gDNA contamination and RNA degradation. RNA was stored at -80°C.

2.6.2 cDNA production

Purified RNA was reverse transcribed using M-MLV reverse transcriptase (Promega) in a two-step reaction. RNA was quantified by Nanodrop and 2μg was used to synthesise cDNA. In the first step 500ng of Oligo dT, 1μL of 25μM random hexamers, 2μL of 5mM dNTP and 2μg of RNA was incubated for 65°C for 5 min. In the second step, RNAse inhibitor (20U/μL), 0.2μL M-MLV reverse transcriptase, 0.1M DTT and 1x M-MLV buffer (Promega) were added to the reaction. Reaction was run at 25°C for 5 min, 50°C for 90min, 70°C for 15 min. Sample was diluted in MilliQ prior to qPCR and stored at -20°C.

2.6.3 qPCR for backbone activity

Real-time PCR used primers specific for the nucTomato, nucEGFP, and human RNA Polymerase 2 (*POLR2A*) (**Table 2.9**). 2uL of cDNA were combined with SYBR Green and 5μM of each primer. All reactions were done on a StepOne Plus Real-time PCR machine. qPCR protocol was 95°C for 10 min then 40 cycles of 95°C 10s and 60°C for 30s with 0.5°C temperature ramping increments. Single amplicon formation was confirmed by melt curve and data analysed by 'QGene' software. Results were normalised to *POLR2A* expression. RT-qPCR was performed in technical triplicate and single amplicons were confirmed via melt curves. Statistics are between three biological replicates.

2.7 Backbone selection curve with increasing hygromycin

2.7.1 Hygromycin selection for multiple inserts

Cell populations with different backbones were derived by lentiviral selection and intial selection with hygromycin. Cell populations were then untreated, treated with selection concentration (140μg/mL) or 500, 1000, and 1500μg/mL of Hygromycin and maintained for three passages. Reporter activity was then quantified in the presence or absence of DMOG by HCI (Section 2.5.1) for the selected pools.

2.8 RQ200674 scaffold analysis from bimodal small molecule screen

2.8.1 Pyridoindole motif selection and assessment from bimodal screen

Screen methods are described in **Chapter 3.1**.

After identification of the RQ200674 scaffold from the 1600 compound bimodal screen, structures from the library containing the motif were grouped by similarity. Data from the original screens was then used to identify activity using +2SD cut offs for Tomato MFI and EGFP MFI from vehicle controls.

2.8.2 Screening of pyridoindole-like compounds

Compounds were provided by the Quinn group (University of Queensland) and arrived in Costar CLS#3603 plates. Compounds were seeded in 1μL of DMSO with either 2.5mM or 5mM of compound. For screening, 100μL of the HIF monoclonal screening cells were seeded at $1x10^4$ cells per well with vehicle and DMOG-treated controls on each plate. Reporter activation was imaged after 48 hours with HCI and cut offs were determined by 3SD from the vehicle (1% DMSO) negative control across three independent biological replicates.

2.9 Super-activator identification

2.9.1 Super activator compound identification and rescreening

The most active compounds in the 36-hour screen were identified from the bimodal screening data. Compounds were provided in 1μL of DMSO at either 2.5mM or 5mM concentrations. HIF screening cells were added to the compounds in 100μL with 1mM of DMOG at $1x10^4$ cells per well. Final solvent concentration was 1.1% DMSO final concentration per well for all wells. Cells were imaged for reporter activation after 48 hours by HCI (Section 2.5.1) for 25μM and 50μM for three independent biological replicates.

2.10 HTS-HCI screening of the Bioaustralis library

2.10.1 Bioaustralis library screening

The Bioaustralis Series I Discovery set compounds were shipped from Bioaustralis and contained 800 molecules that were shipped in 10 individual clear plates. Each well contained 1μg of each compound in 1μL of DMSO. Plates were stored at -80°C prior to screening. To screen, HEK293T HIF screening cells were seeded at $1x10^4$ cells per well in Costar CLS#3603 plates in 50μL 6 hours prior to screening. Compounds were put into solution by incubation in 50μL of cell culture media with 2mM DMOG for 150 minutes with gentle agitation. The full 50μL of media and compound were transferred to the cells in the CLS#3603 plates and incubated. 6 negative (DMSO-treated) and 6 positive (DMOG-treated) controls were included per plate, for a final concentration of 1mM DMOG per compound well with 1.1% DMSO final concentration. Plates were imaged by HCI (Section 2.5.1) at 24 and 48 hours. Z' scores per plate were calculated as per Zhang, et al. [194]. All plates were confirmed to have a Z' of >0.5 within excellent screening range. Reporter output was Z score normalised and hits were determined by the mean + κ scoring[195], where κ was -3SD from the DMOG (positive) control for Tomato MFI and Tomato/EGFP MFI. Z scored compounds were converted to P scores and adjusted with a Benjamini and Hochberg [196] correction. Compounds with EGFP MFI >±2SD from the DMOG-treated control wells were considered non-specific regulators of reporter activity. Compounds that met that criteria had images qualitatively reviewed to confirm they weren't strongly auto fluorescent or obviously confounding results.

2.10.2 Bioaustralis hits validation

Hits were selected based on above criteria and ordered from Bioaustralis as lyophilised powder. Compounds were made into 50mM stocks in DMSO and stored at -20°C. Compounds were screened against the HEK293T HIF reporter cells by HCI (Section 2.5.1). Cells were seeded into 96 well CLS#3603 plates at $1x10^4$ cells per well overnight in 50μL. 1μL of each compound in DMSO was added to 50μL of complete media with 2mM DMOG. The 50μL of compound and DMOG was then added to the reporter cells for final concentrations of 1mM DMOG, 1.1% DMSO. Compound concentrations were 50μM for all compounds or a dose curve of 50μM, 25μM and 10μM. Plates were imaged for the 0hr time point <15min after compound treatment and imaged at the initial (0hr), 24hr and 48hr time points. All compounds

were analysed in triplicate in an arrayed format with HCI (Section 2.5.1) with a minimum of 4 positive and 4 negative controls per plate.

2.10.3 Orthogonal screening with VHL Knockout cell line

The HEK293T HIF reporter VHL knockout (VHL KO) cell line was derived and validated in Allen [197]. Constitutive HIF expression was confirmed by immunoblot. VHL KO HIF reporter was seeded at $1x10^4$ cells per well 24 hours prior to treatment with compounds. VHL KO HIF reporter cells were screened for compound activity as per Section 2.10.2.

2.10.4 Gliorosein toxicity assessment

HEK293T cells were seeded at $1x10^5$ cells/mL in 6 well dishes overnight then treated with DMSO vehicle control (1.1% DMSO), Gliorosein and Glioroseinol for final concentration of 50μM of compound and 1.1% DMSO for consistency with prior assays. Cells were trypsinised, stained 1:2 with trypan blue and counted at 24 and 48 hours. Total number of cells (live & dead) were counted as were number of viable (live) cells that were not stained by trypan blue. Total live cell counts and percentage of unstained cells relative to total cells were presented. Cell counts were calculated as number of live cells per mL of culture for two technical replicates per treatment across 2 biological treatments.

2.10.5 Nuclear shape measurements from High content imaging

Nuclear shape measurements for nuclear area, length, width, and circularity are derived from HCI image data captured as per Section 2.10.1. While highly abnormal nuclei are excluded (as per Section 2.5.1), parameters still allow for a spread of different nuclear phenotypes and were not varied between plates. Nuclear measurements were taken from the EGFP channel and calculated with HCS Studio 3.0. Measurements were taken in parallel with reporter intensity quantification and, are from the same 2000 cell population used to calculate reporter intensity.

2.10.6 Nuclear Shape Score (NSS) for hit filtering

The four features for the measurement of nuclear appearance were selected. Principal component analysis (PCA) was done on the Z scored features using the prcomp function in the R package stats (R version 4.2.2) for each individual compound and control well. PC1 and PC2 were projected on a biplot calculated using the R package ggbiplot (version 0.55). To derive the nuclear shape score (NSS), cut offs for PC1

were set at ±2 and PC2 ±1 to capture DMOG and DMSO control wells within the 95% confidence intervals. Cut offs were scaled outward linearly, given that PCA utilises Euclidian distances to project dissimilarity and were applied uniformly to the Bioaustralis and bimodal inhibitor screening data. Cut offs were scored from most (7) to least (1) similar to the mean of the controls.

2.11 Diabetic foot ulcer bacterial library screening

2.11.1 Bacterial library growth and filtration

Bacterial species were grown in BHI media (Oxoid) with up to 0.2%Tween20 under anoxic conditions at 37°C with constant agitation by Dr. Nan Hao. Cultures were grown in 10mL cultures (**Figure 3.3.3-3.3.4**) or 96 well plates from stationary phase dilutions (**Figure 3.3.5-3.3.6**). In 96 well plates, stationary growth was confirmed by OD_{600} readings every 2 hours for a 72hr period. All cultures screened had an OD_{600} of >0.5 Cultures were spun down at 4000RPM for 15min and filtered through a 0.22μM filter to produce cell-free bacterially-derived supernatants.

2.11.2 Bacterial library supernatant screening

HEK293T cells were assayed for toxicity in response to blank BHI media, with or without 0.2% Tween80 prior to screening. Increasing ratios of media to supernatant were assayed and 10% supernatant to 90% media was well tolerated by cell populations over a 72-hour period with no observed changes in viability or morphology relative to negative controls. HEK293T HIF reporter cell lines were seeded at $1x10^4$ cells per well in 50μL overnight prior to assay. 50μL of 2.2mM DMOG or 0.22% DMSO complete media was added to the cell culture population followed by 10μL of either control or bacterially-derived supernatants for 110μL final volume with final concentrations of 0.1% DMSO or 1mM DMOG with 0.1% DMSO and 10% v/v supernatant. Reporter cells are incubated for 48 hours prior to HCI (Section 2.5.1), and cell populations were reviewed to ensure no increase in toxicity.

2.13 IBD patient sample analysis

2.13.1 IBD patient bacterial culture & supernatant harvesting

Media and cultures were grown by Emma Watson and Swov Dziemborowicz from the CSIRO. Cultures were grown in CSIRO growth media with Inulin, HAMS or 0.2% Galactose supplementation. For initial culturing, 180mL of growth media was mixed with 20mL of inoculate. Inoculate was made from faecal inoculate with minimum

$3.28x10^9$ estimated bacterial count. Faecal samples were made up to 100mL with sterile PBS and glycerol stocks were made from a 50% mixture of inoculate and 50% glycerol. Inoculate or glycerol stock was added to media in a 1:5 ratio. 20mL in 180mL or 2mL for 10mL culture. For iterative growths, 1:5 ratio was maintained at 2mL of the prior sample was used as the inoculate for the next iterative step. Cultures were grown in a sealed environment, in an anaerobic chamber at 37°C with agitation. Cultures were grown for 24 hours, and pH was measured after culturing to confirm successful outgrowth of bacterial species. Cultures were then collected and spun down gently at 5000 rpm for 30 minutes. Supernatants were removed, spun down a second time, and filtered through 0.22μM syringe filters to ensure cell and contaminant free supernatant collection. Supernatants and bacterial pellets were stored at -80°C.

2.13.2 Supernatant screening against HIF-1α

HEK293T HIF reporter cells were seeded at $1x10^4$ cells/well in 100μL with cell culture media and treated with 1mM DMOG or 0.1% DMSO and 10μL of bacterial supernatants or blank media controls. For no media controls, 10μL of complete media was used. Final screening concentrations were 1mM DMOG, 0.1% DMSO and 10% v/v supernatant to media with three technical replicates per biological replicate. Cells were incubated at 37°C for 48 hours and monitored every 24 hours to ensure that there was no bacterial contamination or outsized cell death. At 48 hours, no bacterial contamination was observed and no cell death in the negative controls was observed. Plates were then quantified by HCI (Section 2.5.1). 3SD cut offs from negative media controls were used to bracket for hits of significance.

2.13.3 16s rRNA sequencing

16s rRNA sequencing was performed by Prof. Geraint Rogers and Dr. Steven Taylor at Flinders University. Pelleted bacteria, glycerol stocks and 100mg of raw faecal sample from Section 2.13.1 were supplied to the Rogers lab. gDNA was extracted as per Taylor, et al. [198] and the V1-3 hypervariable region was sequenced as per Taylor, et al. [199] using QIIME software and assigned identity based on 97% sequence identity to reference. Presence and relative abundance are from read depth per sample for each species and used to derive fold change data.

2.13.4 Proteinase K treatments

Supernatants were digested with 1U/mL Proteinase K at room temperature for 2 hours. Proteinase K was then inactivated when samples were boiled at 95°C for 5 minutes and spun down. Treated supernatants were assessed against the HIF reporter after 24 hours as per Section 2.13.2.

2.13.5 3kDa Filtering of bacterial supernatants

3kDa cut off filters (Sigma) were first washed with 1mL milliQ water and spun through for 30min at 14,000 RPM. 1mL of supernatants were then added to 3kDa filters and spun for 1hr at 14,000 RPM at 4°C. Flow through (<3kDa filtrate) and retentate (>3kDa filtrate) were retained. Supernatants were then added to HIF reporter cells as per Section 2.13.2 at 10% v/v, 5% v/v and 2% v/v, with supernatant diluted in milliQ water.

2.13.6 C18 Flash Column Purification

Discovery DSC-18 SPE columns (Sigma) were first washed with 1 column volume (CV) of milliQ water. 1CV of each supernatant was passed through separate columns and flowthrough was collected. 1CV of H_2O, 100% Methanol and Acetonitrile was then passed through the column and flow through was collected. Columns were then washed with milliQ water. Samples were collected and freeze-dried using Alpha 2-4 Lo Plus and RVC 2-25 CD Plus freeze drier (Christ) overnight. Samples were resuspended in 100μL of milliQ water. Resuspended samples were then added to HEK293T HIF reporter cells as per Section 2.13.2.

2.13.7 Metabolomics Analysis

Metabolomics was done on Sample 16-2 3kDa filtered supernatants from the first (Growth #1) and second (Growth #2) iterative growths of bacterial cultures. Metabolomics was performed by Dr Luca Nicolotti at The Australian Wine Research Institutive. 1mL of 3kDa filtered sample was provided. Samples were analysed in two ways. Firstly, samples were analysed for polar metabolites by Hydrophilic interaction liquid chromatography (HILIC) HPLC coupled with High Resolution Fourier Transform Mass Spectrometry (HPLC-HRFTMS). Non-polar metabolites were analysed by Reverse Phase HPLC-HRFTMS. Three technical replicates per sample were analysed and median normalised chromatographic area for each compound was measured. Coefficient variation (%CV) for each identified compound was calculated. Compounds with %CV higher than 25% in both samples were excluded. Ratios, $\log_2$ fold change and adjusted p-values (for technical replicates) was calculated. Compound

identification was done by comparison to external and internal databases by Dr. Nicolotti.

2.13.8 FACS

Polyclonal HEPG2 populations were sub-cultured into 10cm dishes at $2x10^6$ cells per dish overnight and treated with 0.1% DMSO or 100μM Indole for 48 hours. Prior to flow cytometry, HEPG2 cells were trypsinised, washed in complete media and resuspended in resuspended in flow cytometry analysis buffer for analysis followed by filtration through a 40μM nylon cell strainer (Corning Cat#352340). Cell populations were kept on ice prior to sorting. Flow cytometry was done using the BD Biosciences FACS ARIA2 within a biosafety cabinet and aseptic conditions, using an 85μM nozzle. Cell populations were gated by FSC-W/FSC-H, then SSC-W/SSC-H, followed by SSC-A/FSC-A to gate cells. EGFP fluorescence was measured by a 530/30nm detector, and the Tomato fluorescence was determined with the 582/15nm detector. A minimum of 10,000 cells were sorted for all FACS-based analysis. Data is presented as $\log_{10}$ intensity for both fluorescent proteins. Cell counts for histograms are normalised to mode unless stated otherwise. FACS analysis was done on FlowJo™ v10.9.1 software (BD Life Sciences)[200].

2.14 Figure Creation and Software

Unless specified otherwise, error is mean±SD of biological replicates. Diagrams and figures were made with Biorender (www.biorender.com). Statistical analysis and graphs were created with ggplot2 package for R[201] or GraphPad PRISM (Ver. 9.0.0).

Chapter 3. Results

Statement of Authorship

Title of Paper	dFLASH; dual Fluorescent transcription factor Activity Sensor for Histone integrated live-cell reporting and high-content screening
Publication Status	☐ Published ☐ Accepted for Publication ☐ Submitted for Publication ☐ Unpublished and Unsubmitted work written in manuscript style
Publication Details	Pre-print available on Biorivx (DOI: https://doi.org/10.1101/2023.11.21.568191) Intended submission to Nature Communications.

Principal Author

Name of Principal Author (Candidate)	Timothy P. Allen		
Contribution to the Paper	Conceived, designed and performed experiments, generated reagents, compiled and analyzed data, generated figures, wrote manuscript. Contributed to all figures except Figure 4 and supplementary figures 4 & 6.		
Overall percentage (%)	50%		
Certification:	This paper reports on original research I conducted during the period of my Higher Degree by Re ny obligations or contractual agreements with a third pa thesis. I am the primary author of this paper.		
Signature		Date	07.12.2023

Co-Author Contributions

By signing the Statement of Authorship, each author certifies that:

i. the candidate's stated contribution to the publication is accurate (as detailed above);
ii. permission is granted for the candidate in include the publication in the thesis; and
iii. the sum of all co-author contributions is equal to 100% less the candidate's stated contribution.

Name of Co-Author	David C. Bersten		
Contribution to the Paper	Conceived & supervised study. Designed and performed experiments. Contributed panels to Figures 2, 3, Supplementary figures 2, 5 and contributed figure 4 and Supplementary figures 4 & 6 Wrote manuscript.		
Signature		Date	

Name of Co-Author	Murray L. Whitelaw		
Contribution to the Paper	Conceived study wrote manuscript and supervised work.		
Signature		Date	

Please cut and paste additional co-author panels here as required.

Statement of Authorship

Title of Paper	dFLASH; dual Fluorescent transcription factor Activity Sensor for Histone integrated live-cell reporting and high-content screening
Publication Status	☐ Published ☐ Accepted for Publication ☐ Submitted for Publication ☐ Unpublished and Unsubmitted work written in manuscript style
Publication Details	Pre-print available on Biorivx (DOI: https://doi.org/10.1101/2023.11.21.568191) Intended submission to Nature Communications.

Principal Author

Name of Principal Author (Candidate)	Timothy P. Allen
Contribution to the Paper	Conceived, designed and performed experiments, generated reagents, compiled and analyzed data, generated figures, wrote manuscript. Contributed to all figures except Figure 4 and supplementary figures 4 & 6.
Overall percentage (%)	50%
Certification:	This paper reports on original research I conducted during the period of my Higher Degree by o any obligations or contractual agreements with a third this thesis. I am the primary author of this paper.
Signature	Date 7.12.23

Co-Author Contributions

By signing the Statement of Authorship, each author certifies that:

i. the candidate's stated contribution to the publication is accurate (as detailed above);

ii. permission is granted for the candidate in include the publication in the thesis; and

iii. the sum of all co-author contributions is equal to 100% less the candidate's stated contribution.

Name of Co-Author	David C. Bersten
Contribution to the Paper	Conceived & supervised study. Designed and performed experiments. Contributed panels to Figures 2, 3, Supplementary figures 2, 5 and contributed figure 4 and Supplementary figures 4 & 6 Wrote manuscript.
Signature	Date 08.12.23

Name of Co-Author	Murray L. Whitelaw
Contribution to the Paper	Conceived study wrote manuscript and supervised work.
Signature	Date

Please cut and paste additional co-author panels here as required.

Statement of Authorship

Title of Paper	dFLASH; dual Fluorescent transcription factor Activity Sensor for Histone integrated live-cell reporting and high-content screening
Publication Status	☐ Published ☐ Accepted for Publication ☐ Submitted for Publication ☐ Unpublished and Unsubmitted work written in manuscript style
Publication Details	Pre-print available on Biorivx (DOI: https://doi.org/10.1101/2023.11.21.568191) Intended submission to Nature Communications.

Principal Author

Name of Principal Author (Candidate)	Timothy P. Allen		
Contribution to the Paper	Conceived, designed and performed experiments, generated reagents, compiled and analyzed data, generated figures, wrote manuscript. Contributed to all figures except Figure 4 and supplementary figures 4 & 6.		
Overall percentage (%)	50%		
Certification:	This paper reports on original research I conducted during the period of my Higher Degree by Research candidature and is not subject to any obligations or contractual agreements with a third party that would constrain its inclusion in this thesis. I am the primary author of this paper.		
Signature		Date	

Co-Author Contributions

By signing the Statement of Authorship, each author certifies that:

i. the candidate's stated contribution to the publication is accurate (as detailed above);

ii. permission is granted for the candidate in include the publication in the thesis; and

iii. the sum of all co-author contributions is equal to 100% less the candidate's stated contribution.

Name of Co-Author	David C. Bersten		
Contribution to the Paper	Conceived & supervised study. Designed and performed experiments. Contributed panels to Figures 2, 3, Supplementary figures 2, 5 and contributed figure 4 and Supplementary figures 4 & 6 Wrote manuscript.		
Signature		Date	

Name of Co-Author	Murray L. Whitelaw		
Contribution to the Paper	Conceived study wrote manuscript and supervised work.		
Signature		Date	8 Dec 2023

Please cut and paste additional co-author panels here as required.

Name of Co-Author	Daniel J. Peet		
Contribution to the Paper	Supervised work and edited manuscript.		
Signature		Date	8/12/2023

Name of Co-Author	Darryl L. Russell		
Contribution to the Paper	Supervised work.		
Signature		Date	

Name of Co-Author	Ronald J. Quinn		
Contribution to the Paper	Provided small molecule library and associated information.		
Signature		Date	

Name of Co-Author	Miaomiao Liu		
Contribution to the Paper	Provided small molecule library and associated information.		
Signature		Date	

Name of Co-Author	Moganalaxmi Reckdharajkumar		
Contribution to the Paper	Generated reagents.		
Signature		Date	

Name of Co-Author	Alison E. Roennfeldt		
Contribution to the Paper	Conceived, designed, and performed experiments. Contributed panels to figures 2, 3 and supplementary figure 1-3. Analysed data. Edited manuscript.		
Signature		Date	

Please cut and paste additional co-author panels here as required.

Name of Co-Author	Daniel J. Peet		
Contribution to the Paper	Supervised work and edited manuscript.		
Signature		Date	

Name of Co-Author	Darryl L. Russell		
Contribution to the Paper	Supervised work.		
Signature		Date	08-12-2023

Name of Co-Author	Ronald J. Quinn		
Contribution to the Paper	Provided small molecule library and associated information.		
Signature		Date	

Name of Co-Author	Miaomiao Liu		
Contribution to the Paper	Provided small molecule library and associated information.		
Signature		Date	

Name of Co-Author	Moganalaxmi Reckdharajkumar		
Contribution to the Paper	Generated reagents.		
Signature		Date	

Name of Co-Author	Alison E. Roennfeldt		
Contribution to the Paper	Conceived, designed, and performed experiments. Contributed panels to figures 2, 3 and supplementary figure 1-3. Analysed data. Edited manuscript.		
Signature		Date	7/12/23

Please cut and paste additional co-aut

Name of Co-Author	Daniel J. Peet		
Contribution to the Paper	Supervised work and edited manuscript.		
Signature		Date	

Name of Co-Author	Darryl L. Russell		
Contribution to the Paper	Supervised work.		
Signature		Date	

Name of Co-Author	Ronald J. Quinn		
Contribution to the Paper	Provided small molecule library and associated information.		
Signature		Date	

Name of Co-Author	Mingmiao Liu		
Contribution to the Paper	Provided small molecule library and associated information.		
Signature		Date	

Name of Co-Author	Meganaluxmi Ravichandrakumar		
Contribution to the Paper	Generated reagents.		
Signature		Date	07/12/2023

Name of Co-Author	Alison E. Roennfeldt		
Contribution to the Paper	Conceived, designed, and performed experiments. Contributed panels to figures 2, 3 and supplementary figure 1-3. Analysed data. Edited manuscript.		
Signature		Date	

Please cut and paste additional co-author panels here as required.

Name of Co-Author	Daniel J. Peet		
Contribution to the Paper	Supervised work and edited manuscript.		
Signature		Date	

Name of Co-Author	Darryl L. Russell		
Contribution to the Paper	Supervised work.		
Signature		Date	

Name of Co-Author	Ronald J. Quinn		
Contribution to the Paper	Provided small molecule library and associated information. nb. Author couldn't be contacted by time of submission		
Signature		Date	8 Dec 2023

Name of Co-Author	Miaomiao Liu		
Contribution to the Paper	Provided small molecule library and associated information. nb. Author couldn't be contacted by time of submission		
Signature		Date	8 Dec 2023

Name of Co-Author	Moganalaxmi Reckdharajkumar		
Contribution to the Paper	Generated reagents.		
Signature		Date	

Name of Co-Author	Alison E. Roennfeldt Text		
Contribution to the Paper	Conceived, designed, and performed experiments. Contributed panels to figures 2, 3 and supplementary figure 1-3. Analysed data. Edited manuscript.		
Signature		Date	

Please cut and paste additional co-author panels here as required.

dFLASH; dual FLuorescent transcription factor Activity Sensor for Histone integrated live-cell reporting and high-content screening

Authors: Timothy P. Allen[1], Alison E. Roennfeldt[1,2], Moganalaxmi Reckdharajkumar[1], Miaomiao Liu[3], Ronald J. Quinn[3#], Darryl L. Russell[2#], Daniel J. Peet[1#], Murray L. Whitelaw[1,4#] & David C. Bersten[1,2*]

Affiliations: 1. School of Biological Sciences, University of Adelaide, Adelaide, South Australia, Australia 2. Robinson Research Institute, University of Adelaide, South Australia, Australia. 3. Griffith Institute for Drug Discovery, Griffith University, Brisbane, Australia 4. ASEAN Microbiome Nutrition Centre, National Neuroscience Institute, Singapore 169857, Singapore. *Corresponding author. #labs that contributed to the work

Abstract

Live-cell reporting of regulated transcription factor (TF) activity has a wide variety of applications in synthetic biology, drug discovery, and functional genomics. As a result, there is high value in the generation of versatile, sensitive, robust systems that can function across a range of cell types and be adapted toward diverse TF classes. Here we present the dual FLuorescent transcription factor Activity Sensor for Histone integrated live-cell reporting (dFLASH), a modular sensor for TF activity that can be readily integrated into cellular genomes. We demonstrate readily modified dFLASH platforms that homogenously, robustly, and specifically sense regulation of endogenous Hypoxia Inducible Factor (HIF) and Progesterone receptor (PGR) activities, as well as regulated coactivator recruitment to a synthetic DNA-Binding Domain-Activator Domain fusion proteins. The dual-colour nuclear fluorescence produced normalised dynamic live-cell TF activity sensing with facile generation of high-content screening lines, strong signal:noise ratios and reproducible screening capabilities (Z' = 0.68-0.74). Finally, we demonstrate the utility of this platform for functional genomics applications by using CRISPRoff to modulate the HIF regulatory pathway, and for drug screening by using high content imaging in a bimodal design to isolate activators and inhibitors of the HIF pathway from a ~1600 natural product library.

Introduction

Cells integrate biochemical signals in a variety of ways to mediate effector function and alter gene expression. Transcription factors (TF) sit at the heart of cell signalling and gene regulatory networks, linking environment to genetic output[182,189]. TF importance is well illustrated by the consequences of their dysregulation within disease, particularly cancer where TFs drive pathogenic genetic programs[1,202,203]. As a result, there is widespread utility in methods to manipulate and track TF activity in basic biology and medical research, predominantly using TF responsive reporters. Recent examples include enhancer activity screening[204] by massively parallel reporter assays, discovery and characterisation of transcription effector domains[205,206] and CRISPR-based functional genomic screens that use reporter gene readouts to understand transcriptional regulatory networks[185,189]. Beyond the use in discovery biology TF reporters are increasingly utilised as sensors and actuators in engineered synthetic biology applications such as diagnostics and cellular therapeutics. For example, synthetic circuits that utilise either endogenous or synthetic TF responses have been exploited to engineer cellular biotherapeutics[207]. In particular, the synthetic Notch receptor (SynNotch) in which programable extracellular binding elicits synthetic TF signalling to enhance tumour-specific activation of CAR-T cells, overcome cancer immune suppression, or provide precise tumour target specificity [208-211].

Fluorescent reporter systems are now commonplace in many studies linking cell signalling to TF function and are particularly useful to study single cell features of gene expression, such as stochastics and heterogeneity[212], or situations where temporal recordings are required. In addition, pooled CRISPR/Cas9 functional genomic screens rely on the ability to select distinct cell pools from a homogenous reporting parent population. Screens to select functional gene regulatory elements or interrogate chromatin context in gene activation also require robust reporting in polyclonal pools[213]. Many of the current genetically encoded reporter approaches, by nature of their design, are constrained to particular reporting methods or applications [183,185]. For example, high content arrayed platforms are often incompatible with flow cytometry readouts and vice versa. As such there is a need to generate modular, broadly applicable platforms for robust homogenous reporting of transcription factor and molecular signalling pathways.[189].

Here we address this by generating a versatile, high-performance sensor of signal regulated TFs. We developed a reporter platform, termed the dual FLuorescent TF Activity Sensor for Histone integrated live-cell reporting (dFLASH), that enables lentiviral mediated genomic integration of a TF responsive reporter coupled with an internal control. The well-defined hypoxic and steroid receptor signalling pathways were targeted to demonstrate that the composition of the modular dFLASH cassette is critical to robust enhancer-driven reporting. dFLASH acts as a dynamic sensor of targeted endogenous pathways as well as synthetic TF chimeras in polyclonal pools by temporal high-content imaging and flow cytometry. Routine isolation of homogenously responding reporter lines enabled robust high content image-based screening (Z' = 0.68-0.74) for signal regulation of endogenous and synthetic TFs, as well as demonstrating utility for functional genomic investigations with CRISPRoff. Array-based temporal high content imaging with a hypoxia response element dFLASH successfully identified novel regulators of the hypoxic response pathway, illustrating

the suitability of dFLASH for arrayed drug screening applications. This shows the dFLASH platform allows for intricate interrogation of signalling pathways and illustrates its value for functional gene discovery, evaluation of regulatory elements or investigations into chemical manipulation of TF regulation.

Results

Design of versatile dFLASH, a dual fluorescent, live cell sensor of TF activity

To fulfil the need for a modifiable fluorescent sensor cassette that can be integrated into chromatin and enable robust live-cell sensing that is adaptable for any nominated TF, applicable to high content imaging (HCI) and selection of single responding cells from polyclonal pools via image segmentation or flow cytometry (**Figure 1c**) a lentiviral construct with enhancer regulated expression of *Tomato*, followed by independent, constitutive expression of *d2EGFP* as both selectable marker and an internal control was constructed (**Figure 1a, b**). Three nuclear localisation signals (3xNLS) integrated in each fluorescent protein ensured nuclear enrichment to enable single cell identification by nuclear segmentation, with accompanying image-based quantification of normalised reporter outputs using high content image analysis, or single-cell isolation using FACS in a signal dependent or independent manner. The enhancer insertion cassette upstream of the minimal promoter driving Tomato expression is flanked by restriction sites, enabling alternative enhancer cloning (**Figure 1a**). The sensor response to endogenous signal-regulated TF pathways was first assessed by inserting a Hypoxia Inducible Factor (HIF) enhancer. HIF-1 is the master regulator of cellular adaption to low oxygen tension and has various roles in several diseases[214-216]. To mediate its transcriptional program, the HIF-1α subunit heterodimerises with Aryl Hydrocarbon Nuclear Translocator (ARNT), forming an active HIF-1 complex. At normoxia[1], HIF-1α is post-translationally downregulated through the action of prolyl hydroxylase (PHD) enzymes and the Von Hippel Lindau (VHL) ubiquitin ligase complex[155]. Additionally, the C-terminal transactivation domain of HIF-1α undergoes asparaginyl hydroxylation mediated by Factor Inhibiting HIF (FIH), which blocks binding of transcription coactivators CBP/p300[36]. These hydroxylation processes are repressed during low oxygen conditions, enabling rapid accumulation of active HIF-1α. HIF-1α stabilisation at normoxia[1] was artificially triggered by treating cells with the hypoxia mimetic dimethyloxalylglycine (DMOG), which inhibits PHDs and FIH, thereby inducing HIF-1α stabilisation, activity and hypoxic gene expression[217]. The well characterised regulation and disease relevance of HIF-1α made it an ideal TF target for prototype sensor development.

Optimisation of dFLASH sensors

Initially, we tested FLASH constructs with repeats of hypoxia response element (HRE) containing enhancers (RCGTG)[177] from endogenous target genes (HRE-FLASH), controlling expression of either nuclear mono (m) or tandem dimer (td)Tomato and observed no DMOG induced Tomato expression in stable HEK293T cell lines (mnucTomato or tdnucTomato, **Supp Figure 1a,b**). Given the HIF response element has been validated previously[177], the response to HIF-1α was optimised by altering the reporter design, all of which utilised the smaller mnucTomato (vs tdnucTomato) to contain transgene size. We hypothesised that transgene silencing, chromosomal site-specific effects or promoter enhancer coupling/interference may result in poor signal induced reporter activity observed in initial construct designs. As such we optimised the downstream promoter, the reporter composition and incorporated a 3xNLS d2EGFP internal control from the constitutive promoter to monitor chromosomal effects and transgene silencing.

Dual FLASH (dFLASH) variants incorporated three variations of the downstream promoter (EF1a, PGK and PGK/CMV) driving *3xNLS EGFP (nucEGFP)* and 2A peptide linked hygromycin (detailed in **Supp Figure 1c**) in combination with alternate reporter transgenes that it expressed mnucTomato alone, or mnucTomato-Herpes Simplex Virus Thymidine Kinase (HSVtK)-2A-Neomycin resistance (Neo). Stable HEK293T and HepG2 HRE-dFLASH cells lines with these backbones were generated by lentiviral transduction and hygromycin selection. The reporter efficacy of dFLASH variant cell lines was subsequently monitored by high content imaging 48 hours after DMOG induction (**Supp Figure 1d, e)**. The downstream composite PGK/CMV or PGK promoters, enabled the strong DMOG induced Tomato or Tomato/GFP expression dramatically outperforming EF1a (**Figure 1b** and **Supp Figure 1d**). The composite PGK/CMV provided bright, constitutive nucEGFP expression in both HepG2 and HEK293T cells which was unchanged by DMOG, whereas nucEGFP controlled by the PGK promoter was modestly increased (~2.5 fold) by DMOG (**Supp Figure 1e**). Substitution of the mnucTomato with the longer mnucTomato-HSVtK-Neo reporter had no effect on DMOG induced reporter induction in EF1a containing HRE-dFLASH cells, still failing to induce tomato expression (**Supp Figure 1f**). CMV/PGK containing dFLASH sensors maintained DMOG induction when either the mnucTomato or the mnucTomato/HSVtK/Neo reporters were utilised (**Supp Figure 1g, h**) although mnucTomato without HSVtK and Neo produced lower absolute mnucTomato fluorescence and a smaller percentage of cells responding to DMOG, albeit with lower background. Taken together these findings indicate that certain backbone compositions prevented or enabled robust activation of the enhancer driven cassette, similar to the suppression of an upstream promoter by a downstream, contiguous promoter previously described[218,219] suggesting that the 3' EF1a promoter results in poorly functioning multi-cistronic synthetic reporter designs[220]. Consequently, the PGK/CMV backbone and the mnucTomato/HSVtK/Neo reporter from **Supp Figure 1** was chosen as the optimised reporter design (HRE-dFLASH). To confirm that the HRE element was conferring HIF specificity, a no response element dFLASH construct in HEK293T cells treated with DMOG produced no change in either mnucTomato or nucEGFP compared to vehicle-treated populations (**Supp Figure 2a**). This result, together with the robust induction in response to DMOG (**Figure 2D**, **Supp Figure 1f**, **1h**), confirms HIF enhancer driven reporter to respond robustly to induction of the HIF pathway (subsequently labelled dFLASH-HIF).

To validate the high inducibility and nucEGFP independence of dFLASH was not specific to the HIF pathway, we generated a Gal4 responsive dFLASH construct (Gal4RE-dFLASH), using Gal4 responsive enhancers[36,37]. HEK293T cells were transduced with Gal4RE-dFLASH and a dox-inducible expression system to express synthetic Gal4DBDtransactivation domain fusion protein. To evaluate Gal4RE-dFLASH we expressed Gal4DBD fused with a compact VPR (miniVPR), a strong transcriptional activator[221] (**Supp Figure 2b, 3a-c**). We observed ~25% of the polyclonal population was highly responsive to doxycycline treatment (**Supp Figure 2b**), with a ~14-fold change in Tomato expression relative to nucEGFP by HCI (**Supp Figure 3c**) demonstrating our optimised dFLASH backbone underpins a versatile reporting platform.

dFLASH senses functionally distinct TF activation pathways

Following the success in utilising dFLASH to respond to synthetic transcription factor and HIF signalling, we explored the broader applicability of this system to sense other TF activation pathways. We chose the Progesterone Receptor (PGR), a member of the 3-Ketosteriod receptor family that includes the Androgen, Glucocorticoid and Mineralocorticoid receptors, as a functionally distinct TF pathway with dose-dependent responsiveness to progestin steroids to assess the adaptability of dFLASH performance. Keto-steroid receptors act through a well-described mechanism which requires direct ligand binding to initiate homodimerization via their Zinc finger DNA binding domains, followed by binding to palindromic DNA consensus sequences. PGR is the primary target of progesterone (P4, or a structural mimic R5020) and has highly context dependent roles in reproduction depending on tissue type[222,223,224]. We inserted PGR-target gene enhancer sequences containing the canonical NR3C motif (ACANNNTGT[223]) into dFLASH, conferring specificity to the ketosteroid receptor family to generate PRE-dFLASH (**Figure 2b,** see **Methods**).

A chimeric TF system was also established with Gal4DBD fusion proteins to create a synthetic reporter to sense the enzymatic activity of oxygen sensor Factor Inhibiting HIF (FIH). This sensor system termed SynFIH for its ability to synthetically sense FIH activity contained Gal4DBD-HIFCAD fusion protein expressed in a doxycycline-dependent manner, in cells harbouring stably integrated Gal4RE-dFLASH. FIH blocks HIF transactivation through hydroxylation of a conserved asparagine in the HIF-1α C-terminal transactivation domain (HIFCAD), preventing recruitment of the CBP/p300 co-activator complex[36]. As FIH is a member of the 2-oxoglutarate dioxygenase family, like the PHDs which regulate HIF post-translationally, it is inhibited by DMOG (**Figure 2C**), allowing induction of SynFIH-dFLASH upon joint Dox and DMOG signalling (**Supp Figure 3d,3e**). dFLASH-based sensors for PGR and Gal4DBD-HIFCAD generated in the optimised backbone used for dFLASH-HIF (**Figure 2a-c**). For the PGR sensor we transduced T47D cells with PRE-dFLASH, as these have high endogenous PGR expression, while for the FIH-dependent system we generated HEK293T cells with Gal4RE-dFLASH and the GAL4DBD-HIFCAD system (dFLASH-synFIH).

Stable polyclonal cell populations were treated with their requisite chemical regulators and reporter responses analysed by either flow cytometry or temporal imaging using HCI at 2hr intervals for 38 hours (**Figure 2**). Flow cytometry revealed all three systems contain a population that strongly induced nucTomato and maintained nucEGFP (**Supp Figure 2**). In HEK293T cells, ~20% of dFLASH-synFIH and ~50% of dFLASH-HIF population induced Tomato fluorescence substantially relative to untreated controls (**Figure 2d, Figure 2f**). The ~20% reporter response to inhibition of FIH activity by DMOG (**Supp Figure 2e, Figure 2f**) is comparable with what was observed for GalRE-dFLASH response to Gal4DBD-miniVPR expression after equivalent selection (**Supp Figure 2b**). The PGR reporter in T47D cells showed ~50% of the population substantively induced Tomato (**Figure 2e, Supp Figure 2d)**. The presence of considerable responsive populations for FIH, PGR, and HIF sensors, reflected in the histograms of the EGFP positive cells (**Figure 2d-f**) indicated that isolation of a highly responsive clone or subpopulations can be readily achievable for a range of transcription response types. Importantly, the induction of dFLASH-synFIH by

Dox/DMOG co-treatment was ablated and displayed high basal Tomato levels in FIH knockout dFLASH-synFIH cells (**Supp Figure 3e**), indicating that the dFLASH-synFIH specifically senses FIH enzymatic activity.

All dFLASH systems showed consistent signal-dependent increases in reporter activity out to 38 hours by temporal HCI enabling polyclonal populations of dFLASH to track TF activity (**Figure 2g-i**). PRE-dFLASH was more rapidly responsive to R5020 ligand induction (~6 hours, **Figure 2h**) than dFLASH-HIF and dFLASH-synFIH to DMOG or Dox/DMOG treatment, respectively (~10 hours, **Figure 2g, i**). Treatment of PRE-dFLASH with estrogen (E2), which activates the closely related Estrogen Receptor facilitating binding to distinct consensus DNA sites to the PGR, or the hypoxia pathway mimetic DMOG, failed to produce a response on PRE-dFLASH (**Figure 2h**). This indicates that the PRE enhancer element is selective for the ketosteroid receptor family (also see below), and that enhancer composition facilitates pathway specificity. We also observed a signal-dependent change in EGFP expression by flow cytometry in the T47D PRE-dFLASH reporter cells (**Supp Figure 2g**) but did not observe a significant change in EGFP expression for HEK293T or HEPG2 dFLASH-HIF (**Supp Figure 1c, Supp Figure 2c**) or in HEK293T dFLASH-synFIH cells (**Supp Figure 2h**), with only a small change with Gal4RE-dFLASH with Gal4DBD-miniVPR (**Supp Figure 2b**). While this change in T47D cells was not detected in the other cellular contexts (see below), it highlights that care needs to be taken in confirming the utility of the constitutive nucEGFP as an internal control in certain scenarios.

Monoclonal dFLASH cell lines confer robust screening potential in live cells

The observed heterogenous expression of dFLASH within polyclonal cell pools is useful in many assay contexts but reduces efficiency in arrayed high content screening experiments and incompatible with pooled isolation of loss of function regulators. Therefore, monoclonal HEK293T and HepG2 dFLASH-HIF, T47D and BT474 PRE-dFLASH and HEK293T dFLASH-synFIH cell lines were derived to increase reliability of induction, as well as consistency and homogeneity of reporting (**Figure 3, Supp Figure 4**). The isolated mcdFLASH-synFIH and mcdFLASH-HIF lines also demonstrated constitutive signal insensitive nucEGFP expression (**Supp Figure 4a,b,i**). While the T47D PRE-mcdFLASH showed a small increase in nucEGFP in response to R5020, this did not preclude the use in normalisation of high content imaging experiments (see below).

No change in EGFP in BT474 PRE-mcdFLASH cells indicates that strong transactivation leading to promoter read through or cell-type specific effects may be at play. Flow cytometry of monoclonal dFLASH cell lines with their cognate ligand inducers (DMOG (**Figure 3b**), R5020 (**Figure 3f**) or Dox/DMOG (**Figure 3j**)) revealed robust homogeneous induction of mnucTomato in all cell lines. Using temporal high content imaging we also found that clonally derived lines displayed similar signal induced kinetics as the polyclonal reporters although displayed higher signal to noise and increased consistency (**Figure 3, Supp Figure 4i**). Using physiologically relevant concentrations of steroids or steroid analogs (10nM-35nM), the PRE-mcdFLASH lines selectively respond to R5020 (10nM) not E2 (35nM), DHT (10nM), Dexamethasone (Dex, 10nM) or Retinoic acid (RA, 10nM) (**Figure 3g, Supp Figure 4i**). In addition,

dose response curves of R5020 mediated Tomato induction indicate that PRE-mcdFLASH line responds to R5020 with an EC_{50} ~200pM, in agreement with orthogonal methods[225] (**Supp Figure 4g, h**). This suggests that the PRE-mcdFLASH responds sensitively and selectively to PGR selective agonist R5020, with the potential for high-content screening for modulators of *PGR* activity. As such, we term this line mcdFLASH-PGR from herein, for its specific ability to report on PGR activity at physiological steroid concentrations.

The temporal HCI of populations (**Figure 2 and Figure 3**) were imaged every 2hrs and do not inherently provide single-cell temporal dynamics of transcriptional responses. Using clonally derived mcdFLASH-PGR or mcdFLASH-HIF lines we also imaged transcriptional responses to R5020 or DMOG, respectively every 15mins (**Supp Video 1 and 2**). High temporal resolution imaging has the potential to monitor transcriptional dynamics in single cells, facilitated by the dual fluorescent nature of dFLASH. Taken together this indicates that clonal lines display improved signal to noise and assay consistency, possibly enabling high content screening experiments.

Typically, high-content screening experiments require high in-plate and across plate consistency, therefore we evaluated mcdFLASH lines (HIF-1α, PGR, FIH) across multiple plates and replicates. System robustness was quantified with the Z' metric[194] accounting for fold induction and variability between minimal and maximal dFLASH outputs. Signal induced mnucTomato fluorescence across replicates from independent plates was highly consistent (Z' 0.68-0.74) and robust (9.3-11.8 fold, **Figure 3 d, h, l**) the signal induced changes in activity for mcdFLASH-HIF and mcdFLASH-FIH were driven by increased mnucTomato, with minimal changes in nucEGFP (**Figures 3e and 3m**). Despite the changes previously observed in nucEGFP mcdFLASH-PGR in T47D cells provided equivalent reporter to the other systems, (**Figure 3h, i**) as a result, monoclonal mcdFLASH cell lines represent excellent high-throughput screening systems routinely achieving Z' scores > 0.5. Importantly, the induction of the mcdFLASH lines (HEK293T and HepG2 mcdFLASH-HIF, T47D mcdFLASH-PGR and HEK293T mcdFLASH-SynFIH) remained stable over extended passaging (months), enabling protracted large screening applications.

dFLASH-HIF CRISPR-perturbations of the HIF pathway

The robust signal window and high Z' score of mcdFLASH-HIF cell line, coupled with facile analysis by flow cytometry and HCI, indicates that the reporter system is amenable to functional genomic screening. We utilised the recently developed CRISPRoffv2.1 system[226] to stably repress expression of VHL, which mediates post-translational downregulation of the HIF-1α pathway [35,154]. We generated stable mcdFLASH-HIF cells expressing a guide targeting the VHL promoter and subsequently introduced CRISPRoffv2.1 from either a lentivirus driven by an EF1a or SFFV promoter (**Figure 4a, b**). Cells were then analysed by flow cytometry 5- or 10-days post selection to determine if measurable induction of mcdFLASH-HIF reporter was modulated by VHL knockdown under normoxic conditions (**Supp Figure 6**, **Figure 4c, 4d)**. As expected, mcdFLASH-HIF/sgVHL cells expressing CRISPRoffv2.1 from either promoter induced the mcdFLASH-HIF reporter in ~35% by 5 days and the majority of cells (~60%) by 10 days as compared to parental cells. Demonstration that mcdFLASH-HIF is responsive to CRISPRi/off perturbations of key regulators of the

HIF pathway illustrates the potential for the dFLASH platform to provide a readout for CRISPR screens at-scale in a larger format including genome-wide screens.

dFLASH facilitates bimodal screening for small molecule discovery

Manipulation of the HIF pathway is an attractive target in several disease states, such as in chronic anaemia[86] and ischemic disease[91] where its promotion of cell adaption and survival during limiting oxygen is desired. Conversely, within certain cancer subtypes[20,227] HIF signalling is detrimental and promotes tumorigenesis. Therapeutic agents for activation of HIF-α signalling through targeting HIF-α regulators were initially discovered using *in vitro* assays. However, clinically effective inhibitors of HIF-1α signalling are yet to be discovered[228]. The biological roles for HIF-1α and closely related isoform HIF-2α, which share the same canonical control pathway, can be disparate or opposing in different disease contexts requiring isoform selectivity for therapeutic intervention[33]. To validate that HIF-1α is the sole isoform regulating mcdFLASH-HIF in HEK293T cells[229] tandem HA-3xFLAG epitope tags were knocked in to the endogenous HIF-1α and HIF-2α C-termini allowing directly comparison by immunoblot[230] and confirmed HIF-1α is predominant isoform (**Supp Figure 5a**). Furthermore, there was no change in DMOG induced mnucTomato expression in HEK293T mcdFLASH-HIF cells when co-treated for up to 72 hours with the selective HIF2a inhibitor PT-2385 (**Supp Figure 5b)**, consistent with the minimal detection of HIF-2α via immunoblot. This confirmed that our HEK293T dFLASH-HIF cell line specifically reports on HIF-1 activity and not HIF-2, indicating that it may be useful for identification of drugs targeting the HIF-1α pathway.

dFLASH-HIF facilitates multiple measurements across different treatment regimens and time points, enabling capture of periodic potentiated and attenuated HIF signalling during a single experiment. Having validated the robust, consistent nature of mcdFLASH-HIF, we exploited its temporal responsiveness for small molecule discovery of activators or inhibitors of HIF-1α signalling in a single, bimodal screening protocol. To test this bimodal design, we utilised a natural product library of 1595 compounds containing structures that were unlikely to have been screened against HIF-1α prior. We first evaluated library compounds for ability to activate the reporter after treatment for 36 hours (**Figure 5a**) or 24 hours (**Figure 5d**). The selection of two different screening time points was to minimise any potential toxic effects of compounds at the later time points. Consistency of compound activity between the two screens was assessed by Pearson correlations (**Supp Figure 7i**, $R = 0.79$, $p < 2.2x10^{-16}$). Lead compounds were identified by their ability to increase mnucTomato/nucEGFP (**Figure 5b, c**) and mnucTomato MFI more than 2SD compared with vehicle controls, with less than 2SD decrease in nucEGFP (21/1595 compounds (1.3%) each expt; **Supp Figure 7a, e**) and an FDR adjusted P score <0.01 across both screens (3/1595 (0.18%) compounds; **Supp Figure 7b, f**). After imaging of reporter fluorescence to determine these compound's ability to activate HIF-1α we then treated the cells with 1mM DMOG and imaged after a further 36-hour (**Figure 5c**) and 24-hour (**Figure 5f**) period. Again, consistency of compound activity was assessed by Person correlation (**Supp Figure 7j, F,** $R = 0.62$, $p < 2.2x10^{-16}$). Lead compounds were defined as those exhibiting a decrease in mnucTomato MFI >2SD from DMOG-treated controls in each screen without changing nucEGFP >2SD relative to the DMOG-treated controls (26/1595 compounds (1.3%) (36hr treatment) and

13/1595 compounds (<1%) (24hr treatment); **Supp Figure 7c, g**), and decrease in mnucTomato/nucEGFP >2SD with an FDR adjusted P score < 0.01 (3/1595 compounds (0.18%) across both expt; **Supp Figure 7d, h**).

dFLASH identified novel and known compounds that alter HIF TF activity.
We confirmed 11 inhibitors and 18 activators of HIF-1α activity identified from the pilot screen at three concentrations (**Supp Figure 8a**, **9a**) identifying RQ500235 and RQ200674 (**Figure 6a, d**) as previously unreported HIF-1α inhibiting or stabilising compounds, respectively. RQ200674 increased reporter activity 2-fold in repeated assays (**Figure 6d**) and stabilised endogenously tagged HIF-1α at normoxia in HEK293T cells (**Supp Figure 8b**). Mechanistically, RQ200674 had weak iron chelation activity in an *in vitro* chelation assay (**Figure 6e**), suggesting it intersects with the HIF-1α pathway by sequestering iron similar to other reported HIF stabilisers. In the inhibitor compound dataset, Celastarol and Flavokawain B downregulated the reporter at several concentrations (**Supp Figure 9b, c**). Celastarol is a previously reported HIF-1α inhibitor[231-233] and Flavokawain B is a member of the chalcone family which has previously exhibited anti-HIF-1α activity[234]. RQ500235 was identified as a HIF-1 inhibitor by mcdFLASH-HIF screening. Dose dependent inhibition of mcdFLASH-HIF (**Figure 6a**) correlated with a dose-dependent decrease in protein expression by immunoblot (**Figure 6C**). We observed significant (p=0.0139) downregulation of HIF-1α transcript levels (**Figure 6D**) and were unable to rescue HIF-1α protein loss with proteasomal inhibition (**Supp Figure 9d**), indicating RQ500235 was decreasing HIF-1α at the RNA level. More broadly however, the identification of these compounds by mcdFLASH-HIF in the bimodal set up demonstrates successful application of the dFLASH platform to small molecule discovery efforts for both gain and loss of TF function.

Discussion

We designed and optimised dFLASH to offer a versatile, robust live-cell reporting platform that is applicable across TF families and allows for facile high-throughput applications. We validated dFLASH against three independent signal-responsive TFs, two with endogenous signalling pathways (dFLASH-PRE for Progesterone receptors; dFLASH-HRE for hypoxia induced transcription factors) and a synthetic system for a hybrid protein transcriptional regulator (dFLASH- Gal4RE). Each dFLASH construct produced robustly detected reporter activity by temporal high-content imaging and FACS after signal stimulation for its responsive TF (**Figure 2,3**). The use of previously validated enhancer elements for HIF[177] and synthetic Gal4 DNA binding domains[36,37] demonstrated that dFLASH can be adapted toward both endogenous and synthetic pathways displaying highly agonist/activator-specific responses, indicating utility in dissecting and targeting distinct molecular pathways. mcdFLASH lines distinct pathways produced highly consistent (Z' = 0.68-0.74) signal induced Tomato induction measured by high content imaging suggesting dFLASH is ideally suited to arrayed high-throughput screening (**Figure 3**). In addition, mcdFLASH lines also displayed homogenous signal induced reporter induction by flow cytometry indicating that pooled high content screening would also be possible.

Indeed, reporter systems like dFLASH have been increasingly applied to functional genomic screens which target specific transcriptional pathways[185,235-237]. CRISPRoff mediated downregulation of the core HIF protein regulator, VHL produced distinct tomato expressing cell pools (**Figure 4**), demonstrating genetic perturbations of endogenous TF signalling pathways. The robust induction of the dFLASH-HIF reporter upon VHL knockdown in the majority of cells indicates that whole genome screening would also be successful[183,185,235,238].

Using the HIF-1α specific reporter line, mcdFLASH-HIF, the application of high-content screening was exemplified. This approach was successful in discovering a novel activator and novel inhibitor of the HIF pathway, as well as previously identified inhibitory compounds. This ratified dFLASH as a reporter platform for arrayed-based screening and demonstrates the utility of the linked nucEGFP control for rapid hit bracketing. The novel inhibitor RQ500235 was shown to downregulate HIF-1α transcript levels, like another HIF-1α inhibitor PX-478[166,239]. As PX-478 has demonstrated anti-cancer activity in several cell lines [165,166] and preserved β-cell function in diabetic models[239], a future similar role may exist for an optimised analogue of RQ500235.

The dFLASH system is characterised by some distinct advantages which may enable more precise dissection of molecular pathways. The ability to control for cell-to-cell fluctuations and to decouple generalised or off-target effects on reporter function may aid the precision necessary for large drug library or genome-wide screening applications[176]. In addition, dFLASH, unlike many other high-throughput platforms can be used to screen genetic or drug perturbations of temporal transcriptional dynamics or as used here at multiple time points. Also, the results indicate that dFLASH is ideally suited to array-based functional genomics approaches[240] allowing for multiplexing with other phenotypic or molecular outputs[241,242 189,243].

The dFLASH approach has some limitations. The fluorescent nature of dFLASH limits the chemical space by which it can screen due to interference from auto-fluorescent compounds. In addition, we acknowledge that fluorescent proteins require O_2 for their activity and this limits the use of mnucTomato as a readout of hypoxia. Also, while the backbone design has been optimised for a robust activation of a variety of transcription response pathways, the mechanistic underpinning of this is unclear and could be further improved, providing insights into the sequence and architectural determinants of enhancer activation in chromatin. In addition to the strong effect of the dFLASH downstream promoter on upstream enhancer activity it is clear that either the distance between contiguous promoter/enhancer or the sequence composition of the linker has a functional consequence on enhancer induction.

The incorporation of robust native circuits such as those described here (Hypoxia or Progesterone) has the potential to allow the manipulation or integration of these pathways into synthetic biology circuitry for biotherapeutics. In these cases, it is critical that robust signal to noise is achieved for these circuits to effectively function in biological systems. Further, the use of a synthetic approach to 'sense' FIH enzymatic activity through the HIF-CAD:P300/CBP interaction opens up the possibility that other enzymatic pathways that lack effective *in vivo* activity assay may also be adapted. We also envisage that dFLASH could be adapted to 2-hybrid based screens as a complement to other protein-protein interaction approaches.

The ability to temporally track TF regulated reporters in populations and at the single-cell level enable dFLASH to be used to understand dynamics of transcriptional responses as has been used to dissect mechanisms of synthetic transcriptional repression[205,206] or understand notch ligand induced synthetic transcriptional dynamics[244]. For instance, synthetic reporter circuits have been used to delineate how diverse notch ligands induce different signalling dynamics Nandagopal, et al. [244]. The large dynamic range of the dFLASH-PGR and HIF reporter lines in conjunction with the high proportion of cells induced in polyclonal pools (**Figure 2**) also suggests dFLASH as a candidate system for forward activity-based enhancer screening. These approaches have been applied to dissect enhancer activity or disease variants with other similar systems such as lentiviral-compatible Massively Parallel Reporter Assays (LentiMPRA)[245,246]. However, the use of the internal control normalisation provided by dFLASH may be useful in separating chromosomal from enhancer driven effects in forward enhancer screens.

Given dFLASH has robust activity in both pooled and arrayed formats, it offers a flexible platform for investigations. dFLASH can be used to sense endogenous and synthetic transcription factor activity and represents a versatile, stable, live-cell reporter system of a broad range of applications.

Main Figures

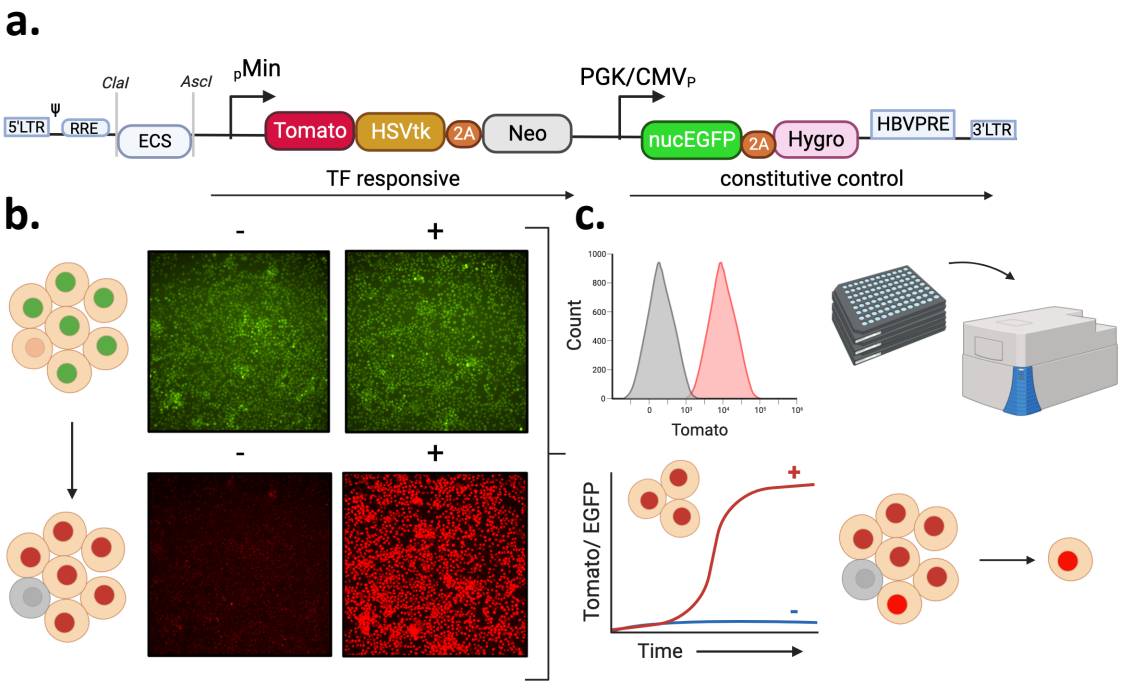

Figure 1. Summary of dFLASH LV-REPORT construction, utility, and validation (**a**) The dFLASH system utilises the lentiviral LV-REPORT construct, consisting of a cis-element multiple cloning site for enhancer insertion, followed by a minimal promoter that drives a transcription factor (TF) dependent cassette that encodes three separate expression markers; a nuclear Tomato fluorophore with a 3x C-terminal nuclear localisation signal (NLS), Herpes Simplex Virus Thymidine Kinase (HSVtK) for negative selection and Neomycin resistance (Neo) for positive selection separated by a 2A self-cleaving peptide (2A). This is followed by a downstream promoter that drives an independent cassette encoding EGFP with a 3x N-terminal NLS, and a Hygromycin resistance selection marker separated by a 2A peptide. (**b**) This design allows for initial identification of the EGFP fluorophore in nuclei, independent of signal. Expression of the Tomato fluorophore is highly upregulated in a signal-dependent manner. Images shown are monoclonal HEK293T dFLASH-HIF cells. Populations were treated for 48 hours ±DMOG induction of HIF-1α and imaged by HCI. (**c**) This system can be adapted to a range of different applications. This includes (clockwise) flow cytometry, arrayed screening in a high throughput setting with high content imaging, isolation of highly responsive clones or single cells from a heterogenous population or temporal imaging of pooled or individual cells over time.

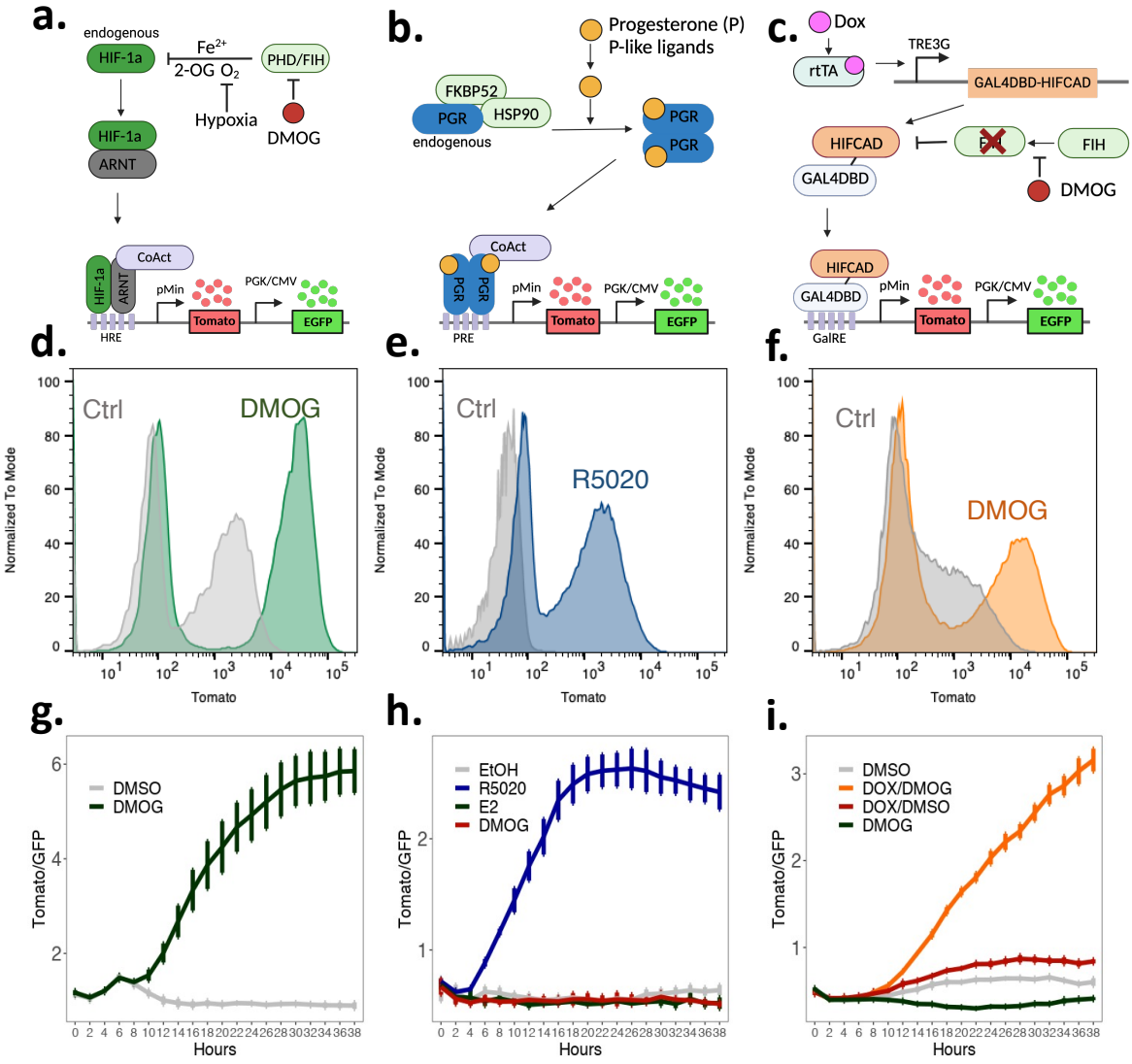

Figure 2. dFLASH provides sensitive readouts to three distinct TF pathways
(**a-c**) Three distinct enhancer elements enabling targeting of three different signalling aspects. (**a**) Hypoxic response elements (HRE) provide a read out for HIF-1α activation; (**b**) Progesterone response elements (PRE) derived from progesterone receptor target genes facilitate reporting of progestin signaling; (**c**) Gal4 response elements (GalRE) enable targeting of synthetic transcription factors to dFLASH such as a GAL4DBD-HIFCAD fusion protein that provides a FIH-dependent reporter response. (**d-f**) Flow cytometry histograms showing Tomato expression following 48 hr treatments of the indicated dFLASH polyclonal reporter cells (**d**) HEK293T; 1mM DMOG or 0.1% DMSO (Ctrl), (**e**) T47D; 100nM R5020 or Ethanol (Ctrl), (**f**) HEK293T; 1μg/mL Doxycycline (Dox) and 1mM DMOG or Dox and 0.1% DMSO (Ctrl). (**g-i**) Reporter populations as in **d-f** were temporally imaged for 38 hours using HCI directly after treatment with (**g**) 0.5mM DMOG or 0.1% DMSO, (4 replicates) (**h**) 100nM R5020, 35nM E2, 0.5mM DMOG or 0.1% Ethanol (EtOH) (4 replicates), (**i**) 0.1% DMSO, 1mM DMOG, 100ng/mL Dox and 0.1% DMSO, or 100ng/mL Dox and 1mM DMOG (4 replicates).

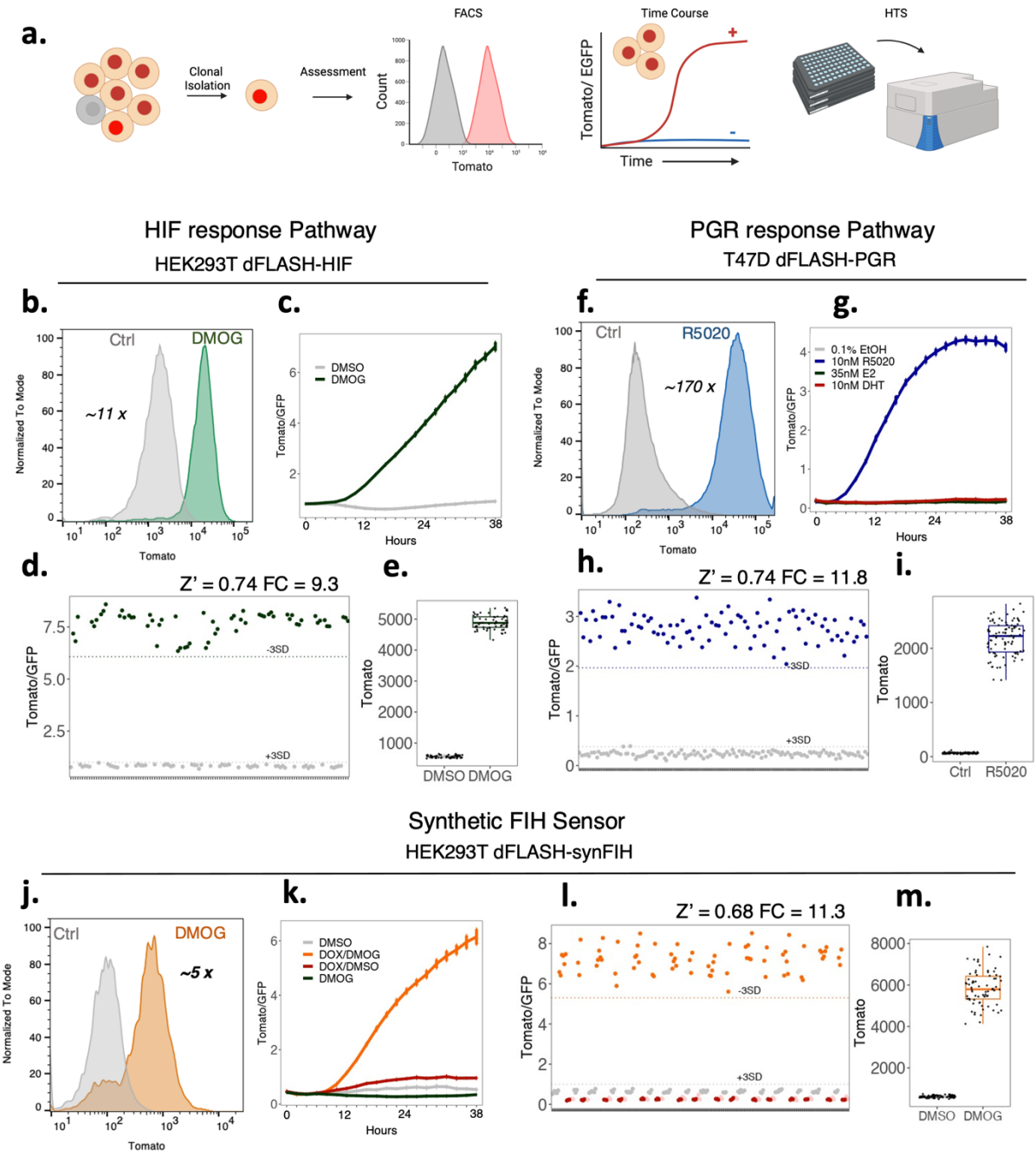
a.
Clonal Isolation
Assessment
FACS
Count
Tomato
Time Course
Tomato/ EGFP
Time
HTS
HIF response Pathway
HEK293T dFLASH-HIF
PGR response Pathway
T47D dFLASH-PGR
b.
Ctrl
DMOG
~11 x
Normalized To Mode
Tomato
c.
DMSO
DMOG
Tomato/GFP
Hours
f.
Ctrl
R5020
~170 x
g.
0.1% EtOH
10nM R5020
35nM E2
10nM DHT
d.
Z' = 0.74 FC = 9.3
-3SD
+3SD
e.
DMSO DMOG
h.
Z' = 0.74 FC = 11.8
i.
Ctrl R5020
Synthetic FIH Sensor
HEK293T dFLASH-synFIH
j.
~5 x
k.
DMSO
DOX/DMOG
DOX/DMSO
DMOG
l.
Z' = 0.68 FC = 11.3
m.
DMSO DMOG

Figure 3. Derivation of robust, screen-ready dFLASH clonal lines
(**a**) Schematic for derivation and assessment of robustness for clonal lines of (**b-e**) HEK239T dFLASH-HIF (mcdFLASH-HIF), (**f-i**) T47D dFLASH-PGR (mcdFLASH-PGR) and (**j- m**) HEK293T dFLASH-synFIH (mcdFLASH-synFIH) were analysed by flow cytometry, temporal HCI over 38 hours and for inter-plate robustness by mock multi-plate high throughput screening with HCI. (**b-e**) mcdFLASH-HIF was (**b**) treated with DMOG for 48 hours and assessed for Tomato induction by flow cytometry relative to vehicle controls with fold change between populations displayed and (**c**) treated with vehicle or 0.5mM DMOG and imaged every 2 hours for 38 hours by HCI (mean ±sem, 8 replicates). (**d-e**) mcdFLASH-HIF was treated for 48 hours with 1mM DMOG or vehicle (6 replicates/plate, n = 10 plates) by HCI in a high throughput screening setting (HTS-HCI) for (**d**) normalised dFLASH expression and (**e**) Tomato MFI alone. (**f – i**) T47D mcdFLASH-PGR was (**f**) assessed after 48 hours of treatment with 100nM R5020 by flow cytometry for Tomato induction and (**g**) treated with 10nM R5020, 35nM E2, 10nM DHT and vehicle then imaged every 2 hours for 38 hours by temporal HCI for normalised dFLASH expression (mean ±sem, 8 replicates). (**h-i)** T47D mcdFLASH-PGR was assessed by HTS-HCI at 48 hours (24 replicates/plate, n = 5 plates) for (**h**) dFLASH normalised expression and (**i**) Tomato MFI alone. (**j**) HEK293T dFLASH-synFIH was assessed, with 200ng/mL and or Dox and 1mM DMOG by flow cytometry for dFLASH Tomato induction (**k**) mcdFLASH-synFIH was treated with 100ng/mL Dox, 1mM DMOG and relevant vehicle controls and assessed for reporter induction by temporal HCI (mean ±sem 4 replicates). (**l-m**) mcdFLASH-synFIH cells were treated with 200ng/mL Dox (grey), 1mM DMOG (red), vehicle (pink) or Dox and DMOG (orange) and assessed by HTS-HCI after 48 hours (24 replicates/plate, n = 3 plates) for (**l**) normalised dFLASH expression or (**m**) Tomato MFI induction between Dox and Dox and DMOG treated populations. Dashed lines represent 3SD from relevant vehicle (+3SD) or requisite ligand treated population (-3SD). Fold change for flow cytometry and HTS-HCI (FC) is displayed. Z' was calculated from all analysed plates by HTS-HCI. Z' for all plates analysed was > 0.5.

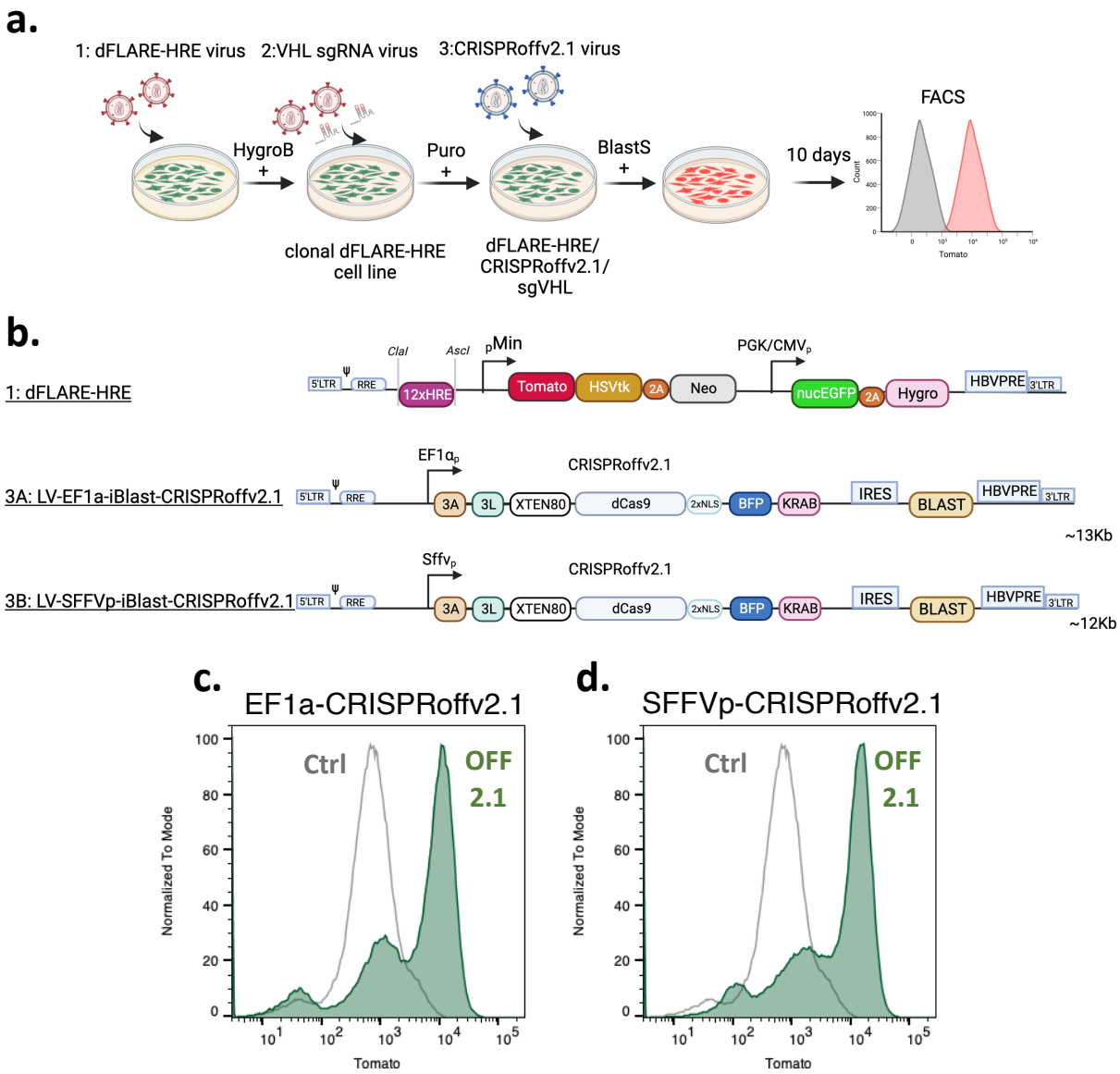

Figure 4. Near homogenous activation of mcdFLASH-HIF by CRISPRoff knockdown of VHL.

(**a**) Clonal (1) mcdFLASH-HIF lines derived post-hygromycin (HygroB) selection were transduced first with the (2) sgRNA vector targeting *VHL* transcriptional start site, followed by puromycin selection (Puro). This pool was subsequently transduced by the (3) CRISPRoffv2.1 virus and selected with blasticidin (BlastS) prior to flow cytometry (on day 5 and 10 post Blasticidin selection). (**b**) The (1) dFLASH vector with the HRE enhancer was transduced as were 2 variants of the CRISPRoffv2.1 vector with either (**3A**) EF1α promoter or (**3B**) SFFV promoter driving the dCas9 expression cassette. (**c, d**) Flow cytometry for dFLASH-HIF induction in response to the CRISPRoffv2.1 VHL knockdown relative to parental line (Ctrl) with (**c**) EF1a or (**d**) SFFV expression constructs after 10 days of selection.

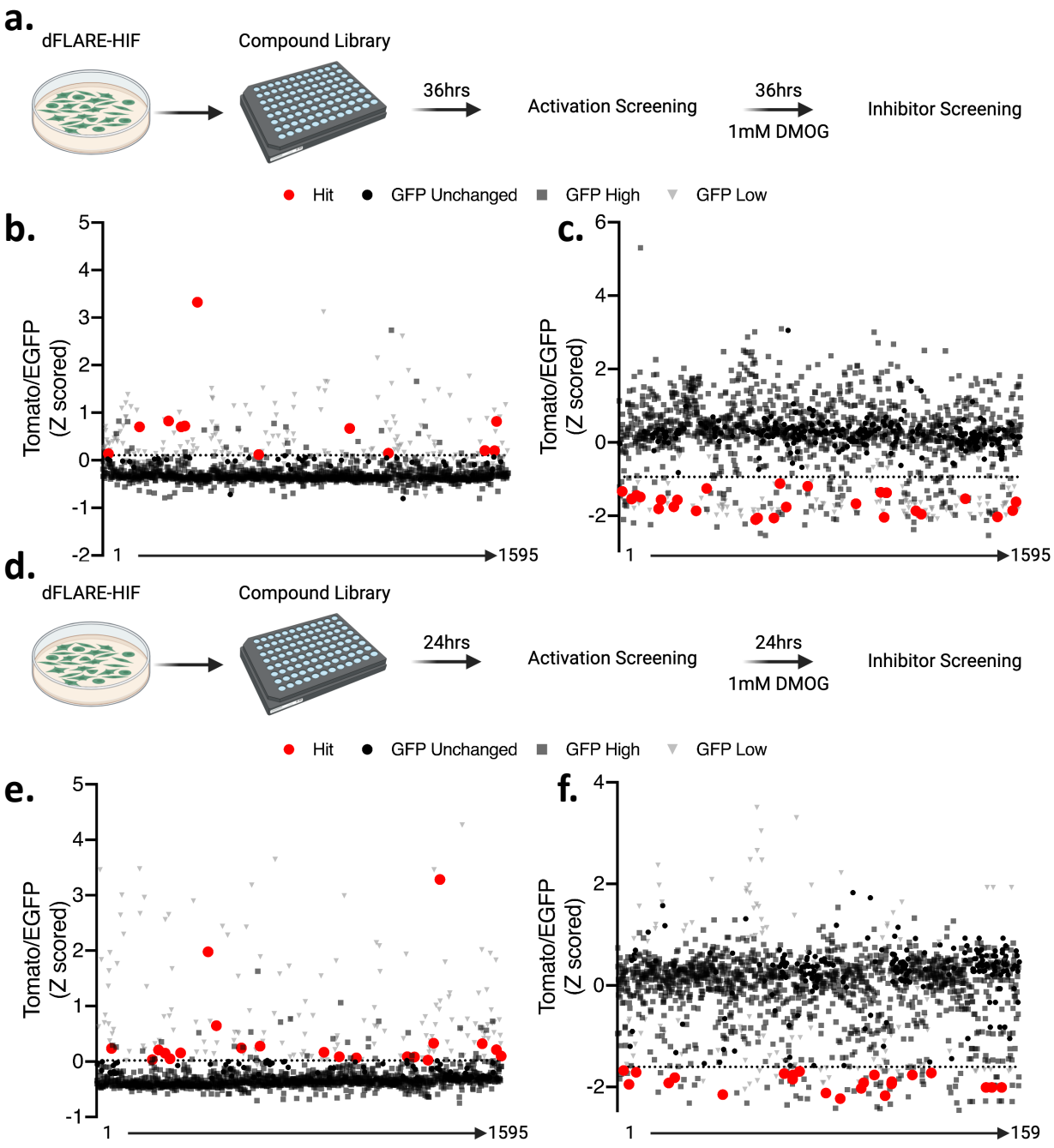
a.
dFLARE-HIF
Compound Library
36hrs
Activation Screening
36hrs
1mM DMOG
Inhibitor Screening
Hit
GFP Unchanged
GFP High
GFP Low
b.
c.
Tomato/EGFP (Z scored)
1
1595
d.
dFLARE-HIF
Compound Library
24hrs
Activation Screening
24hrs
1mM DMOG
Inhibitor Screening
Hit
GFP Unchanged
GFP High
GFP Low
e.
f.
Tomato/EGFP (Z scored)
1
1595
159

Figure 5. Bimodal small molecule screening of the HIF signalling pathway with dFLASH-HIF identifies positive and negative regulators

(**a**) HEK293T mcdFLASH-HIF cells were treated with a 1595 compound library and incubated for 36 hours prior to (**b**) the first round of HCI normalised dFLASH activity. Compounds that changed EGFP >±2SD are shown in grey and excluded as hits. Compounds that increase Tomato/EGFP >2SD from the vehicle controls (dashed line) are highlighted in red. After the activation screen, the compound wells were then treated with 1mM DMOG for 36 hours prior to the second round of HCI. Compounds that decreased dFLASH activity greater than 2SD from DMOG controls (dashed line) are shown in red. Compounds that changed EGFP >±2SD are shown in grey and excluded as hits. Normalised dFLASH output (Z scoring) for all analysed wells. (**d-f**) The screening protocol of (**a-c**) was repeated using 24 hr points for HCI.

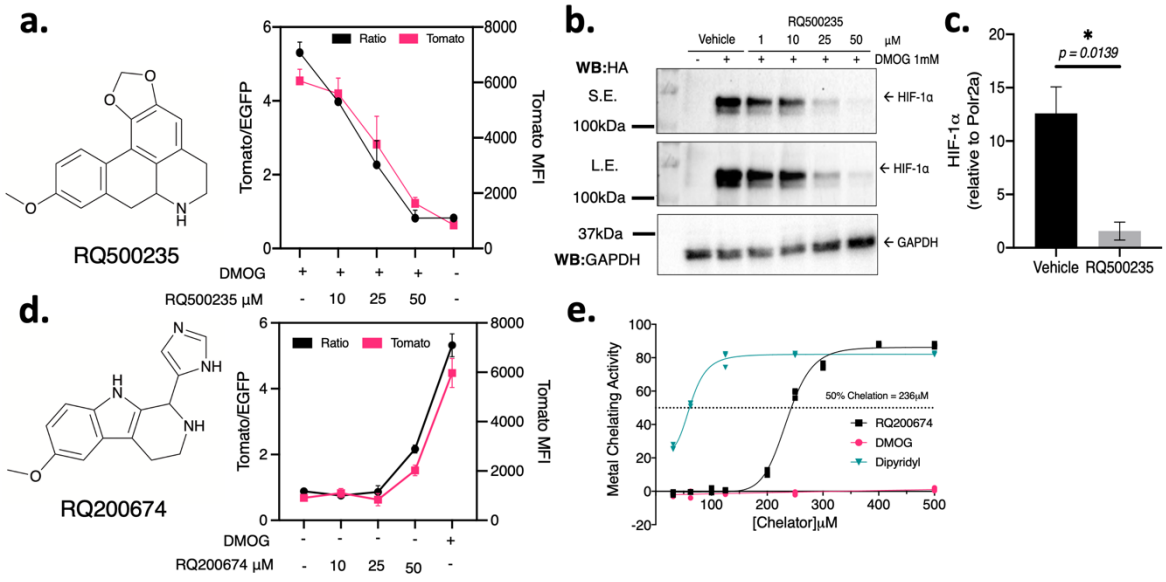

Figure 6. **Investigating mechanisms for HIF-1α regulation by hit dFLASH-HIF inhibitor RQ500235 and hit activator RQ200674**

(**a, b**) Inhibitor RQ500235 identified from the bimodal screen (**a**) represses DMOG induced Tomato in dFLASH-HIF cells in a dose dependent manner (n=2, Tom MFI, red; Tom normalised to EGFP, black) and (**b**) decreases expression of HIF-1α protein as assessed by immunoblot of whole cell extracts from endogenous HA-Flag tagged HIF-1α in HEK293T cells. S.E.= short exposure; L.E.= long exposure. (**c**) RT-PCR shows HIF-1α transcript is significantly decreased in HEK293T cells treated for 6 hours with RQ500235 (n =3, *p=0.0139). (**d**) Activator RQ200674 identified from the bimodal screen recapitulated activation of dFLASH-HIF at 50µM in HEK293T cells (n = 2). (**e**) *in vitro* iron chelation assay of RQ200674 displays weak chelating activity at 236µM from line of best fit (n = 3) compared to positive control iron chelator and HIF-1α activator, dipyridyl.

Supplementary Figures

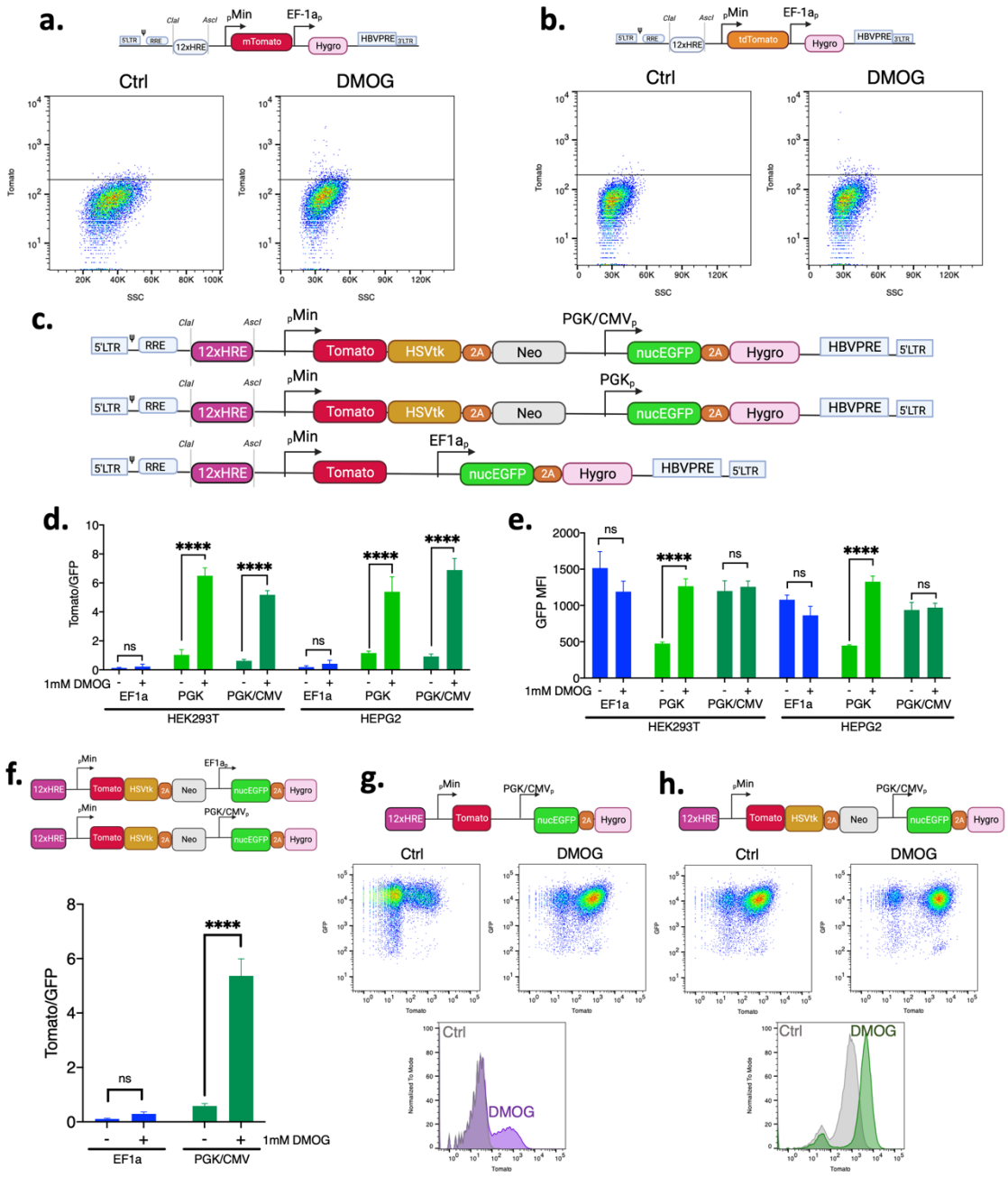

Supplementary Figure 1. Optimised dFLASH design produces a robust HIF sensor.

(**a-b**) HEK293T cells with HRE-dFLASH constructs without EGFP and (**a**) expressing monomeric Tomato or (**b**) dimeric Tomato were treated -/+ 1mM DMOG for 48 hours and quantified by FACS. Tomato MFI >200AU was used to compare induction (black line). (**c-e**) HEK293T and HEPG2 cells were transduced with HRE-dFLASH reporters that had different downstream promoters controlling EGFP or Tomato cassette composition and treated for 48 hours -/+ 1mM DMOG prior to HCI. The (**d**) Tomato/EGFP MFI ratio and (**e**) EGFP MFI for each backbone variant was then compared (Data from three independent biological replicates). (**f**) HEK293T cells transduced with reporter constructs containing the downstream PGK/CMV or EF1a

promoters were compared for DMOG induction by HCI after 48 hours of -/+ 1mM DMOG treatment (Data from three independent biological replicates). Significance was assessed with a Two-Way ANOVA (**** $p < 0.001$, ns = not significant). (**g**,**h**) HEK293T cells with the HRE enhancer and different dFLASH backbone compositions of (**g**) PGK/CMV dFLASH with Tomato alone as the upstream cassette or (**h**) dFLASH-HIF were treated for 48-hours -/+ 1mM DMOG prior to EGFP analysis and Tomato induction by FACS.

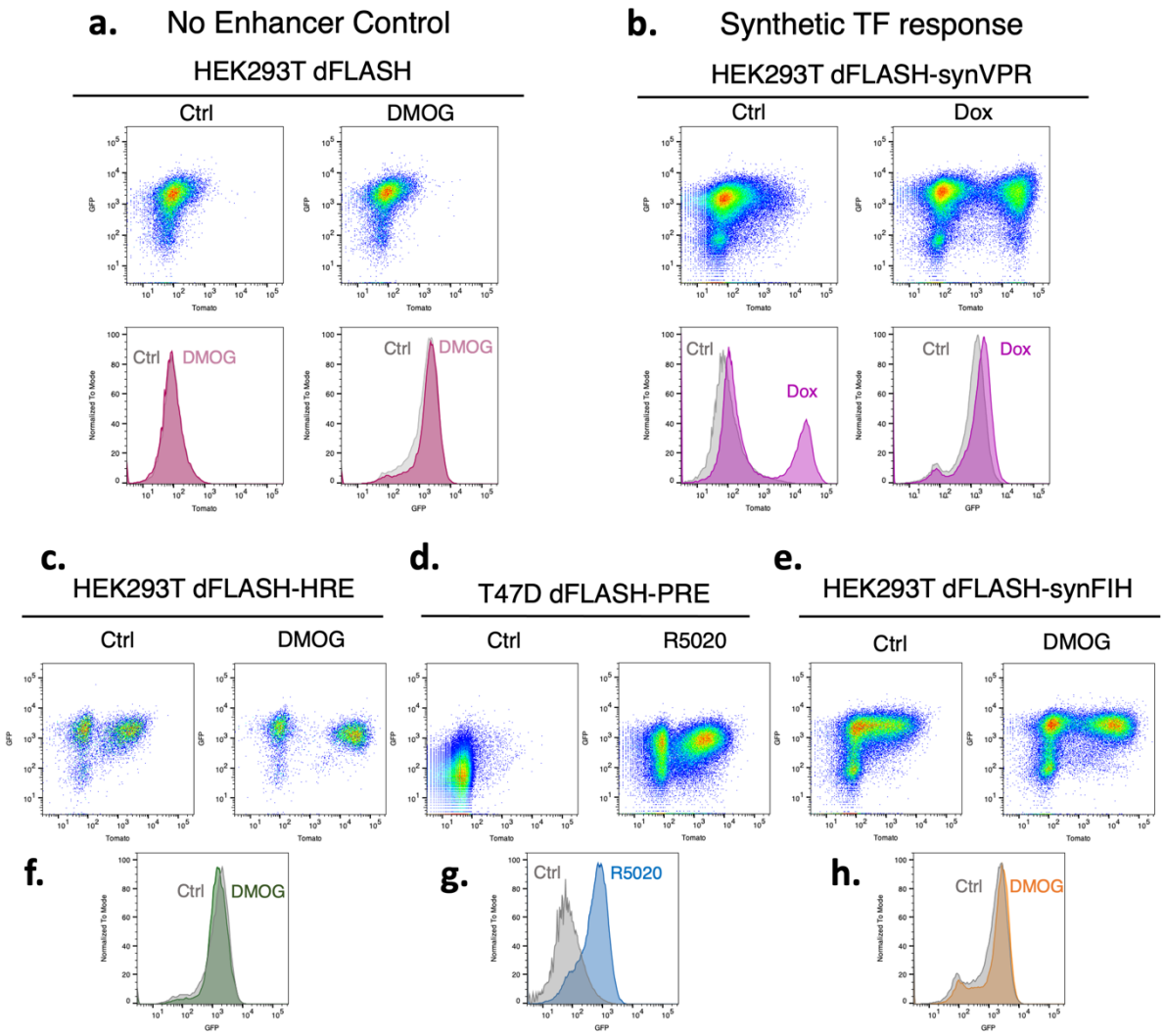

Supplementary Figure 2. dFLASH provides a TF-responsive, versatile reporter platform in heterogenous cell pools.

(**a-b**) HEK293T cells were transduced with (**a**) dFLASH with no enhancer and treated with 1mM DMOG or 0.1% DMSO (Ctrl) or (**b**) GalRE-dFLASH and Gal4DBD-miniVPR and treated with H_2O (Ctrl) or 1μg/mL Dox for 48 hours prior to FACS. Dot plots of populations' Tomato and EGFP intensity with or without activating chemicals and histograms comparing EGFP and Tomato MFI between control and treated populations are shown. (**c-h**) Dot plots and EGFP histograms for control and chemical treated (**c, f**) dFLASH-HIF, (**d, g**) dFLASH-PR polyclonal pools (*to accompany* ***Figure 2a-c***) and (**e, h**) dFLASH-synFIH.

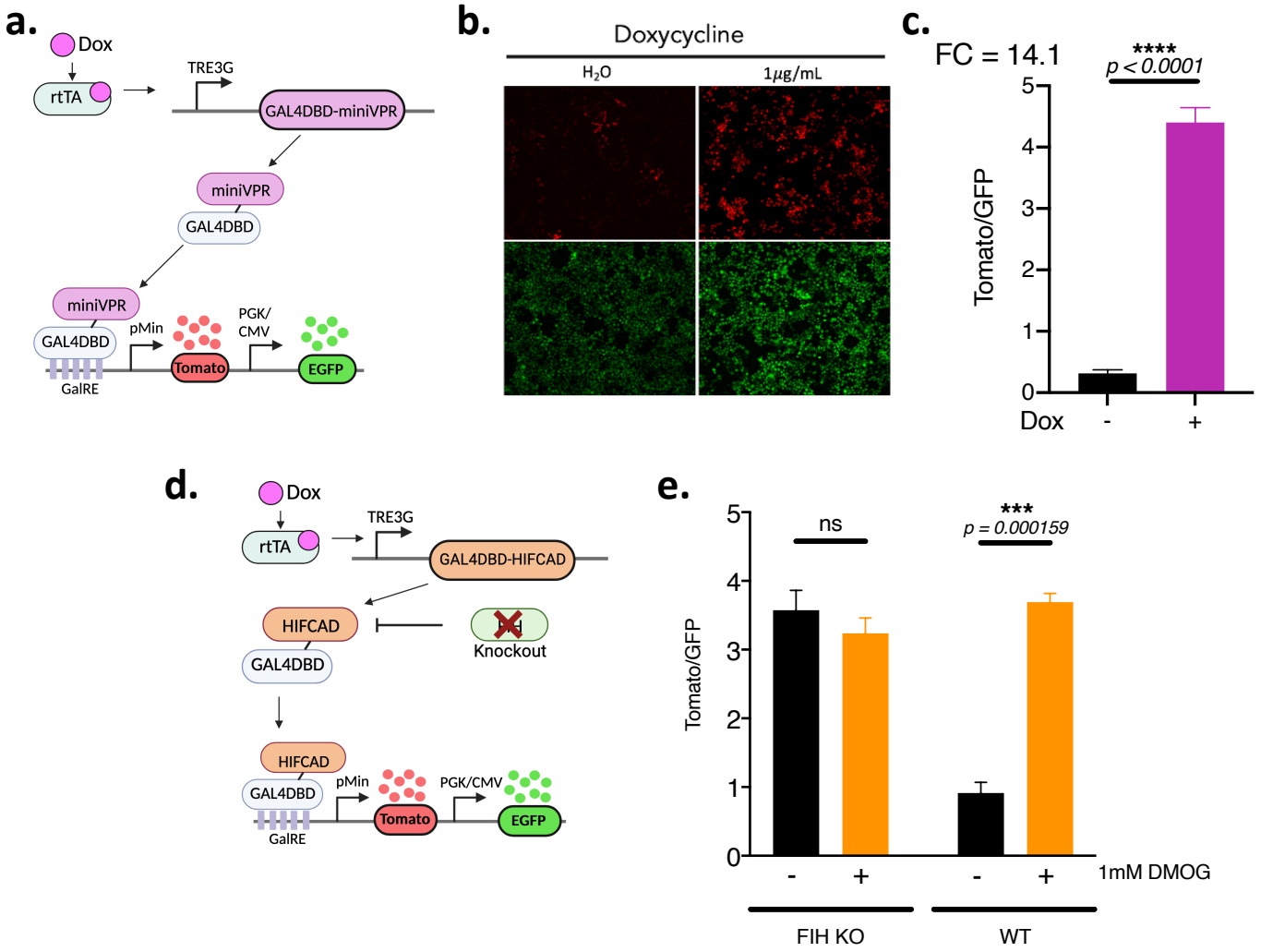

Supplementary Figure 3. Synthetic transcription factors drive a strong response from the GalRE-dFLASH reporter and can respond to endogenous signaling pathways.

(**a**) GAL4DBD-miniVPR is expressed from an independent dox-inducible vector that subsequently binds to GalRE-dFLASH. (**b**,**c**) HEK293T GalRE-dFLASH cells were transduced with GAL4DBD-miniVPR expression construct and were treated -/+ doxycycline for 48 hours prior to HCl for (**b**) Tomato expression (top panels) and EGFP expression (bottom panels). (**c**) Normalised fluorescence intensity was also quantified for treated populations (n=3, mean ±sem). FC is Fold change between the populations. (**d, e**) To confirm HEK293T dFLASH-synFIH system was FIH dependent, (**d**) GalRE-dFLASH and GAL4DBD-HIFCAD vectors were transduced into HEK293T cells with FIH knocked out. (**e**) FIH KO cells were compared with wildtype HEK293T dFLASH-synFIH (WT) in a 200ng/mL dox background for DMOG-dependent reporter induction by HCl (n=3). (**c, e**) Significance was assessed by t-test with Welch's correction (ns = not significant, *** p <0.001, ****p <0.0001).

HIF response Pathway

HEK293T dFLASH-HRE

HepG2 dFLASH-HRE

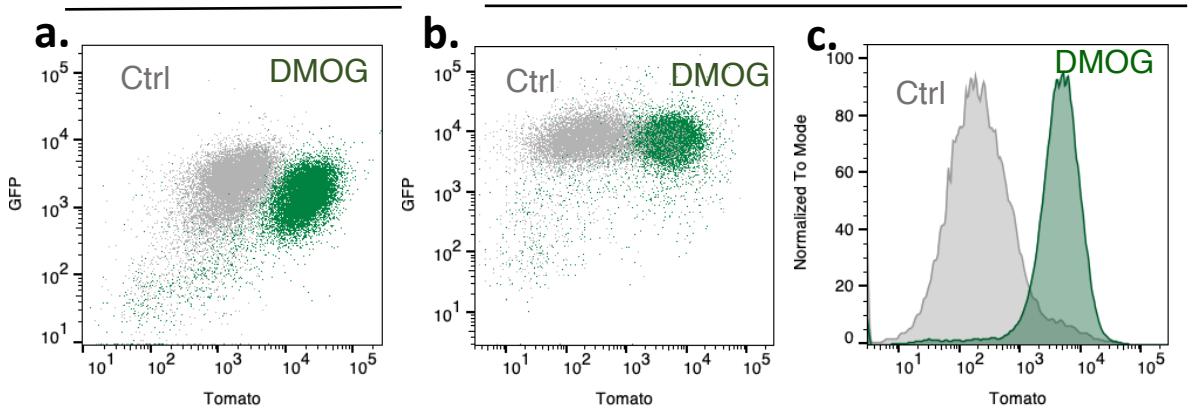

PGR response Pathway

T47D dFLASH-PRE

BT474 dFLASH-PRE

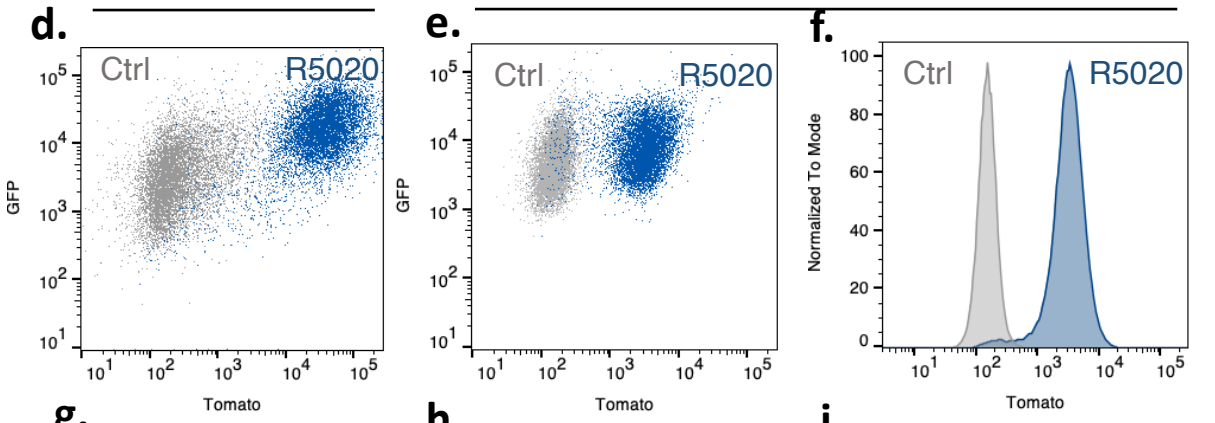

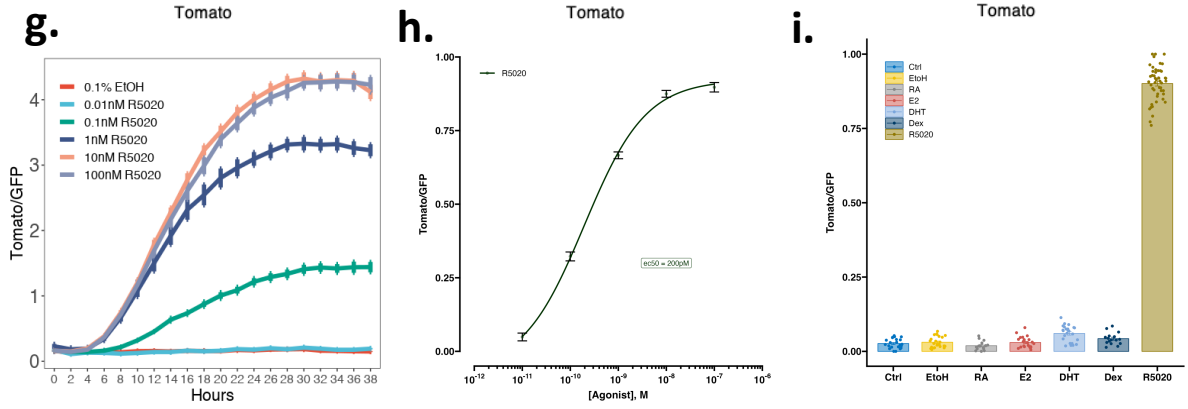

Synthetic FIH Sensor

HEK293T dFLASH-synFIH

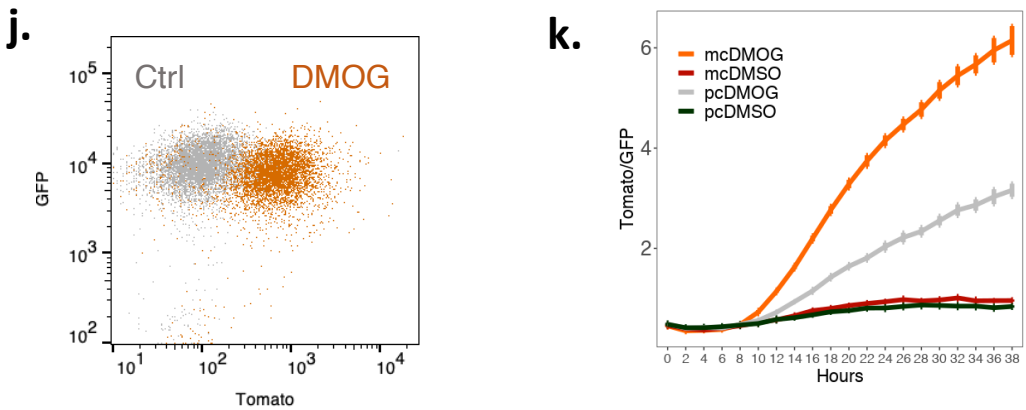

Supplementary Figure 4. Clonal dFLASH cell lines enable improved reporting across different cell types.

(**a-c**) Flow cytometry of clonal dFLASH-HIF cell lines for (**a**) HEK293T (*see also* ***Figure 3b***) and (**b,c**) HepG2 cells after 48 hours -/+ 0.5mM DMOG. (**d-h**) dFLASH-PGR functionality was assessed by flow cytometry in (**d**)T47D (*see also* ***Figure 3f***) and (**e,f**) BT474 cells after 48 hours -/+ 100nM R5020. (**g,h**) T47D dFLASH-PGR cells were treated with increasing concentrations of R5020 (0.01-100nM, 8 replicates per group) and (**g**) imaged over 38 hours with temporal HCI or (**h**) imaged at 48 hours to determine sensitivity to R5020. (**i**) Comparison of inductions of the T47D mcdFLASH-PGR line to different steroids (10nM R5020, 35nM E2, 10nM DHT, 10nM Dex, 10nM RA) by HCI after 48 hours of treatment. (**g**) and (**i**) are the mean±sem of normalised Tomato/GFP (within each expt) from n = 3 independent experiments (24 replicates), except Dex and RA (n=2 (16 replicates)). (**j, k**) Clonally derived HEK293T dFLASH-synFIH cells were (**j**) analysed by flow cytometry after 48 hours of 200ng/mL Dox -/+ 1mM DMOG (*see also* ***Figure 3k***) with (**k**) showing temporal HCI comparisons between monoclonal (mc) and polyclonal (pc) lines (*see also* ***Figure 2j***).

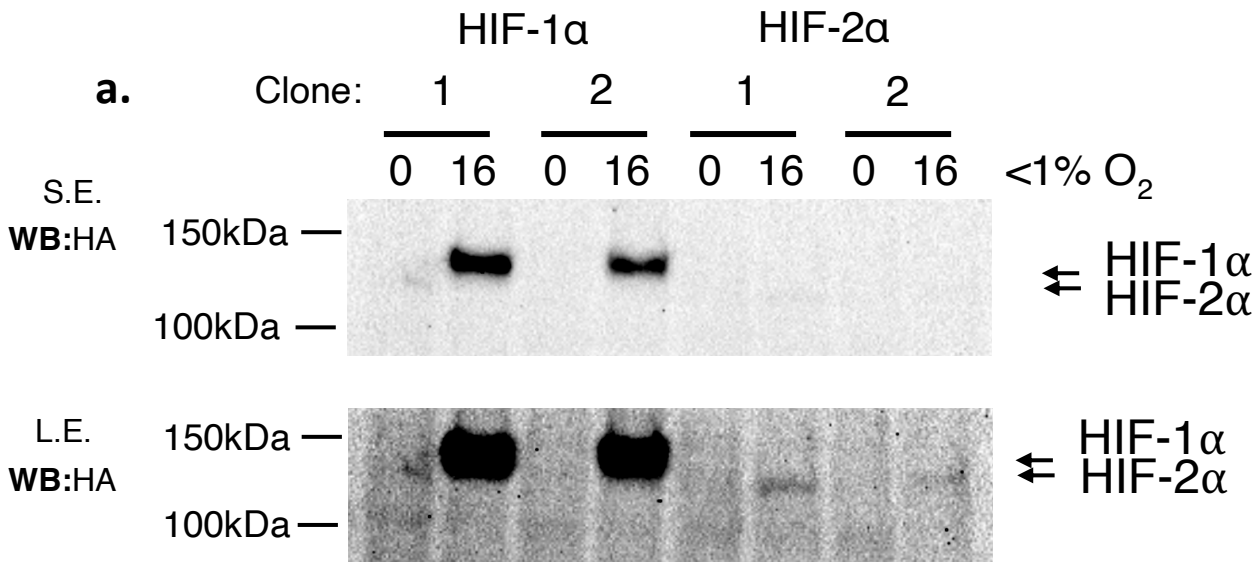
HIF-1α
HIF-2α
a.
Clone: 1 2 1 2
0 16 0 16 0 16 0 16 <1% O2
S.E.
WB:HA
150kDa
100kDa
HIF-1α
HIF-2α
L.E.
WB:HA
150kDa
100kDa
HIF-1α
HIF-2α

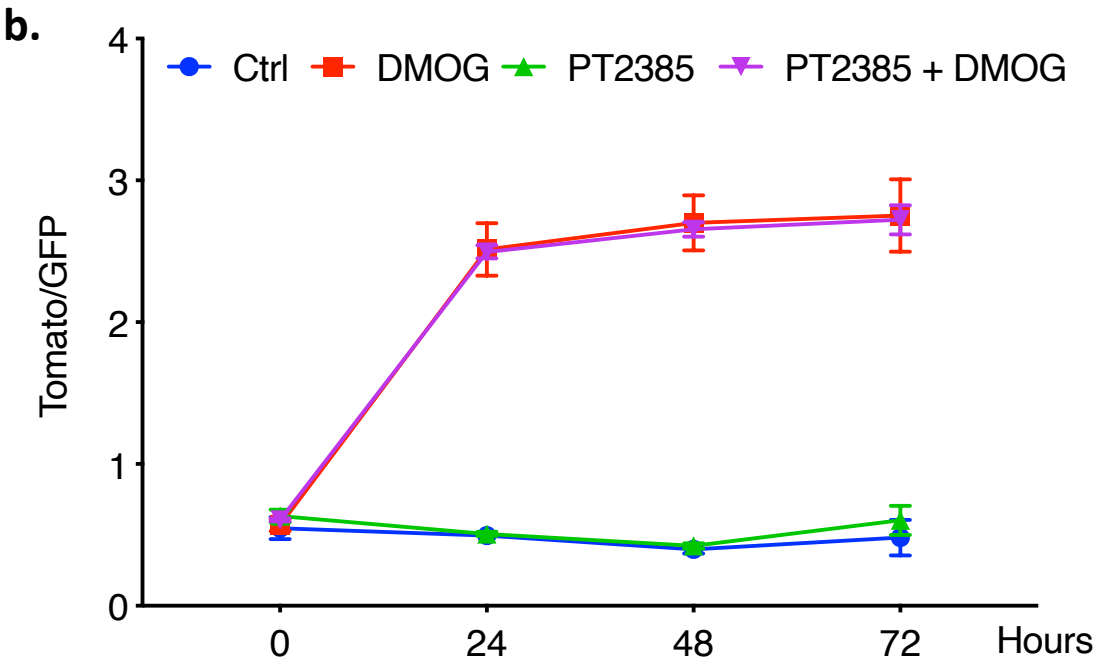
b.
Ctrl
DMOG
PT2385
PT2385 + DMOG
Tomato/GFP
0
1
2
3
4
0
24
48
72
Hours

Supplementary Figure 5. HIF-1α is the predominant isoform that affects the dFLASH reporter in HEK293T cells

(**a**) Monoclonal HEK293T cells with endogenously HA-Flag tagged HIF-1α or HIF-2α were treated with hypoxia (<1% O_2) for 16 hours prior to anti-HA immunoblotting of whole cell extracts. S.E.= short exposure; L.E.= long exposure. Representative of three independent experiments. (**b**) mcdFLASH-HIF cells were treated -/+ 1mM DMOG and -/+ 10μM of the HIF-2α antagonist (PT-2385) as indicated and quantified by HCI over 72-hour period.

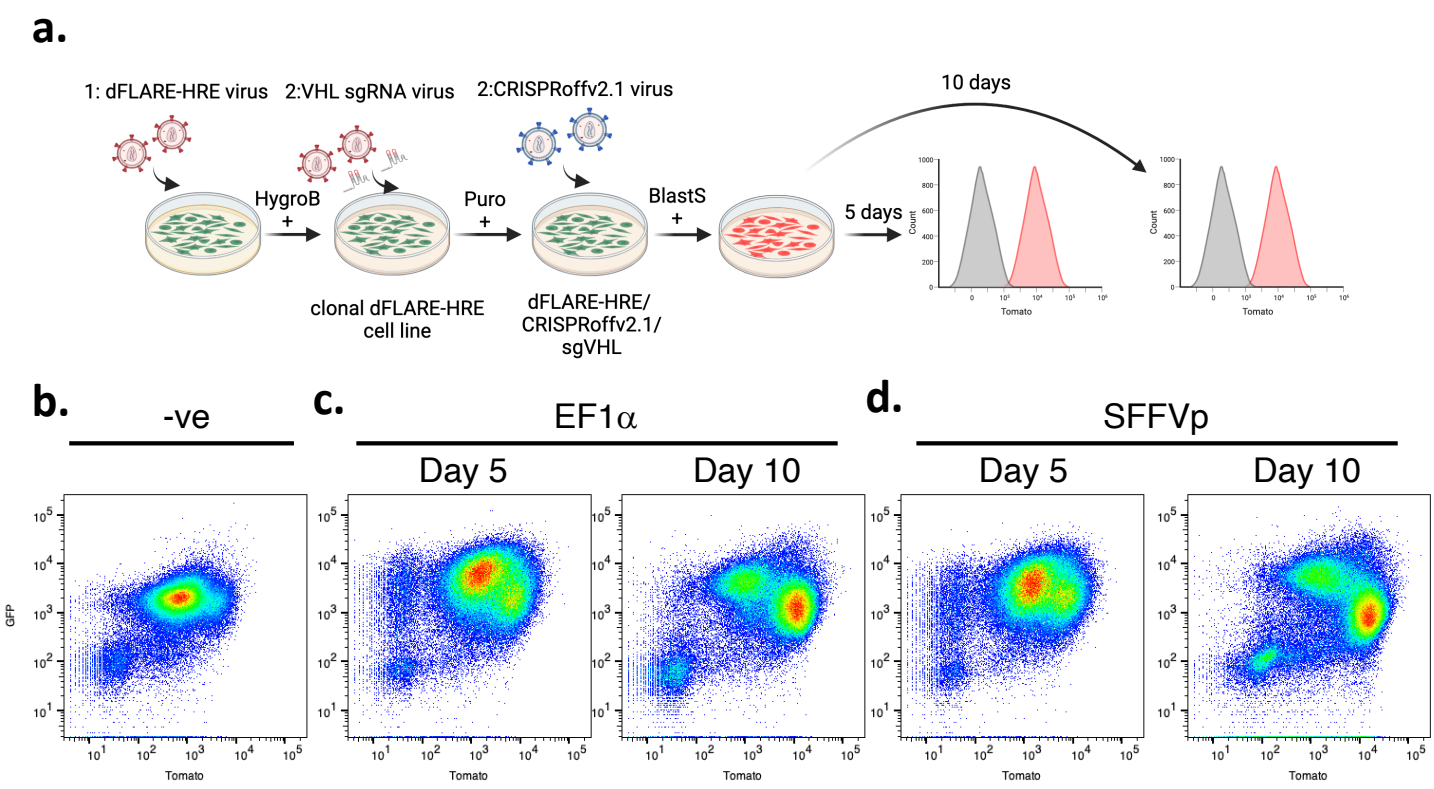

Supplementary Figure 6. CRISPRoff mediated VHL knockdown induces mcdFLASH-HIF reporter lines.

(**a**) HEK293T cells were first transduced with dFLASH-HRE and a clonal reporting line was derived after hygromycin (HygroB) treatment. This line was in turn transduced with the VHL sgRNA vector and selected with puromycin (Puro). This line was then transduced with the CRISPRoffv2.1 vector and selected with blasticidin S (Blast) and populations were subjected to flow cytometry after 5 days or 10 days of selection for analysis of reporter expression. (**b-d**) dot plots for dFLASH expression from the (**b**) non-CRISPRoff parental line, (**c**) EF1a-CRISPRoffv2.1 transduced and (**d**) SFFVp-CRISPRoffv2.1 populations after 5 or 10 days of blasticidin selection (*see also* ***Figure 4***).

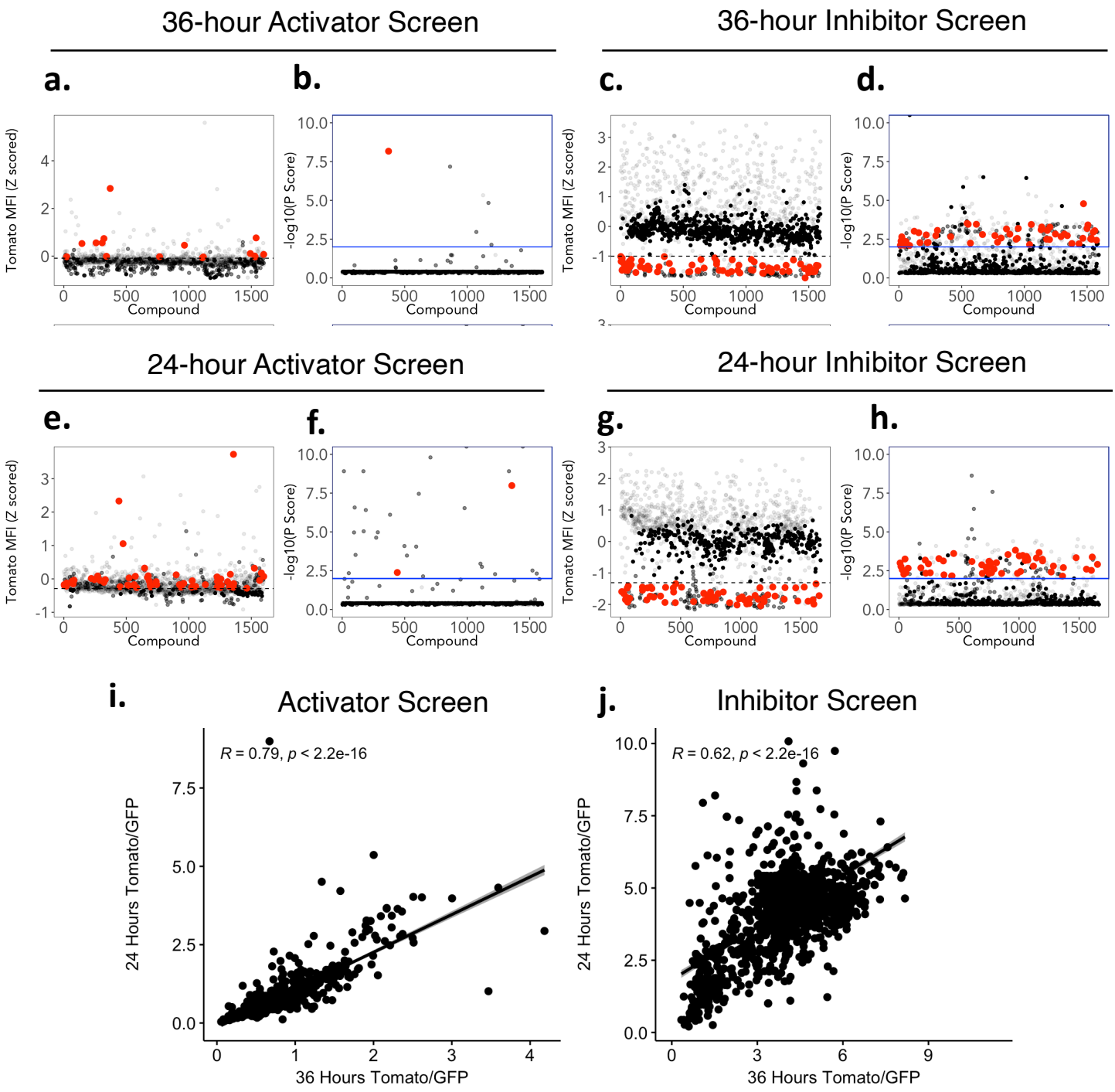
36-hour Activator Screen
36-hour Inhibitor Screen
a.
b.
c.
d.
Tomato MFI (Z scored)
-log10(P Score)
Compound
24-hour Activator Screen
24-hour Inhibitor Screen
e.
f.
g.
h.
i.
Activator Screen
j.
Inhibitor Screen
R = 0.79, p < 2.2e-16
R = 0.62, p < 2.2e-16
24 Hours Tomato/GFP
36 Hours Tomato/GFP

Supplementary Figure 7. Hit selections and assessment of bimodal screen reproducibility between independent screens for activators and inhibitors of HIF-1α.

Compound-induced dFLASH-HIF reporter activity was used to score hits from the (**a-d**) 36-hour or the (**e-h**) 24-hour bimodal screens according to Tomato MFI and adjusted P scores. Lines indicate cut offs for hit criteria with hits shown in red for each metric and dismissed compounds that change EGFP >±2SD shown in grey. (**i, j**) Pearson correlations of the Tomato/EGFP between the 36-hour and the 24-hour screens for (**i**) reporter activation ($R = 0.62$, $p < 2.2x10^{-16}$) or (**j**) reporter inhibition ($R = 0.62$, $p < 2.2x10^{-16}$) for all 1595 compounds screened. Line indicates line of best fit, grey boundary is 95% confidence interval.

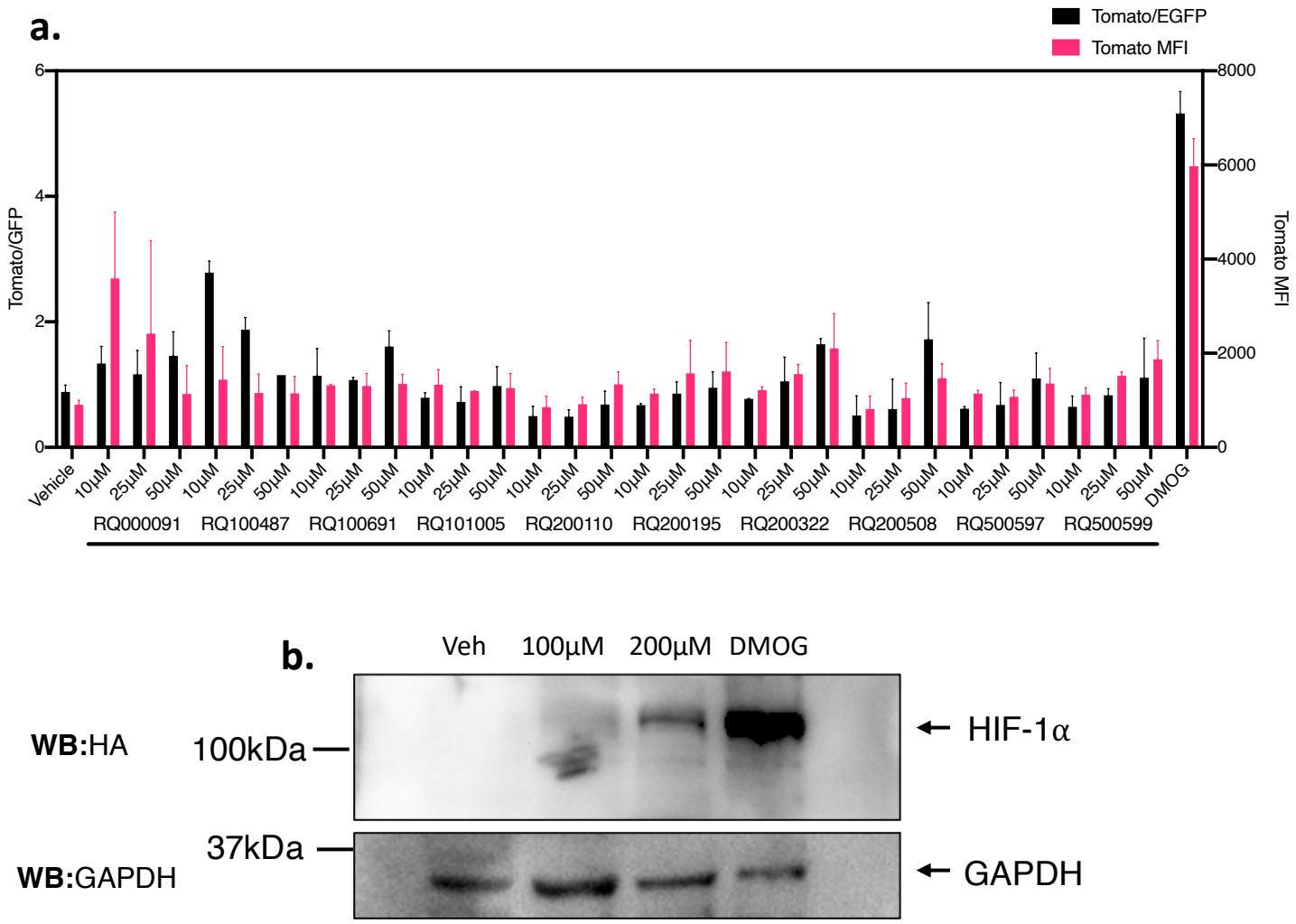

Supplementary Figure 8. Rescreening of activator hits from 1595 compound small molecule screen reveals RQ200674 causes normoxic stabilisation of HIF-1α

(**a**) The 11 top performing hits from the activator screens, including RQ200674 (*see also* ***Figure 6d***) were rescreened against HEK293T mcdFLASH-HIF at 10μM, 25μM and 50μM. Comparisons between Tomato/GFP and Tomato MFI dFLASH induction shown against vehicle (-ve Ctrl) and 1mM DMOG (+ve Ctrl) treated populations (n=2). (**b**) Immunoblot of whole cell extracts from HEK293T cells containing endogenously HA-Flag tagged HIF-1α and treated as indicated with vehicle (0.1% DMSO),1mM DMOG (+ve Ctrl), or 100μM and 200μM of RQ200674 for 18 hours. Representative of 2 independent experiments.

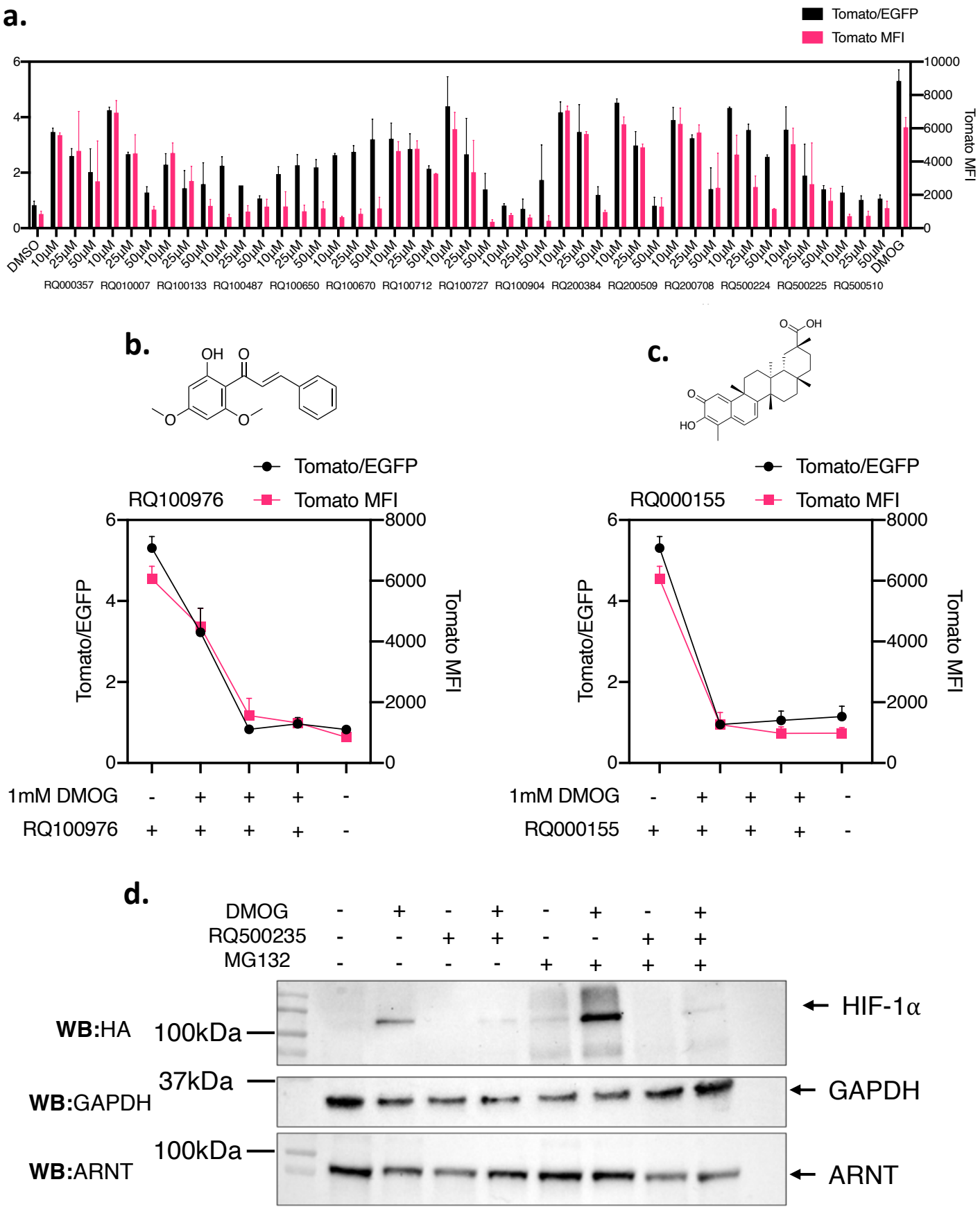
a.
Tomato/EGFP
Tomato MFI
Tomato MFI
DMSO
RQ000357 RQ010007 RQ100133 RQ100487 RQ100650 RQ100670 RQ100712 RQ100727 RQ100904 RQ200384 RQ200509 RQ200708 RQ500224 RQ500225 RQ500510
DMOG
b.
OH
O
O
O
c.
O
OH
O
HO
RQ100976
Tomato/EGFP
Tomato MFI
Tomato/EGFP
Tomato MFI
1mM DMOG - + + + -
RQ100976 + + + + -
RQ000155
Tomato/EGFP
Tomato MFI
Tomato/EGFP
Tomato MFI
1mM DMOG - + + + -
RQ000155 + + + + -
d.
DMOG - + - + - + - +
RQ500235 - - + + - - + +
MG132 - - - - + + + +
WB:HA
100kDa
HIF-1α
37kDa
WB:GAPDH
GAPDH
100kDa
WB:ARNT
ARNT

Supplementary Figure 9. Flavokawain B, Celastarol and RQ500235 decrease dFLASH-HIF and proteasomal inhibition doesn't rescue RQ500235 impact on HIF-1α.

(**a-c**) The 18 top inhibitory compounds, including (**b**) Flavokawain B (RQ100976),(**c**) Celastarol (RQ000155) and RQ500235 (*see also* ***Figure 6a***) were rescreened against dFLASH-HIF at 10μM, 25μM and 50μM in 1mM DMOG treated 293T dFLASH-HIF cells (24 hours). Comparisons between Tomato/GFP and Tomato MFI dFLASH induction shown against 0.1% DMSO (-ve Ctrl) and 1mM DMOG (+ve Ctrl) treated populations (n=2). (**d**) Immunoblot of whole cell extracts from HEK293T cells with endogenously HA-Flag tagged HIF-1α following a 12 hr treatment period with with the indicated combinations of 1 mM DMOG (full12 hr), 50μM RQ500235 (final 6 hr) and 10μM MG132 (final 3 hr). Representative of 2 independent experiments.

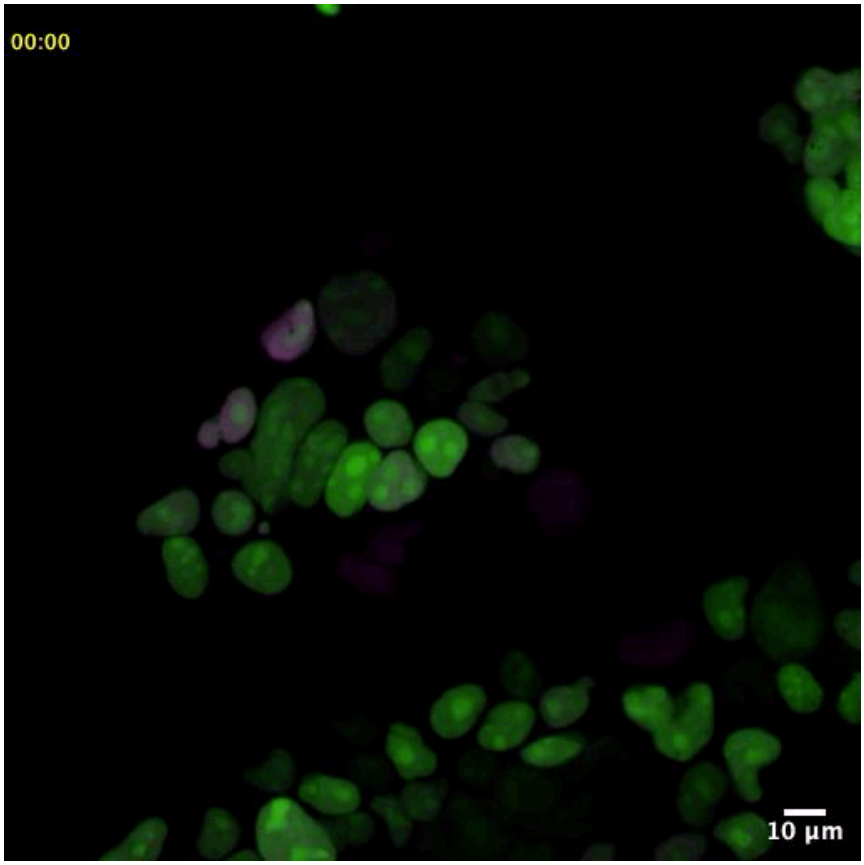

Supplementary Movie 1. Single cell temporal dynamics of HEK293T mcdFLASH-HIF cells
HEK293T mcdFLASH-HIF cells were seeded at $1x10^5$ cells/dish in Poly-D-Lysine coated plates overnight prior to imaging with spinning disk confocal microscopy at 40x magnification. Cells were imaged every 15 min for 48 hours for Tomato (Magenta) and EGFP (Green) expression. Time stamps are given in top left.

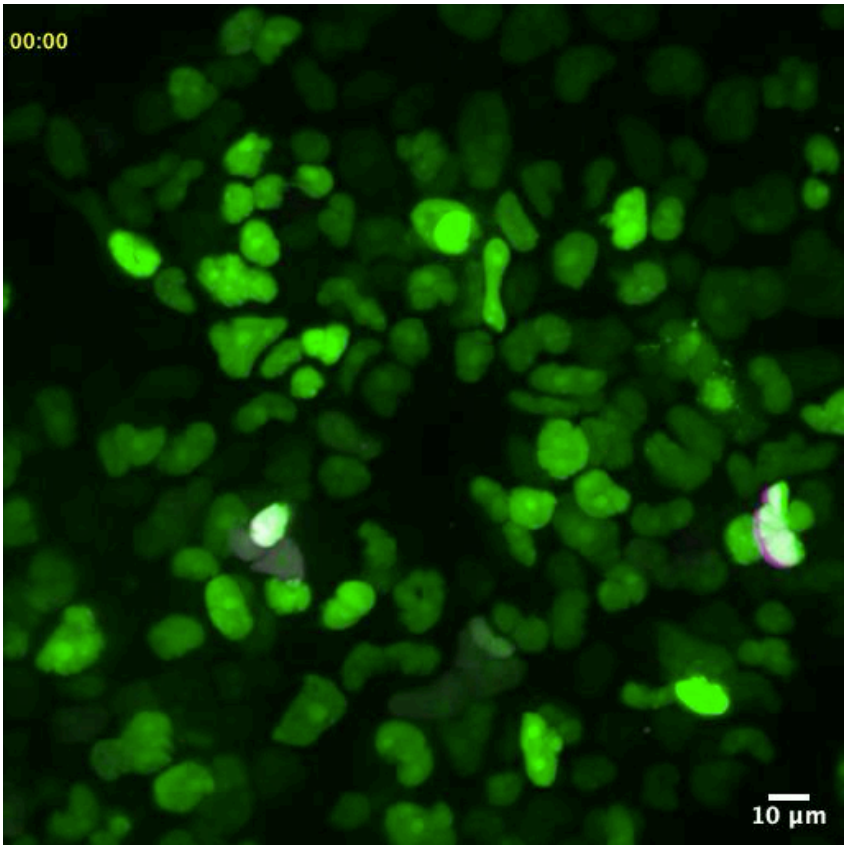

Supplementary Movie 2. Single cell temporal dynamics of T47D mcdFLASH-PGR cells
T47D mcdFLASH-PGR cells were seeded at $5x10^5$ cells/dish in Poly-D-Lysine coated plates overnight prior to imaging with spinning disk confocal microscopy at 40x magnification. Cells were imaged every 15 min for 48 hours for Tomato (Magenta) and EGFP (Green) expression. Time stamps are given in top left.

Methods:

Plasmid Construction. cDNAs were amplified using the Phusion polymerase (NEB) and assembled into ClaI/NheI digested pLV410 digested backbone by Gibson assembly[223]. Sequence verified LV-REPORT plasmid sequences and constructs are listed in **Supplementary Table 1**. Briefly, the plasmids contained an upstream multiple cloning sites followed by a minimal promoter (derived from the pTRE3G minimal promoter) and then followed by a reporter construct mnucTomato/HSVtk-2a-Neo or other variants). This was then followed by a constitutive promoter (EF1a, PGK or PGK/CMV) driving the expression or hygromycinR cassette with or without a 2a linked d2nucEGFP (**Supplementary Figure 1C**).

To improve the performance of our previously reported lentiviral inducible expression systems[247], the PGK promoter in Tet-On3G IRES Puro was replaced by digestion with MluI/NheI and insertion of either EF1a-Tet-On3G-2A-puro, EF1a-Tet-On3G-2A-BlastR or EF1a-Tet-On3G-2A-nucTomato using Phusion polymerase (NEB) amplified PCR products from existing plasmids. Plasmids were cloned by Gibson isothermal assembly and propagated in DB3.1 cells (Invitrogen). We also generated a series of constitutive lentiviral plasmids as part of this work pLV-EgI-BlastR (EF1a-Gateway-IRES-BlastR), pLV-EgI-ZeoR (EF1a-Gateway-IRES-ZeoR), pLV-EgI-HygroR (EF1a-Gateway-IRES-HygroR), pLV-SFFVp-gI-BlastR (SFFVp-Gateway-IRES-BlastR), pLV-SV40p-gI-BlastR (SV40p-Gateway-IRES-BlastR). These plasmids were constructed by isothermal assembly of G-Blocks (IDT DNA) or PCR fragments, propagated in ccbD competent cells, sequence verified and deposited with Addgene (**Supplementary Table 1**).

The Lentiviral backbone expression construct pLV-TET2BLAST-GtwyA was then using to insert expression constructs cloned into pENTR1a by LR Clonase II enzyme recombination (Cat#11791020, Thermo). GAL4DBD-HIFCAD (727-826aa) and the GAL4DBD[37] were cloned into pENTR1a by ScaI/EcoRV or KpnI/EcoRI respectively. The miniVPR sequence[221] was cloned into the pENTR1a-GAL4DBD construct at the EcoRI and NotI sites. The pENTR1a vectors were then Gateway cloned into the pLV-TET2PURO-GtwyA vector. pENTR1a-CRISPRoffv2.1 was generated by inserting an EcoRI/NotI digested CRISPRoff2.1 (CRISPRoff-v2.1 was a gift from Luke Gilbert, Addgene #167981) into pENTR1a plasmid. pLV-SFFVp-CRISPRofv2.1-IRES-BLAST and pLV-EF1a-CRISPRofv2.1-IRES-BLAST were generated by pENTR1a by LR Clonase II enzyme recombination (Cat#11791020, Thermo). All Lentiviral plasmids were propagated in DH5a without any signs of recombination.

Enhancer element cloning. The 12x HRE enhancer from hypoxic response target genes (PGK1, ENO1 and LDHA) was liberated from pUSTdS-HRE12-mCMV-lacZ[177] with XbaI/SpeI and cloned into AvrII digested pLV-REPORT plasmids. Progesterone responsive pLV-REPORT-PRECat PRECat was cloned by isothermal assembly of a G-Block (IDT-DNA) containing enhancer elements from 5 PGR target gene enhancers (Zbtb16, Fkbp5, Slc17a11, Erfnb1, MT2)[248] into AscI/ClaI digested pLV-REPORT(PGK/CMV). Gal4 response elements (5xGRE) were synthesised (IDT DNA) with ClaI/AscI overhangs and cloned into Cla/AscI digested pLV-REPORT(PGK/CMV). Sequences are in **Supplementary Table 2.**

Mammalian cell culture and ligand treatment. HEK293T (ATCC CRL-3216), HEPG2 (ATCC HB-8065) line were grown in Dulbecco's Modified Eagle Medium (DMEM high glucose) + pH 7.5 HEPES (Gibco), 10% Foetal Bovine Serum (Corning 35-076-CV or Serana FBS-AU-015), 1% penicillin-streptomycin (Invitrogen) and 1% Glutamax (Gibco). T47D (ATCC HTB-133) or BT474 (ATCC HTB-20) were grown in RPMI 1640 (ATCC modified) (A1049101 Gibco) with 10% Foetal Bovine Serum (Fisher Biotech FBS-AU-015) and 1% penicillin-streptomycin[249]. Cells were maintained at 37^0C and at 5% CO_2.Clonal lines were isolated by either limiting dilution or FACS single cell isolation into 96 wells trays. Resultant monoclonal populations were evaluated for single colony formation or assessed by HCI or FACS. Ligand treatments were done 24 hours after seeding of cells in requisite plate or vessel.

Standard concentrations and solvent, unless specified otherwise, are 200ng/mL Doxycycline (Sigma, H_2O), 0.5mM or 1mM DMOG (Cayman Scientific, DMSO), 100nM R5020 (Perkin-Elmer NLP004005MG, EtoH), 35nM Estradiol (E2, Sigma E2758, EtOH), 10nM all-trans retinoic acid (RA, Sigma #R2625), 10nM Dihydrotestosterone (DHT, D5027), 10nM Dexamethasone (Dex, Sigma D4902), 10μM PT-2385 (Abcam, DMSO).

Lentiviral Production & stable cell line production. Near confluent HEK293T cells were transfected with either psPAX2 (Addgene #12260) and pMD2.G (Addgene #12259) or pCMV-dR8.2 dvpr (Addgene #8455), pRSV-REV (Addgene; #12253) and pMD2.G along with the Lentivector (described above) and PEI (1μg/μl, polyethyleneimine) (Polysciences, USA), Lipofectamine 2000, or Lipofectamine 3000 at a 3μl:1μg ratio with DNA. Media changed 1-day post-transfection to complete media or Optimem. Virus was harvested 1-2 days post-transfection, then viral media was filtered (0.45μM or 0.22μM, Sartorius) before the target cell population was transduced at a MOI < 1. Cells were incubated with virus for 48 hours prior media being exchanged for antibiotic containing complete media. Standard antibiotic concentrations were 140μg/mL hygromycin (ThermoFisher Scientific #10687010), 1μg/mL Puromycin (Sigma; #P8833) or 10μg/mL Blasticidin S (Sigma; CAT#15205).

Generation of CRISPR knockout or knockdown cell lines. Generation of CRISPR knockout guides and plasmids against FIH has been previously described[250]. These guides were transfected into HEK293T cells and with PEI at a 3μg:1μg ratio then clonally isolated as above. Knockouts were confirmed with PCR amplification and sanger sequencing coupled with CRISPR-ID[251]. FIH knockouts were selected via serial dilution and confirmation of knockout by sequencing and T7E1 assay. The VHL sgRNA guides were selected from the Dolcetto CRISPRi library[252] with BsmBI compatible overhangs (**Supplementary Table 3**). These oligos were annealed, phosphorylated then ligated into BsmBI-digested pXPR050 (Addgene#9692), generating XPR-050-VHL. Monoclonal HEK293T LV-REPORT-12xHRE cell lines were transduced with the XPR-050-sgVHL virus, and stable cell lines selected with Puromycin. Subsequently, LV-SFFVp-CRISPRoffv2.1-IRES-BlastR or LV-EF1a-CRISPRoffv2.1-IRES-BlastR virus was infected into HEK293T LV-REPORT-12xHRE/XPR-050-sgVHL stable cells and selected with Blasticidin S (15μg/ml) for 5 days. FACS was used to assess activation of the dFLASH-HRE reporter in parental (dFLASH-HRE/sgVHL) or CRISPRoffv2.1 expressing cells at day 5 or day 10 after Blasticidin S addition.

CRISPR knock-in of tags to endogenous HIF-1α and HIF-2α. CRISPR targeting constructs clones targeting adjacent to the endogenous HIF-1α and HIF-2α stop codons[32]. Constructs were cloned into px330 by ligating annealed and phosphorylated oligos with BbsI digested px330, using hHIF-1α and hHIF-2α CTD sgRNA (**Supplementary Table 3**). Knock-in of HA-3xFlag epitopes into the endogenous HIF-1α or HIF-2α loci in HEK293T cells was achieved by transfection with 0.625 μg of pNSEN, 0.625μg of pEFIRES-puro6, 2.5μg of px330-sgHIF-α CTD, and 1.25μg of ssDNA HDR template oligo containing flanking homology to CRISPR targeting site the tag insertion and a PAM mutant into ~$0.8x10^6$ cells using PEI (3:1). 48 hours after transfection, the medium was removed from cells and replaced with fresh medium

supplemented with 2 μg/ml puromycin for 48 hours and the cell medium was changed to fresh medium without puromycin. 48 hours later cells were seeded by limiting dilution into 96-well plates at an average of 0.5 cells/well. Correct integration was identified by PCR screening using HIF-1α and HIF-2α gDNA screening primers (**Supplementary Table 4).** Positive colonies reisolated as single colonies by limiting dilution. Isolated HIF-1α and HIF-2α tag insertions were confirmed by PCR, sanger sequencing and western blotting.

High Content Imaging (HCI). Cells were routinely seeded at $1x10^4$ to $5x10^4$ cells per well in black walled clear bottom 96 well plates (Costar Cat#3603), unless otherwise stated. Cell populations were imaged in media at the designated time points at 10x magnification and 2x2 binning using the ArrayScan™ XTI High Content Reader (ThermoFisher). Tomato MFI and EGFP MFI was imaged with an excitation source of 560/25nm and 485/20nm respectively. Individual nuclei were defined by nuclear EGFP expression, nuclear segmentation and confirmed to be single cells by isodata thresholding. Nuclei were excluded from analysis when they couldn't be accurately separated from neighbouring cells and background objects, cells on image edges and abnormal nuclei were also excluded. EGFP and Tomato intensity was then measured for each individual nucleus from at least 2000 individual nuclei per well. Fixed exposure times were selected based on 10-35% peak target range. Quantification of the images utilised HCS Studio™ 3.0 Cell Analysis Software (ThermoFisher). For assessment of high throughput robustness of each individual reporting line in a high throughput setting (HTS-HCI), replicate 96 well plates were seeded for the HIF (10 plates), PGR (5 plates) and synFIH (3 plates) monoclonal reporter lines and imaged as above at 48 hours. For the HIF line, each plate had 6 replicates per treatment (vehicle or DMOG) per plate. For the PGR, 24 replicates per treatment, either vehicle or R5020 per plate were present with edge wells excluded. 24 replicates per treatment were also used for synFIH, with system robustness assessed between the DOX/DMSO and DOX/DMOG treatment groups. Z' and fold change (FC) for the Tomato/EGFP ratio for each individual plate was then calculated as per Zhang, et al. [194]:

$$Z' = 1 - \frac{(3\sigma_{c+} - 3\sigma_{c-})}{|\mu_{c+} - \mu_{c-}|}$$

Z' for every plate across each system was confirmed to be >0.5. Overall robustness of each system is the average of every individual Z' and FC for each system. For temporal high content imaging, HIF, PGR and synHIF lines were seeded in plates and treated with requisite ligands immediately prior to HCI. Four treatment replicates per plate were used to assess the polyclonal population. 4 treatments per plate were used to assess the synFIH monoclone (DOX, DMSO, DOX/DMSO, DOX/DMOG), with 100ng/μL Doxycycline utilised, and 8 treatments per plate (vehicle, DMOG or R5020) were used to assess the PGR and HIF monoclonal lines. Plates were humidified and maintained at 37^0C, 5% CO_2 throughout the imaging experiment. Plates were then imaged every 2 hours for 40-48 hours. At every timepoint, a minimum 2000 nuclei were resampled from each well population.

T47D mcdFLASH-PGR R5020 Dose response curve EC50 calculation. T47D mcdFLASH-PGR cells were treated with increasing doses of 0.01-100nM R5020 and quantified by HCI after 48hrs. Tomato/GFP values were min/max normalised ($x' =$

$\frac{(X-x_{min})}{(x_{max}-x_{min})}$) within each experiment (n = 3) and the EC50 constant and curve fitted using the drc R package from Ritz, et al. [253].

Bimodal small molecule screen to identify activators or inhibitors of the hypoxic response pathway. Library of natural and synthetic compounds was supplied by Prof. Ronald Quinn and Compounds Australia, available by request. 5mM of each of the 1595 compounds were spotted in 1μL DMSO into Costar Cat#3603 plates and stored at -80°C prior to screening. Plates were warmed to 37°C prior to cell addition. Monoclonal HIF HEK293T reporter cells were seeded at $0.5x10^4$ cells per well across 20 Costar Cat#3603 plates pre-spiked with 5mM of compound in 1uL of DMSO in 100uL. On each plate, 4 wells were treated with matched DMSO amounts to compound wells as were four 1mM DMOG controls. Plates were then imaged using HCI (described above) at 36 hrs or 24 hours for reporter activation. Wells were then treated with 100uL of 2mM DMOG (for 1mM DMOG final, 200uL media final). 4 vehicle and 8 DMOG-treated controls (excluding the initial controls from the activator screen) were used for the inhibitor screen. Cells were imaged again 36 hours (Screen 1) or 24 hours (Screen 2) after treatment with 1mM DMOG in the compound wells. Data was Z scored and control wells were used to establish gating for abnormal expression of Tomato and EGFP fluorophores. For the activator screen, compounds within +/- 2SD EGFP MFI of vehicle wells were counted as having unchanged transcriptional effects. Compounds with Tomato/EGFP ratio greater than +2SD of vehicle controls was counted as a putative hit. For the inhibitor screen, compounds within +/- 2SD EGFP MFI of DMOG controls were counted as having unchanged GFP expression and Compounds with Tomato/EGFP ratio lower than -2SD from the DMOG control were considered putative inhibitors. To correct for false positives within each screen, Z scored compounds were converted to their respective P score and adjusted with a Benjamini and Hochberg [196] correction. Pearson correlations were then used to compare compound expression between screens with the base R package (4.4.0). Putative activators and inhibitors identified in the screens were re-spotted at 1mM, 2.5mM and 5mM in 1μL of DMSO in Costar Cat#3603 96 well trays. Activators were rescreened by HCI after 24 hours against $1x10^4$ cells HIF reporter monoclones in biological duplicate against with vehicle and 1mM DMOG controls in 100μL. Inhibitors were rescreened by HCI after 24 hours in duplicate against $1x10^4$ cells HIF reporter monoclones with 1mM DMOG to compound wells. Final compound concentrations were 10μM, 25μM and 50μM respectively and Tomato MFI and Tomato/EGFP ratio for each compound was assessed.

Reverse Transcription and Real Time PCR. Cells were seeded in 60mm dishes at $8x10^4$ cells per vessel overnight before treatment for 48 hours with 1mM DMOG or 0.1% DMSO. Cells were lysed in Trizol (Invitrogen), and RNA was purified with Qiagen RNAEasy Kit, DNaseI treated and reverse transcribed using M-MLV reverse transcriptase (Promega). cDNA was then diluted for real time PCR. Real-time PCR used primers specific for *HIF-1α*, and human RNA Polymerase 2 (*POLR2A*) (**Supplementary Table 4**). All reactions were done on a StepOne Plus Real-time PCR machine utilising SYBER Green, and data analysed by 'QGene' software. Results are normalised to *POLR2A* expression. RT-qPCR was performed in triplicate and single amplicons were confirmed via melt curves.

Flow cytometry analysis and sorting (FACS). Prior to flow cytometry, cells were trypsinised, washed in complete media and resuspended in resuspended in flow cytometry sort buffer (Ca^{2+}/Mg^{2+}-free PBS, 2%FBS, 25mM HEPES pH 7.0) for cell sorting) prior to cell sorting or flow cytometry analysis buffer (Ca^{2+}/Mg^{2+} free PBS, 2%FBS, 1mM EDTA, 25mM HEPES pH 7.0) for analysis followed by filtration through a 40μM nylon cell strainer (Corning Cat#352340. Cell populations were kept on ice prior to sorting. Flow cytometry was performed either using the BD Biosciences BD LSRFortessa or the BD Biosciences FACS ARIA2 sorter within a biosafety cabinet and aseptic conditions, using an 85*μ*M nozzle. Cell populations were gated by FSC-W/FSC-H, then SSC-W/SSC-H, followed by SSC-A/FSC-A to gate cells. EGFP fluorescence was measured by a 530/30nm detector, and the Tomato fluorescence was determined with the 582/15nm detector. A minimum of 10,000 cells were sorted for all FACS-based analysis. Data is presented as log_{10} intensity for both fluorophores. Tomato induction was gated from the top 1% of the negative control population. Cell counts for histograms are normalised to mode unless stated otherwise. FACS analysis was done on FlowJo™ v10.9.1 software (BD Life Sciences)[200].

Time Lapse Spinning Disc Confocal Microscopy. HEK293T mcdFLASH-HIF and T47D mcdFLASH-PGR cells were seeded at $1x10^5$ or $5x10^5$ cells per dish respectively, onto 50*μ*g/mL poly-D-lysine *μ*-Dish 35 mm, high Glass Bottom dishes (Ibidi, #81158） in FluoroBrite DMEM (Gibco, A1896701)/10% FBS/ 1% Pens/1% Glutamax/10mM HEPES pH7.9 and incubated overnight at 37°C with 5% CO2 prior imaging. Cells were treatment with either 0.5mM DMOG (mcdFLASH-HIF) or 100nM R05020 (mcdFLASH-PGR) immediately prior to imaging with a CV100 cell voyager spinning disk confocal Tomato (561 nm, 50% laser, 400ms exposure and 20% gain) and EGFP (488 nm, 50% laser, 400ms exposure and 20% gain) fluorescence for 48 hours post treatment with 15min imaging intervals. Images were captured at 40x with an objective lens with a ~30μm Z stack across multiple fields of view. Maximum projected intensity images were exported to Image J for analysis and movie creation.

Cell Lysis and Immunoblotting. Cells were washed in ice-cold PBS and lysates were generated by resuspending cells in either cell lysis buffer (20mM HEPES pH 8.0, 420mM $NaCl_2$, 0.5% NP-40, 25% Glycerol, 0.2mM EDTA, 1.5mM $MgCl_2$, 1mM DTT, 1x Protease Inhibitors (Sigma)) (**Supp Figure 4**) or urea lysis buffer (6.7M Urea, 10mM Tris-Cl pH 6.8, 10% glycerol, 1% SDS, 1mM DTT) (**Figure 6, Supp Figure 8, 9**). Quantification of protein levels was done by Bradford Assay (Bio-Rad). Lysates were separated on a 7.5% SDS-PAGE gel and transferred to nitrocellulose via TurboBlot (Bio-Rad). Primary Antibodies used were anti-HIF1α (BD Biosciences #), anti-HA (HA.11, Biolegend #16B12), anti-Tubulin (Serotec #MCA78G), anti-GAPDH (Sigma #G8796), anti-ARNT (Proteintech #14105-1-AP). Primary antibodies were detected using horseradish peroxidase conjugated secondary antibodies (Pierce Bioscience #). Blots were visualised via chemiluminescence and developed with Clarity Western ECL Blotting substrates (Bio-Rad).

***In vitro* iron chelation activity assay.** Chelation of iron for RQ200674 was measured by a protocol adapted from Wong, et al. [254] for use in 96 well plate format. 0.1mM $FeSO_4$ (50μL) and 50μL of RQ200674, Dipyridyl (positive control) or DMOG

solutions were incubated for 1hr at room temperature prior to addition of 100μL of 0.25mM Ferrozine (Sigma) and incubated for a further 10 minutes. Absorbance was measured at 562nM. Chelation activity was quantified as:

$$Chelation\ activity = \frac{(A_{control} - A_x)}{A_{control}} \times 100$$

Where $A_{control}$ is absorbance of control reactions without RQ200674, DP or DMOG and A_x is absorbance of solutions with compound.

Statistical Analysis. All data in graphs were presented as a mean ± sem unless otherwise specified. Significance was calculated by a Two-Way ANOVA with Tukey multiple comparison or unpaired t-test with Welches correction where appropriate using Graphpad PRISM (version 9.0.0). All statistical analysis is from three independent biological replicates

Figure Creation. Schematics and diagrams were created with BioRender (BioRender.com) and graphs were made either with ggplot package in R[201] and GraphPad PRISM (version 9.0.0).

Data Availability. Source data are provided with this paper. Additional data, including full construct sequences, are available from corresponding authors upon request. Constructs not available on Addgene can be requested from corresponding authors.

Acknowledgements. We thank Nicholas Smith, Alexander Pace, and members of our laboratories for critical feedback and helpful discussions. We also wish to acknowledge Adelaide Microscopy and the AHMS and SAHMRI Flow Cytometry facilities for technical assistance. We acknowledge Compounds Australia (www.compoundsaustralia.com) for their provision of specialized compound management and logistics research services to the project. This work was supported by Australian Government Research Training Scholarships (T.P.A, A.E.R), The Emeritus Professor George Rodgers AO Supplementary Scholarship (T.P.A, A.E.R). The Playford Memorial Trust Thyne Reid Foundation Scholarship (A.E.R). The George Fraser Supplementary Scholarship (A.E.R), The University of Adelaide Biochemistry Trust Fund (D.J.P. and M.L.W) and the Bill and Melinda Gates Foundation Contraceptive Discovery Program [OPP1771844] (D.C.B, D.L.R).

Author contributions. Study was initially conceived by D.C.B and M.L.W. T.P.A, D.C.B., A.E.R designed and performed experiments. T.P.A, D.C.B., M.L.W, M.L. and R.J.Q. performed and analysed the bimodal screening campaign. M.R. and A.E.R. derived FIH KO cell line. T.P.A, D.C.B and M.L.W wrote the manuscript with input from all authors. Work was supervised by D.J.P, D.L.R. & M.L.W.

Source Data. Source data for figures is available with this manuscript.

Competing interests. The authors declare no competing interests.

Correspondence and requests for materials. Should be addressed to David C. Bersten.

Supplementary Table 1: Synthetic toolkit for generation of reporter cell lines

Deposit Name:	Availability	Purpose
Dual fluorescent reporter constructs:		
pLV-REPORT(EF1a)	Addgene #172326	Reporter with mnucTomato and EF1a downstream promoter
pLV-REPORT(EF1a)-TTN	Addgene #172327	Reporter with mnucTomato-HSVtk-2A-NeoR and EF1a downstream promoter
pLV-REPORT(PGK)	Addgene #172328	Reporter with mnucTomato-HSVtk-2A-NeoR and PGK downstream promoter
pLV-REPORT(PGK/CMV)	Addgene #172330	Reporter with mnucTomato-HSVtk-2A-NeoR and PGK/CMV downstream promoter
12xHRE-pLV-Report-EF1a	Addgene: #172333	Reporter with HRE enhancer
12xHRE-pLV-REPORT(PGK)	Addgene #172334	Reporter with HRE enhancer
12xHRE-pLV-REPORT(PGK/CMV)	Addgene #172335	Reporter with HRE enhancer
PREcat-pLV-REPORT(PGK/CMV)	By Request	Reporter with a PR-responsive concatemer, with enhancers from 5 target genes, containing 6 PR response elements.
5xGRE-pLV-REPORT(PGK/CMV)	Addgene #172336	Reporter with GRE enhancer
12xHRE-pLV-REPORT(EF1a)	By Request	Reporter with HRE
12xHRE- pLV-REPORT(EF1a)-tdnucTomato	By Request	Reporter with tdnucTomato and EF1a downstream promoter
Protein expression constructs:		
pLV-TET2Puro	By Request	Doxycycline-inducible expression vector
pLV-TET2BlastR	By Request	Doxycycline-inducible expression vector
pLV-TET2nucTomato	By Request	Doxycycline-inducible expression vector
pLV-TET2Puro-gal4DBD-miniVPR-HA	Addgene #207171	Doxycycline-inducible expression vector for GAL4DBD-miniVPR
pLV-TET2Puro-gal4DBD-HIFCAD	Addgene #207173	Doxycycline-inducible expression vector for GAL4DBD-HIFCAD (727-826) with Myc tag
pEF-IRES-puro6 gal4DBD-HIFCAD myc tag	Addgene #207171	Constitutively expresses GAL4DBD-HIFCAD (727-826) with Myc tag
pEF-IRES-puro6 gal4DBD-HIFCAD pGalO linker	Addgene #207172	Constitutively expresses GAL4DBD-HIFCAD (727-826) with Myc tag
pENTR1a-CRISPRoffv2.1	Addgene #207174	Lentiviral expression vector for CRISPRoffv2.1 with BFP tag
pLV-EgI-NeoR	Addgene #207175	Gateway-compatible lentiviral expression plasmid with Neomycin resistance
pLV-EgI-BlasR	Addgene #207176	Gateway-compatible lentiviral expression plasmid with Blasticidin resistance
pLV-EgI-HygroR	Addgene #207177	Gateway-compatible lentiviral expression plasmid with Hygromycin resistance
pLV-EgI-ZeoR	Addgene #207178	Gateway-compatible lentiviral expression plasmid with Zeocin resistance

Supplementary Table 2: Sequences for enhancer cloning

PRECat (G-block)
gaattacaaaaacaaattacaaaaattcaaaattttatcgatTGCATGCCTGCTTACATAAGGAAGTACAGAGTGTA CCAAAACAGCAGACCCAAAAAAAGCCTGAAATGTGAGAACCCCAAAACTGTACAGCTTGTATT TCAGGAAGCAAAACTGAGGACGCAAGCCGTCTTCATGGAATAATACATCCTGTTCCCACAAGT GACGTTAGCTTCCAGACTGTGCACAGAGTGCACACTTCACCCAGTGTGTGTCATCATGGTCAC ACAGTGTTCTTTCCGTGGTCACATCTGTGTCCACATTTCCTCCTTTTGATGGGAACAAAGCAGT CATGTTAGGAAGGGAAAGGACACGGTGTTTAATCACACAATCCATGGACAGCCGTGGGCATC CAGTAATGCCTGGAATGAGTCAAGAAGGCATTGCCCCAGTTTTCACTAAGAGCTGCGAGGACA GCCTGTCCTGTTACAACCCACCCACAGCCTCCGTTGAGGCGCGCCAGCTTTAGGCGTGTACG GTGGGCGCCTATAAAAGC
5xGRE
GGTACCAGCTTGCATGCCTGCAGGTCGGAGTACTGTCCTCCGAGCGGAGTACTGTCCTCCGA GCGGAGTACTGTCCTCCGAGCGGAGTACTGTCCTCCGAGCGGAGTACTGTCCTCCGAGCGG AGAC

Supplementary Table 3: Index of all sgGuide oligos used

	Upper (5'-3')	**Lower (5'-3')**
VHL Knockdown sgGuide	CACCGCCGGGTGGTCTGGATCGCGG	AAACCCGCGATCCAGACCACCCGGC
hHIF-1α CTD sgRNA	CACCGTGAAGAATTACTCAGAGCTT	AAACAAGCTCTGAGTAATTCTTCA
hHIF-2α CTD sgRNA	CACCGCCTCCTCAGAGCCCTGGACC	AAACGGTCCAGGGCTCTGAGGAGGC

Supplementary Table 4: Primer sets for qPCR and PCR confirmation

	Forward (5'-3')	**Reverse (5'-3')**
qPCR HIF-1α	TATGAGCCAGAAGAACTTTTAGGC	CACCTCTTTTGGCAAGCATCCTG
qPCR PolR2a	GCACCATCAAGAGAGTGCAG	GGGTATTTGATACCACCCTCT
HIF-1α gDNA primers	GGCAATCAATGGATGAAAGTGGATT	GCTACTGCAATGCAATGGTTTAAAT
HIF-2α gDNA primers:	ACCAACCCTTCTTTCAGGCATGGC	GCTTGGTGACCTGGGCAAGTCTGC

Chapter 3.1

Chapter 3.1E. Extended Data for Thesis:

Addition to: dFLASH; dual FLuorescent transcription factor Activity Sensor for Histone integrated live-cell reporting and high-content screening.

Results & Discussion:

HIF-1α causes a transcription change on the EF-1a promoter backbone that doesn't get translated into a detectable change with High Content Imaging

FACS analysis of HEK293T cells with the Tomato-HSVtK-Neo FLASH-HIF was compared to probe heterogeneity of the PGK/CMV or EF-1a downstream promoter populations. Consistent with prior results, the EF-1a backbone produced no DMOG-dependent Tomato increase compared with the PGK/CMV backbone (**Figure 3.1.1A**). We next asked if the EF-1a backbone was unresponsive to HIF-1α and RT-qPCR of the PGK/CMV backbone compared with the EF-1a backbone (**Figure 3.1.1B**) showed that there was a significant (PGK/CMV $p < 0.05$; EF-1a $p < 0.01$) upregulation of Tomato mRNA produced by DMOG stimulation of the HEK293T dFLASH-HIF-1α cell populations after 48 hours for both backbones. There are differences in the degree of upregulation by the two backbones however, as the EF-1a increased Tomato mRNA by 3.7-fold compared to 15.7-fold by the PGK/CMV backbone (**Figure 3.1.1B**). If the EF-1a backbone is incapable of producing enough Tomato MFI to overcome the detection threshold of the HCI, this would explain why there is no significant change in the EF-1a backbone population by HCI compared with the RT-qPCR result which shows that the EF-1a backbones are HIF-1α responsive, albeit to a lesser degree than the PGK/CMV population.

High content imaging is the mean level of expression from the population and, unlike FACS, doesn't readily represent the heterogeneity of the cellular population at a single-cell level. However, the FACS analysis in **Figure 3.1.1A** suggests a rather

homogenous reporter population in the presence of DMOG. From the RT-qPCR, it is unclear if this change in Tomato mRNA is broadly consistent across the polyclonal pool or if there is an outsized impact from a small minority of cells that are strongly inducing the reporter and correspondingly Tomato mRNA. Coupled with the FACS analysis however, this points toward there being a small upregulation of Tomato mRNA that doesn't overcome the threshold for detection, pointing toward some mechanism of inhibition mediated by the EF-1a promoter.

EF-1a reporter inhibition cannot be rescued by increased selection pressure

To attempt to improve the expression from the EF-1a construct, we next asked if increasing the level of selection would favour clones with a higher proportion of reporter activity or multiplicity of infection to overcome the inhibitory mechanism of EF-1a. HEK293T cells were cultured with increasing levels of hygromycin for 4 passages across 2 independent replicates. In addition to the parental line there was a 140μg/mL (the original selection concentration), 500μg/mL, 1000μg/mL, and a 1500μg/mL of hygromycin added to the cultures over this period. We then treated the replicates with and without 1mM DMOG and imaged with HCI.

We observed that there was little to no impact on reporter function by HCI increasing the selection pressure for any of the backbones when evaluating the Tomato MFI (**Figure 3.1.1C**) but some increase in EGFP MFI (**Figure 3.1.1D**) for the populations. The Tomato MFI readings for the EF-1a backbone didn't substantially increase with higher selection pressure however the EGFP readings with 500 to 1500 μg/mL of Hygromycin saw a more consistent level of expression above that of the 140μg/mL and untreated control. This suggests that selection is favouring a higher expression or presence of the EGFP gene, and correspondingly the reporter yet this doesn't increase the Tomato MFI to a substantial degree. We see a similar trend occur with the PGK and the PGK/CMV backbones, with a slightly elevated EGFP MFI that doesn't elevate Tomato MFI background. This result supports the assertation that the EF-1a inhibition of activity is not a consequence of reporter copy number, given the high level of EGFP that increased with selection observed in the EF-1a backbone, but because of an unknown repressive mechanism exerted by the EF-1a promoter.

The ability of proximal transgenic promoters inhibiting expression has been reported previously[255,256]. Promoter suppression was originally described by Emerman and Temin [256] where they placed two selection cassettes under two different promoters and could differentially select for either gene in cell populations. They proposed a chromatin-mediated inhibition effect, supported by later work where silenced promoters had decreased DNAase I sensitivity[219] and reversal of inhibition by the insertion of a chromatin insulator region to local DNA topology[218]. Furthermore, recent data evaluating dual promoter circuit design in HEK293T cells showed that EF-1a promoters were weaker than mCMV and hPGK promoter inclusion[220]. These data supports our decision to develop screening systems with the PGK/CMV promoter. It also presents a surprising consequence to promoter selection within dual promoter contiguous elements, an important factor that may inform other synthetic design approaches.

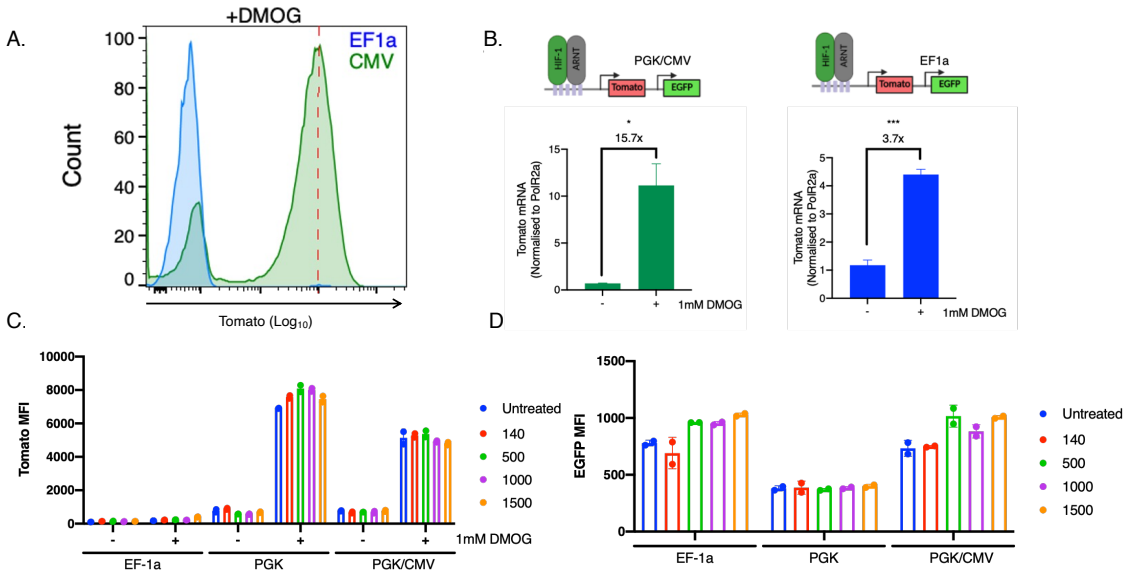

Figure 3.1.1. The EF1a backbone is transcriptionally responsive, but not functionally responsive to HIF-1α induction and inhibition appears as an intrinsic property that cannot be selected out.

(A) FACS and (B) RT-qPCR of polyclonal HEK293T cells with either the PGK/CMV (green) or EF-1a (blue) of HRE-dFLASH backbones with the Tomato-HSVtK-Neo expression cassette treated with 1mM DMOG for 48 hours. (B) Mean of 3 independent experiments shown, significance evaluated with one way ANOVA and Dunnett's post-hoc multiple comparisons. *p<0.05, ****p < 0.001. (C-D) HCI of HEK293T cells with either the EF1a, PGK or PGK/CMV dFLASH reporter backbones treated with increasing levels of hygromycin post-selection. (C) Tomato MFI of the cell populations with vehicle or 1mM DMOG for 48 hours, (D) EGFP of the DMOG treated population for the three backbones. Data from 2 biological replicates. Error bars are mean±SD.

Structurally similar pyridoindole scaffolds display a diverse set of activities on the dFLASH system

As part of our small molecule discovery efforts, we identified a novel activator of the reporter system that we suggest is able to stabilise HIF-1α through iron chelation, RQ200674. The iron chelation mediated by RQ200674 may fully explain its HIF-1α stabilisation effect. Many HIF stabilisers in clinical trials are iron chelators[257,258] but have known off-target effects[259] and more potency compared RQ200674. However, it also contained a pyridoindole motif, which is structurally similar to AhR agonists that bind in the PAS-B area[260] but also have been linked with improved ischemic recovery[261,262], where HIF-1α is known help drive tissue repair[91,93].

Therefore, we investigated if structural analogues containing the pyridoindole motif would have a similar impact on the reporter system, through a similar mechanism to stabilise HIF-1α. We initially looked in our original screening data for structures that contained the motif and identified 14 compounds (including RQ200674). We then were able to subcategorise them into 4 groups based on similarity (**Figure 3.1.2**). Group 4 is the most diverse. Group 1-3 are all more closely related structurally, with larger carbon chains surrounding the pyridoindole motif in the case of Group 1 and Group 2. Group 3 has a less complex superstructure they have one or two non-aromatic rings with various ester functional groups. Evaluating the compounds from the 24-hour (**Figure 3.1.3A**) and 36-hour (**Figure 3.1.3**) screening data revealed that the only compound that increased Tomato MFI to the same degree as AR-Q200674 had a 2-fold change in EGFP compared with other compounds (RQ101049). Other than AR-Q200674, only three other compounds didn't increase EGFP relative to the negative controls (RQ000026, AR-Q500341, RQ100691), indicated by the dashed lines (**Figure 3.1.3B, 3D**) at both time points. Therefore, there was no indication from this dataset that the pyridoindole motif was a general pro-HIF scaffold.

Screening of other pyridoindole compounds doesn't reveal any strong HIF-1α activators

We screened 27 other compounds containing the pyridoindole structural motif for HIF-1α activation on HEK293T FLASH-HIF (**Figure 3.1.4**) at 25μM and 50μM. As we were retesting these compounds from initial screening pool, where they were not identified as hits, we utilised 3SD cut offs instead of the 2SD cut-offs for increased stringency and to capture "near miss" compound activity based on our original criteria. One compound, RQ101078, exceeded the 3SD cut off for Tomato/EGFP used to detect activation of the reporter at 25μM (**Figure 3.1.4A**). It also had a large upregulation in Tomato MFI compared to controls and other compounds (**Figure 3.1.4C**) and the EGFP values were only slightly over the EGFP cut off relative to the controls (**Figure 3.1.4B**). We can conclude that it appears to act as a weak activator of the reporter.

Most of the compounds screened were not active. This is consistent with our conclusion, based on the earlier compounds (**Figure 3.1.3**), that the pyridoindole scaffold was not a pro-HIF scaffold as only 1 of 27 increased the reporter. Additionally, RQ101078 did increase the reporter but didn't meet all the hit criteria, unlike RQ200674. It did not further increase reporter activity at 50μM either, suggesting that further titrating this compound may not also further increase reporter activity. As a result, we concluded that RQ101078 was not a strong enough lead to investigate further.

Overall, we conclude that the pyridoindole structural motif is a poor predictive scaffold for discovery of HIF-1α activators. Of the 40 motif-containing structures assessed across the primary (**Figure 3.1.3**) and secondary assays (**Figure 3.1.4**) only two, RQ200674 and RQ101078, showed increased in reporter activity. There was no general increase in reporter activity across different pyridoindole compared with DMSO controls. While this motif does have diverse biological activity in other systems[262], our hypothesis that the motif was contributing to the HIF-1α activation mechanism doesn't hold true beyond potentially facilitating iron binding in the case of RQ200674 due to the attached imidazole moiety.

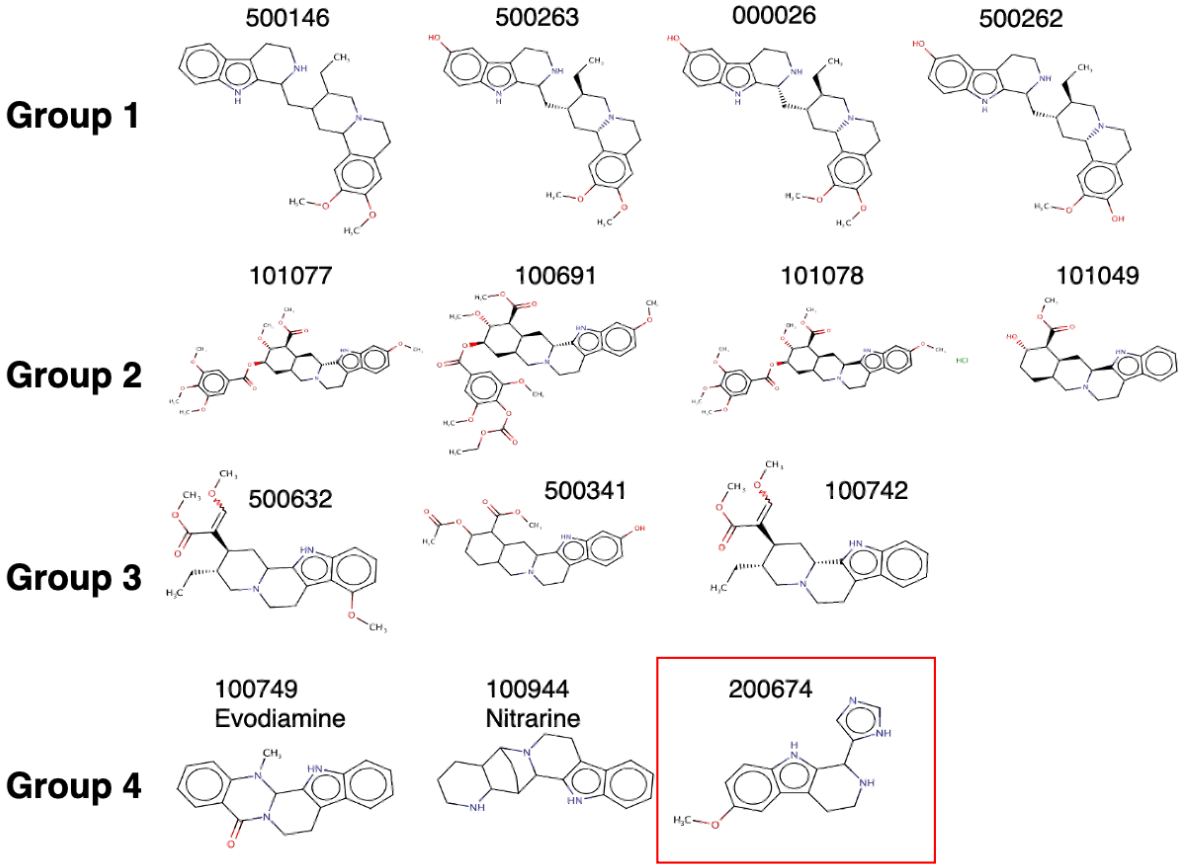

Figure 3.1.2. Pyridoindole structures from the library screen
Structures of the pyridoindole-containing compounds from the original library screening classified into 4 groups. Red box denotes AR-Q200674, the most potent activator identified.

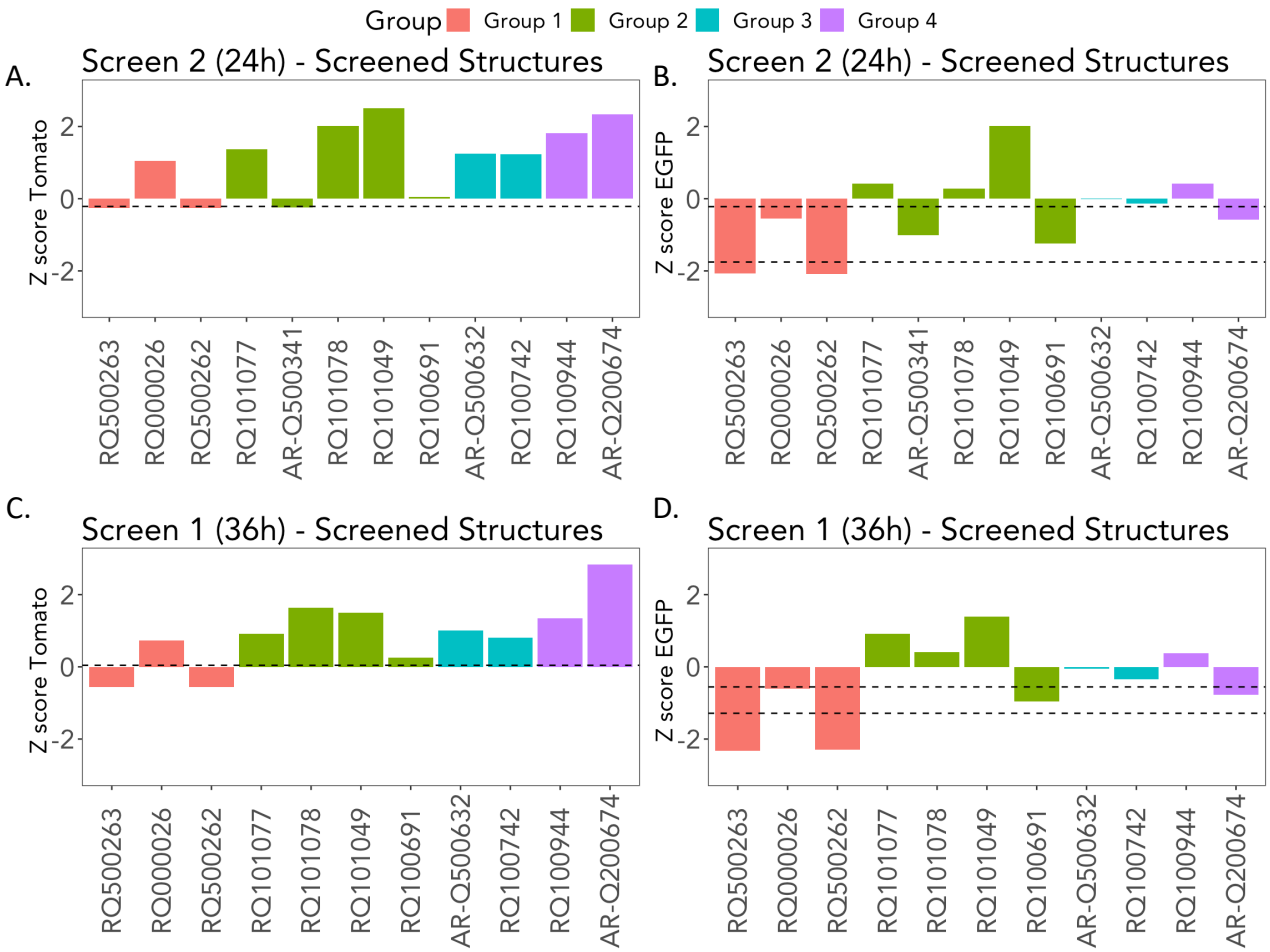

Figure 3.1.3. Pyridoindole structures apart from RQ200674 do not upregulate the reporter

(A-D) Reporter data from the structures in **Figure 3.1.2** from the (A, B) 24 hour and (C, D) 36-hour library screen against HEK293T FLASH-HIF. Data is the Z scored (A, C) Tomato or (B, D) EGFP MFI from the original 1600 compound screen. Dashed lines are (A, C) 3SD above DMSO controls for Tomato MFI or (B, D) the upper and lower bounds of 3SD from the EGFP fluorescence of the DMSO controls used for gating hits in the original screen.

Figure 3.1.4. Screening of Pyridoindole-like compounds reveals no strong activators of the HIF-1α reporter

(A-C) HEK293T FLASH-HIF cells (A) Tomato/EGFP ratio, (B) control gene EGFP MFI and (C) HIF-1α-dependent Tomato MFI. Cells were treated with either 25μM or 50μM of one of 27 different pyridoindole-containing compounds after 48 hours were imaged by HCI after 48 hours. Dashed line represents 3SD above DMSO controls for each fluorescent protein.

Putative "super activators" from the Quinn small molecule screen appear to slightly increase Tomato MFI above other DMOG-treated, compound-treated populations

Upregulation of HIF-1α by other pathways, such as through regulation of the mTOR pathway[51] or NF-κB signalling[263] would be a plausible explanation for increased reporter expression by a "super activator" compound. Additionally, there has been a allosteric activator for the related isoform HIF-2α reported, which bound to the PAS-B pockets and stimulated a small level of elevated function[163]. As a result, the compounds that increase Tomato MFI above the DMOG control were of interest.

In the screen for compound activity against DMOG-treated mcdFLASH-HIF cells with the Quinn library (**Figure 3.1.5A**) we could see that there were several compounds that appeared to increase the activity of the reporter. As the reporter was already elevated from DMOG-treatment, these compounds appear to be "super activators". This activity was observed in the 38-hour screen (**Figure 3.1.5A**) for three identified compounds that passed FDR analysis ($p < 0.05$ of adjusted p values) and Z score was > 2. This was not the case for the 24-hour screen, where these compounds were inactive, but the induction may be time dependent. Looking at the Tomato and EGFP values however (**Figure 3.1.5C, D**) revealed upregulation at 24 hours (**Figure 3.1.5D**) of both EGFP and Tomato that caused the decreased ratio measured in **Figure 3.1.5B**. Additionally, this EGFP upregulation was not observed at 38 hours in the initial screen (**Figure 3.1.5C**).

We then assayed the three compounds, RQ100129, RQ202016, and AR-Q200664 at 25μM and 50μM after 48 hours against HEK293T FLASH-HIF (**Figure 3.1.5E-G**). Unlike in the 38-hour screen, we did not see a large upregulation mediated by these compounds (**Figure 3.1.5E**). Interestingly, when we looked at the EGFP (**Figure 3.1.5F**) and Tomato (**Figure 3.1.5G**) separately we saw both fluorescent proteins were upregulated at least 3SD above controls for all three compounds.

This means that their mode of action was not specific to the HIF-1α pathway. These compounds appeared to be non-specific upregulation of the reporter through an unknown mechanism. While this is interesting and could be followed up through qPCR, translational inhibition and protein stability assays, the lack of specificity to the HIF-1α pathway means the compounds were not investigated further.

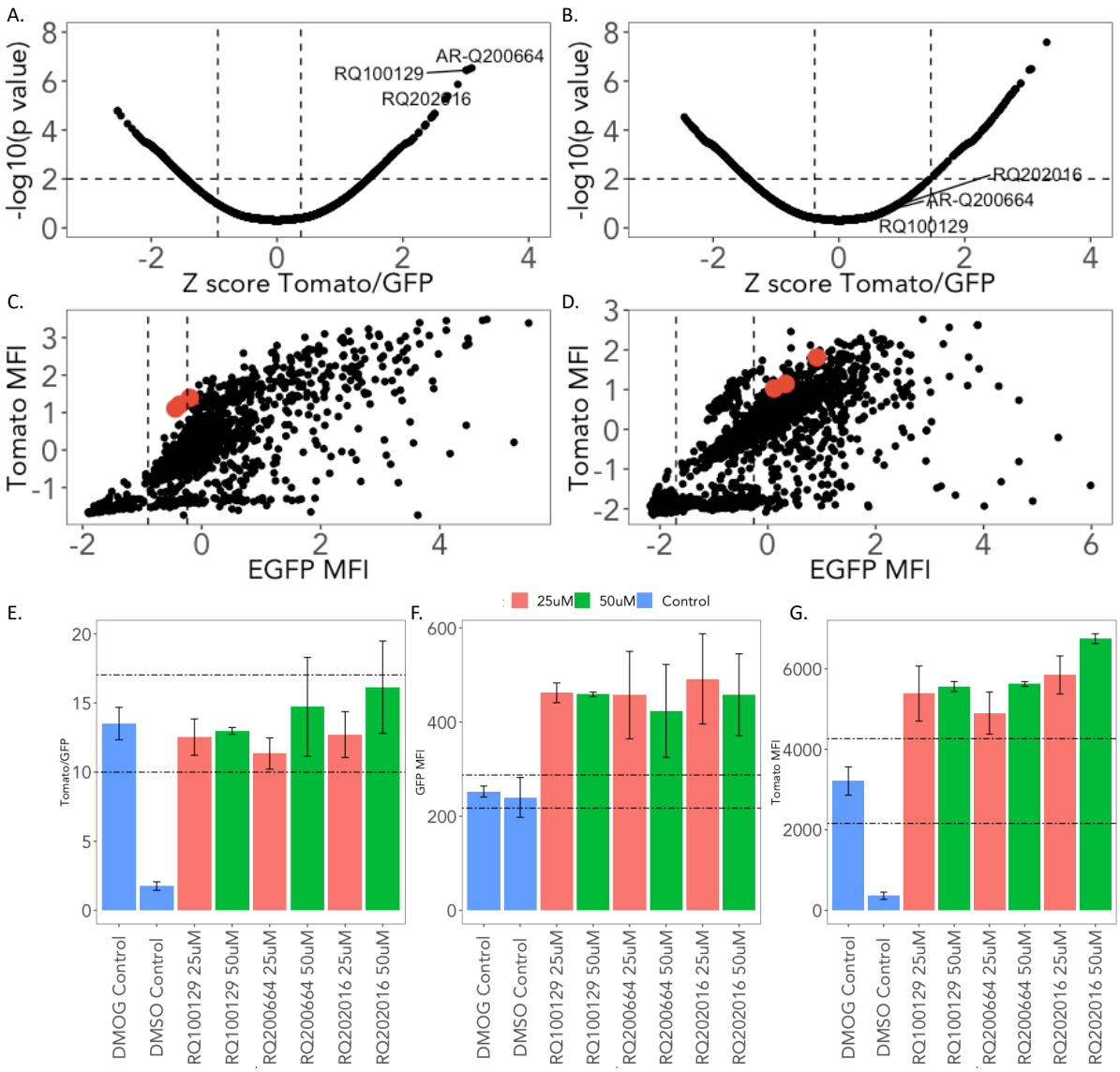

Figure 3.1.5. Compounds that appeared to upregulate Tomato expression as do not display consistent activity over the reporter

(A, B) Z scored Tomato/EGFP plotted against -log10 p-values for the (A) 36-hour and (B) 24-hour 1600 compound small molecule screening data for 1mM DMOG treated HEK293T FLASH-HIF cells. Compounds indicated are putative activators at 36 hours. Horizontal dashed line indicates p = 0.05. Vertical dashed lines indicate 2SD from DMOG treated controls.

(C, D) Z scored Tomato MFI plotted against Z scored EGFP MFI from the above (C) 36-hour and (D) 24-hour screens. Red dots indicate location of putative super activators. Dashed lines represent 2SD cut offs of EGFP fluorescence from the DMOG controls.

(E-G) HEK293T FLASH-HIF cells treated with 1mM DMOG and 25μM (red) or 50μM (green) of putative super activators. Cells were quantified by HCI after 48 hours for (E) Tomato/EGFP ratio, (F) EGFP MFI, and (G) Tomato MFI relative to vehicle controls (blue). Dashed lines indicate 3SD from the DMOG control for each metric. Data is mean of two independent biological replicates.

Chapter 3.2
Screening of a rare metabolite library with HRE-dFLASH and integration of morphology metrics into screening pipeline

HIF-1α and natural products

Prior attempts at HIF-1α inhibitor discovery have utilised some natural product libraries sourced from plant life and marine environments[264]. These have reported some success. Using a range of natural product sources[265,266] the Nagle group found several antagonists of a transient luciferase reporter for HIF in T47D cells[267]. The mechanism behind these inhibitory compounds are diverse, including inhibition of protein translation[265] and mitochondrial respiration[266]. Another thread that is present throughout this group's profiling of natural products and HIF biology is, among most HIF-1 inhibitors, a narrow window of concentrations between the proposed primary function of inhibiting HIF and cytotoxicity that occludes function and prevents these compounds from progressing to clinical implementation[264,265].

Natural products, however, remain a viable pool of potential drug-like compounds with the poorly explored and annotated microbial chemosphere eclipsing that found within eukaryotes[268]. One of the challenges with developing whole-cell assays for drug screening is effectively filtering toxic compound interference from pathway-dependent activity, particularly in the case of HIF-1α where inhibition of core processes may have substantive molecular feedback onto factor expression and stabilisation. While our previous efforts with a natural product library curated by the Quinn group were successful in defining a novel activator and inhibitor, the Bioaustralis library offers a different spectrum of compounds compared with what was supplied by the Quinn group and is solely comprised of microbial compounds and semi-synthetic derivatives, including rare metabolites.

Bioaustralis library selection:

We previously performed a successful bimodal protocol to screen a large library for HIF-1α agonists and antagonists, however that approach exhibited a reduced Z' score. Therefore, for the smaller Bioaustralis library, we screened the compounds only for

their ability to inhibit HIF-1α. The decision to focus on inhibition over activation was additionally driven by the fact that inhibitors for HIF-1α have been proposed as potential drug candidates in multiple cancer contexts[20,76,176,269]. Prior clinical trials with inhibitors, such as Acriflavine, have not resulted in clinical success. For example, Acriflavine interacts directly with the HIF-1α/ARNT dimer but also has DNA intercalating activity which, despite its demonstrated anti-cancer properties, is an off-target effect that complicates clinical usage[270]. As a result, there is an existing gap for an effective HIF-1α inhibitor without a pleiotropic side-effect profile. As noted previously, natural products do commonly result in off-target effects, however they also provide entry points for combinatorial chemistry and refinement[271]. Finally, there are several well-studied mechanisms for activation of HIF-1α, with numerous compounds that can upregulate HIF-1α expression, while in contrast true inhibitors of HIF-1α are more elusive and thus provide the more biologically interesting avenue of investigation. As the Bioaustralis discovery set contains several rare microbial metabolites from fungal and environmental sources, it therefore offers a preliminary launching pad for investigating if there are novel microbial products that can act as regulators of HIF-1α.

Screening the Bioaustralis library for HIF-1α inhibitors

As there were only single aliquots of each compound supplied in HCI-incompatible plates, the library of compounds was resuspended in 50μL of media with a 2x DMOG concentration. The full 50μL of media was then added to monoclonal HEK293T dFLASH-HIF cells seeded in screening plates at $1x10^4$ cells in 50 uL per well (**Figure 3.2.1**).

The reporter was imaged at 24- and 48-hours post-treatment, due to the optimised time course with the dFLASH-HIF reporter but also to capture slow-acting compounds and chart changes between the two time points to assess activity over an extended time course.

The compounds were scored initially for Tomato/GFP readout with false discovery rate analysis at a $p< 0.01$ significance and a 3SD decrease in Tomato/GFP ratio from DMOG control wells at both time points (**Figure 3.2.2A, C**)**.** Compounds whose EGFP MFI changed more that 3SD from the control wells were excluded from analysis due to non-specific effects.

57 hits from the 812 compounds (7% of total) met this hit criteria at one time point and 35 met the criteria (4% of total) across both time points. These compounds decreased Tomato MFI >2SD from the mean of compound population and more that 3SD from the DMOG controls (**Figure 3.2.2B, D**). Compounds were also assessed for consistent trends across the two time points. We then followed up with a qualitative review of the HCI images for all 35 hits across the two time points. This was to confirm there was there no clear interference with the results such as autofluorescence, cell debris, or compound falling out of solution.

From the screening data we unexpectedly observed that there were compounds that appeared to be upregulating the reporter (**Figure 3.2.3**). Some of these compounds at both 24 and 48 hours had Tomato/EGFP increase above three standard deviations (**Figure 3.2.3A, B)**. There has been a reported HIF-2α agonist[163] and pathways that can upregulate HIF-1α[51] , hence the interest in these compounds. Looking at the Tomato MFI (**Figure 3.2.3C, D**), reveals that at both time points, none of these compounds upregulated Tomato MFI above the 3SD cut off and indeed, sit near the mean of the other compounds. Their EGFP expression shows that they were below the average expression of the other compounds, although several still met control

determined cut offs (**Figure 3.2.3E, F**) yet this falsely inflated their normalised reporter readout. These were deemed as most likely false activators, with follow up experiments planned to verify them as such.

Selection of lead compounds

From the list of 57 hits, with 35 overlapping, across the 2 time points, we selected 12 compounds for follow up analysis that were active at 24 and 48 hours, 9 potential inhibitory compounds and 3 of the putative false activators split up into three categories.

The first subcategory (**Cat. 1, Figure 3.3.4**) are 3 compounds initially identified as being potential up-regulators but failed to increase Tomato MFI (**Figure 3.2.3**). We selected these compounds to confirm our prior analysis designating them as false positives on the reporter screen and to ensure that our downstream confirmation pipeline would detect such compounds. This is of particular importance, as Sparsomycin and Anisomycin are known protein synthesis inhibitors, and an abnormal morphology was observed for Monensin A treated cells that caused heterogeneity of reporter activity within the cell populations.

The second subcategory (**Cat. 2, Figure 3.3.5**) selected was a cluster of 6 top performing hits from the library. These hits had no connecting structural relationship but decreased the reporter the most efficiently and could be readily sourced for further experimentation.

The third category (**Cat. 3, Figure 3.3.6**) comprised a set of 3 closely related quinone-like compounds that seemed to downregulate dFLASH-HIF. They had a clear structural similarity, but within the library there was a closely related structure that had no impact on the reporter system, Gliroseniol, which may thus provide clues to key functional groups. For similar reasons we included tetrahydroxyquinone within Cat.3, as this compound again had no activity in the original screen but contains simpler functional groups around the common quinone scaffold in this group.

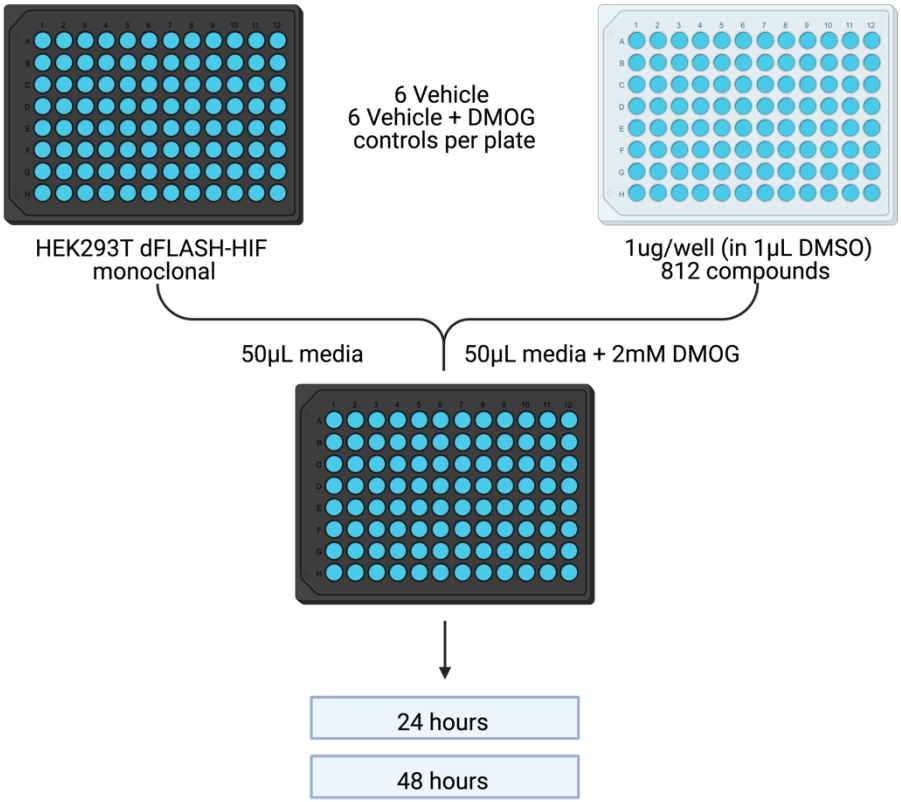

Figure 3.2.1. Experimental set up for the inhibition screen with the Bioaustralis compound library

HEK293T dFLASH-HIF monoclonal cells were seeded in a 96 well screening plate at $1x10^4$ cells per well in 50µL. The Bioaustralis library in screening-incompatible plates was warmed to 37°C and then resuspended in 50µL in media with 2mM DMOG (a 2x stock on final) and incubated by shaking for 1hr. The 50µL of media with the Bioaustralis library was then transferred to the screening plates with HEK293T dFLASH-HIF cells (for 1mM DMOG final) and then incubated for 24 hour and 48 hours prior to imaging. 6 DMSO vehicle controls and 6 DMOG vehicle controls were included per plate.

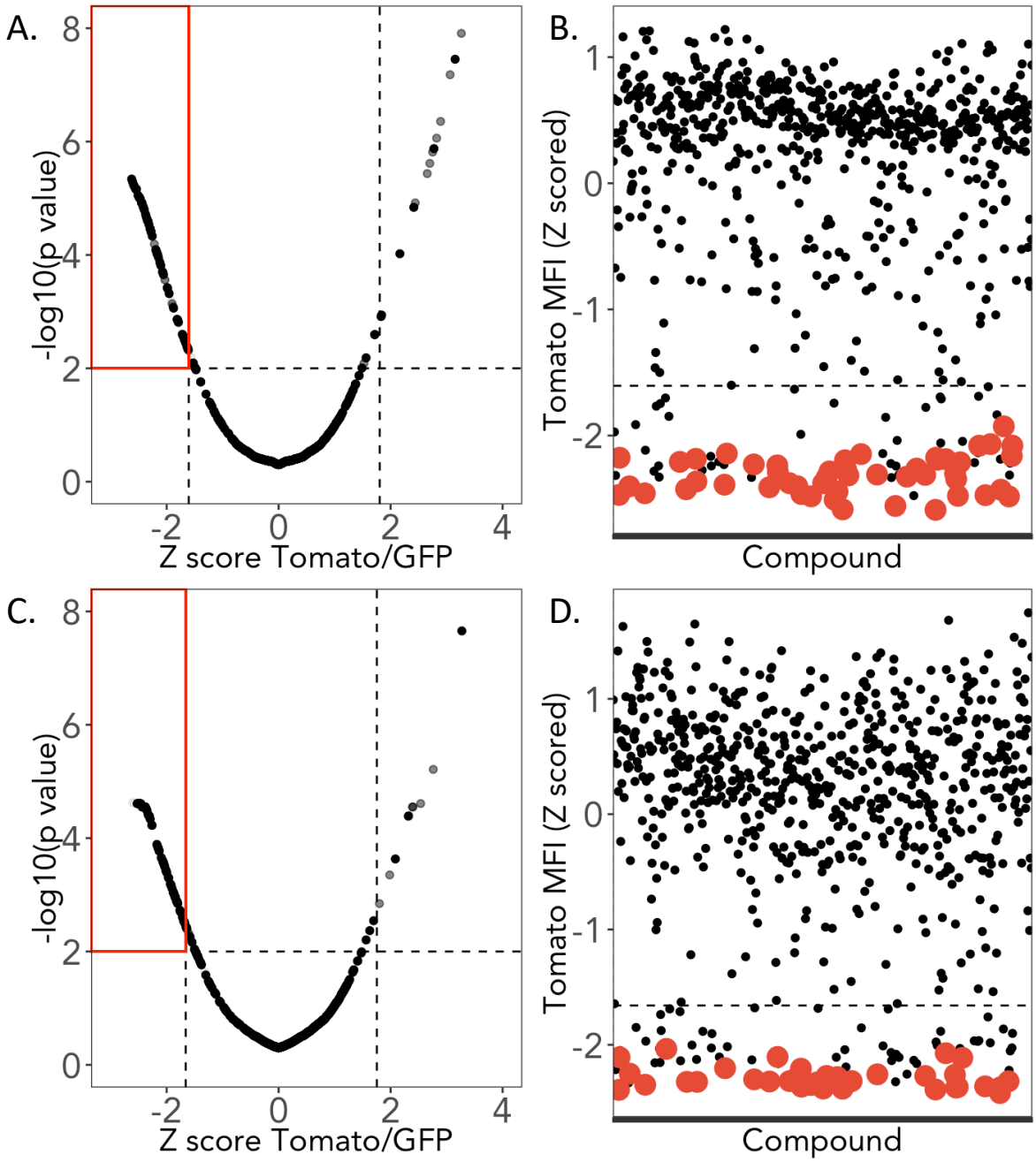
A.
-log10(p value)
Z score Tomato/GFP
B.
Tomato MFI (Z scored)
Compound
C.
-log10(p value)
Z score Tomato/GFP
D.
Tomato MFI (Z scored)
Compound

Figure 3.2.2. Identification of putative negative regulators of HIF-1α activity from a diverse fungal and microbial metabolite library

HEK293T dFLASH-HIF monoclonal cells were incubated with 1ug/ml of the Bioaustralis library compounds and 1mM DMOG and imaged after (A) 24 and (C) 48 hours. Data was Z scored and subjected to False Discovery Rate analysis ($p < 0.01$, horizontal line) to narrow down hits (red box) that were greater than 3SD from DMOG controls (vertical dashed lines). Compounds that had EGFP changes >3SD from controls were excluded (grey dots) (B, D) Compounds that met that criteria were confirmed to decrease Tomato MFI more than 3SD (horizontal dashed line) at (B) 24 hours and (D) 48 hours without altering EGFP control gene beyond 3SD are highlighted in red.

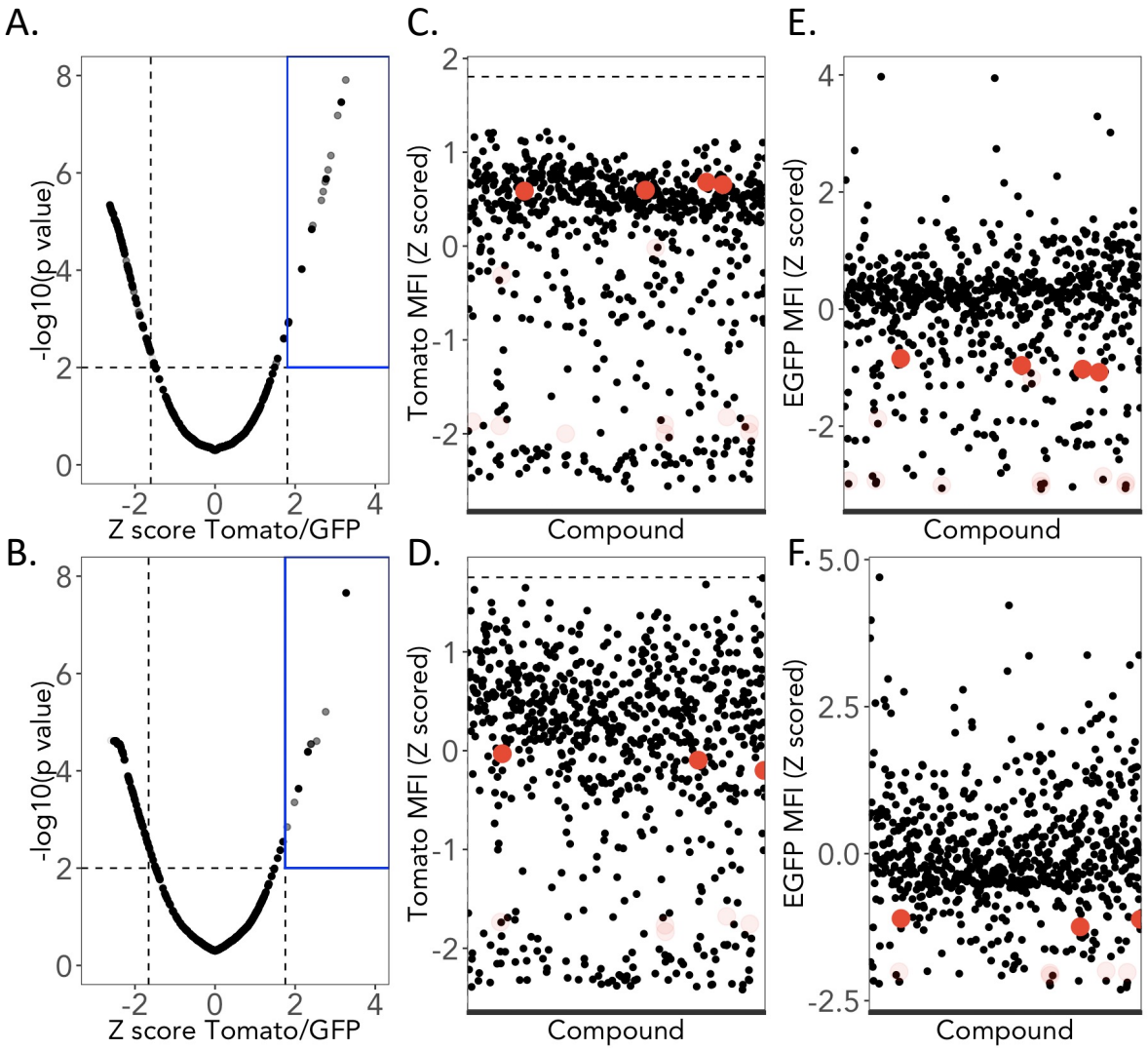

Figure 3.2.3. No compound upregulates HIF-1α-dependent reporter expression

(A, B) Screening data from **Figure 3.2.2** for (A) 24 hours or (B) 48 hours highlighting compounds that putatively upregulate reporter expression (blue box). Dashed lines represent the >3SD cut off for Tomato/EGFP from DMOG controls (vertical) or p <0.01 (horizontal). Compounds that change EGFP >3SD from DMOG controls are excluded (grey dots) (C-F) Putative activators (red circles) (C, D) Tomato MFI or (E, F) EGFP MFI expression at (C, E) 24 hours or (D, F) 48 hours. Dashed line indicates >3SD Tomato MFI cut off from DMOG controls. Activators that did not meet EGFP cut off but did meet Tomato/EGFP threshold in A and B are opaque red circles.

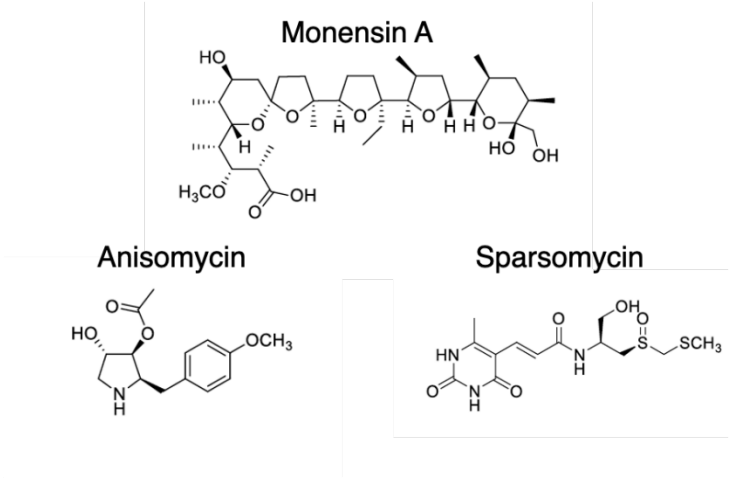

Figure 3.2.4. Structures of the Category 1 (Cat. 1) compounds
Chemical structures of the 3 compounds that were identified as increasing Tomato/EGFP ratio in DMOG treated cells through suppression of EGFP.

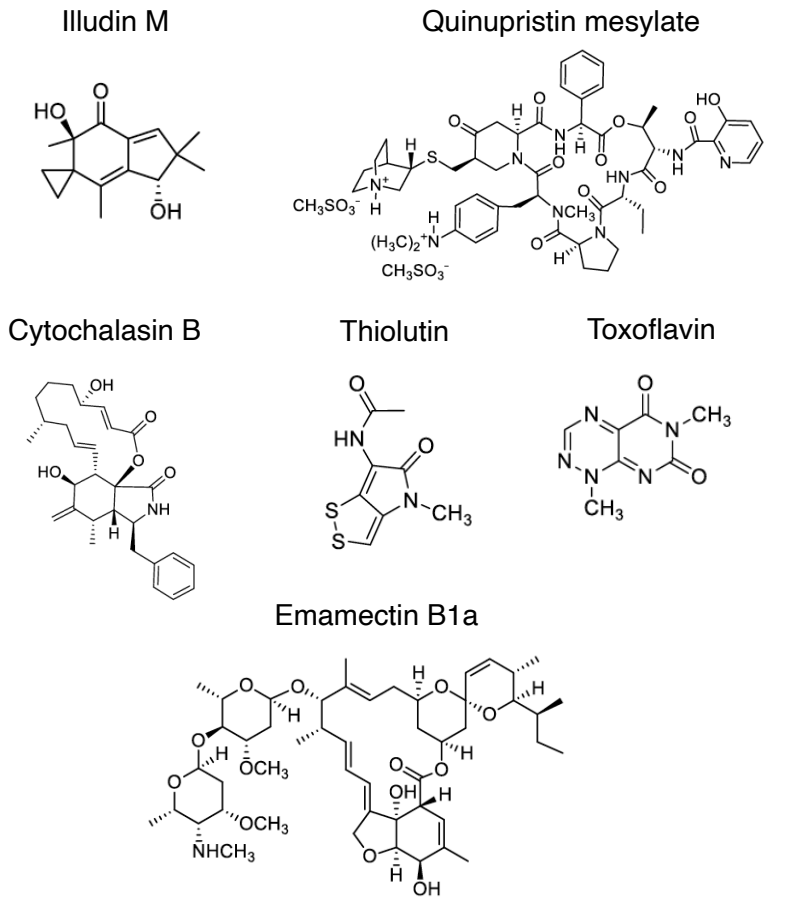

Figure 3.2.5. Structures of the Category 2 (Cat. 2) compounds

Chemical structures of six structurally diverse putative HIF-1α inhibitors from the small molecule screening in **Figure 3.2.2**.

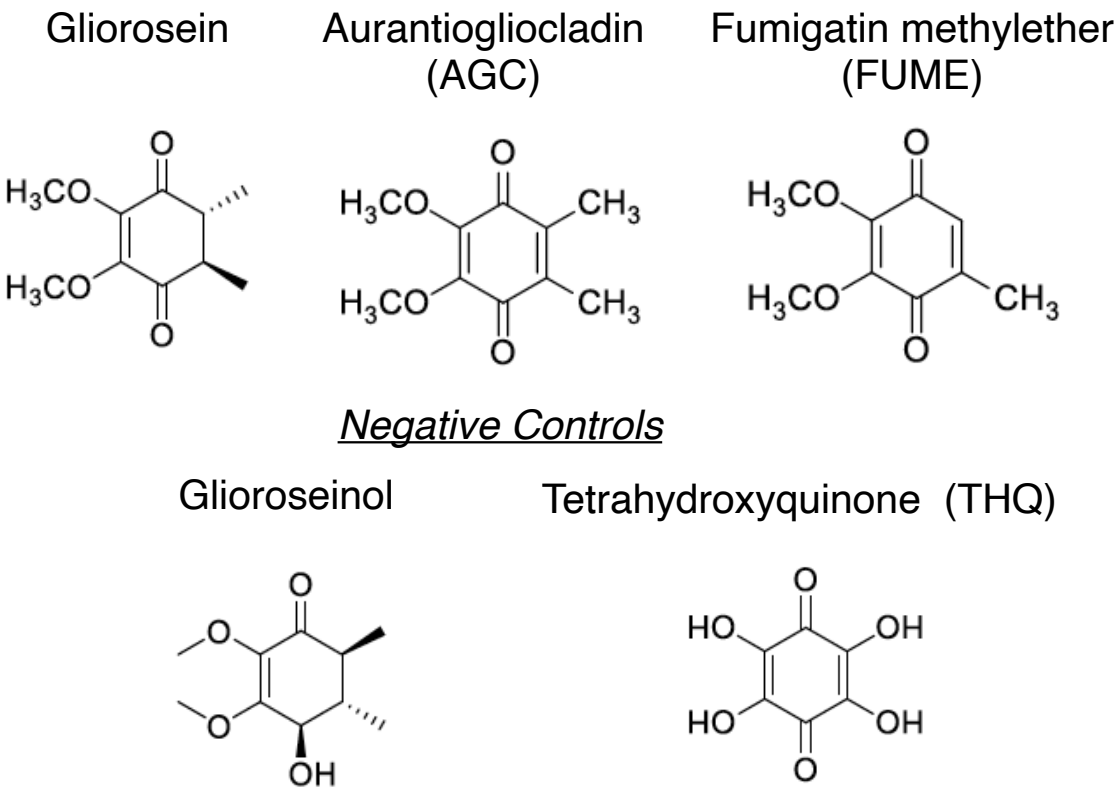

Figure 3.2.6 Structures of the Category 3 (Cat. 3) compounds

Chemical structures of three structurally related putative HIF-1α inhibitors from the small molecule screening in **Figure 3.2.2**. Also included are two negative controls with similar structural backbones, Glioroseinol and Tetrahydroxyquinone (THQ).

Rescreening of compounds of interest against the dFLASH-HIF system

Having selected several lead compounds, we then sought to confirm their activities in follow-up validation assays. We treated HEK293T dFLASH-HIF with 1mM DMOG and 50μM of the compounds above and repeated the initial screening protocol, imaging at 0-, 24-, and 48-hours (**Figure 3.2.7** – **Figure 3.2.9**).

Cat. 1:

These compounds did not upregulate Tomato/GFP compared to DMOG in contrast with their earlier reported activity (**Figure 3.3.3**). At 48 hours there was a significant reduction by all 3 compounds ($p < 0.001$) (**Figure 3.3.7**) that was unexpected. Anisomycin has been previously reported inhibit protein synthesis in mammalian tissue culture and activate JNK signalling to induce apoptosis[272] and Sparsomycin is also known to block protein synthesis via blocking ribosomal translocation[273]. Monensin A has a reported wide spectrum activity in cellular systems[274], incorporating anti-proliferative effects[275] that may impact expression of the reporter.

While we expected off-target effects, we predicted we'd see similar reporter response to what we observed in the original screen; a decrease in EGFP and potentially Tomato that would cause an increase in Tomato/EGFP at 48 hours. Instead, the result we see culminates in reporter downregulation, suggesting that these compounds are non-specifically regulating the reporter. It should be noted however, that the 50μM concentration, selected as this is near the mean concentration for most of the lead compounds, is a higher screening concentration for the Cat 1 compounds Sparsoymcin (27nM) and Anisomycin (38nM), which may also explain the discrepancy. Importantly, these compounds met the EGFP cut offs which is our primary filter for screen interference, suggesting that further selection metrics may need to be included into screening design to capture these types of compounds that may confound results.

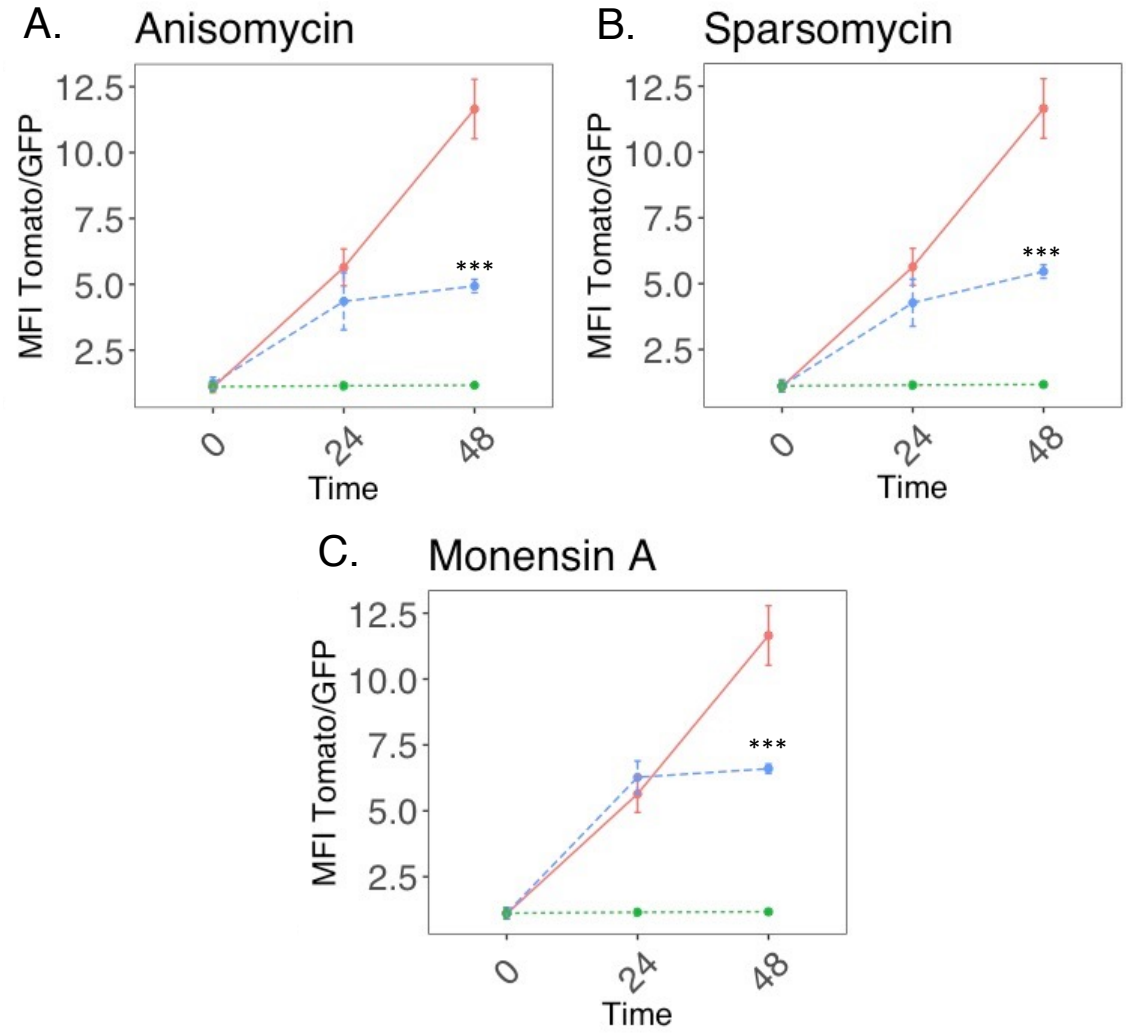

Figure 3.2.7. Determination of false activator activity in subsequent rescreening (A-C) HEK293T dFLASH-HIF reporter activity at 0, 24 and 48 hours after 1mM of DMOG and 50μM compound treatment for the **Cat. 1** compounds. DMOG (Red) and DMSO (Green) controls are shown for comparison (n =3). Significance assessed by one way ANOVA against DMOG controls with Welch's correction and Dunnett's post-hoc test (*p<0.05, **p<0.01, ***p<0.001).

Cat. 2 & Cat. 3:

Overall, the **Cat. 2** and **Cat. 3** compounds replicated the activity we observed in our initial screen, where they inhibited the expression of the reporter to a significant degree at the 24- and 48-hour time points.

The **Cat. 2** structures at 50μM significantly downregulated the reporter ($p < 0.001$) at 24 and 48 hours (**Figure 3.2.8**) in alignment with the screening data. Interestingly, at 0 hours, Emamectin B1a (**Figure 3.2.8F**) produced a significant change compared to DMOG. This was unexpected and suggests that Emamectin B1a did interfere with reporter output non-specifically. The rapid increase meant that it was unlikely to be a HIF-1α mediated response, as we previously only detected HIF-1α-mediated changes after 6 hours. Follow-up analysis of blank media spiked with compound did confirm it was weakly auto-fluorescent.

The bioactive **Cat. 3** compounds downregulated the reporter significantly ($p < 0.001$) relative to the DMOG control (**Figure 3.2.9C-E**) while there was no consequential inhibition observed for the two negative controls (**Figure 3.2.9A, B**). There was a small decrease in Tomato/EGFP for the THQ negative control (**Figure 3.2.9B**), however, while significant, that decrease is not large especially when compared with the observed inhibition from the other **Cat 3** compounds. Like Emamectin B1a, FUME had elevated reporter activity at the 0-hour time point. The increase is only observed for FUME and not the other closely related inhibitors, therefore, this appears to be FUME specific and, again like Emamectin B1a, there is no increase in reporter activity in response to DMOG treatment for these cell populations.

Two compounds, FUME and Emamectin B1a, had elevated activity at 0 hours through an undefined cause but their reporter cells did not increase activity over the course of the assay. Emamectin B1a treatment had cellular toxicity at and above 15 μM in a human bronchial epithelial cell line[276]. Their auto-fluorescence may explain the elevated 0-hour time point, although the period is very short between treatment and imaging. These compounds were included in downstream analysis, despite this

activity, as Emamectin B1a and FUME met all the screening thresholds and EGFP expression across replicates did not change more than 3SD relative to DMOG control cells.

Another important observation is **Cat. 2** and **Cat. 3** compounds (**Figure 3.2.8, Figure 3.2.9**) cause reporter activity to decrease to the same level of the vehicle control. This can be indicative of two potential outcomes, either the HIF-1α pathway is being effectively suppressed by the activity of these compounds in a way that isn't impacting the viability of cell culture, or the activity of the compounds is preventing the action of DMOG to activate the HIF-1α pathway.

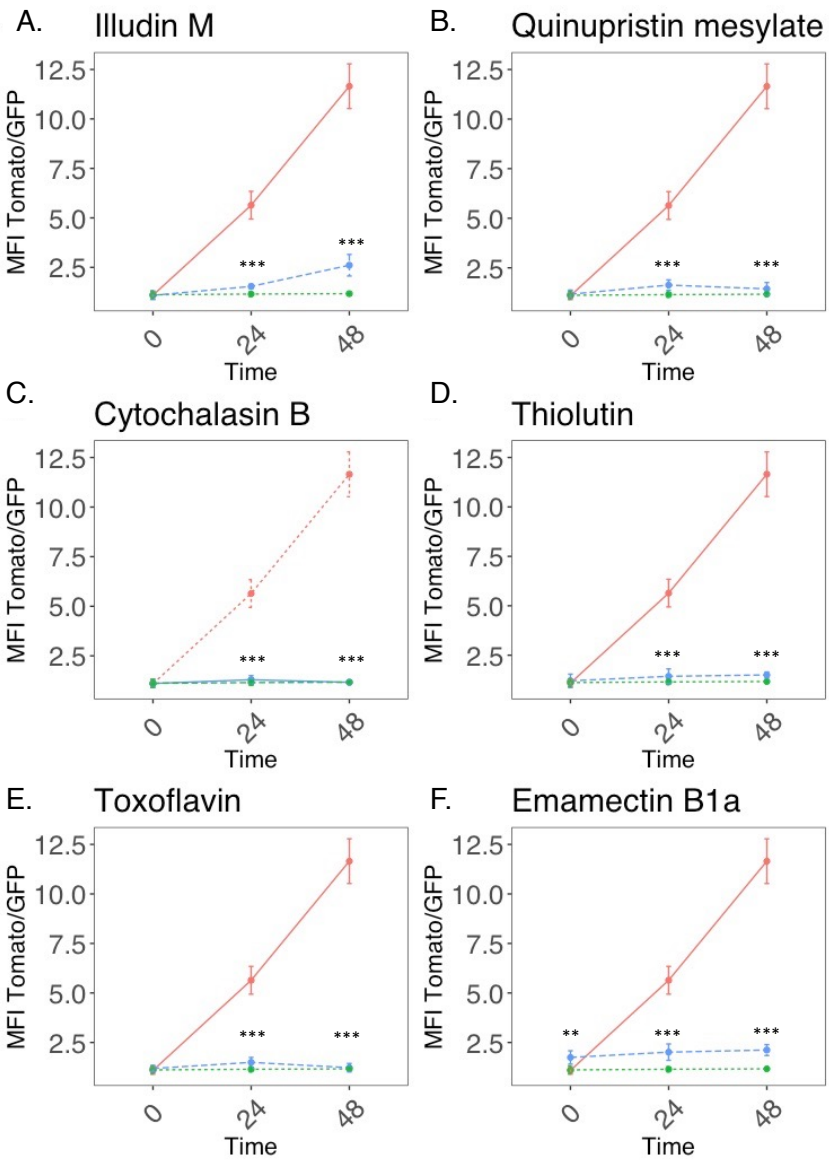

Figure 3.2.8. Rescreening of most potent hits from the Bioaustralis screen
(A-F) HEK293T dFLASH-HIF cells at 0, 24 and 48 hours after simultaneous treatment of 1mM of DMOG and 50μM of the putative **Cat. 2** inhibitors from the screen in **Figure 3.2.2** (Blue), and DMOG (Red) and DMSO (Green) controls (n =3). Error is standard deviation. Significance assessed by one way ANOVA against DMOG controls with Welch's correction and Dunnett's post-hoc test (*p<0.05, **p<0.01, ***p<0.001).

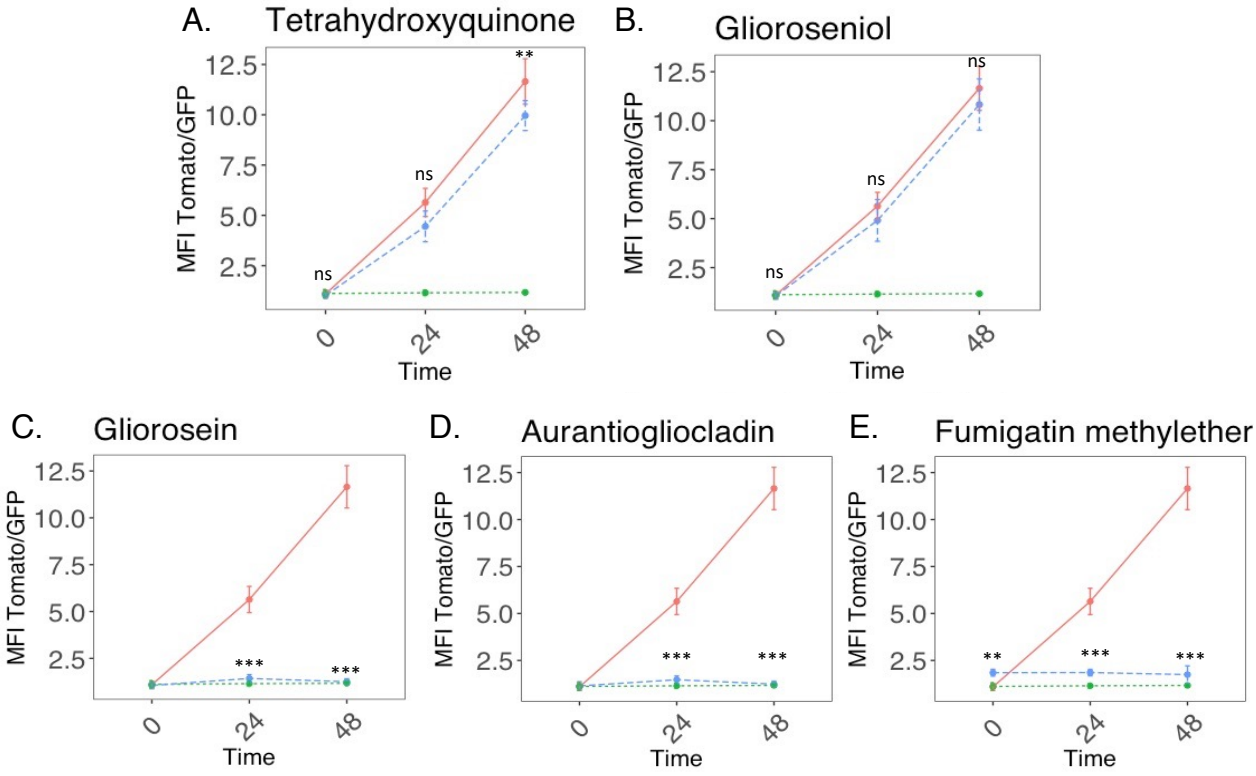

Figure 3.2.9. Rescreening of structurally similar hits identified from initial Bioaustralis screen.

(A-E) HEK293T dFLASH-HIF cells at 0, 24 and 48 hours after simultaneous treatment of 1mM of DMOG and 50μM of **Cat. 3** compounds from the screen in **Figure 3.2.2** (Blue), DMOG (Red) and DMSO (Green) controls (n =3). (A, B) are negative control compounds and (C-E) are putative inhibitors. Error is standard deviation. Significance assessed by one way ANOVA against DMOG controls with Welch's correction and Dunnett's post-hoc test (*p<0.05, **p<0.01, ***p<0.001).

VHL Knockout line reveals that inhibitors block DMOG-dependent HIF-1α induction

The inhibitors from **Cat. 2** and **Cat. 3** had consistent inhibition against DMOG-stimulated HEK293T dFLASH-HIF. DMOG is cleaved intracellularly[277] to compete with 2-OG binding to block the action of 2-oxoglutarate dioxygenases. Therefore, it was imperative that we confirmed these compounds could inhibit HIF-1α and not block the action of DMOG. To do so we counter-screened the compounds at 10μM, 25μM and 50μM against a HEK293T dFLASH-HIF monoclonal line with the Von Hipple Lindau (VHL) complex knocked out (VHL KO dFLASH-HIF) and imaged at 24- and 48-hours, consistent with the original screen. As VHL controls ubiquitination of HIF-1α prior to degradation (**Figure 3.2.10A**), the VHL KO stabilises HIF-1α at normoxia (**Figure 3.2.10B,C**) which in turn constitutively upregulates the reporter. Importantly, in HEK293T cells this reporter readout is only for HIF-1α as HEK293Ts do not express HIF-2α[229].

Cat. 2:

Only two **Cat. 2** compounds, Thiolutin and Emamectin B1a, had a sizable decrease on HIF-1α-dependent Tomato MFI expression and one compound, Toxoflavin, had a small decrease in Tomato MFI (**Figure 3.2.11D-F**). 10μM of Emamectin B1a caused a massive spike in EGFP relative to all other compounds, suggesting a strong off-target interference effect. The other three compounds, Illudin M, Quinupristin mesylate and Cytochalasin B (**Figure 3.2.11A-C**), did not inhibit HIF-1α-dependent Tomato MFI expression. Declines in the Tomato/EGFP ratio for **Cat. 2** compounds are due to compound-induced changes on EGFP expression. For example, Thiolutin (**Figure 3.2.11D**) decreases Tomato expression for all three concentrations at 24 and 48 hours but also has a similar decline in EGFP expression at 48 hours, indicating a loss of specificity for the HIF-1α reporter and a more general off-target effect. The decline in the EGFP reporter expression, that was not seen previously, coupled with no compound decreasing Tomato MFI without changing the EGFP reporter considerably leads to the conclusion that these compounds are not real HIF-1α inhibitors. Instead,

it is more plausible that they were blocking the action of DMOG in upregulating reporter expression than halting HIF-1α function.

Cat. 3

The negative controls, Glioroseinol and THQ show no change on the Tomato reporter expression relative to the non-compound controls, with the decreased Tomato/EGFP at 48 hours (**Figure 3.2.12A, B**) caused by a slight EGFP increase. This is consistent with the result of the prior assay, where neither compound inhibited DMOG-induced reporter activity. This supports the use of the VHL KO as an orthogonal screen as the negative controls behave as expected in this cell line.

Importantly, there is no decline in Tomato MFI close to what was observed for the prior assays for the three putative **Cat. 3** inhibitors. At 50μM there is some decline in Tomato MFI for Gliorosein and FUME while AGC decreased Tomato MFI to a small degree at 25μM and 50μM. These small changes are alongside noisy EGFP readings for cells treated with these compounds from 24 to 48 hours. AGC and FUME at 25μM increase EGFP expression, again not something observed prior, while decreasing EGFP at 50μM relative to the other compounds. Gliorosein at 50μM has an elevated EGFP reading that then changes to a lower-than-expected reading at 48 hours. These changes cause considerable variability in the Tomato/EGFP ratio, which in VHL-positive cells was consistently near background levels. This suggests these compounds may have a similar mode of action to the **Cat. 2** compounds, whereby these block HIF-1α activation by DMOG rather than inhibiting HIF-1α directly.

Overall, the **Cat. 2** (**Figure 3.2.11**) and **Cat. 3** compounds (**Figure 3.2.12**) did not greatly inhibit Tomato expression from the VHL KO reporter. This (1) contrasts with prior results that show consistent downregulation of reporter activity and (2) mechanistically suggests the inhibitors are blocking DMOG's ability to upregulate the reporter and disrupting normal cell function rather than specifically targeting the HIF-1α pathway.

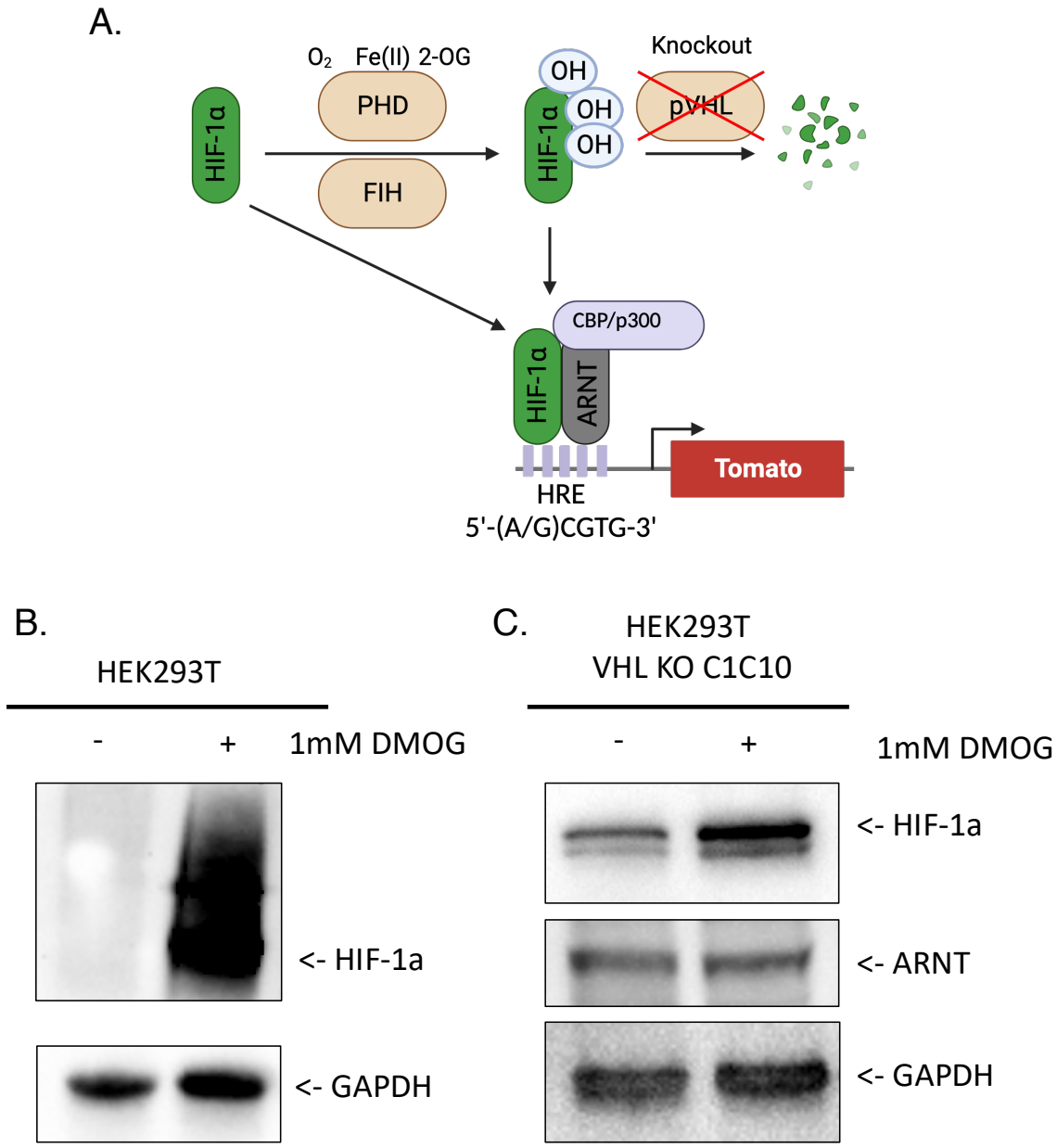

Figure 3.2.10 VHL knockout in HEK293T dFLASH-HIF cells resulted in constitutive HIF-1α expression.
(A) Deletion of the Von Hipple Lindau complex (VHL), which mediates the PHD-dependent degradation of HIF-1α in the presence of oxygen, 2-oxoglutarate (2-OG) and iron, leads to stabilised HIF-1α under Normoxia and constitutive HIF-1α activity.
(B) Immunoblot of HEK293T line showing DMOG-dependent HIF-1α induction under normoxic conditions. Representative of three independent experiments.
(C) Immunoblot of the VHL knockout HIF reporter cell line at normoxia, shows stabilised HIF-1α in the vehicle control compared with 24-hour 1mM DMOG treatment with no impact on ARNT or loading control GAPDH. Representative of 2 independent experiments.

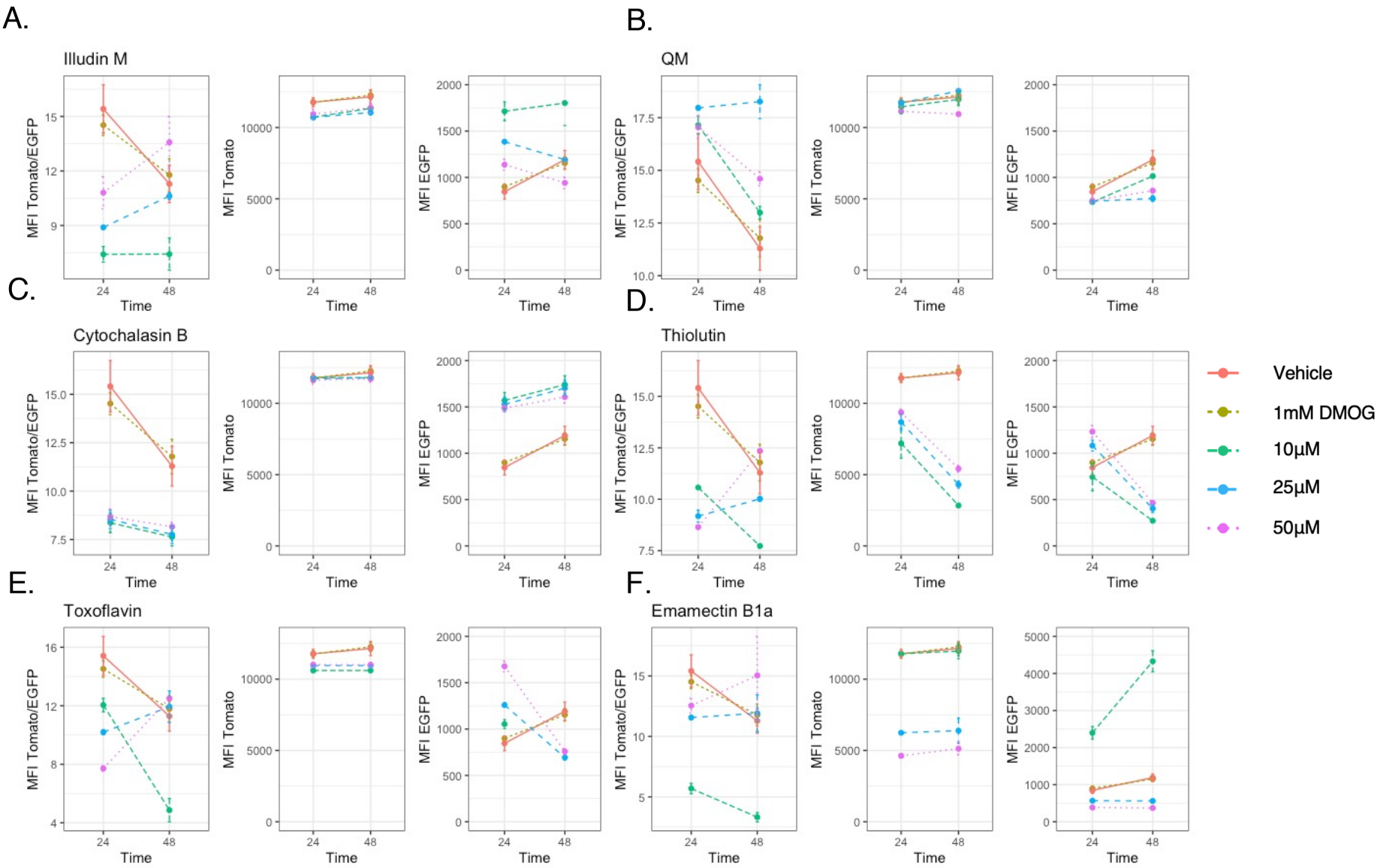
A.
Illudin M
B.
QM
C.
Cytochalasin B
D.
Thiolutin
E.
Toxoflavin
F.
Emamectin B1a
MFI Tomato/EGFP
MFI Tomato
MFI EGFP
Time
24
48
Vehicle
1mM DMOG
10μM
25μM
50μM

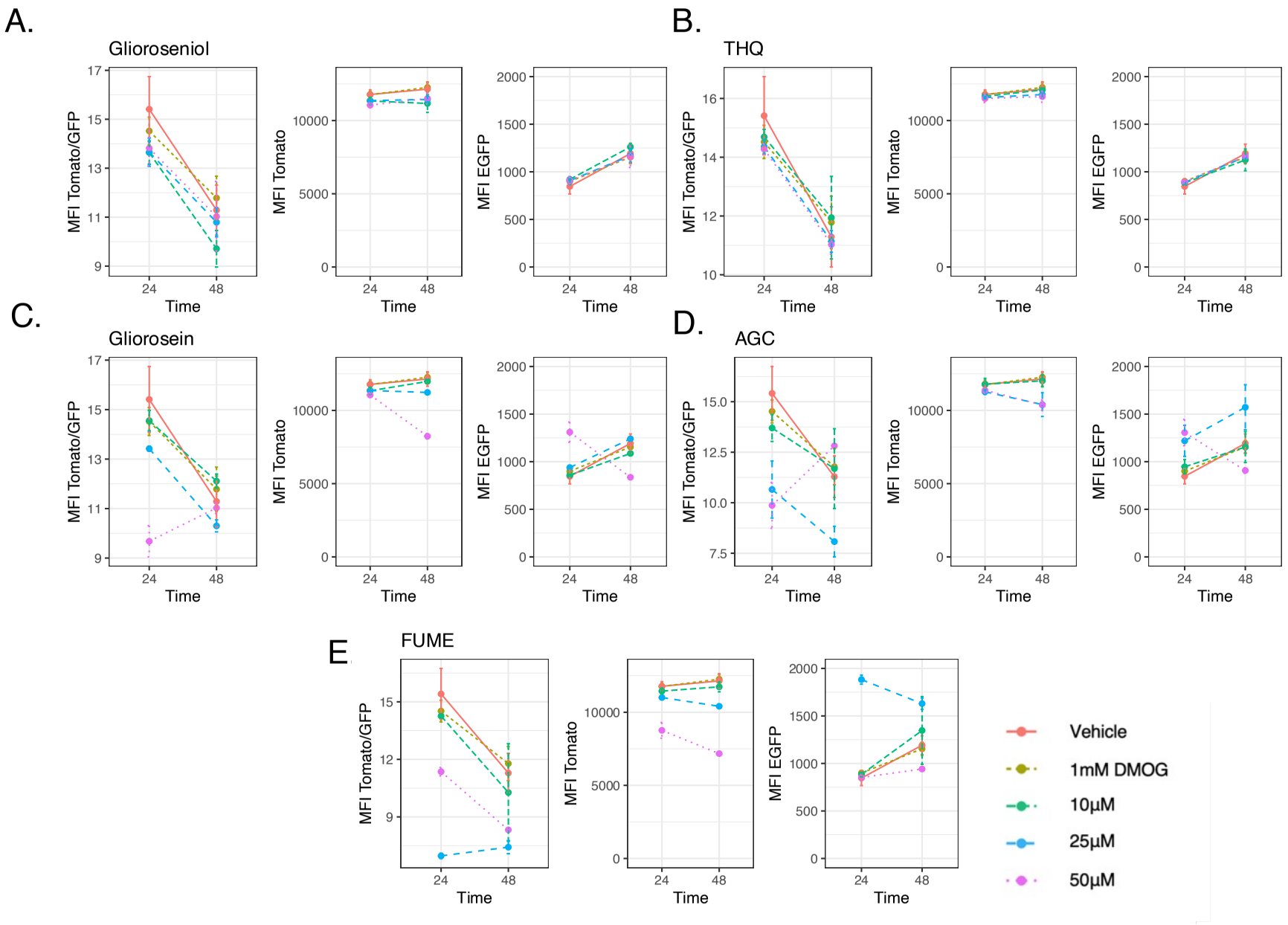
A.
Glioroseniol
B.
THQ
C.
Gliorosein
D.
AGC
E
FUME
MFI Tomato/GFP
MFI Tomato
MFI EGFP
Time
24
48
Vehicle
1mM DMOG
10μM
25μM
50μM

Figure 3.2.11. Cat. 2 compounds do not inhibit VHL KO dFLASH-HIF cells
(A-F) HEK293T dFLASH-HIF cells with VHL KO were imaged by HCI at 24 and 48 hours after treatment with 10μM (green), 25μM (blue) and 50μM (pink) of the **Cat. 2** compounds relative to 0.1% DMSO vehicle (red) and 1mM DMOG (yellow) control. Data is mean ±SD of two independent experiments.

Figure 3.2.12. Cat. 3 inhibitors do not inhibit Tomato MFI expression
(A-E) HEK293T dFLASH-HIF cells with VHL KO were imaged by HCI at 24 and 48 hours after treatment with 10μM (green), 25μM (blue) and 50μM (pink) of the (A, B) negative controls and (C-E) putative inhibitors of the **Cat. 3** compounds relative to 0.1% DMSO vehicle (red) and 1mM DMOG (yellow) control. Data is mean ±SD of two independent experiments.

Gliorosein causes considerable cytotoxicity at the prior time points

The unexpected behaviour of these compounds in the counter screen meant that we wanted to assess if these compounds were having a deleterious impact on the reporter cells. Mechanistically, it appears as though these compounds block DMOG's activity *in cellulo* rather than HIF-1α, given they don't inhibit the Tomato reporter in the VHL KO cell line. Therefore, we questioned if these compounds had a cytotoxic effect that we weren't able to detect in our current screening pipeline. We have used EGFP as a control in a prior successful screen for HIF modulators and used it to successfully exclude several interfering compounds (such as the **Cat. 1** compounds). However, it provides a constitutive transcriptional readout that encodes a bright EGFP who's destabilisation may not fully reflect cell viability.

To assess the possibility that the **Cat. 3** compounds impact cellular viability we treated HEK293T cells, the parent line for both dFLASH-HIF and the VHL KO cell line, with 50μM of the negative control Glioroseinol and closely matched lead compound Gliorosein, given the latter decreased both Tomato and EGFP in the VHL KO line. Cell populations were assessed for viability by cell counts with live dead staining at 24 and 48 hours after treatment (**Figure 3.2.13**). Glioroseinol had no negative impact on cellular viability at 24 and 48 hours. Glioroseinol has been used as a negative control in prior experiments this is consistent with seeing no effect of this compound on our reporter cell lines in prior assays. Gliorosein however saw a 29.9% drop in cellular viability compared with Glioroseinol, its closest structurally similar negative control (**Figure 3.2.13A**). Additionally, after 24 hours of growth there was large decline in the number of live cells within the Gliorosein-treated population compared with controls. We could not separate the activity of this toxic compound (Gliorosein) and a legitimate lead compound by activity on the dFLASH-HIF reporter output alone. It also implies the structurally related compounds, FUME and AGC, are likely toxic as well as they resulted in similar reporter outcomes. Unlike more traditional target-discovery approaches that utilise luciferase reporter assays however, we utilised High Content Imaging, an approach that we can potentially leverage for higher quality lead compound selection.

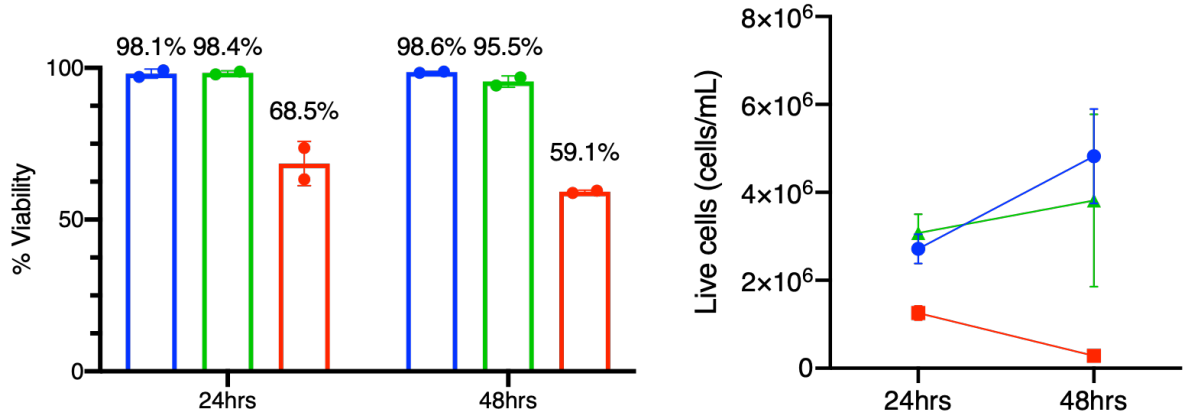

Figure 3.2.13. Gliorosein has significant toxicity compared with negative control Glioroseinol.
HEK293T cells were seeded identically at 1x10^6 cells/mL then treated with a DMSO negative control (blue), 50μM of negative control Glioroseinol (green) and 50μM of Gliorosein (red) for 24 and 48 hours. (A) Viability and (B) total cell counts were performed using at these time points (n = 2) using Live/Dead staining. Data is means of two biological replicates, means and standard deviations are shown.

High content imaging facilitates integration of cellular morphology in profiling chemical-dependent phenotypes

High content imaging platforms are integrating more advanced methods of categorising cellular morphologies within a tissue culture setting. This has been increasingly used in screening on a phenotypic level[278]. Identification of cellular features has been used to discern abnormal phenotypes in high throughput protocols. For example, Rohban, et al. [279] artificially expressed 220 genes with different functionality and used detectable morphological signatures induced by this overexpression to capture known gene and morphological change correlations. Additionally, Hasle, et al. [212] used only nuclear shape as a filter for alternate gene expression profiles associated with paclitaxel resistance on a single-cell basis, validating that nuclear morphology can reflect fundamental changes in molecular processes. We therefore began investigating if this would allow for us to detect false positives or confounding compounds within our primary screening data alongside assay of our control gene.

Evaluating if nuclear shape can be used for better hit weighting for integration into dFLASH-HIF screening pipelines

Given that nuclear morphology has been previously assessed in many cell lines as a predictor of senescence or apoptosis[280-282] we looked at what metrics we might capture regarding nuclear shape given our EGFP and Tomato act as proxies for nuclear stains. As part of the imaging process, we capture four main metrics of nuclear shape in our original screening data (**Figure 3.2.14**): (1) nucleus area, (2) nucleus size, (3) length to width ratio of the nucleus (also known as nuclear aspect), and (4) perimeter to area ratio, which is a measure of nuclear sphericity or roundness. While area and size are co-dependent, their similarity enables us to confirm consistency in our analysis approach. These metrics have been previously used in morphology assessments and used to generate nuclear irregularity indexes[282] for detection of cellular senescence.

The DMOG and DMSO treated controls for nuclear area and size (**Figure 3.2.14A, B**) were slightly elevated compared with most compound treated wells, however many of the identified putative inhibitors increased nuclear size and area above the controls and most compounds 25% above the average of the DMOG controls. There are more pronounced differences between the controls and the identified hits when measuring the perimeter to area ratio (**Figure 3.2.14D**) and nuclear aspect (length/width ratio of the measured nuclei) (**Figure 3.2.14C**).

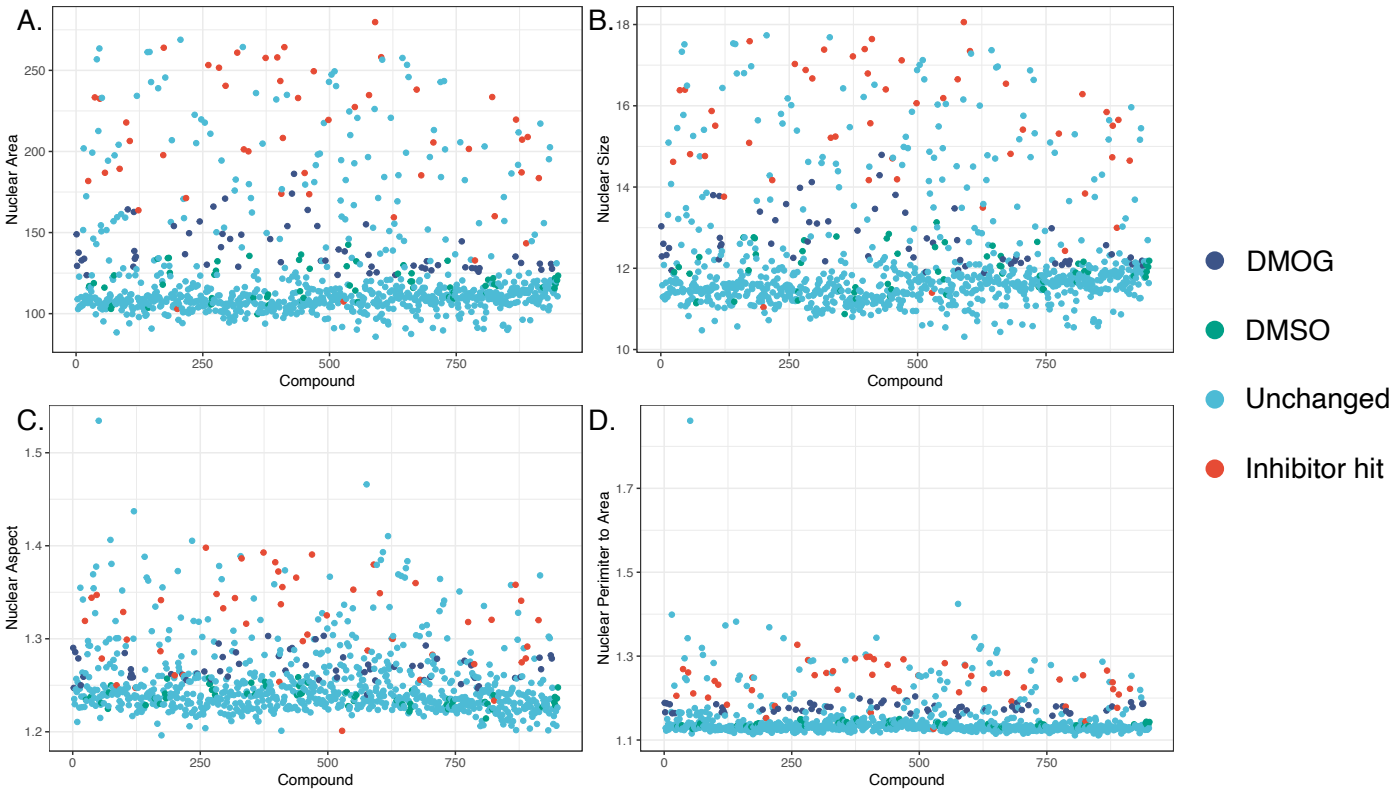

Figure 3.2.14. Breakdown of individual nuclear measurements from the Bioaustralis library
Averages of the 2000 cells per well analysed for control and compound wells from the Bioaustralis library for 4 nuclear shape metrics: (A) Nuclear area (B) Nuclear size (C) Length to Width ratio of the nucleus and (D) The perimeter to area ratio (P2A) of the nucleus. DMSO control (purple), DMOG controls (green), inactive compound wells (light blue) and inhibitor hits (red) are shown for every metric.

Nuclear parameters can be used to "score" cellular populations

To analyse these differences more in depth, we collapsed these measurements into a single output that would allow us to visualise if there was a meaningful overperformance of the inhibitor hits compared with the controls. The presence of so many inhibitors changing the size of the nuclei, and our efforts above in failing to successfully confirm activity, suggested that morphology may be used as a predictor of toxicity prior to screening efforts. Indeed, similar approaches and gating of nuclear size have been previously employed, as apoptosis or necroptosis can alter nuclear size [243,283], thus nuclear size gating can potentially decrease false positives.

We used Principal Component Analysis (PCA)[284] to project the combined output of these 4 measurements into 2D space (**Figure 3.2.15**). To differentiate compounds that differ from the controls and what we can define as a "normal" nuclear shape we scored these hits based on proximity to the controls and, due to the Z score normalisation, sit closest to 0 for the principal coordinates. This thresholding is indicated by the boxes in **Figure 3.2.15**. Populations that fell in the smallest box were considered closest to normal therefore scored highest, hits that fell in the second smallest box were then scored lower and so forth. The box sizes were scaled linearly out from the area of the first box that captured the bulk of the population. This allowed us to score all cell populations in an unbiased fashion.

Having weighted the nuclear shape of the compounds we then looked to see where the selected hits, that were false positives, scored against these parameters (**Figure 3.2.16**). Most of the selected hits (dark blue) scored less than 6, where some DMSO and DMOG controls sat at 24 hours. At 48 hours, with few exceptions, all controls were scored as 7. Of note there are two distinct population clusters, a set of compounds that scored <3, indicating abnormal nuclei, and those that scored >4, clustering closely to the bulk of the wells and controls. This indicates that our current nuclear threshold could be used to exclude those compounds from downstream analysis, under the assumption that radically different nuclei is indicative of cellular toxicity. This in turn would remove several of the selected compounds, based on our initial thresholding, which turned out to be non-specific interfering compounds.

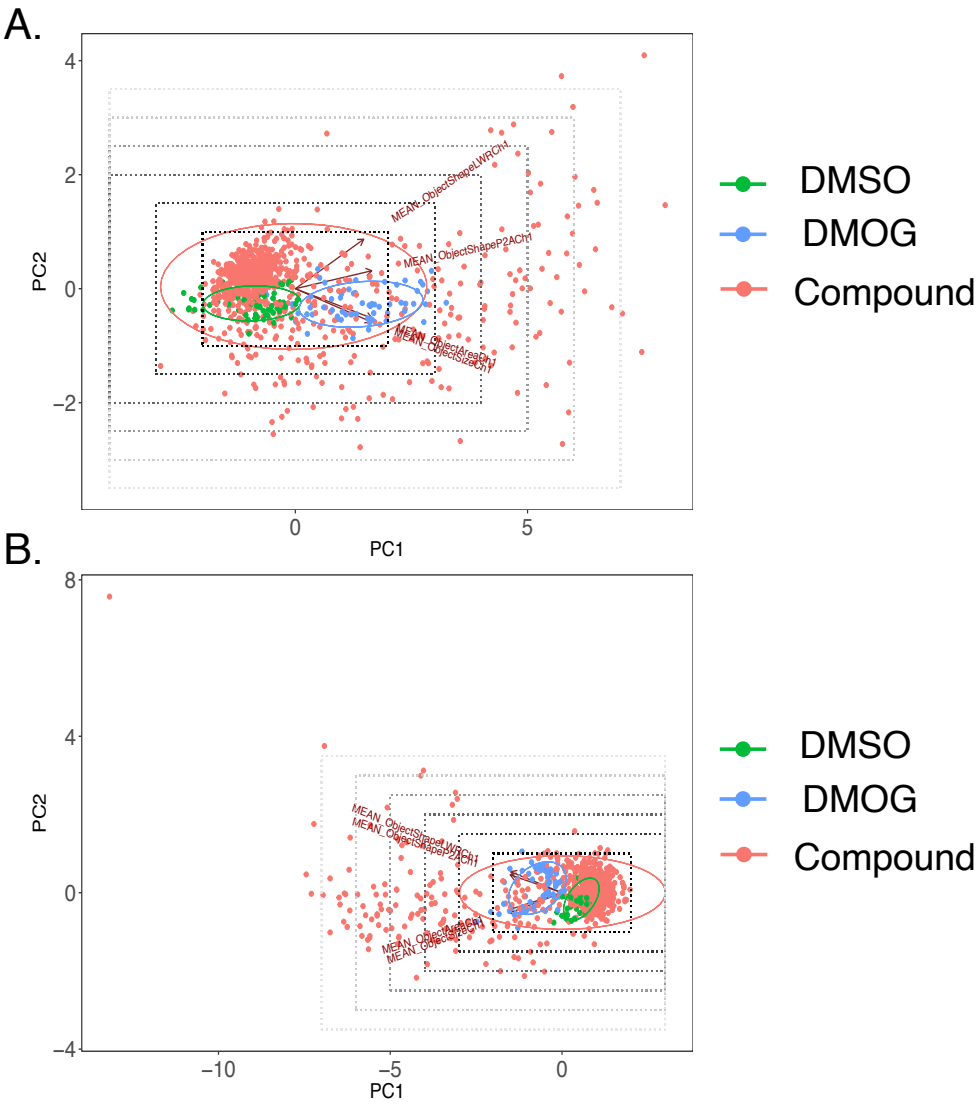

Figure 3.2.15. Unbiased weighting of compounds based on nuclear shape parameters compared with controls.
PCA plots of the 4 nuclear features from the (A) 24 hours and (B) 48 hours from the small molecule screen in **Figure 3.2.2**. Weighting scheme was then applied to these PCA plots (C, D), where the black and grey denote the linearly decreasing scoring (smallest box = 7, largest = 1) of nuclear size compared to many of the compounds. Ellipses represent the 95% confidence interval for the respective population.

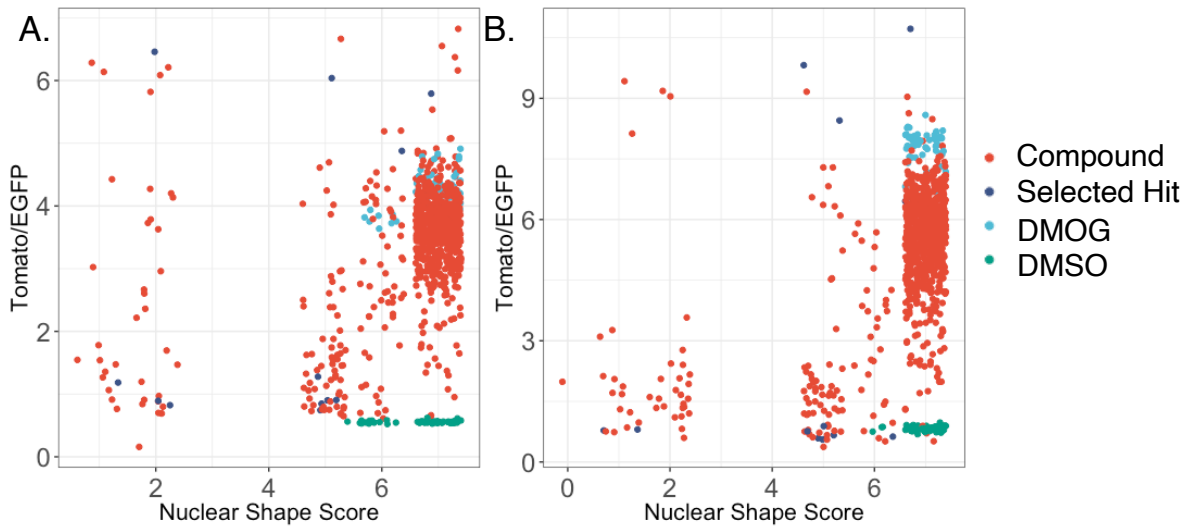

Figure 3.2.16. Most wells score highly nuclear shape parameters, enabling identification of a subset of low-scoringabnormal nuclei with decreased reporter expression.

Nuclear shape scores of compounds from **Figure 3.2.15** for (A) the 24 hour and (B) 48-hour time points scored from most abnormal (1) to most normal (7) against unnormalized Tomato/EGFP values from the original library screen (**Figure 3.2.2**). Red indicates wells treated with compounds; dark blue are compounds that were selected for subsequent rescreening based on our original hit criteria. DMSO (green) and DMOG (light blue) controls are also shown.

We also looked to see if there was a time-dependent changes in nuclear shape. We'd expect some fluctuations, given the live cell environment and normal cell-cycle changes in nuclear morphology, however that might not appear at the population level, as the data is representative of 2000 individual cells., Some compound-treated populations appear to be changing more significantly between 24 to 48 hours than others. Therefore, we compared these nuclear scores against the Z-scored Tomato/GFP ratios for the 57 compounds that were identified as hits against our original criteria (**Figure 3.2.17**).

We set a cut off (**Figure 3.2.17**) of a nuclear shape score (NSS) of 5 (out of 7) and a Z score of -2 and assessed these compounds for changes in nuclear score between 24 and 48 hours. 3 of the 11 chosen compounds (Illudin M, Emamectin B1a and Thiolutin) failed to meet those criteria for at least one time point and a fourth, Cytochalasin B, saw a change in score between 24 and 48 hours. Additionally, only 26 of the 57 compounds (45.6%) met the criteria at one time point and 11 (19.6%) met the cut off criteria at both time points. 7 of those 11 compounds were not chosen as part of our initial rescreening set. Interestingly, Gliorosein, and the closely related structure AGC, met the selection criteria at both time points, which suggests that while this filter removed many potential hits it is limited in how it can infer mechanism. Despite that, this filter removes some compounds that were found not to function in retesting, therefore supporting the use of the nuclear filter in future experimental workflows with the dFLASH system as it can provide a valuable addition to the lead selection process.

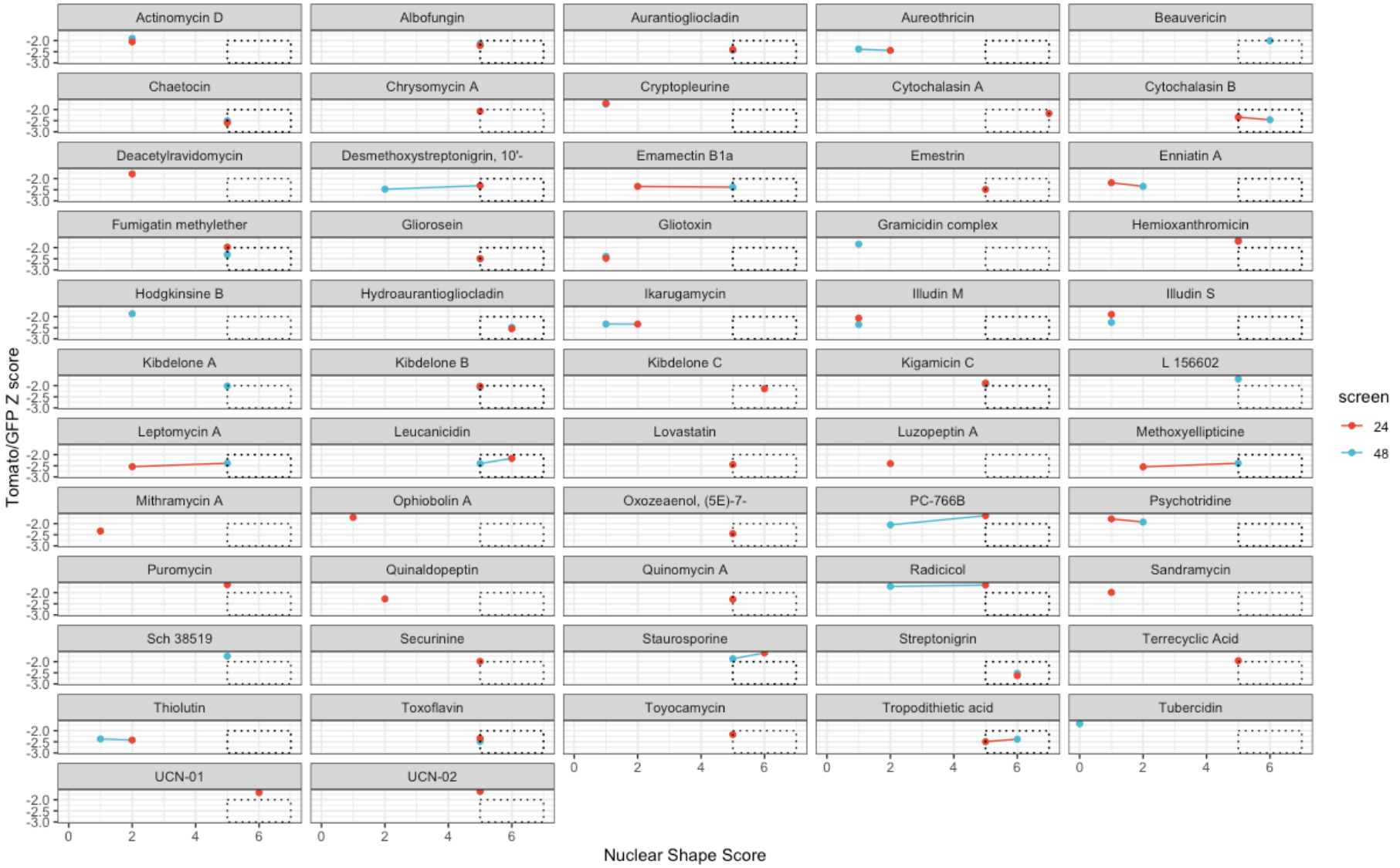
Actinomycin D
Albofungin
Aurantioglioclad in
Aureothricin
Beauvericin
Chaetocin
Chrysomycin A
Cryptopleurine
Cytochalasin A
Cytochalasin B
Deacetylravidomycin
Desmethoxystreptonigrin, 10'-
Emamectin B1a
Emestrin
Enniatin A
Fumigatin methylether
Gliorosein
Gliotoxin
Gramicidin complex
Hemioxanthromicin
Hodgkinsine B
Hydroaurantioglioclad in
Ikarugamycin
Illudin M
Illudin S
Kibdelone A
Kibdelone B
Kibdelone C
Kigamicin C
L 156602
Leptomycin A
Leucanicidin
Lovastatin
Luzopeptin A
Methoxyellipticine
Mithramycin A
Ophiobolin A
Oxozeaenol, (5E)-7-
PC-766B
Psychotridine
Puromycin
Quinaldopeptin
Quinomycin A
Radicicol
Sandramycin
Sch 38519
Securinine
Staurosporine
Streptonigrin
Terrecyclic Acid
Thiolutin
Toxoflavin
Toyocamycin
Tropodithietic acid
Tubercidin
UCN-01
UCN-02
-2.0
-2.5
-3.0
0
2
4
6
Tomato/GFP Z score
Nuclear Shape Score
screen
24
48

Figure 3.2.17. Hit refinement utilising reporter activity against nuclear shape weighting.
Inhibitor hits from 24 hours (red) and 48 hours (blue) the Bioaustralis screen (**Figure 1**) and changes between the time points, indicated by the line, are plotted against the nuclear scoring from **Figure 13**. Hit cut off is a nuclear score > 5 and Z score < -2 (black box).

Nuclear filter assessment supports the discovery of the novel HIF-1α inhibitor

We next checked if this filter would work when applied to our other inhibitor screen (**Quinn library, Chapter 3.1.1**) that identified a transcriptional inhibitor of HIF-1α. The PCA plots for the same metrics from the Quinn library screen are similar to those from the Bioaustralis screen (**Figure 3.2.18A, B, Figure 3.2.15**). There are some outlier DMOG-treated populations in the 24-hour time point (**Figure 3.2.18B**) but the ellipses, which represent 95% confidence intervals, are centred toward the middle of the PCA plot suggesting these to be edge cases.

The compound-treated wells cluster into two distinct bins, the compound populations that have an NSS>4 and those that have an NSS<3 at both time points (**Figure 3.2.18C, D**). This is identical to what we observed earlier with the Bioaustralis screen compounds with this filtering method (**Figure 3.2.16**). This supports the exclusion of compounds that have an NMS<3. Interestingly, there are less abnormally detected nuclei at 36-hour screen than the 24-hour screen, indicating that there may be a time-dependent effect from certain compounds.

Finally, we then looked to see how our identified inhibitor, RQ500235, performed against this scoring metric. In both the 36-hour (**Figure 3.2.18C**) and 24-hour (**Figure 3.2.18D**) RQ500235 had an NSS of 7. There were 3 putative inhibitors out of 25 at 36-hours and 2 putative inhibitors at 24 hours that were previously identified as not changing EGFP relative to controls, at 24-hours that had an NMS<3. This suggests that the EGFP filtering was largely effective at removing interfering compounds however, it also shows that NMS filtering can assist in lead refinement. Additionally, when selecting between similarly scoring hits for lead assessment, NMS ranking, in this case, would favour selection of a real HIF-1α inhibitor.

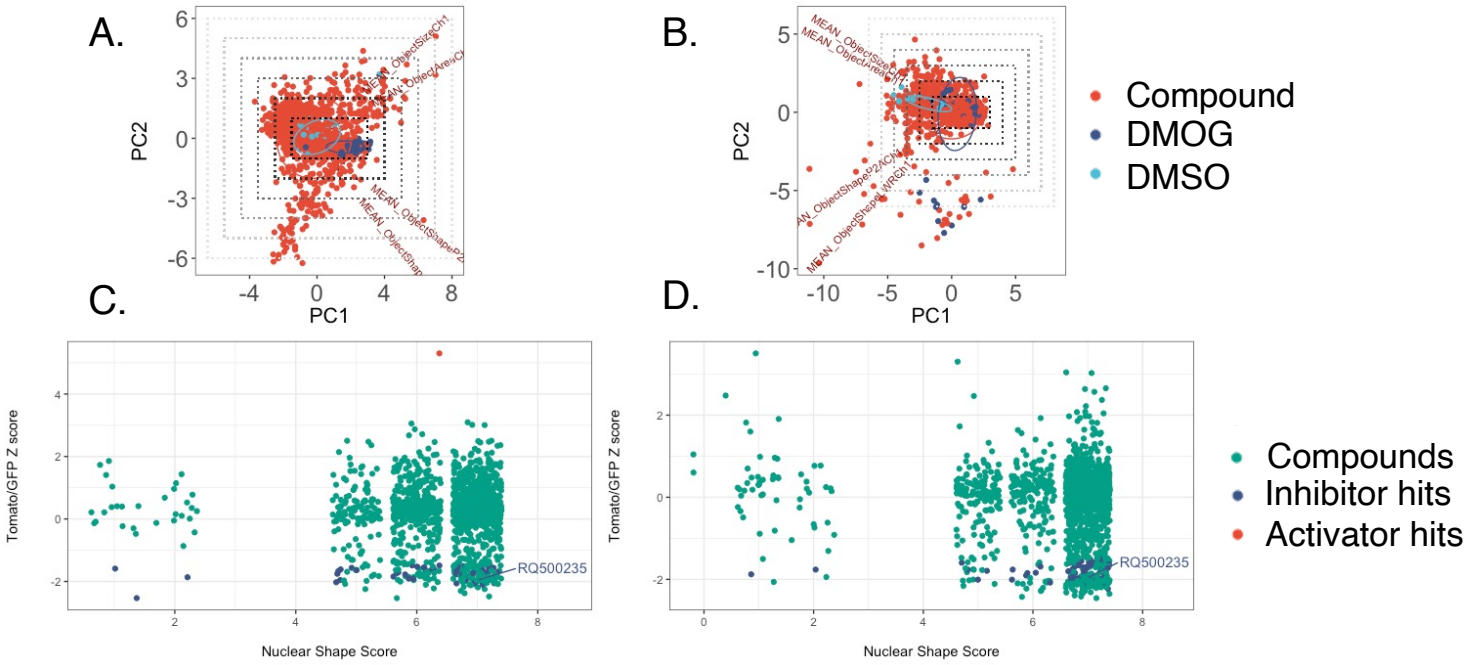

Figure 3.2.18 Nuclear shape scoring on the Quinn library inhibitor screen would further help hit refinement and validates RQ500235 selection as a lead compound.

The pilot inhibitor screen (from **Chapter 3.1**) was used to confirm the use of the nuclear filter for hit discovery. (A, B) PCA biplots of the (A) 36 hour and (B) 24-hour inhibitor screens with the same thresholding approach as the Bioaustralis screen (**Figure 3.2.15**) were used to determine nuclear normality. The Z scored Tomato/EGFP output from cell populations were then compared against the nuclear shape score for the (C) 36 hour and (D) 24-hour screen. Populations are classified based on their original screening criteria as inert compounds (green), putative activators (red) and putative inhibitors (blue). Position of RQ500235, the novel inhibitor, is indicated for both time points.

Discussion:

Improvements to the screening pipeline and revealed shortcomings in prior approaches

The drug discovery pipeline that we pursued in the investigation of this Bioaustralis screen was heavily dependent on the dFLASH system, as we previously demonstrated its robustness and pathway-specific nature (**Chapter 3.1**). Our screening strategy was similar in concept to that described by the Inglese group [176,285,286]. It consisted of an initial screen to look for HIF-1α inhibitors in the presence of DMOG, an approach we had prior success with in identifying a HIF-1α inhibitor from the Quinn library. Importantly, we had an independent EGFP transcriptional control that filtered compounds that changed the EGFP intensity beyond 3 standard deviations from that of control EGFP expression, which was highly consistent across plates. Evaluating both the Tomato MFI and EGFP MFI separately and as a ratio generated a list of 35 hits across both 24 and 48 hours and enabled us to discount potential, but false positive, "super-activators" of HIF-1α (**Figure 3.2.3**). Then we sought to confirm the initial screen results across three independent replicates under the same screening conditions and concentrations with measurements at 0, 24 and 48 hours to establish kinetic profiles for the putative inhibitors (**Figure 3.2.7-3.2.9**). Then we sought to evaluate these compounds against an orthogonal screening approach that utilised a VHL KO (**Figure 3.2.10-3.2.12**). The conflict between the prior screening line data and lack of performance with the orthogonal screen informed us that our selection of lead compounds was poor and did not provide specific activity against the biological process we were targeting.

The deployment of an orthogonal screen aims to differentiate compounds that have a direct impact on the target pathway or are having an off-target effect [285]. The orthogonal screening with the VHL KO (**Figure 3.2.10-3.2.12**) suggested the reported chemical effects from the lead compounds to be from interference of the chemical induction of our reporter, accompanied by potential toxic side effects as seen for Gliorosein (**Figure 3.2.13**). As a result, the conclusions that we can draw from this are that (a) our follow-up validation assays with concentration repeats and the VHL KO

orthogonal screen appear to accurately eliminate interfering compounds and (b) these compounds passed our pre-existing criteria, where large changes in EGFP were the sole readout for toxic or off-target effects. Therefore, we demonstrate that a dFLASH pipeline can be robust in removing interfering compounds but also that our current approach is unable to recognise these compounds prior to a re-screening phase.

Selection of the VHL KO as the orthogonal screening assay was due to several considerations. VHL acts as the primary ubiquitin ligase for the degradation of HIF-1α [154,287] and knockdowns of VHL are known to drive stabilised HIF expression independent of oxygen concentrations[25] (**Figure 3.2.10**). Therefore, the knockout drives constitutive reporter expression which in turn allows for an inducer-free assessment of the cell-based reporter. DMOG acts as a non-specific hydroxylase inhibitor [131,288] and as a result our output was dependent upon DMOG mode of action not being impacted by the activity of the putative inhibitors. The VHL KO, however, unlike the DMOG screening approaches provides a pre-existing reservoir of HIF-1α and Tomato. If these compounds did interfere with HIF-1α message production, similar to what was reported for PX-478 [166] and RQ500235 which inhibited HIF-1α transcript levels, or interacted directly with the HIF-1α dimer like acriflavine[169] we would expect a decrease in Tomato expression in the VHL KO line. As no consistent changes were observed without matched off-target effects for these compounds over the 48-hour period, they are therefore unlikely to functionally interact with the reservoir of HIF-1α.

This suggests that the biological activity we predicted early on was a consequence of interference from these compounds on our reporter system. This finding is supported by the cytotoxic activity of Gliorosein when compared with Glioroseinol, which suggests that cytotoxicity over the 48-hour period prevents induction of HIF-1α and sufficient transcriptional activation of the reporter in comparison with the vehicle controls. These results and screening pipeline establish that the dFLASH system in conjunction with genomic editing can enable easy generation of orthogonal approaches alongside the primary screening approach for effective pipeline design[286,289]. However, despite the success of the downstream pipeline in capturing

false positives, it may remain possible to increase screen robustness by using the information-rich dataset generated from high content imaging to establish filters, based on factors like cell morphology.

Nuclear morphology as a criterion for higher quality lead selection.

High Content approaches enable categorisation of cellular morphology [290-292] in addition to our particular application, being the capturing of fluorescent protein intensity [293]. As we saw a hit rate of ~4% from our initial screening efforts, we assumed we were filtering out many low-quality hits from the library. As previously mentioned, included within our dataset were measurements of nuclear shape and this allows us to associate activity of compounds with a morphological phenotype comprised of 4 measurements of nuclear shape (**Figure 3.2.14**). Abnormal nuclear shape has been previously suggested to be used as a filter for HTS design[283] as nuclear shape change has been associated with apoptotic pathways, demonstrated by Maria, et al. [294] when assessing apoptotic V79 cell nuclear morphology with TUNEL assays and Feulgen-DNA staining. Similar size-based filters have been applied to large scale, imaged-based screens before. Yan, et al. [243] used similar nuclear measurements to what we describe above to look for regulators of nuclear size in a pooled CRISPR-screen format on a single-cell basis.

It must be noted that many factors can impact nuclear shape [280,281] and by applying an exclusionary nuclear morphology filter, we would be making the presumption that aberrations in nuclear morphology are deleterious to cellular health and are discounting the potential impact of the compound on our HIF pathway. This is supported somewhat in our follow-up analysis, as we do see the selected quinone compounds, including Gliorosein which is known to be toxic (**Figure 3.2.13**), have different nuclear morphology scores to the controls (**Figure 3.2.16**). It may not always hold true however, as nuclear shape is known to be altered by disruption of BRG1, a SWI/SNF chromatin remodelling complex [295,296] that has been linked with HIF signalling[297,298]. As a result, we instead proposed using nuclear morphology as a different weighting parameter to compounds that meet our hit criteria, as in our system the EGFP expression is assessed to exclude compounds that dysregulate

transcription. Additionally, we are evaluating the nuclear shape of 2000 individually nuclei per treated population to control for heterogeneity and cell cycle dependent effects that would be magnified in single-cell analysis done by other screening approaches[243]. Indeed, nuclear morphology analysis and filtering would result in low weighting of compounds we initially considered, based on Tomato and EGFP intensity alone, strong hits and would favour an investigation into alternate compounds.

While traditional reporters are single output for a distinct factor, like a classical luciferase screen [299], by factoring in the Tomato and EGFP intensities, the ratio of their expression and the four measured nuclear dimensions we are able to establish a more detailed criteria of hit selection. Cell phenotypes and reporter outputs have been combined previously, such as in the creation of the ORACL system for categorising similar drug classes by combining cytoplasmic, nuclear and specific protein fluorescent tags in a high content setting[300]. We aim for a similar outcome, whereby we can eliminate compounds that induce abnormal morphology while retaining on-target specificity in single-pass screening attempts. When we investigate the nuclear shape against Tomato/GFP cut offs we find that the majority of compounds (7 of 11) preferentially selected were those not chosen for re-evaluation (**Figure 3.2.17**), however Cytochalasin B, Gliorosein, AGC and FUME met the selection criteria but Emamectin B1a and Illudin M would have been excluded based on these criteria. Finally, we applied this nuclear filter against our validated pilot screen (**Figure 3.2.18**), having pulled out RQ500235 that decreased HIF-1α protein level. We saw a very similar trend to the Bioaustralis screen, with several compounds having a <3 NSS, including some compounds that met our hit criteria. Therefore, we can conclude that the nuclear filter would help remove some false positives and leads to a narrower hit pool.

Future directions and emerging horizons

Future development of these high content screening pipelines and methods will be centred on increasing integration of machine learning features for classification and hit identification. These analyses enable more complete annotation of compound bioactivity when coupled with high content imaging[301,302]. In our current pipeline we

automate the measurements of cellular parameters within each population and use features from that classification to define our outcome, specifically the intensity of reporter fluorescent proteins and, as shown above, are trying to integrate other cellular features for hit sorting. As part of this approach, we generate thousands of images per screen, an example being that for a single 96 well plate with a maximum of 16 “fields” (images) possible per well we have an upper boundary of 1,536 images per plate, across the 10 plates used in the Bioaustralis library screen that equates to a maximum of 15,360 images per time point. This in turn provides a lot of quantitative data that can be further utilised to understand the bioactivity of compounds on the cells through measurements of cell morphology [302], however there is no clear-cut standard for how to integrate these approaches into classical drug discovery efforts. Despite this, there are “trained” models on pre-existing data or there are unbiased discovery methods that can be used to integrate more complex datasets into discovery pipelines.

Deep-learning methods to classify cellular phenotypes down to a single cell level [278] have begun to be used, however can be hampered by requiring training datasets prior to deployment [303]. Therefore, as a computational approach, we favoured using Principal Coordinate Analysis (PCA) to interpret our nuclear measurements and interpret their phenotype [304,305]. This presents an unbiased view and facilitates future upscaling in experimental features through the addition of more detailed measurements. There do remain open questions in how accurate this nuclear morphology filter is at predicting viable hits. While our current data shows that it would have filtered out the current crop of “noisy” compounds, there is no guarantee that the hits it does select through re-weighting would be on-target. What this analysis does offer however, is another metric to classify hits beyond reporter output, and shows there to be a correlation between a change in nuclear size and non-pathway modulators of cellular function. Indeed, PCA analysis of screening data is being more heavily utilised [306] and is the first step toward implementing more advanced machine-learning feature extraction to classify drug hits, and should improve efficiency as feature analysis becomes more complex and the dFLASH system matures as a drug discovery platform.

Chapter 3.3 Leveraging dFLASH to probe for microbiome-mediated TF signalling

The diverse signalling nature of the human microbiome

There are many uncharacterised secondary metabolites, a diverse class of bacterial small molecules which mediate a swathe of biological interactions such as survival and host signalling[307], that are produced by the human microbiome that are important for host-signalling. Consequently, there has been an expansion in functional screening against microbial species and isolates. For example, recently bioactive cell-free supernatants from *Clostridium* were shown to downregulate NF-κB following fractionation of crude supernatants[308]. Identification of proximally located genes that drive production of metabolites are classified as biosynthetic gene cassettes (BGCs) and are considered a primary driver of small molecule diversity in the microbiome[309,310].

In silico prediction of BGCs has identified over 400,000 across microbial species however, only ~2000 have a known associated function, indicative of the untapped synthetic potential of the microbiota[311]. Study of how these BGCs influence host biology in a physiological niche is complicated, as most environments contain multiple species that can cooperatively modulate the metabolome[307,312]. This was demonstrated by Chevrette, et al. [307] whom generated a small three-member commensal community and saw significant shifts in the produced metabolome with the deletion of a single BGC in a single species. Additionally, the microbiome contains a complex enzymatic mileu of potential modifying enzymes that can react with small molecules, adding an extra layer of diversity that cannot easily be predicted[313]. Therefore, the complexity of the human microbiome results in an extremely diverse metabolome that is poorly characterised and has vast signalling potential.

Utilisation of cell-based reporters for functional characterisation of microbial interactions

Because of this complexity, there has been an increase in utilising cell-based bioassay approaches for discovery of novel metabolite interactions with signalling pathways. Prior approaches have lent on expression of BGCs in heterologous organisms, which have met with some success but remove these synthetic components from a cross-

signalling environment[314]. Chen, et al. [192] performed a cell-free supernatant screen with 144 bacterial monocultures isolated from IBD patients against 314 GPCRs in a luciferase-based assay. Similar work was done by Colosimo, et al. [315] where they fractionated bioreactor culture supernatants prior to luciferase screening against GPCRs *in cellulo*. Importantly, these protocols represent a move away from prior approaches that favoured *in silico* detection of BGCs[316,317] , toward unbiased empirical detection of important signalling molecules that arise in the human microbiome. This is advantageous given that there is a predicted large level of redundancy of biosynthetic pathways within the human microbiome[315], poor annotation of the existing microbial metabolome and issues with *in silico* approaches being unable to capture the enzymatic diversity present[144].

Investigating functional TF interactions with the microbiome

Current leading efforts that are focused on deconvolution of microbiome-generated bioactive components utilise reductive experimental pipelines[190-192,318]. This is to combat the complex mixture of signalling metabolites produced by the microbial niche. This reductive approach is exemplified by the generation of monocultures from patient isolates coupled with target-driven discovery efforts[191,192]. While this has been successful in identifying signalling components in forward chemical screens or genotoxic assays, it's predicated on the hypothesis that in disease cases, such as IBD, single species or strains can generate pathogenic components that signal to the host (**Figure 3.3.1**).

While this is valid for some molecular mechanisms, it does narrow and remove the diversity from the metabolome that is representative of what is seen in a physiological setting. By removing individual strains from the collaborative biosynthetic environment[319], the range of produced metabolites is narrowed and thus can fail to detect potentially consequential microbial-host signalling mechanisms. This is due to biosynthetic pathways and gene clusters producing metabolites that cross-signal between species or strains[311] (**Figure 3.3.1**), thereby producing secondary metabolites with host-signalling potential.

As a result, when experimentally testing for functional connections that may have physiological relevance, investigating multi-strain cultures or bulk patient

metabolomes in a target-discovery setting is more reflective of disease state and may provide a more accurate assessment of the microbial-derived compounds present in a host signalling environment. While this complicates down-stream identification of pathways that produce hit molecules, it offers the potential for unearthing novel signalling interactions that would be overlooked using refractive approaches.

Investigation into microbial metabolite mediated TF signalling against HIF-1α

We became interested in exploring if complex microbial metabolomes were cross signalling to the HIF pathway due to ubiquitous expression and multi-tissue functions of HIF, its role in certain microbiome-linked pathologies like inflammatory bowel disease, and our broader hypothesis that potentially all bHLH-PAS TFs can be regulated by ligand binding. Given the prevalence of cell-based biosensors in the field, we also wondered if dFLASH could be a suitable tool for these investigations.

We targeted two disease phenotypes where HIF-1α signalling has been linked with modulating disease phenotypes and took two different approaches toward investigating the microbial populations' signalling potential.

The first context we investigated was the microbiome of Diabetic Foot Ulcers (DFUs). DFUs are chronic wounds that are a co-morbidity that arise in diabetic patients due in part to their microbiome and have a high incidence of infection[104]. Hyperglycaemia has also been shown to disrupt HIF-1α signalling through increased degradation of HIF-1α protein matched with decreased expression in DFU biopsies[98,99]. DFU's have impaired healing that has been linked with decreased VEGF expression, a HIF-1α target gene, which may underpin defective wound repair[106,320]. This is supported by increased HIF-1α signalling, resultant from prolyl-hydroxylase inhibition, increasing wound healing in different diabetic murine models[98,106]. While there is a known effect from hyperglycaemia, we theorised that there may be additional microbiome-mediated signalling that prevents HIF-1α stabilisation or activity that might modulate disease progression.

The second context we investigated was Inflammatory Bowel Disease (IBD) microbiome signalling to host HIF-1α. There are significant changes that are observed in IBD patient microbiomes that appear to have disease signifigance[144,145,321,322] and the pathogenesis of IBD is perceived to involve distortion in the host-microbiome molecular relationship[128]. These changes in the microbiome have been correlated with disease severity. Schirmer, et al. [322] monitored the disease progression of 405 paediatric Ulcerative Colitis (UC) patients, one of the two subtypes of IBD, between initiation of treatment to 52 weeks post-treatment and observed shifts in microbial taxa that correlated with improved patient outcomes.

HIF-1α activation via prolyl hydroxylase inhibition attenuated epithelial damage, a hallmark of IBD, in murine models of colitis[130,134,323]. This is due to HIF defined roles in helping regulate epithelial barrier proteins such as Claudin-1[111,324] and intestinal trefoil factor (ITF)[113,325], the role of HIF-1α in production of anti-inflammatory Th17 cells[122,326] and promotion of cellular survival under conditions of inflammatory hypoxia[125,327] There are known interactions between HIF-1α and the microbiota, with HIF-1α being stabilised by high levels of butyrate and short chain fatty acids (SCFA)[138-140] produced by bacterial species, which decline within periods of IBD-associated microbiome dysbiosis[321]. These results, coupled with other anti-inflammatory pathways HIF regulates[148] mean that HIF-1α is considered a protective factor that combats IBD. It is because of this role that we wanted to investigate if we could detect pro- or anti-HIF-1α signalling from IBD patient microbiomes.

The investigation into potential DFU microbiota was different to our IBD approach due to the source material. With the DFU context we utilised monocultures or artificial mock communities from a patient-isolated library, more in line with the literature for cell-based bioassays for determination of functional metabolites[190-192] which also would simplify downstream analysis. However, it comes with many of the caveats discussed above. For the IBD cultures we assayed cell-free supernatants from anaerobic cultures derived from patient stool samples, to capture a more diverse metabolome and try to maintain the biosynthetic environment *in vitro*.

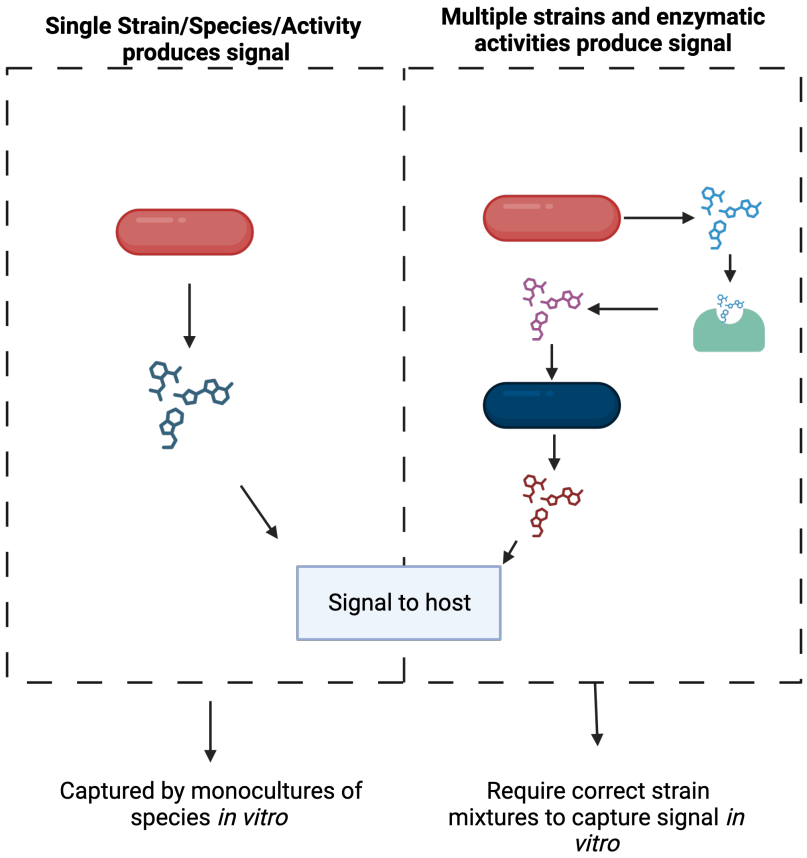

Figure 3.3.1. Two predominant modes of metabolite production from the microbiota.
Bacterial species in the microbiome produce metabolites from biosynthetic gene clusters. These signalling metabolites can be formed from a single species (left) or result from multiple metabolic processes via enzymatic activity across strains or species that produce the causative signal as a result of the mixed biotic environment present *in vivo* and in co-culture experiments (right). This informs experimental approaches to capture functional metabolites.

Results:

Isolation of bacterial species to modulate the dFLASH-HIF from Diabetic wounds

Dr. Nan Hao (University of Adelaide) isolated a small library of individual bacterial species from 20 patients with DFUs. Therefore, we designed a rapid *in cellulo* pipeline (**Figure 3.3.2.**) to investigate if any of these species were producing HIF signalling molecules. Dr. Hao cultured 26 individual bacterial strains from 11 different patients as monocultures in aerobic or anaerobic conditions (**Table 3.3.1.**). This limited library included 10 strains of *Finegoldia magna* which has been found to be one of the most common commensal anaerobes isolated from infected DFUs[328], *Morganella Morganii* of which certain strains can produce genotoxic metabolites[191] and *Enterococcus faecalis* which appeared in our 16s rRNA sequencing of some IBD patient samples discussed below (**Figure 3.3.9**). The inclusion of multiple strains of the same species is an attempt to capture intra-species diversity, which can be highly variable. As there have been some described cases of inhibition of HIF-1α [151,153] and promotion of HIF-1α stability by bacterial species[138,139,329], we tested these monocultures for both their ability to activate and inhibit HIF-1α *in cellulo* using dFLASH-HIF. We relied solely on reporter readout, without applying nuclear filtering. This was due to the smaller sample sizes utilised, as our current nuclear filter relies only on 4 metrics and requires baseline values to be established. Without a larger dataset (like in **Chapter 3.2**), it is potentially unreliable and may obfuscate real findings. Additionally, the EGFP gene has been shown to act as a reasonable proxy for non-specific interference in our screening campaigns.

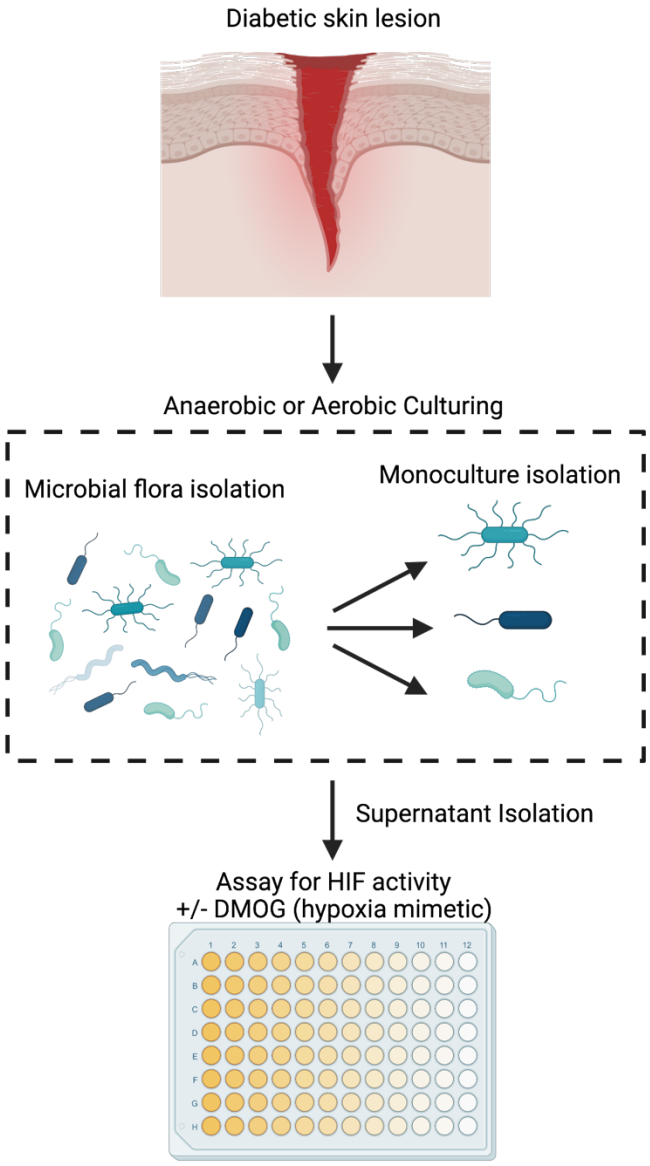

Figure 3.3.2 dFLASH-HIF screening of bacterial monocultures derived from diabetic patient skin lesions

Bacterial species were first isolated from skin lesion swabs in patients with diabetic foot ulcers (DFUs) and then single colonies were isolated and grown up independently as monocultures. Species identity was confirmed by MALDI-TOF mass spectrometry. Colonies were then cultured as single bacterial species. The supernatants from the liquid cultures could then be isolated, filtered and added directly to HEK293T dFLASH-HIF cells for HIF activation (- DMOG) or inhibition (+ DMOG).

Individual bacterial isolates from diabetic foot ulcers do not significantly impact the HIF-1α sensor

Prior to screening bacterial isolates, we confirmed that the bacterial growth media (BHI, see **Methods**) was non-toxic to our cellular system or auto fluorescent by co-culturing cells with 10% v/v both blank supernatant, supernatant with 0.2% Tween or supernatant with *F. magna* (ATCC) grown in BHI for 48 hours and observing cell growth by widefield microscopy. We then screened by HCI 52 different bacterial isolates across 32 different bacterial species for activation and inhibition (**Figure 3.3.3, 3.3.4**) of HIF-1α, by the addition of 10% v/v cell-free supernatant to culture medium and vehicle containing the monoclonal dFLASH-HIF cell line and co-incubating for 48 hours. To control for having species cultured in BHI and BHI + 0.2% Tween both blank medias were anaerobically incubated and included as positive and negative controls, with no difference between the two blank medias observed (**Figure 3.3.3**). Media controls presented in **Figure 3.3.3B-3.3.5** are BHI + 0.2% Tween. For a species to be considered a candidate lead for downstream investigation, a 3SD cut off was set from the media controls for both the Tomato MFI and the Tomato/EGFP ratio. Both measurements were used to account for induced changes in the independent EGFP control gene, a proxy measurement for off-target or deleterious effects.

There was no significant upregulation of the reporter across any of the bacterial supernatants in **Figure 3.3.3**. Where ratio increases were observed, such as *S. simulans* in **Figure 3.3.3B**, it was due to EGFP and not Tomato MFI changes. Additionally, there were observed differences between different strains. The *M. morganii* strain in **Figure 3.3.3A** that decreased EGFP expression was isolated from patient 10, whereas the strain in **Figure 3.3.3B,** where a much smaller change was observed, was isolated from patient 4. The lack of reporter response however indicates that there is no positive regulation occurring between these cultures and the HIF pathway. The detection of off-target effects, however, does ratify that this approach does facilitate sensing of microbial products, given the changes seen in the EGFP gene.

Screening for inhibition of HIF signalling in the presence of DMOG similarly showed no comprehensive downregulation of the reporter (**Figure 3.3.4**). There was no significant change in Tomato MFI (the readout for HIF-1α expression) for any of the individual bacterial strains that corresponded with an altered Tomato/EGFP ratio except for *S. simulans* (**Figure 3.3.4B**). It had an increase of >3SD for Tomato/EGFP with an increase in Tomato MFI. The Tomato MFI did not increase >3SD and a decrease in EGFP expression was also observed that caused the elevated Tomato/EGFP ratio. Coupled with the increased background observed for *S. simulans* in the activation screen (**Figure 3.3.3B**), *S. simulans* appears to be non-specifically regulating dFLASH-HIF. At increased concentrations, it therefore may be possible to see an enhanced effect, however, in a monoculture setting there should be higher than physiological levels of potential metabolites and toxicity over 10% of total volume precluded testing higher supernatant ratios. As a result, we conclude that none of the candidate species in monoculture were regulating the HIF reporter.

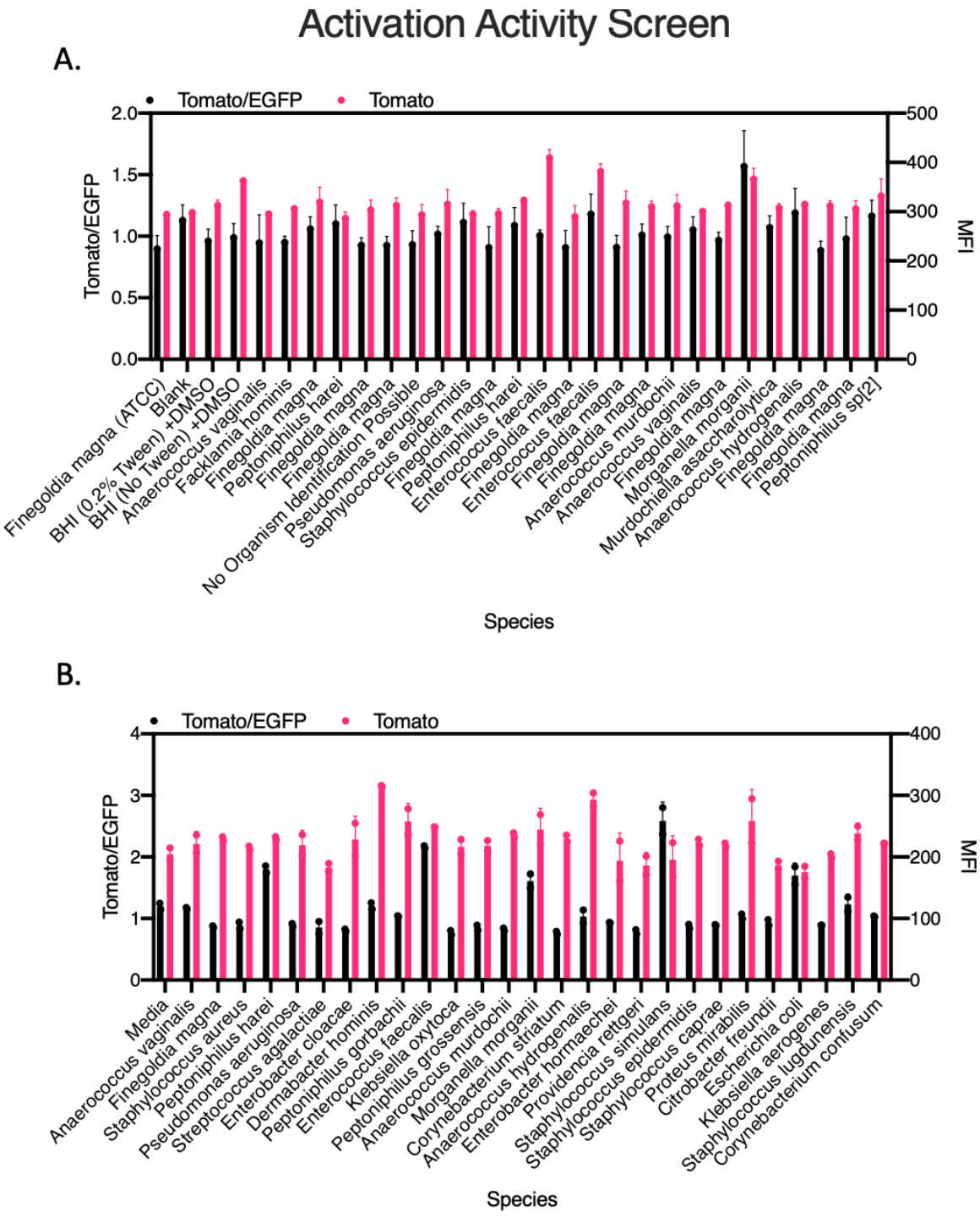
Activation Activity Screen
A.
Tomato/EGFP
Tomato
Tomato/EGFP
MFI
Species
Finegoldia magna (ATCC)
Blank
BHI (0.2% Tween) +DMSO
BHI (No Tween) +DMSO
Anaerococcus vaginalis
Facklamia hominis
Finegoldia magna
Peptoniphilus harei
Finegoldia magna
Finegoldia magna
No Organism Identification Possible
Pseudomonas aeruginosa
Staphylococcus epidermidis
Finegoldia magna
Peptoniphilus harei
Enterococcus faecalis
Finegoldia magna
Enterococcus faecalis
Finegoldia magna
Anaerococcus murdochii
Finegoldia magna
Anaerococcus vaginalis
Finegoldia magna
Morganella morganii
Murdochiella asaccharolytica
Anaerococcus hydrogenalis
Finegoldia magna
Finegoldia magna
Peptoniphilus sp[2]
B.
Tomato/EGFP
Tomato
Tomato/EGFP
MFI
Species
Media
Anaerococcus vaginalis
Finegoldia magna
Staphylococcus aureus
Peptoniphilus harei
Pseudomonas aeruginosa
Streptococcus agalactiae
Enterobacter cloacae
Dermabacter hominis
Peptoniphilus gorbachii
Enterococcus faecalis
Klebsiella oxytoca
Peptoniphilus grossensis
Anaerococcus murdochii
Morganella morganii
Corynebacterium striatum
Anaerococcus hydrogenalis
Enterobacter hormaechei
Providencia rettgeri
Staphylococcus simulans
Staphylococcus epidermidis
Proteus mirabilis
Citrobacter freundii
Escherichia coli
Klebsiella aerogenes
Staphylococcus lugdunensis
Corynebacterium confusum

A.

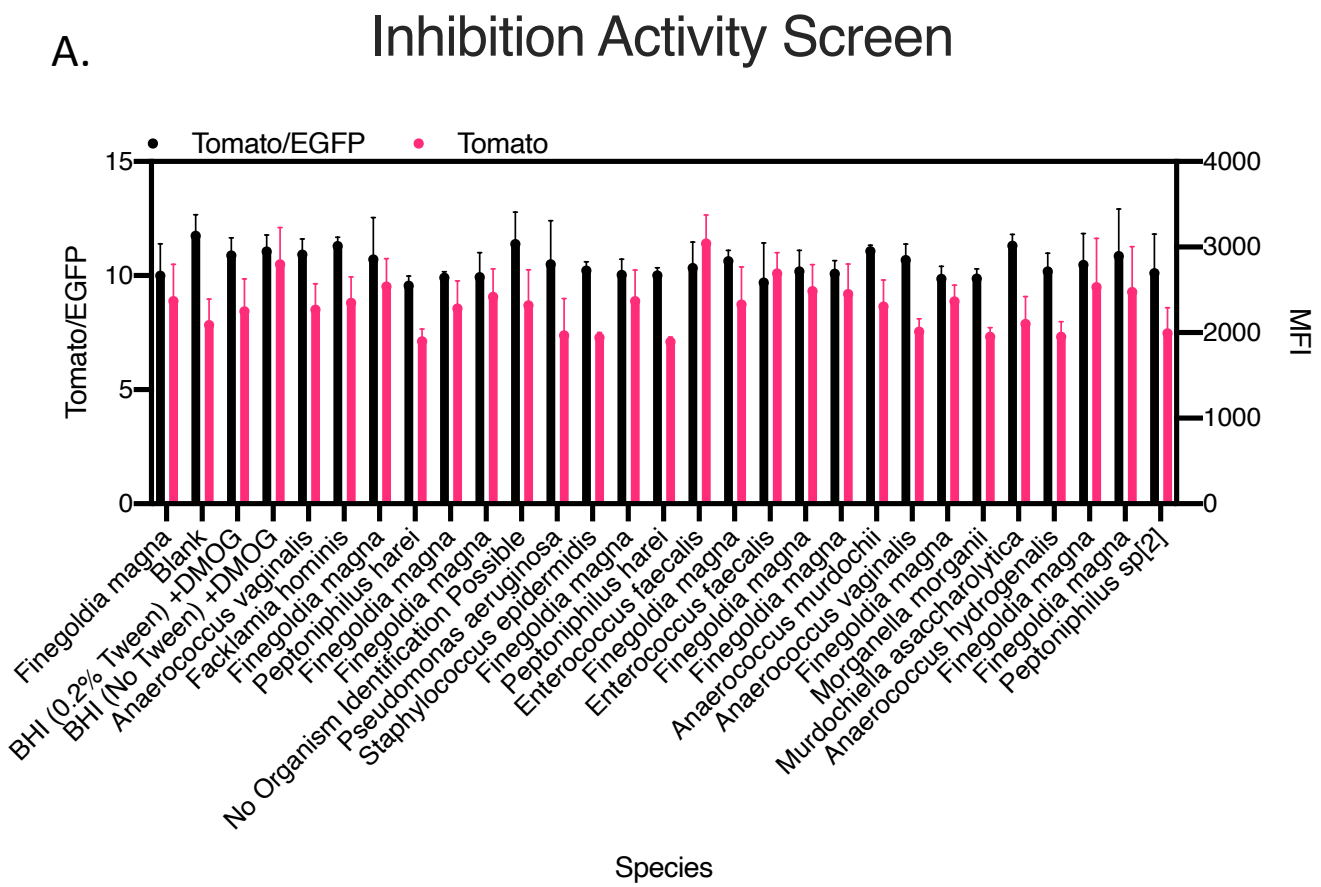
Inhibition Activity Screen
Tomato/EGFP
Tomato
Tomato/EGFP
MFI
15
10
5
0
4000
3000
2000
1000
0
Finegoldia magna
Blank
BHI (0.2% Tween) +DMOG
BHI (No Tween) +DMOG
Anaerococcus vaginalis
Facklamia hominis
Finegoldia magna
Peptoniphilus harei
Finegoldia magna
Finegoldia magna
No Organism Identification Possible
Pseudomonas aeruginosa
Staphylococcus epidermidis
Finegoldia magna
Peptoniphilus harei
Enterococcus faecalis
Finegoldia magna
Enterococcus faecalis
Finegoldia magna
Anaerococcus murdochii
Finegoldia magna
Anaerococcus vaginalis
Finegoldia magna
Morganella morganii
Murdochiella asaccharolytica
Anaerococcus hydrogenalis
Finegoldia magna
Finegoldia magna
Peptoniphilus sp[2]
Species

B.

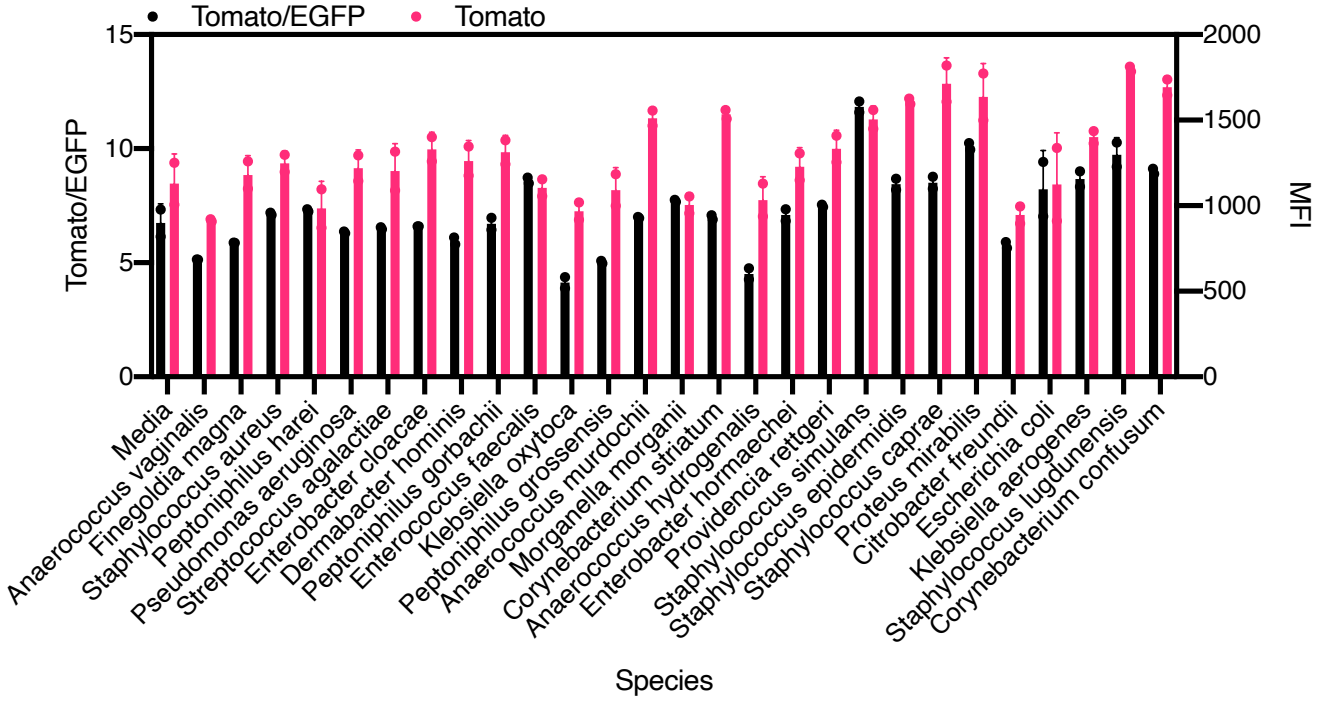
Tomato/EGFP
Tomato
Tomato/EGFP
MFI
15
10
5
0
2000
1500
1000
500
0
Media
Anaerococcus vaginalis
Finegoldia magna
Staphylococcus aureus
Peptoniphilus harei
Pseudomonas aeruginosa
Streptococcus agalactiae
Enterobacter cloacae
Dermabacter hominis
Peptoniphilus gorbachii
Enterococcus faecalis
Klebsiella oxytoca
Peptoniphilus grossensis
Anaerococcus murdochii
Morganella morganii
Corynebacterium striatum
Anaerococcus hydrogenalis
Enterobacter hormaechei
Providencia rettgeri
Staphylococcus simulans
Staphylococcus epidermidis
Proteus mirabilis
Citrobacter freundii
Escherichia coli
Klebsiella aerogenes
Staphylococcus lugdunensis
Corynebacterium confusum
Species

Figure 3.3.3 Pilot screening for bacterial monocultures for activation of the HIF-1α pathway.
(A, B) HEK293T dFLASH-HIF cells with 0.1% DMSO (vehicle) were imaged by HCI for reporter expression after 48 hours of treatment with supernatants from stationary phase cultures of individual bacterial species added at 10% v/v final. Tomato/EGFP ratio (black) and Tomato MFI (pink) are shown for all species (mean±SD). Data is from 1 supernatant growth and from (A) three biological replicates or (B) two biological replicates of reporter cell treatments with three technical replicates per biological replicate. A +3SD cut off for hits of interest was applied to both the Tomato and Tomato/EGFP readings relative to the media (blank) control. No bacterial supernatants met both cut offs.

Figure 3.3.4 Pilot screening of bacterial monocultures for inhibition of HIF-1α
(A, B) HEK293T dFLASH-HIF cells with 1mM DMOG were imaged by HCI for reporter expression after 48 hours of treatment with supernatants from stationary phase cultures of individual bacterial species added at 10% v/v final. Tomato/EGFP ratio (black) and Tomato MFI (pink) are shown for all species (mean±SD). Data is from 1 supernatant growth and from (A) three biological replicates or (B) two replicates of reporter cell treatments. A -3SD cut off for hits of interest was applied to both the Tomato and Tomato/EGFP readings relative to the media (blank) control. No bacterial supernatants met both cut offs.

Creation of mock communities did not identify putative HIF-1α regulation.

As none of the monocultures were bioactive against the reporter, we therefore thought to try a co-culture approach with the isolated species from patient DFUs. The creation of *in vitro* mock communities is increasingly standard practice as it more closely resembles the *in vivo* environment and produces a more complex secondary metabolome due to cross-feeding and the shared biotic environment[307,330,331]. As a result, we investigated if co-cultures would gain pro- or anti-HIF-1α activity as an emergent property. The 5 most commonly occurring species that were isolated by *in vitro* subculturing from DFUs were pooled into a base community (**Figure 3.3.5A**). Equal volumes from stationary phase cultures were added to form a 5 member "base" community culture. To that base culture, the bacterial species isolated from 12 patients were then added from stationary monocultures, forming a mock patient-associated co-culture. In addition, six 10-species communities were created with different combinations of bacteria from the monoculture library. These mixed cultures were then screened for activity against the dFLASH-HIF system.

Initially, we investigated if the base cultures would impact HIF-1α signalling (**Figure 3.3.5B**). We observed a small level of increased reporter activity relative to the media in one replicate however this effect was not significant across three independent co-culture formations. The small, non-significant increase that is observed relative to blank media may be an emergent property however it is small magnitude and equally likely to be a product of assay variability. Interestingly, we observed that all the patient-derived mock communities increased Tomato MFI relative to the media control (**Figure 3.3.5C**) but no differences to the control were observed when co-treated with DMOG (**Figure 3.3.5D**). These activation events are small and similar in magnitude to what was observed with the base culture (**Figure 3.3.5B**). A similar pattern was also observed with the 10-species communities (**Figure 3.3.5E**) where many of them had increased Tomato MFI expression relative to the media control, on par with 5 species base culture however with more variation of EGFP. There are numerous proposed ways by which bacterial species may upregulate HIF-1α, such as through lipopolysaccharide[332], butyrate[138-140] or production of iron scavenging compounds[149].

However, as we'd expect an increased bacterial abundance in culture compared to *in vivo*, we would expect a potent activator of the HIF-1 pathway to induce a greater magnitude effect to be a valid candidate for follow up investigations.

Taken together, although we observe minor changes that indicate potential weak pro-HIF-1α from co-culture conditions, this effect was small in magnitude and not significant. As a result, we conclude that there were no substantive interactions between the diabetic cultures and the HIF-1α pathway under these culture conditions. While that doesn't preclude the existence of interactions *in vivo*, this reductive approach did not produce strongly active metabolites. While we were unable to find a strongly active supernatant, we did routinely detect off-target interactions from these supernatants, through fluctuations in the EGFP control gene which does indicate that we are maintaining some bioactivity from these cultures. This, coupled with uses of similar strategies[190-192], suggests the experimental flow through is valid. As we optimised conditions that enables supernatant screening in an arrayed-based setting, higher-throughput screening conditions would be possible with an expanded library. Finally, it also suggests that co-culture, over monoculture, approaches may provide more promise for future investigations, given they provide the potential for a richer metabolome to sample.

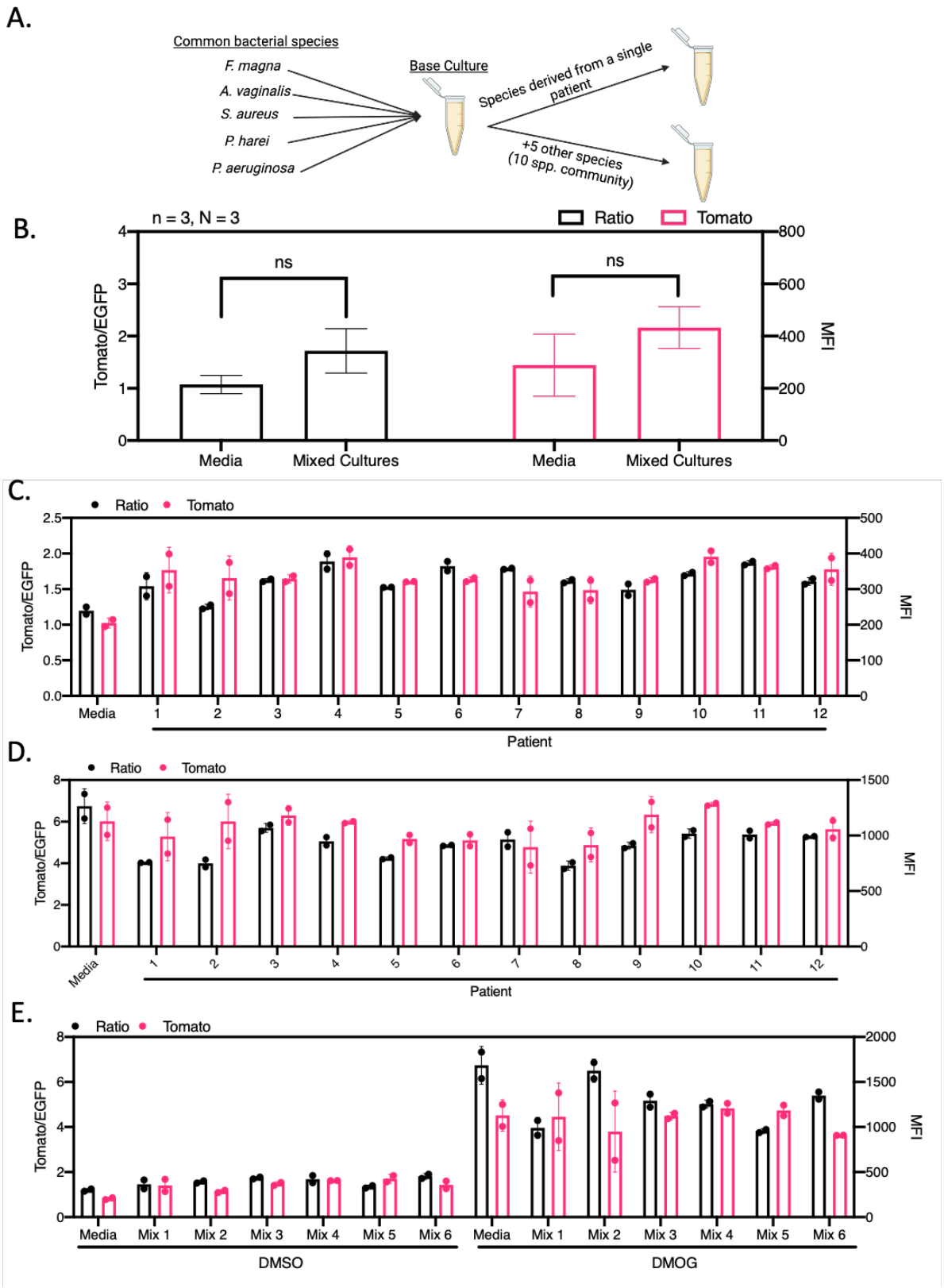
A.
Common bacterial species
F. magna
A. vaginalis
S. aureus
P. harei
P. aeruginosa
Base Culture
Species derived from a single patient
+5 other species (10 spp. community)
B.
n = 3, N = 3
Ratio
Tomato
ns
ns
Tomato/EGFP
MFI
Media
Mixed Cultures
Media
Mixed Cultures
C.
Ratio
Tomato
Tomato/EGFP
MFI
Media
1
2
3
4
5
6
7
8
9
10
11
12
Patient
D.
Ratio
Tomato
Tomato/EGFP
MFI
Media
1
2
3
4
5
6
7
8
9
10
11
12
Patient
E.
Ratio
Tomato
Tomato/EGFP
MFI
Media
Mix 1
Mix 2
Mix 3
Mix 4
Mix 5
Mix 6
Media
Mix 1
Mix 2
Mix 3
Mix 4
Mix 5
Mix 6
DMSO
DMOG

Figure 3.3.5. Pilot screening of mock bacterial communities from common species demonstrate putative HIF-1α sensor activation.
(A) A mock community of the 5 most common species isolated from the 20-patient DFU cohort by Dr Nan Hao were pooled into a single base culture. That base culture was added with species unique to 12 individual patients or mixed with 5 other common species isolated from the 20-patient cohort, forming six 10 species communities. (B) HCI of HEK293T mcdFLASH-HIF cells treated for 48 hours with 10% v/v of the 5 species co-culture and 0.1% DMSO. Data is from three independent cultures (N = 3) and reporter assays were done in triplicate per culture growth (n = 3). (C, D, E) The 5 species co-culture base from (B) were (C, D) combined with species isolated from 12 independent patients to form representative cultures or (E) 5 diverse species to form a novel emergent mixture. mcdFLASH-HIF cells were treated with 10% v/v for these supernatants for 48 hours and (C, E) 0.1% DMSO or (D) 1mM DMOG. Data is from one culture growth (N = 1) and reporter assays were done in biological duplicate, each with 3 wells per plate.

Patient cohort for screening of complex microbial supernatants

In contrast with our refractive method for detection of HIF-1α microbial modulators from *in vitro* isolated cultures we also looked to isolate activity from a more complex microbial community. In collaboration with Dr. Michael Conlon at the CSIRO, we asked if anaerobic cultures of IBD patient gut microbiomes would be producing pro- or anti-HIF signalling molecules. To test this hypothesis, we developed an approach that would facilitate screening the microbial metabolome from a small cohort of IBD patients utilising dFLASH-HIF as our reporter (**Figure 3.3.6**).

Four paediatric IBD patients (**Table 3.3.2**) provided samples over a course of disease treatment, from initial presentation at clinic (Visit 1) to various points over the course of their treatment (Visit 2-4). Acute inflammation in patients was assessed by calprotectin quantification. Calprotectin detection in faecal samples is a marker of intestinal inflammation, due to the leakage of neutrophils into the intestinal lumen during inflammation, hence has been widely used as a biomarker of IBD-associated gut inflammation[333]. Elevated faecal calprotectin levels have been shown to be correlated with decreased microbial diversity, a hallmark of the IBD microbiome[322]. Therefore, this cohort provides a pre-treatment baseline microbiome and captures how treatment progression, which corresponded with lower levels of acute inflammation, might influence the putative signalling. Of the four patients, 3 were diagnosed with Crohn's disease (CD) and one with Ulcerative Colitis (UC). Both diseases fall under the banner of IBD however there are distinct subtype differences regarding location of inflammation within the intestinal tract and inflammation occurrence coupled with potentially differing roles of the microbiota within disease progression. Evidence in support of this are the emergent efforts to profile and diagnose CD by microbial dysbiosis, a change in species of the microbiome[334], which has been suggested to be more dramatic than that observed for UC[144]. As a result, we were curious if there would be any dramatic differences between patient WCH6 (UC) and the other three CD patients.

To capture these patient microbiomes at different points of their disease progression and hence different microbial diversity, 100mg faecal samples from these patients were provided and used for anaerobic outgrowths to form representative cultures of

the species present within the patient's gut environment utilising the CSIRO's gut modelling technique (CSIRO, unpublished data). Two sources were used in the establishment of these anaerobic cultures. The first was raw faecal material (denoted as "raw') (**Figure 3.3.6**) to establish anaerobic cultures. Secondly, after initial culturing of these samples, glycerol stocks were taken (denoted as "gly" or "glycerol") and used to establish future cultures. The base anerobic media also had one of three different supplements, high amylose starch (HAMS), Inulin or Galactose as they can stimulate differential growth of bacterial species, giving a broader diversity of metabolites for screening[335]. These supernatants were then to be mixed in culture with our established cell-based screening systems.

When optimising blank supernatants for addition over the HEK293T mcdFLASH-HIF system (**Figure 3.3.6**) we observed no broad changes in cell morphology up to a 1:5 (20%) supernatant to cell culture concentration across all three cell culture media however a slight decrease in cell confluency. At 30% of total there was broad cell growth reduction and morphology changes that can be observed. As a result, we therefore selected 10% of total (1:10) as our screening concentration, consistent with our DFU screening project, as there was no observed impact on cell growth and prior efforts have used a similar ratio albeit with a different bacterial growth media and culture strategy.

Table 3.3.2. Summary of the pediatric naïve IBD patient cohort that donated faecal samples for anaerobic outgrowth and microbial metabolite screening

Patient ID	Diagnosis	Visit information	Sample collection date	Calprotectin (ug/g)	Sample ID (screening)
WCH6	Ulcerative Colitis	Baseline (Visit 1)	13/12/2016	2312	6-1
		Visit 3	23/5/2017	<100	6-3
WCH10	Crohn's Disease	Baseline (Visit 1)	21/2/2017	3600	10-1
		Visit 2	19/6/2017	1867	10-2
		Visit 4	1/4/2018	135	10-4
WCH14	Crohn's Disease	Baseline (Visit 1)	7/7/2014	1532	14-1
		Visit 4	23/4/2018	105	14-4
WCH16	Crohn's Disease	Baseline (Visit 1)	17/5/2017	9570	16-1
		Visit 2	10/8/2017	179	16-2
		Visit 4	25/5/2018	1790	16-4

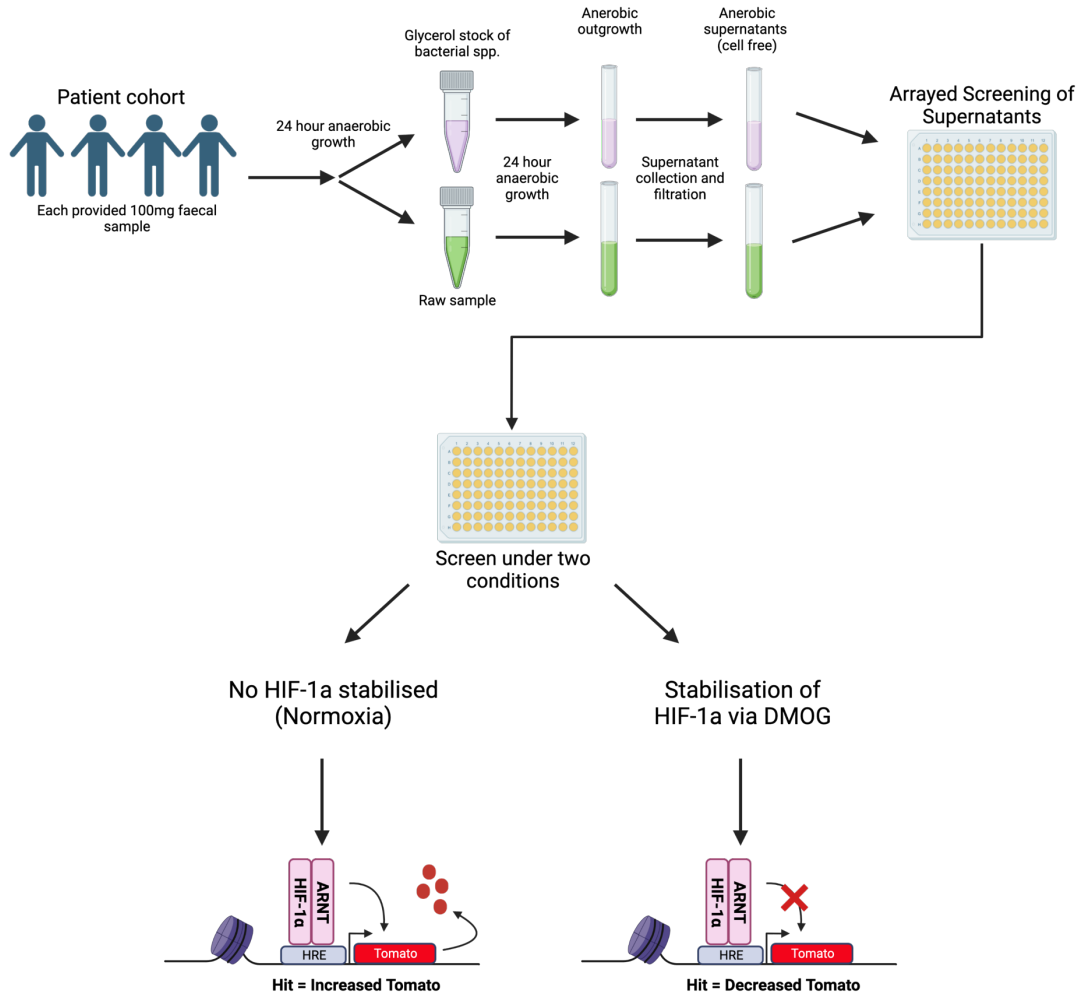

Figure 3.3.6 Screening strategy for capturing metabolites produced from IBD patient microbiomes

Complex microbiome cultures were derived from samples from 4 IBD patients (summarised Table 3.3.2). Anerobic bacterial cultures were established from either glycerol stocks from prior outgrowths or direct from raw faecal samples (Raw). These cultures were then spun down and filtered to derive a cell-free supernatant mixture of the aqueous metabolites produced by those bacterial species. This supernatant was then added to HEK293T dFLASH-HIF cells. Supernatants were assayed for their impact on reporter assays in the presence of DMOG (for inhibition of HIF-1α) or DMSO (for activation of the HIF-1α pathway).

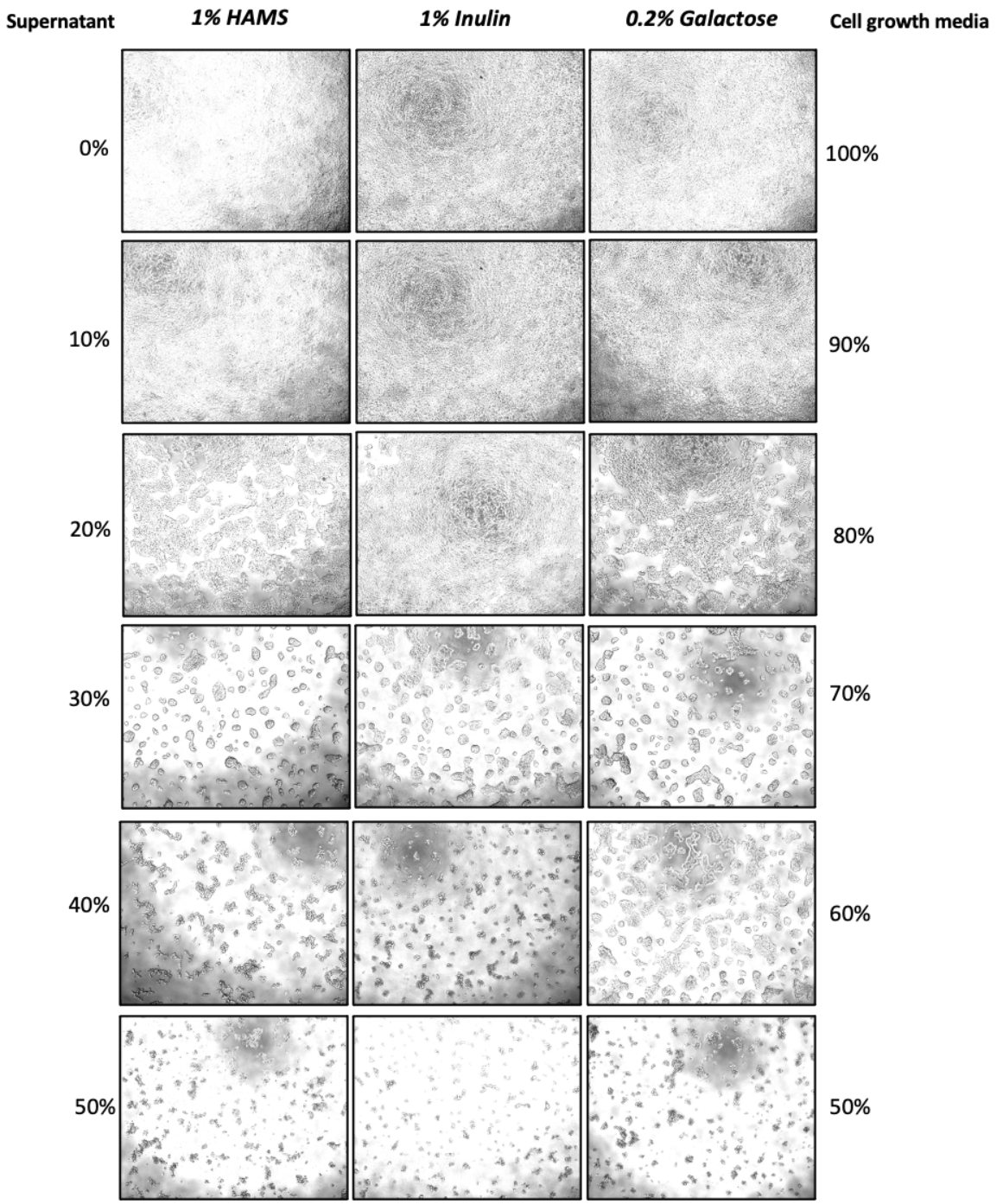

Figure 3.3.7 Bacterial media is tolerated up to 20% v/v in HEK293T cells
Anaerobic growth media contained the three supplements, 1% HAMS, 1% Inulin, and 0.2% Galactose used to derive mixed microbial populations from IBD patient samples were cultured under anoxia for 24 hours in 96 well plates. These supernatants were then added to HEK293T cells at increasing concentrations (0% v/v to 50% v/v) for 24 hours prior to widefield microscopy for assessment of cellular populations. Images are representative of two biological replicates.

Screening of IBD supernatants for activation or inhibition of the HIF-1α reporter

The initial screen of supernatants against HEK293T dFLASH-HIF was performed with and without the addition of DMOG to capture agonistic and antagonistic activity against the HIF-1α reporter system. To determine samples of interest across the initial screen we used a cut off three standard deviations (3SD) from the -DMOG (for activation) or +DMOG (for inhibition) blank media treated controls for each of the three different media supplements, 1% High Amylose Starch (HAMS), 1% Inulin or 0.2% Galactose. There were no observed differences in control assays to assess blank media (Raw) Vs blank media with glycerol additions (to match the addition of glycerol samples), nor for controls (DMSO, DMOG) -/+ media added.

Across media supplements we observed some weak upregulation of the reporter by 5 culture supernatants (**Figure 3.3.8C, Figure 3.3.8E**) with the maximum upregulation of 2-fold sitting just above cut off that was highly consistent across biological replicates, however no sample was upregulated with HAMS media supplementation (**Figure 3.3.8A**). Agonistic activity from the microbiota onto HIF-1α has been previously reported through a butyrate-dependent mechanism[138,139], proposed to be through inhibition of PHD2. Therefore, there is a prior reported mechanism that may explain the upregulation in reporter activity that we observe. Of note, there are no samples that are both upregulated across glycerol-derived (gly) and faecal-derived (raw) samples. This is suggestive of variation in species composition between the two different preparations. There is also no consistent upregulation that is observed for the same sample across the different media groups. There is expected to be sample to sample variations due to the alternate media supplementations and alternate species compositions to be present, which may explain the lack of consistency.

As there have been several described mechanisms of HIF upregulation by microbial products, the small levels of upregulation of the reporter are likely to be consequence from one of those described interactions and therefore is not a surprising result. It does, however, show that we may be able to detect putative interactions between the complex supernatant mixture and our *in cellulo* genetic reporter like prior approaches[190,192].

Antagonism by microbial species against HIF-1α signalling through a direct HIF-1α protein interaction has not been previously reported. When screening for HIF-1α inhibition, we observed a consistent downregulation of two glycerol stock samples (10-2 gly, 16-2 gly) that fell below the 3SD cut off for HAMS (**Figure 3.3.8B**) and Galactose (**Figure 3.3.8F**) and was near basal expression in all medias, including Inulin (**Figure 3.3.8D**). The cells treated with the two bioactive media types also see a decrease in cell proliferation which was observed during culturing, resulting in sparser wells relative to controls. These supernatants decrease Tomato MFI with no significant change in EGFP, our off-target effect proxy, by HCI quantification. There was no downregulation in the raw samples for the same patients however, with all raw samples having no effect on the DMOG-induced reporter (**Figure 3.3.8**). This downregulation, that was consistent between bio replicates, was unexpected but indicates a change that occurs between the raw samples and the glycerol stocks causes this effect.

There are some open questions regarding this result and the underlying biology. In the crude supernatant it's uncertain if this is the action of a metabolite or protein factor. Protein factors have been previously detected in supernatant screening[191]. The downregulation was also seen only in the glycerol-derived supernatants and not the raw sample. This raises the question as to whether or not this effect is artificial and of physiological importance. These concerns however are matched against seeing a clear downregulation of the HIF reporter *in cellulo* from the supernatant, hence delineation of the mechanism may elucidate a novel signalling mechanism between the microbiome and HIF biology.

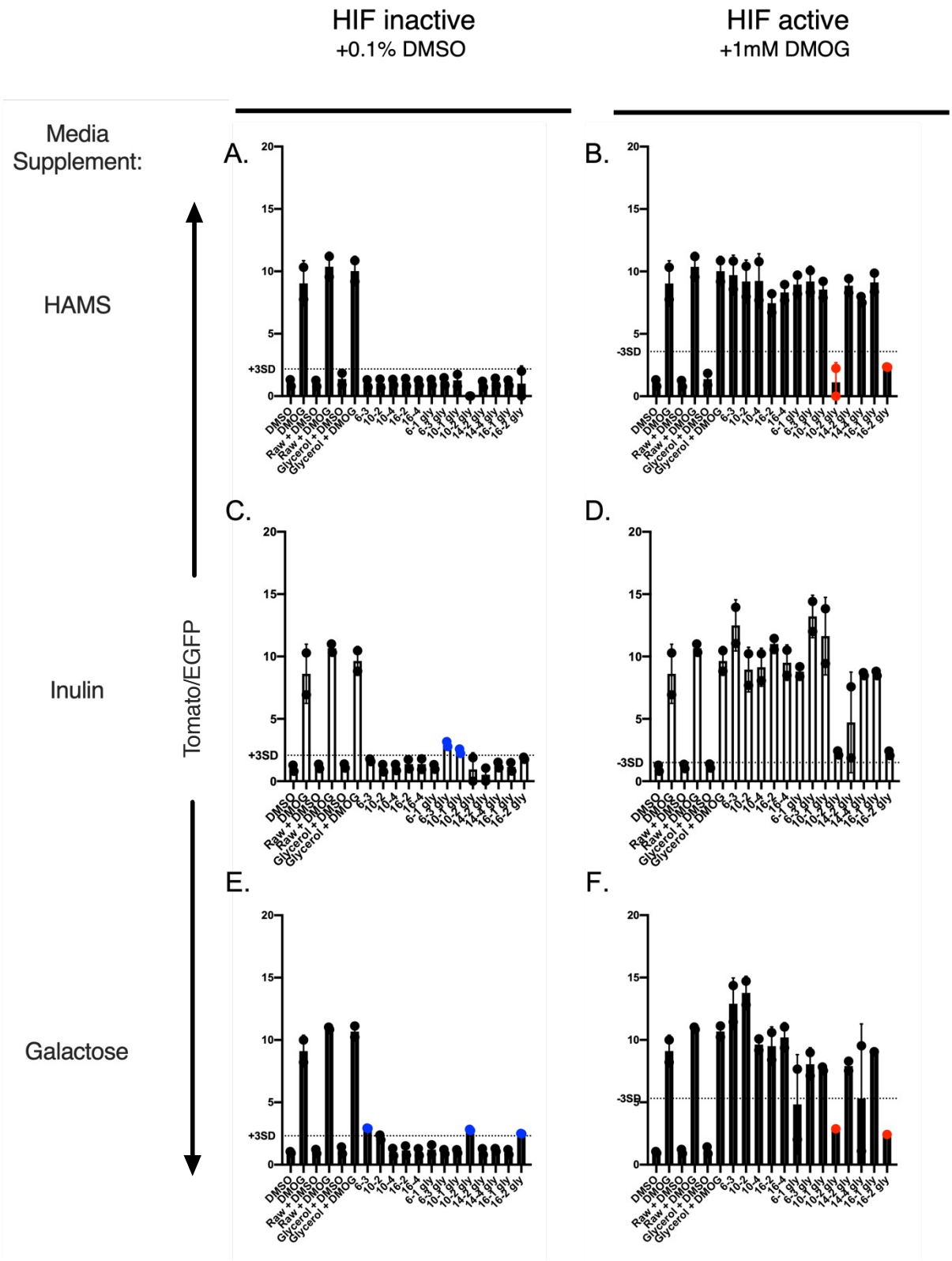
HIF inactive
+0.1% DMSO
HIF active
+1mM DMOG
Media Supplement:
HAMS
Inulin
Galactose
Tomato/EGFP
A.
B.
C.
D.
E.
F.
+3SD
-3SD
DMSO
DMOG
Raw + DMSO
Raw + DMOG
Glycerol + DMSO
Glycerol + DMOG
6-3
10-2
10-4
16-2
16-4
6-1 gly
6-3 gly
10-1 gly
10-2 gly
14-1 gly
14-2 gly
16-1 gly
16-2 gly

Figure 3.3.8 Arrayed screen of anaerobic cultured supernatants from IBD patient samples identifies several strong inhibitor fractions
(A-F) HEK293T dFLASH-HIF cells reporter expression was imaged by HCI after cells were treated with one of 13 patient samples, 5 derived from faecal samples and 8 from glycerol stocks (gly) or media controls with glycerol (Glycerol + DMSO, Glycerol + DMOG) or without (Raw + DMSO, Raw + DMOG) for 48 hours with vehicle or 1mM DMOG. Non-supernatant controls are also included (DMSO, DMOG). Patient microbiomes grown in bacterial growth media with (A, B) 1% HAMS, (C, D) 1% Inulin or (E, F) 0.2% Galactose supplementation were assessed for their ability to (A, C, E) activate or (B, D, F) inhibit HIF-1α expression at 10% v/v. (A, C, E) Dashed lines represents 3SD above the raw media control mean reporter expression treated with DMSO. Samples above this line are highlighted in blue. (B, D, F) Dashed lines represent 3SD below the mean reporter expression of the raw media control treated with DMOG. Samples below this line are highlighted in red. Data is mean of 2 biological replicates with 2 technical replicates per sample.

Downregulation by supernatants replicated in confirmatory assays

Given the downregulation of the reporter that was observed we then sought to confirm that this change that was observed in the primary screening was significant and that the samples, after -80^{o}C storage were still bioactive. In the follow-up assay (**Figure 3.3.9**) there is significant downregulation (**Figure 3.3.9D**) with 16-2 for all three medias relative to media-matched controls ($p<0.001$) and HAMS and Galactose for 10-2 ($p< 0.0001$). We see that, across the three replicates there was a lot more consistency of effect for 16-2 than for 10-2. This confirms that there is no change in the raw samples but a consistent decline across independent replicates with the two bioactive glycerol-derived samples even with a freeze-thaw cycle after -80^{o}C storage.

Also of note is that the effect appears to drop the reporter about to down to basal expression, indicating that the supernatants were completely abolishing DMOG-driven upregulation of the HIF-1α pathway. 14-2 was also included in the rescreening, as there was a decrease in the glycerol sample in the initial screen (**Figure 3.3.9D**) however it did not decrease reporter output significantly in comparison to the controls in the inulin sample (**Figure 3.3.9B**) and no change at all was observed for HAMS (**Figure 3.3.9A**) or Galactose (**Figure 3.3.9C**). Therefore, 16-2 gly and 10-2 gly appear to consistently downregulate the HIF-1α cell-based reporter.

The consistency of action for the supernatants, something not observed with the DFU mock communities, across the initial assays suggests that there is a real anti-reporter activity that is a result of a bacterial product. That this occurs in the glycerol stocks and not in the raw samples suggests that there is something being consistently differentially enriched in the glycerol samples. Therefore, we targeted the glycerol samples specifically to investigate the mechanism of action of these supernatants.

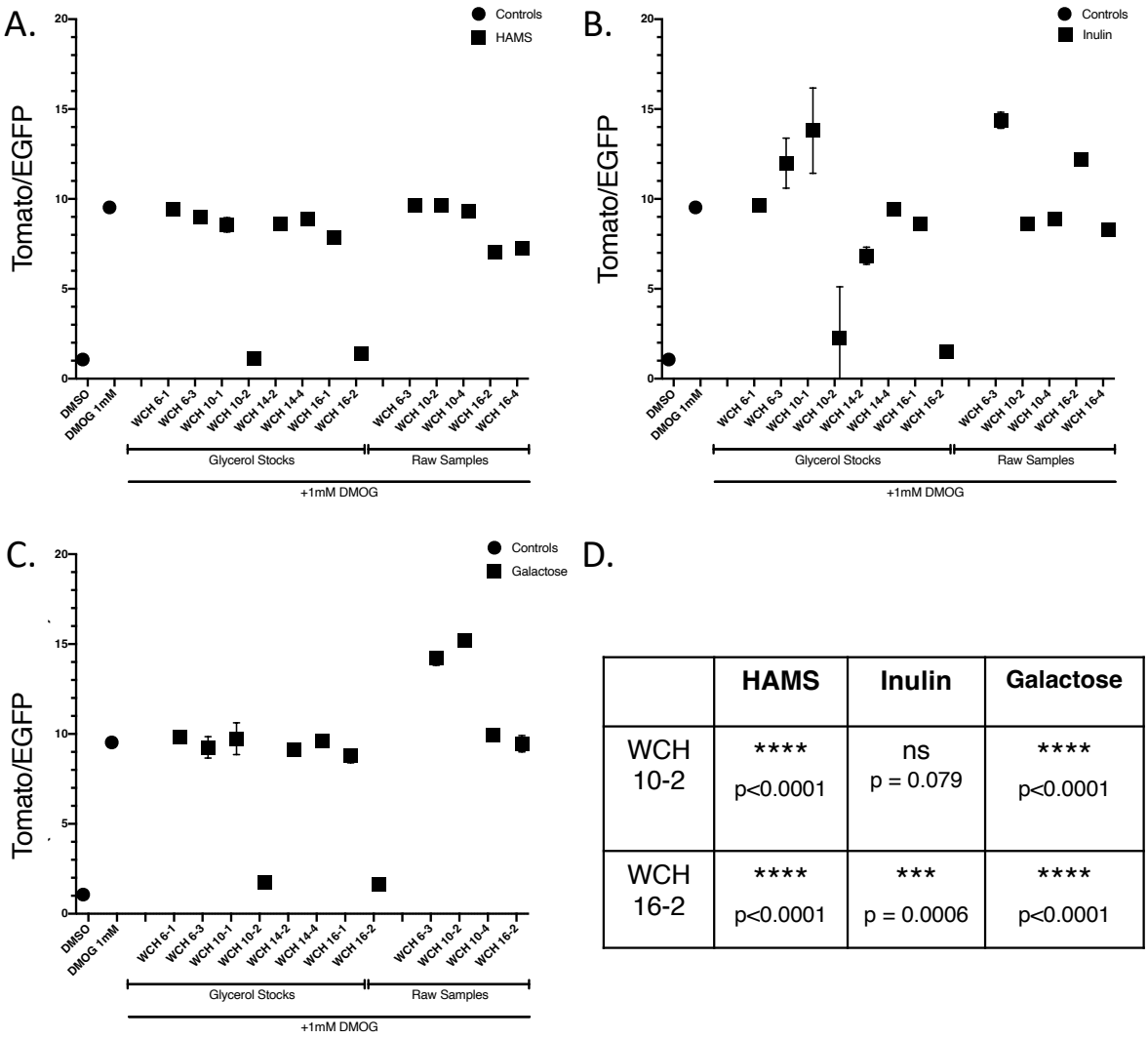

	HAMS	Inulin	Galactose
WCH 10-2	**** p<0.0001	ns p = 0.079	**** p<0.0001
WCH 16-2	**** p<0.0001	*** p = 0.0006	**** p<0.0001

Figure 3.3.9 Supernatant reporter inhibition effect observed for glycerol stock samples replicates in confirmatory screen with different media supplements.

(A-C) Bacterial supernatants at 10% v/v with either (A) 1% HAMS, (B) 1% Inulin or (C) 0.2% Galactose supplementation from **Figure 3.3.8** were re-assayed at 10% v/v for their ability to decrease reporter expression in HEK293T dFLASH-HIF cells treated with 1mM DMOG after 6+ months of -80*C storage. Controls are matched blank media samples to media supplement. Data is mean of 3 biological replicates, with 2 technical replicates per biological replicate. (D) Significance for Glycerol stock samples WCH 10-2 and WCH 16-2 across the three media supplements was assessed by one-way ANOVA and Dunnett's post-hoc analysis relative to the DMOG positive control.

No differential enrichment of species observed by 16s rRNA sequencing

As we observed differences in the activity between raw and glycerol derived samples we wanted to investigate if there was a clear difference in microbial diversity that may explain the reporter downregulation that we see or give a clear lead species to investigate. We sent glycerol and raw outgrowths for samples from patients 10 and 16 (**Table 3.3.2**) with matched glycerol stocks and raw samples, where possible, for 16s rRNA sequencing and analysis by the Rogers Lab at Flinders University for a population level overview. The sequencing for the samples identified relative abundances of 95 different Operational Taxonomic Units (OTUs) that were present across all 16 samples, separated into inactive (**Figure 3.3.10A**) and active (**Figure 3.3.10B**) pools.

In every anaerobic culture, one of four OTUs comprised nearly 50% of the cultured species (**Figure 3.3.10A, B**), except for 16-2 HAMS Fermentation 1. This is not surprising, as complex anaerobic cultures can often result in selection for a subset of anaerobic species and can struggle to capture the original sample diversity [336,337]. The expansion of four different predominant OUT's (*Escherichia-Shigella [Escherichia* and *Shigella* cannot be differentiated by 16s rRNA sequencing hence share an OTU], *Enterococcus and Clostridium sensu stricto 1, Bifidobacterium*), with *Escherichia-Shigella* increasing by 10% in glycerol stocks compared to raw sample growths (**Figure 3.3.11A**). However, we observed there being no differential enrichment of these dominant species in active samples for 10-2 and 16-2 (**Figure 3.3.10C, D**, **Figure 3.3.11B, C**). As none of these species were greatly increased in the glycerol stocks, for which we'd expect to be a marker of increased activity, we concluded it was unlikely that these OTUs were the driver of the reporter downregulation.

When we looked for enrichment of low abundance species between all the glycerol and raw samples, we saw that there was an increase in several lowly abundant OTUs in 16-2 and 10-2 glycerol samples (**Figure 3.3.12**). As a result, we then looked specifically as to which species were enriched between raw and glycerol samples for 16-2 and 10-2 (**Figure 3.3.10B, C**).

There was a large (~14 fold) enrichment in *Lactobacillus* species in all the glycerol stocks, with a 17-fold increase in the 10-2 sample (**Figure 3.3.10C, Appendix Table 3.3.3**.) *Lactobacillus* has previously been reported to potentially downregulate HIF-1α

transcription in a breast cancer cell line[338], however the study lacked a proposed mechanism that might explain this effect and they described cytotoxic effects on their cell line of choice. However, that would only explain the activity of one of the two potential samples as *Lactobacillus* wasn't within the top 17 enriched species for 16-2 glycerol stock (**Table 3.4.2A**). This suggests that it's an unlikely candidate to be causative in the 16-2 samples. Therefore, we cannot discount there being a similar mechanism between the two samples but there is no clear, enriched species across both bioactive samples that would explain the reporter phenotype.

The only other clade that increased to a similar degree overall was the *Escherichia-Shigella*, increasing from 7% in raw samples to 17% in glycerol stocks (**Figure 3.3.11A**) but were not detected in active 16-2 HAMS samples (**Figure 3.3.12C**). HIF-1α induction during bacterial infection *in cellulo* has been shown for *Enterobacteriaceae,* which encompasses both *Escherichia* and *Shigella* spp[149,339]. This mechanistically, for certain members of the larger genus, was suggested to occur by excretion of iron-chelating siderophores[149]. This activity is the opposite to the downregulation of the HIF-1α reporter we observe, presumably because of our mixed species/metabolite culture, again suggesting novel activity.

This experiment led us to focus on pursuing a "compound-first" instead of a "species-first" approach to understanding the cause of the observed reporter decreases. There were several species that were able to be detected in the glycerol stocks that were not able to be detected in the raw samples, however most were lowly abundant relative to other species in the overall culture (**Figure 3.3.12B**). This means that it would be hard to isolate those lowly appearing species with traditional sub-cultivation methods under anoxia. Additionally, this sequencing approach doesn't provide information on a strain-level, therefore the diversity at a sub-genus level is also unknown and would require either cultureomics or more in depth metagenomic sequencing. Therefore, we began to investigate if the activity we observe is a result of a protein or a metabolite produced by these cultures.

A.

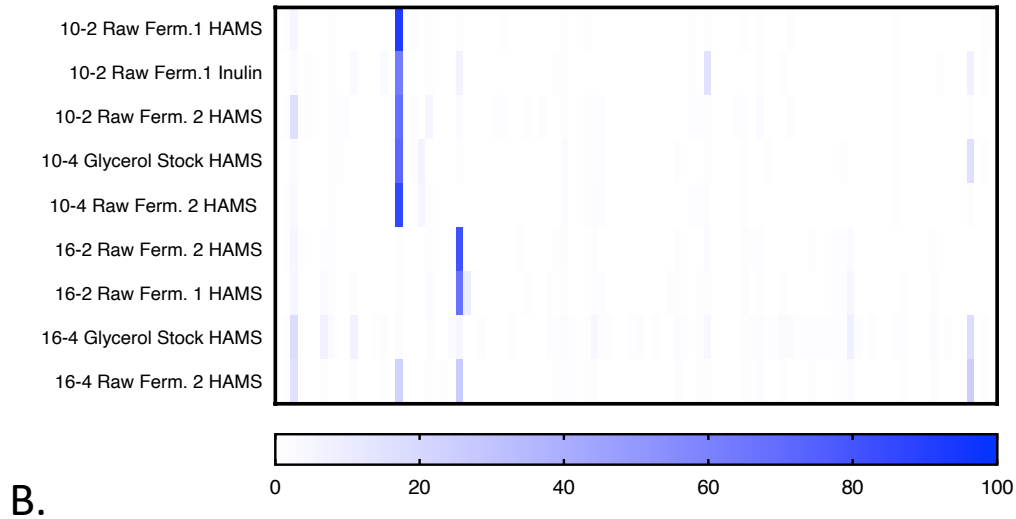
10-2 Raw Ferm.1 HAMS
10-2 Raw Ferm.1 Inulin
10-2 Raw Ferm. 2 HAMS
10-4 Glycerol Stock HAMS
10-4 Raw Ferm. 2 HAMS
16-2 Raw Ferm. 2 HAMS
16-2 Raw Ferm. 1 HAMS
16-4 Glycerol Stock HAMS
16-4 Raw Ferm. 2 HAMS
0
20
40
60
80
100

B.

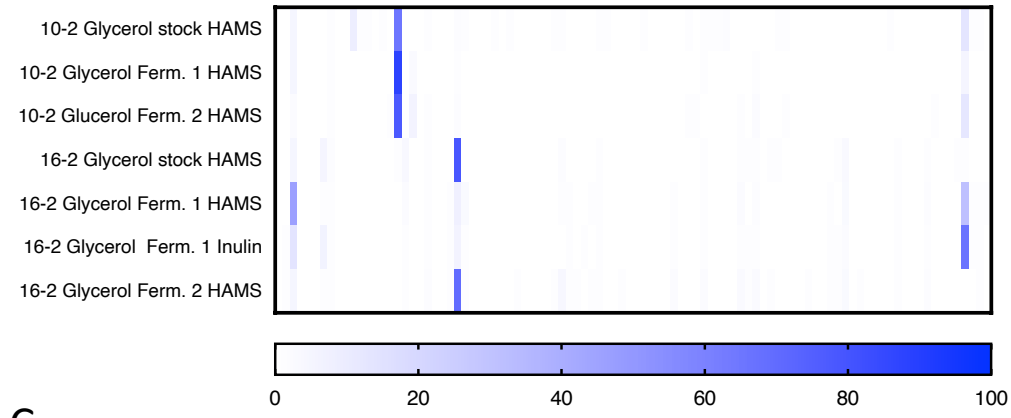
10-2 Glycerol stock HAMS
10-2 Glycerol Ferm. 1 HAMS
10-2 Glucerol Ferm. 2 HAMS
16-2 Glycerol stock HAMS
16-2 Glycerol Ferm. 1 HAMS
16-2 Glycerol Ferm. 1 Inulin
16-2 Glycerol Ferm. 2 HAMS
0
20
40
60
80
100

C.

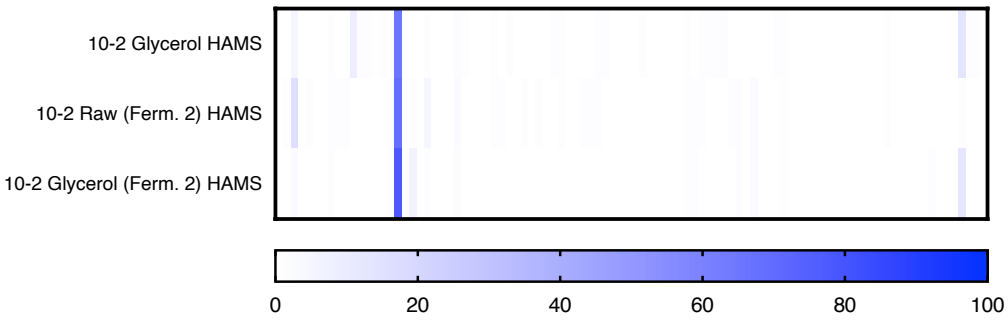
10-2 Glycerol HAMS
10-2 Raw (Ferm. 2) HAMS
10-2 Glycerol (Ferm. 2) HAMS
0
20
40
60
80
100

D.

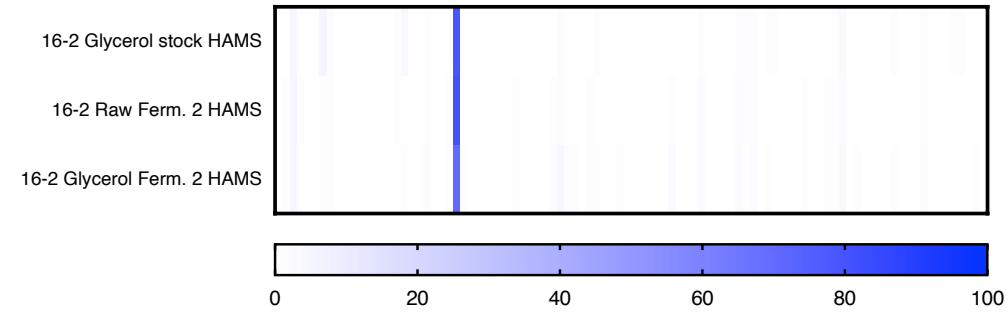
16-2 Glycerol stock HAMS
16-2 Raw Ferm. 2 HAMS
16-2 Glycerol Ferm. 2 HAMS
0
20
40
60
80
100

Figure 3.3.10. 16s rRNA sequencing of bioactive and inactive species present in the anaerobic cultures doesn't reveal clear trends in differential species enrichment.

(A, B) 16s rRNA sequencing of bacterial populations samples identify 95 different OTUs from patients WCH16 and WCH10 across samples that (A) didn't downregulate the dFLASH-HIF reporter or (B) downregulated the dFLASH-HIF reporter. (C, D) population comparison of glycerol stock diversity or HAMS anaerobic outgrowths for raw and glycerol derived samples for samples (C) 10-2 and (D) 16-2. Data is presented at percentage of the population each bacterial taxonomy is present in the total population. Enriched species are summarised in **Appendix Tables 3.3.1A - 3.33A** and **Figure 3.3.11, Figure 3.3.12**.

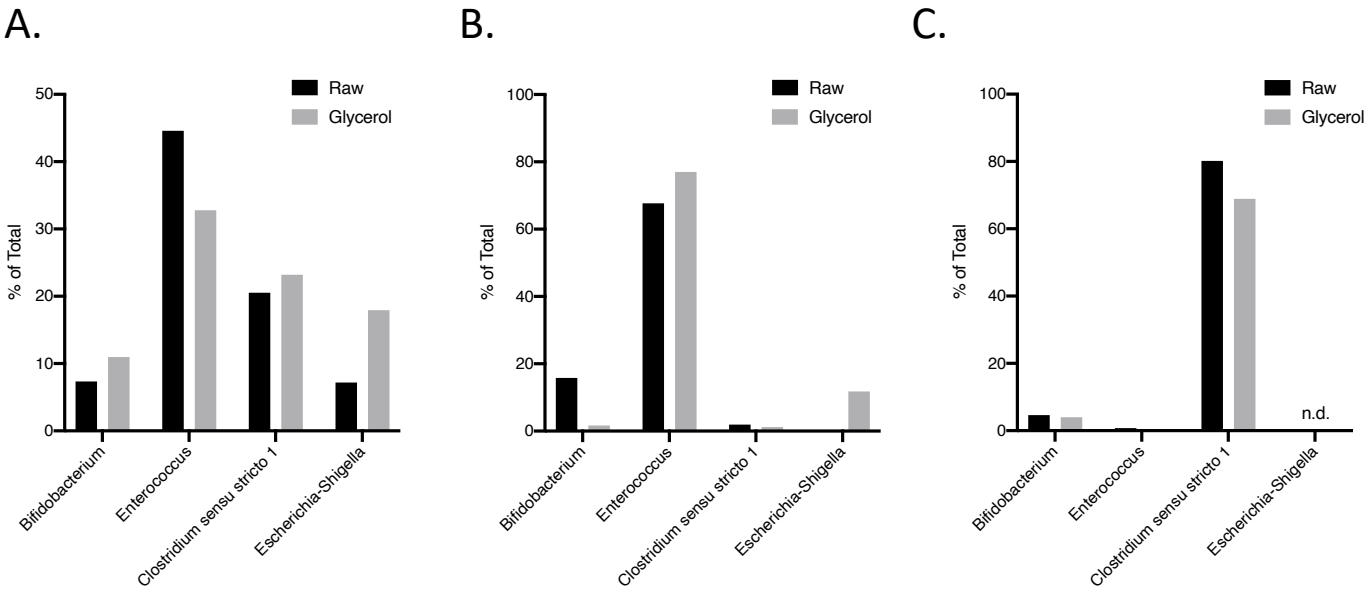

Figure 3.3.11. Four most enriched species between active and inactive samples set do not reveal clear trend for differential enrichment of a dominant species.
(A) 16s rRNA sequencing identified 4 OTUs that where abundant (>5% of overall population) between all the analysed inactive samples (**Figure 3.3.10A**) compared with the active samples (**Figure 3.3.10B**). (B, C) Abundance for (B) 10-2 and (C) 16-2 of raw and glycerol samples from fermentation 2 with HAMS supplementation of the 4 biggest populations from the pooled analysis.

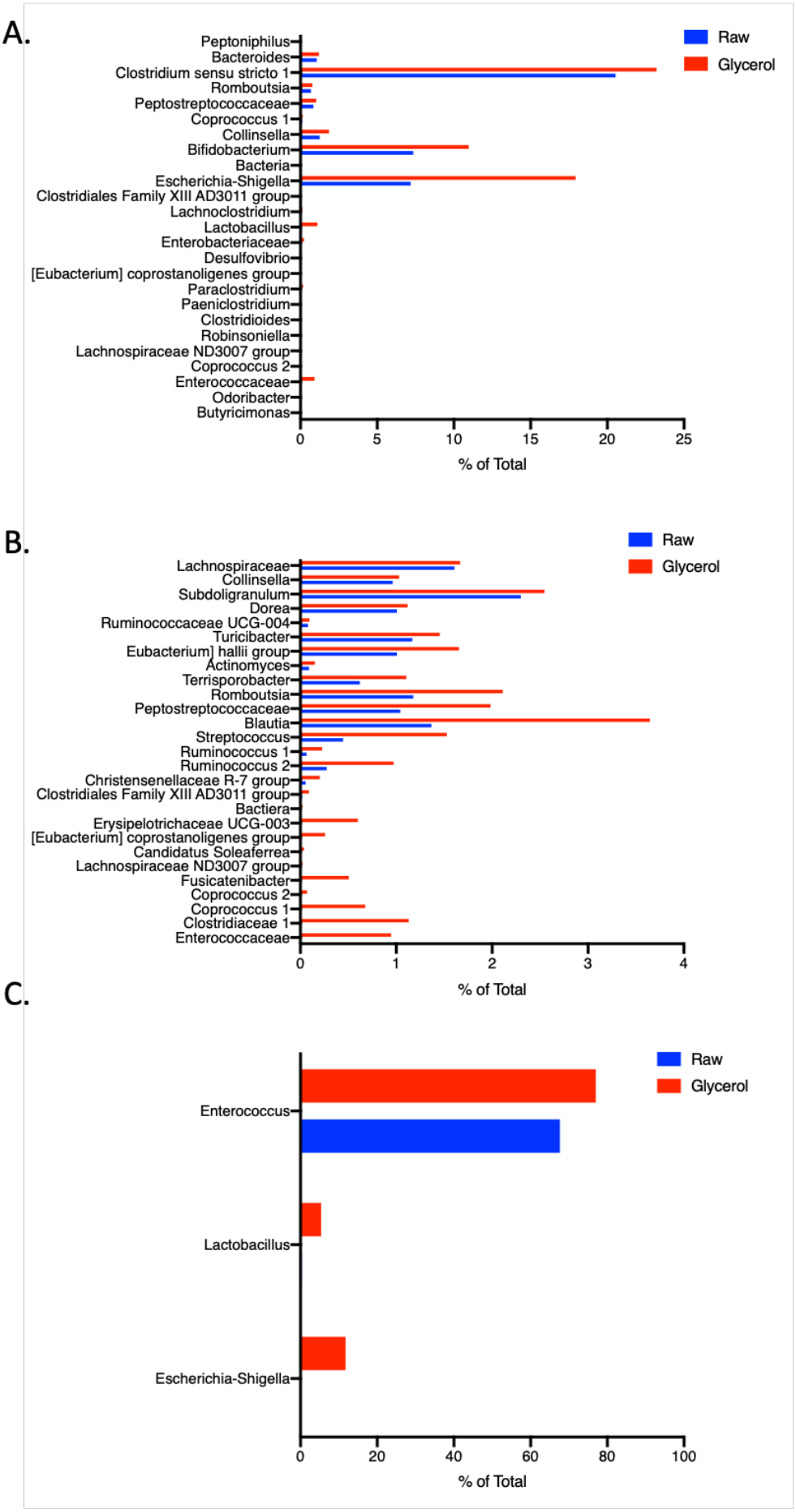
A.
Raw
Glycerol
Peptoniphilus
Bacteroides
Clostridium sensu stricto 1
Romboutsia
Peptostreptococcaceae
Coprococcus 1
Collinsella
Bifidobacterium
Bacteria
Escherichia-Shigella
Clostridiales Family XIII AD3011 group
Lachnoclostridium
Lactobacillus
Enterobacteriaceae
Desulfovibrio
[Eubacterium] coprostanoligenes group
Paraclostridium
Paeniclostridium
Clostridioides
Robinsoniella
Lachnospiraceae ND3007 group
Coprococcus 2
Enterococcaceae
Odoribacter
Butyricimonas
0
5
10
15
20
25
% of Total
B.
Raw
Glycerol
Lachnospiraceae
Collinsella
Subdoligranulum
Dorea
Ruminococcaceae UCG-004
Turicibacter
Eubacterium] hallii group
Actinomyces
Terrisporobacter
Romboutsia
Peptostreptococcaceae
Blautia
Streptococcus
Ruminococcus 1
Ruminococcus 2
Christensenellaceae R-7 group
Clostridiales Family XIII AD3011 group
Bactiera
Erysipelotrichaceae UCG-003
[Eubacterium] coprostanoligenes group
Candidatus Soleaferrea
Lachnospiraceae ND3007 group
Fusicatenibacter
Coprococcus 2
Coprococcus 1
Clostridiaceae 1
Enterococcaceae
0
1
2
3
4
% of Total
C.
Raw
Glycerol
Enterococcus
Lactobacillus
Escherichia-Shigella
0
20
40
60
80
100
% of Total

Figure 3.3.12. Differential enrichment of less abundant OTUs between Glycerol stock derived and Raw sample derived anaerobic cultures.
Proportion of each sample population for raw-derived cultures (blue) compared with glycerol stock cultures (red) for (A) glycerol cultures compared with raw samples, (B) HAMS media growths for 16-2 compared with 16-2 raw sample in Fermentation 2 and (C) HAMS media growth of 10-2 glycerol stock compared with raw sample for Fermentation 2.

Activity of the supernatant appears to be consistent with a small molecule

We sought to determine if the activity that we observed from the supernatant was the result of a protein factor or a small molecule. To do so we took a three-pronged approach to isolate metabolites from the supernatants and track if downregulation was still observed (**Figure 3.3.13A**). This approach was (1) to use enzymatic digestion of proteins within the supernatants, (2) filter supernatants through a 3kDa cut off filter to remove all but small peptides, (3) pass supernatants through a C18 flash column and extract with solutes of decreasing polarity. As a negative control we used 6-1, which was inactive in the prior assays but still is derived from a microbial community from an IBD patient. For these downstream assays we selected the HAMS-derived supernatants as they were the most consistent between all assays.

We used proteinase K (PK), a serine protease, to digest any protein content within the supernatants. Supernatants were treated with 1U/mL Proteinase K at room temp for 20 minutes prior to addition to HEK293T dFLASH-HIF reporter cells and measured after 24 hours for their ability to repress the DMOG induced reporter (**Figure 3.3.13B).** Across two replicates it's clear that, post-PK treatment reporter repression is maintained for both 10-2 and 16-2 and that the PK treatment doesn't prevent upregulation of the reporter with the negative control (6-1). Additionally, as with the initial reporter assays, repression from these samples closely matched basal reporter expression.

We generated a <3kDa fraction from the supernatant that we then applied to the HEK293T dFLASH-HIF cells at 2uL (2% v/v), 5uL (5% v/v) or 10uL (10% v/v) at 24 hours (**Figure 3.3.13C**) or 48 hours (**Figure 3.3.13D**). 3kDa filtration has been used previously to separate protein content from metabolite fractions[191]. Within the <3kDa supernatant fraction we observed there was a consistent downregulation of the reporter in the presence of DMOG for the 10-2 and 16-2 samples at the highest concentration (10% v/v) at both time points (**Figure 3.3.13C, D**). 16-2 was more active than 10-2 as at 5% v/v it decreased reporter to the same extent as the 10% v/v sample as well. There was no observable decrease relative to the DMOG-alone control by the 6-1 sample at either time point, again suggesting that the bioactive component for 10-2 or 16-2 is <3kDa in size, which rules out most proteins excepting for small peptides.

We selected 16-2, as it was active at a lower concentration, to run through a C18 flash column, extracting column flow through (FT), H_2O, Methanol (MeOH) and Acetonitrile (AcCN) extracts from the samples. These were added to HEK293T cells prior to the assay and no gross morphological defects were observed (Data not shown). Samples were then freeze-dried and resuspended before being added again to DMOG treated HEK293T mcdFLASH-HIF cells at either 2uL (2% v/v) or 5uL (5% v/v) against HEK293T dFLASH-HIF after 48 hours (**Figure 3.3.14**). We observed a large decrease in Tomato fluorescent protein expression (HIF-1α activity readout) with 16-2 at 2% v/v for the flow through and the H_2O fraction, not the input (consistent with **Figure 3.3.13D** at 2% v/v) and at 5% v/v we see a decrease in the input, FT, H_2O and MeOH phase. This indicates that we are isolating the activity from the C18 column, once again consistent with the activity observed being from a small molecule.

The C18 purified supernatants were then run against HEK293T dFLASH-HIF cells with the VHL knockout (**Figure 3.3.14B**) and imaged by HCI. This VHL knockout inclusion is important, as all prior work for HIF-1α inhibition was done in the presence of DMOG. If the supernatant was blocking the action of DMOG or via some other mechanism, then the reporter suppression effect would be lost, as was seen in **Chapter 3.2**. At 5% v/v there was the Tomato downregulation without large change in the EGFP internal control for the same samples as **Figure 3.3.14B**, excepting a small uptick with the methanol sample that was seen in the GFP control. This shows the effect is not DMOG-dependent as it downregulated the constitutive VHL KO reporter.

Overall, the results from the three-pronged approach point toward the activity being consistent with a more polar small molecule. It was resistant to proteinase K degradation post-heat treatment, passed through a 3kDa filter, which are inconsistent with a protein factor. The C18 column shows activity in FT and H_2O at 2% v/v and in the MeOH phase at 5% v/v for both dFLASH-HIF and VHL KO dFLASH-HIF. This suggests that the potential metabolite (given the prior results) is likely more polar in nature, which would be consistent with its presence in the aqueous supernatant.

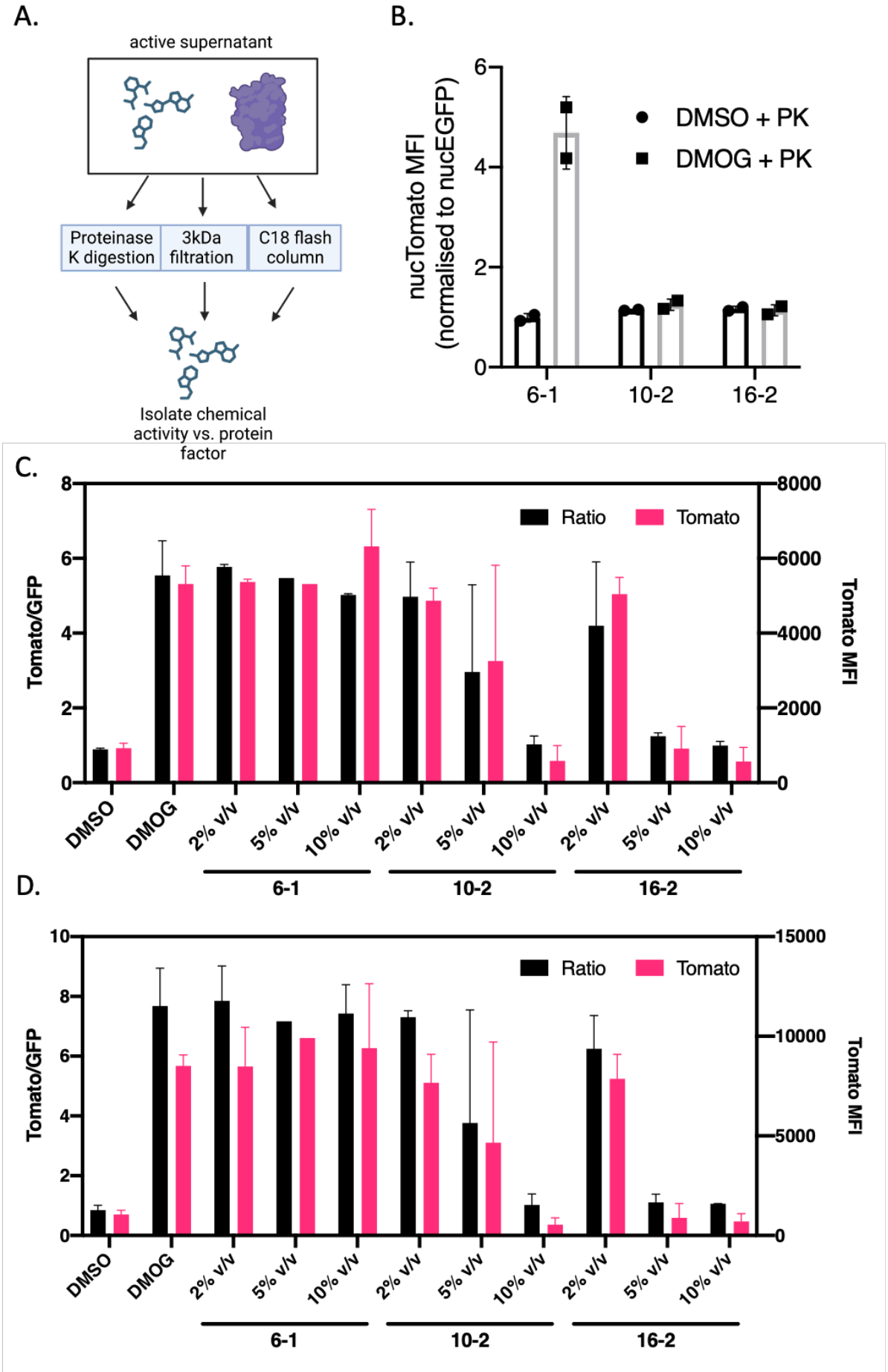
A.
active supernatant
Proteinase K digestion
3kDa filtration
C18 flash column
Isolate chemical activity vs. protein factor
B.
nucTomato MFI (normalised to nucEGFP)
DMSO + PK
DMOG + PK
6-1
10-2
16-2
C.
Tomato/GFP
Tomato MFI
Ratio
Tomato
DMSO
DMOG
2% v/v
5% v/v
10% v/v
6-1
10-2
16-2
D.
Tomato/GFP
Tomato MFI
Ratio
Tomato
DMSO
DMOG
2% v/v
5% v/v
10% v/v
6-1
10-2
16-2

Figure 3.3.13 Determination that the bioactivity observed is consistent with a small molecule and not a protein factor.
(A) Outline of the three approaches, (1) Proteinase K digestion, (2) 3kDa Filtration and (3) C18 column purification, used to determine if the bioactivity in 10-2 and 16-2 is due to a protein or small molecule/metabolite. (B) 6-1, 10-2 and 16-2 supernatants were treated with 1U/mL proteinase K prior to addition at 10% v/v to HEK293T dFLASH-HIF cells and imaged for reporter expression after 24 hours with 0.1% DMSO or 1mM DMOG. Data is mean of 2 biological replicates. (C, D) Tomato/EGFP ratio of 6-1, 10-2 and 16-2 supernatants were passed through a 3kDa cut off filter and the <3kDa fraction was added to HEK293T dFLASH-HIF cells at 10%, 5% or 2% v/v and imaged at (C) 24 hours or (D) 48 hours after treatment with 1mM DMOG (n = 2, except 6-1 5% v/v, n = 1).

A.

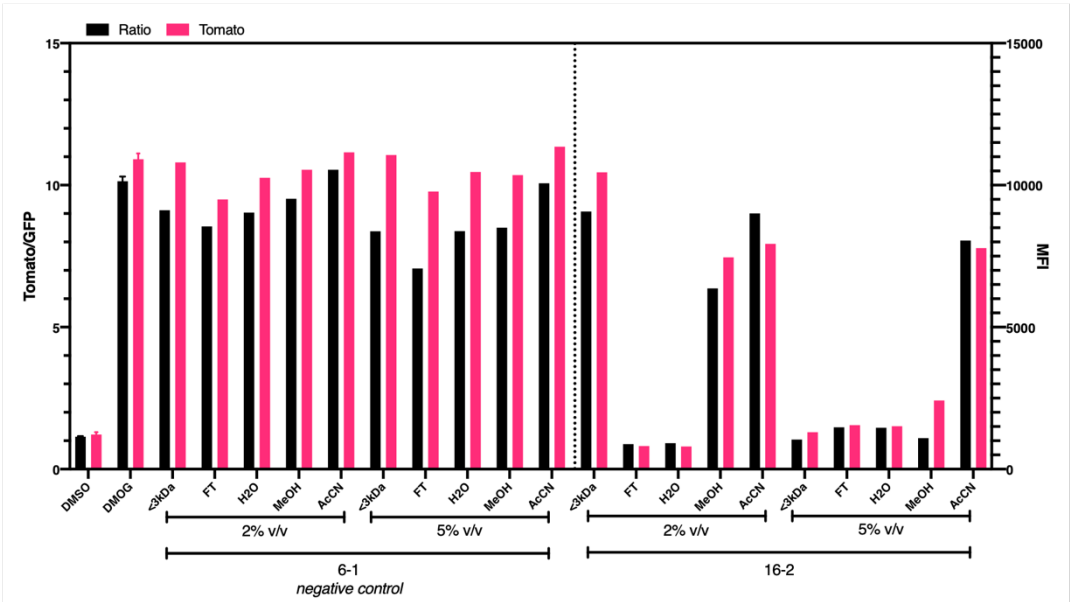

B.

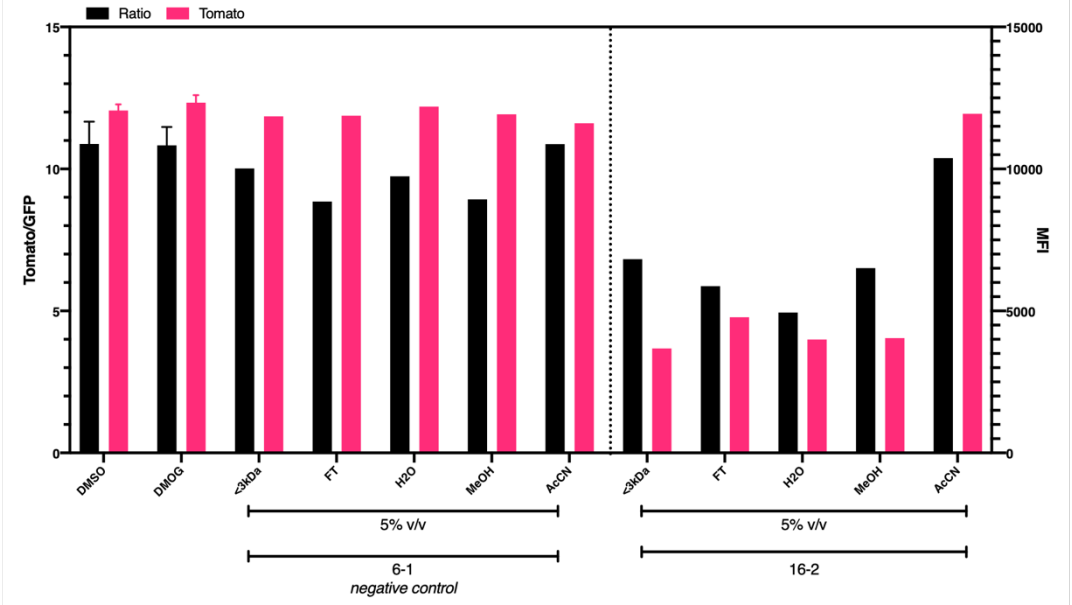

Figure 3.3.14 Activity is maintained post-C18 column purification of <3kDa active fractions

(A, B) 6-1 and 16-2 <3KDa fractions were passed through a C18 flash column. Elutions were freeze dried and reconstituted in H_2O prior to addition at (A) 2% or (A, B) 5% v/v to HEK293T (A) dFLASH-HIF treated with 1mM DMOG or (B) VHL KO dFLASH-HIF cells for 48 hours prior to imaging for reporter expression. N=1.

Iterative growth strategy failed to increase putative metabolite concentration

The results of **Figure 3.3.13** and **Figure 3.3.14** showed that the supernatant was broadly consistent with a metabolite and the results pointed toward the sample being found only in glycerol stock-derived cultures. We therefore hypothesised that a series of iterative growths of the anaerobic cultures would increase and select for the presence of the unknown metabolite that was causing the reporter downregulation (**Figure 3.3.15A**). We based this on the appearance of activity post-glycerol stock outgrowth thus thought that the activity was being selected for under our anerobic growth conditions. Therefore, we grew three cultures in iteration with the HAMS growth media, an initial culture (Growth #1) from the glycerol stock, then sub-cultured that into a second outgrowth (Growth #2) and then sub-cultured a second time for the third outgrowth (Growth #3) on the assumption that it would increase the abundance of the metabolite (and metabolite producing BGC) which would allow for easier downstream detection.

When we assayed these supernatants against HEK293T dFLASH-HIF (**Figure 3.3.15B**) we saw that, while Growth #1 maintained the significant downregulation at 10% v/v, 5% v/v, and 2% v/v in the presence of DMOG ($p<0.001$), anti-reporter activity was completely lost with Growth #2 relative to negative control sample 6-3. Activity Growth #1 we saw that at 2% v/v we did have a significant downregulation, but reporter activity was 50% greater than 5% v/v showing we can titrate activity which again would be expected for a soluble factor. This was a surprising result; however, it does provide two very closely matched samples that can be targeted in a comparative manner to attempt to determine the bioactive compound.

Importantly, we also saw that, consistent with **Figure 3.3.13**, 3kDa filtration produced downregulation of dFLASH-HIF with Growth #1 that was not seen for Growth #2 at 48 hours at 24 or 48 hours (**Figure 3.3.15C, D**). In Growth #2 across the concentration gradient, we observed no change comparing the unfiltered sample with either the retentate or the eluant, suggesting that the putative metabolite is not present with the sample. We saw that the bioactivity was maintained in both the retentate (>3kDa fraction) and the <3kDa eluted fraction. The presence in the retentate is expected, given the supernatant was not fully centrifuged through the 3kDa filter. The presence in the eluant however shows that the putative metabolite can move through the filter.

Activity of the eluant for Growth #1 suggest that we can target the <3kDa fraction as a lower complexity fraction to generate a candidate list of potentially active compounds.

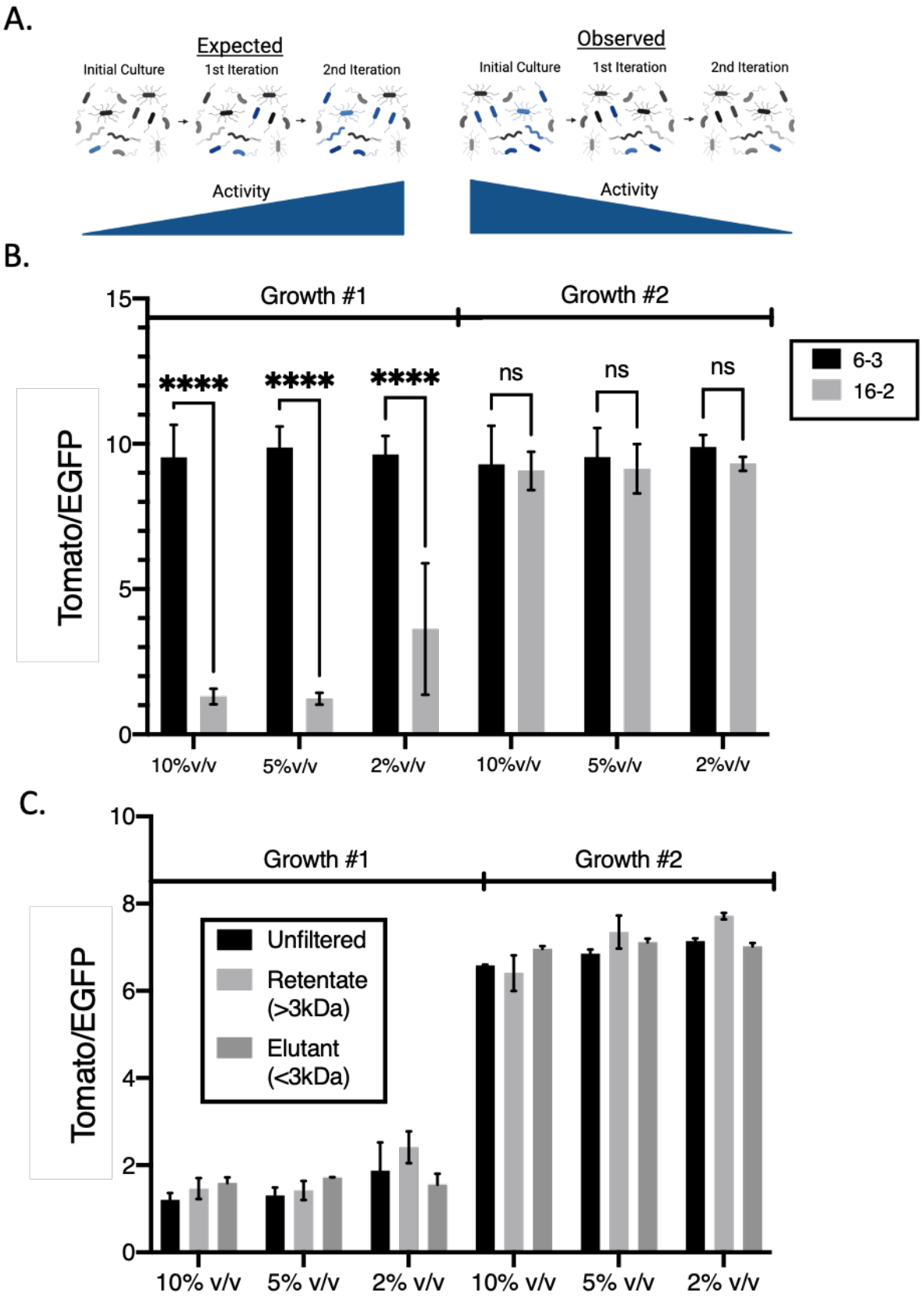
A.
Expected
Initial Culture
1st Iteration
2nd Iteration
Activity
Observed
Initial Culture
1st Iteration
2nd Iteration
Activity
B.
Growth #1
Growth #2
Tomato/EGFP
15
10
5
0
****
****
****
ns
ns
ns
6-3
16-2
10%v/v
5%v/v
2%v/v
10%v/v
5%v/v
2%v/v
C.
Growth #1
Growth #2
Tomato/EGFP
10
8
6
4
2
0
Unfiltered
Retentate (>3kDa)
Elutant (<3kDa)
10% v/v
5% v/v
2% v/v
10% v/v
5% v/v
2% v/v

Figure 3.3.15 Iterative growths to attempt to increase bioactivity instead causes a loss of activity

(A) We expected our iterative growth strategy to positively select for the bacterial species that was causing the bioactivity, thereby enriching for activity given that our current anaerobic growth strategy appears to be favourable for production of the metabolite. (B, C) Glycerol stocks of 16-2 (bioactive) and 6-3 (negative control) were outgrown with the iterative growth strategy and the initial (Growth #1) culture and the first subculture (Growth #2) were assayed against HEK293T dFLASH-HIF at 10%, 5% and 2% v/v in the presence of DMOG and (B) imaged at 48 hours for reporter quantification. Data is mean of 3 independent biological replicates, three technical replicates per biological replicate. Significance was assessed with a student t-test with Welch's correction at each concentration matched to the negative control. (C) 16-2 supernatants from Growth #1 and Growth #2 were passed through a 3kDa filter and unfiltered sample, eluant (<3kDa) and retentate (>3kDa) was assayed by HCl for activity against DMOG-treated HEK293T dFLASH-HIF cells at 48 hours at 2%, 5% or 10% v/v. Data is mean of 3 biological replicates with 2 technical replicates per biological replicate.

Differential enrichment of metabolites provides putative leads for future investigations

To investigate if there are differentially enriched metabolite species between Growth 1 and Growth 2, we had the samples analysed by Metabolomics South Australia for untargeted profiling of the complex samples with High Resolution Fourier Transform Mass Spectroscopy (HRFTMS), focusing on both polar and non-polar metabolites (**Figure 3.3.16A**). Polar metabolites were identified by Hydrophilic Interaction Liquid Chromatography (HILIC)[340] and more non-polar secondary metabolites by Reverse Phase chromatography (RP)[341]. 145 polar metabolites were identified by HILIC-HRFTMS, and 214 metabolites were identified by RP-HRFTMS, with putative identities assigned by matching of m/z profile against the internal Metabolomics South Australia and METLLIN databases. Metabolites were also cross-referenced against the Human Metabolome Project[342], where possible.

While there could have been some overlap in identified metabolites between the two methods, none of the metabolites identified as being enriched >4-fold were enriched in both processes. While there were metabolites that were lower in growth 1 relative to growth 2, our hypothesis was that there would be a metabolite that was enriched in growth 1 relative to growth 2 that was the causative agent. As a result, we focused on the compounds that were enriched in the two processes 4-fold or higher (**Figure 3.3.16B, C**).

Bacterial secondary metabolites are identifiable in RP-HRFTMS

From the 56 secondary metabolites identified as being upregulated more than 4-fold in the RP-HRFTMS, only 20 have a putative identity, and among those compounds upregulated more than 16-fold only 6 of the 28 have a putative identity (**Figure 3.3.16C**). Most other identified secondary metabolites are vitamin-derivatives (e.g. Pathenol, Vitamin C) or are metabolites associated with amino acid metabolism (e.g. leucylasparagine). The large number of unknown metabolites (63% of detected secondary metabolites, 40% of polar metabolites) are of interest. It's unsurprising that

we detected so many, given that despite extensive efforts[342] much of the human microbial metabolome remains unannotated.

From those upregulated compounds two are known products from the excretory pathway, Stercobilin and Glycylprolylhydroxyproline, likely originating from the original stool sample. Their presence in growth 1 is as a contaminant, which would be greatly decreased when sub-cultured in growth 2. Stercobilin is a bacterial product from the end point of heme breakdown and a major component of faeces[343]. Glycylprolylhydroxyproline is an oligopeptide detected in urine from collagen breakdown[344]. It is unlikely that these contaminants are the causative agents however, they have not been linked with HIF-associated effects in the literature previously and Stercobilin has only been correlated with inflammation[343].

HILIC-HRFTMS identifies differentially enriched drug-like scaffolds

We investigated the enriched hits in the polar compounds (**Figure 3.3.16B**), given that bioactivity was maintained post-elution from a C18 column in the aqueous phase (**Figure 3.3.14**). There were 25 metabolites that were upregulated more than 4-fold, 13 of which were upregulated more than 16-fold in Growth 1. 15 of these metabolites were assigned putative identities, but 10 could not be identified. Of the 15 known metabolites, we identified several metabolites that are upregulated in faecal samples, fitting with the source of the microbial cultures, or are known metabolites from bacterial cultures.

From the 15 known metabolites, two are members the benzimidazole family of compounds. 1H-Benzimidazol-5-ol was enriched 6-fold and 2-aminobenzimidazole was enriched 9-fold in growth 1. Benzimidazole derivatives have been reported as scaffolds for derivation of PHD inhibitors[345] and HIF-1α inhibitors[346,347]. It's important to note however, that these compounds are heavily modified from the scaffolds we identify. Additionally, this scaffold, and the benzimidazole family, has known diverse activity *in cellulo* due functioning as a privileged scaffold enabling extensive modification for side groups[348,349]. Therefore, these two metabolites are of interest in future investigation into the causative downregulation that is observed. Two separate instances of 2,5-piperazinedione are also highly enriched in the HILIC-HPFTMS

analysis. 2,5-piperazinediones are cyclic peptides and are simple molecular scaffolds that have a diverse range of activities and are commonly occurring bacterial metabolites[350]. The 2,5-piperazinediones presence confirms that our samples contain non-ribosomal peptides (NRPs)[309], a pool of diverse signalling molecules that could be candidate bioactive molecules.

It's important to note the caveats with these results, (1) These are putative structural identifications and may not be accurate, and (2) these metabolites provide a candidate list for future investigations that, due to limitations in time, go beyond the scope of this thesis. While we have identified several metabolites that confirm we have a diverse pool of potential ligands within the bioactive supernatant and potential lead compounds from this analysis, there is still a program of work to determine the mechanism that explains the reporter downregulation.

Figure 3.3.16. **Metabolomics of polar and secondary metabolites show differentially enriched metabolites between Growth 1 and Growth 2.**
(A) <3kDa fractions from growth 1 and growth 2 from **Figure 3.2.15** were analysed for differential enrichment by Hydrophilic Interaction Liquid Chromatography (HILIC) High Resolution Fourier Transform Mass Spectroscopy (HRFTMS) for polar compounds or Reverse Phase HRFTMS for secondary metabolites. (B) 145 compounds were identified by HILIC-HRFTMS. 12 compounds were enriched 4-fold (blue) and 13 compounds were enriched 16-fold (red) with $p < 0.05$. (C) 214 compounds were identified by RP-HRFTMS. 28 compounds were enriched 4-fold (blue) and 28 compounds were enriched 16-fold (red). Metabolites were further classified putative identity (Known, Circle) or not (Unknown, Triangle). Data is from three technical replicates per sample.

Adaption of dFLASH toward the Aryl Hydrocarbon Receptor

While this project was primarily focused on HIF-1α, as that is our well validated screen-ready system, we also began to design a system to target the Aryl Hydrocarbon Receptor (AhR). AhR is a well characterised sensor of microbial products[351,352]. There has been a significant interest in the role of AhR in the gut microenvironment, given its role in IL-22 expression and Th17 cell balance[352-354], which also involves crosstalk with HIF-1α signalling[123,355].

As a result, we developed an initial dFLASH sensor of AhR (**Figure 3.3.17A**). It contained 10 repeats of the 30bp AhR response element from CYP1A1[356]. When XRE-dFLASH was transduced into HEPG2 cells, creating HEPG2 dFLASH-AhR, there was a clear response from the population to AhR ligands, Indole and Kynurenic acid (**Figure 3.3.17C**). The ligand responses from the polyclonal cells didn't form a population with a large level of separation from the negative control, indicating a much smaller signal window which complicates screening efforts. While a monoclonal line of HEPG2 dFLASH-AhR population also increased Tomato expression post-ligand treatment (**Figure 3.3.17D**) the level of expression remains much lower in than the HIF-1α screening line and there was a significant fluctuation in EGFP expression.

The current AhR reporter underperforms when compared with the HIF-1α and PR dFLASH systems, the other endogenous dFLASH reporters. While there are several differences between these transcription factors and their co-activators, there is also a significant difference in enhancer construction for XRE-dFLASH compared to the other systems. PRE-dFLASH and HRE-dFLASH have multiple response elements per repeating unit in the enhancer, while XRE-dFLASH has a single response element per repeating element. Additionally, each concatemeric unit was much smaller than that of SRE-dFLASH and HRE-dFLASH. Therefore, while XRE-dFLASH does respond, the signal may be greatly improved by redesigning the enhancer element to include more endogenous response elements and their flanking contexts.

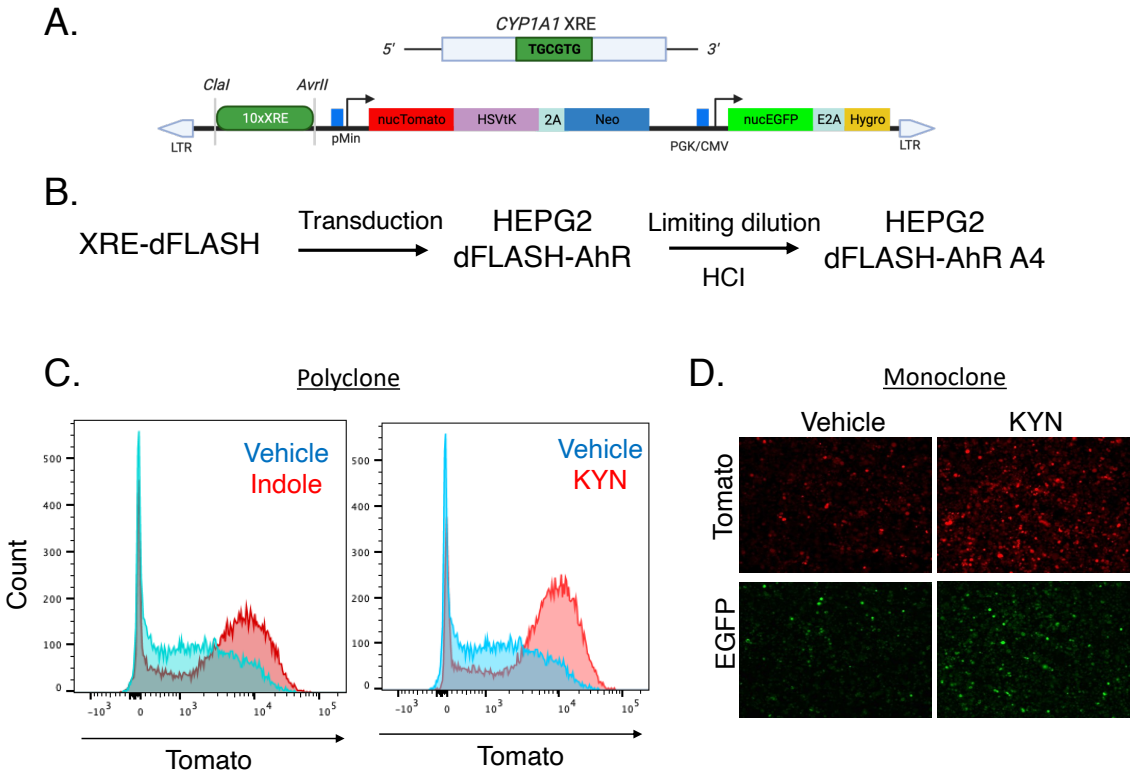

Figure 3.3.17 Initial variants of dFLASH-AhR constructs demonstrate ligand response but lack sensitivity

(A) A single CYP1A1 Xenobiotic Response Element (XRE) was multimerised 10 times and cloned into dFLASH, creating XRE-dFLASH. (B) transduction into HEPG2 cells, generating HEPG2 dFLASH-AHR polyclone. Monoclonal derivation was done through limiting dilutions to 1 cell per well of the polyclone and selection of the most response clone, A4, by HCI. (C) Tomato MFI from polyclonal HEPG2 dFLASH-AhR treated with 0.1% DMSO (vehicle), 100μM Indole or 100μM of Kynurenic acid (KYN) for 48 hours was assessed by flow cytometry. Representative of 2 independent experiments. (D) dFLASH-AhR A4 monoclones were treated with 0.1% DMSO or 100μM Kynurenic acid for 48 hours prior to widefield imaging for Tomato (Cy3) or EGFP (FITC) expression. Images are representative of 3 independent replicates.

Discussion:

dFLASH is a robust system for investigating functional links between microbiota and host signalling pathways.

There have been several proposed mechanisms previously made between HIF-1α and different microbial species, such as *P. aeruginosa*[153,357], hence our interest in using supernatant screening to probe for potential bioactivity. Supernatant screening has been performed against other signalling pathways recently, for example, Chen, et al. [192] describe a forward chemical screen where they took a large library of individual strains and screened them against a GPCR luciferase reporter library for activity. This group have also applied a similar strategy toward DNA damage agents[191] and next generation GPCR reporters[190]. Reporter screens against intracellular transcription factors has also been done, where supernatants from bacteria engineered to express single genes from microbiota are screened in parallel against fluorescent reporters[314]. Therefore, we have confidence that our experimental approach was sound in probing for interactions between these species and HIF-1α.

One of the major aims of this project was to investigate if dFLASH would be a suitable reporter to investigate functional connections between microbial species and cellular models. While fluorescent screening systems have also been deployed in refractive screening systems for NF-κB[314], this approach relied on heterologous expression of isolated commensal genes in a model bacterium instead of an unbiased exposure to the biotic environment offered by combining live cell culture with bacterial supernatants. We found that HEK293T dFLASH-HIF cells tolerated a range of different media types and did not observe dramatic cytotoxicity under any screening condition, although some slowed cell-growth was observed with certain bioactive samples. This allowed us to screen against three types of bacterial culture; monocultures (**Figure 3.3.3- 3.3.5**), multi-species co-culture models (**Figure 3.3.5**) and larger scale patient-derived *in vitro* cultures (**Figure 3.3.7-3.3.9**), at 10% v/v of supernatant, consistent with other, similar supernatant approaches[190-192]. While our screening of monocultures and mock communities was ultimately unsuccessful in defining a novel interaction with HIF-1α (**Figure 3.3.3-3.3.5**), we did observe multiple instances where reporter expression was altered non-specifically by microbial supernatant addition. This

suggests that we are sampling the microbial biotic environment with this reporter. Furthermore, based on our small molecule screening ability and the results from the IBD patient sample screening, it also suggests that dFLASH enables selection of on-target activity from background interference.

No DFU associated strain or mock colony regulated HIF-1α

With the DFU-isolated strains we tried two approaches, screening monocultures (**Figure 3.3.3-3.3.4**) and mock communities (**Figure 3.3.5**), to probe for a functional interaction between any of these species and the HIF-1α reporter. While we did see an increase in mean reporter expression with the 5-member community compared to the media control, it was statistically insignificant and small in magnitude (**Figure 3.3.5**). This highlights some of the complications and caveats with functional screening of the microbiota. Firstly, there is a lot of diversity in microbial products that result from a shared biotic environment *in vivo*, with cross-species/cross-strain signalling lost *in vitro*. This has been demonstrated with the jump from monoculture to co-culture models *in vitro*, with multi-species coculture models producing different secondary metabolites[312,330]. Secondly, many of the BGC are silenced under standard culture conditions[307]. Therefore the bulk of the biosynthetic potential of the microbiome is considered untapped by experimental methods[358,359], particularly as it's known that BGCs for one process can synthesis intermediates for other pathways[360]. Additionally, some commensal species aren't readily culturable as single colony isolates[337] which introduces an inherent bias in the library composition. Ultimately however, we do conclude that there is no impact on HIF-1α signalling from any of the patient-derived strains.

Despite this, these assays were still informative, despite not having the desired results. They allowed us to demonstrate that dFLASH can be utilised as a high throughput screening platform applied toward investigating microbial products. dFLASH offers a competitive advantage over prior reporter systems. First the internal control that, as was seen with the EGFP changes to monoclonal DFU isolates (**Figure 3.3.3**), can detect off-target reporter modulation. Second, it's an image-based approach which enables identification of deleterious phenotypes. While this wasn't relevant for the

DFU monocultures, it was for the IBD samples discussed below. Overall, the screening of the DFU cultures ratified our experimental approach, as we could detect reporter inference and highlights issues with current refractive screening methods for delineating bacterial-host signalling events.

Identification of the bioactive IBD sample, implications and future directions.

We took a different culturing approach when probing the activity of the IBD-patient derived cultures. While the issues surrounding *in vitro* silencing and loss of diversity still apply, instead of single colony isolates we used bulk microbiome cultures from patient derived samples. This strategy, known as culture enrichment, does introduce differences in populations compared with uncultured microbiomes however can enrich for less common taxa[361]. As shown by the 16s sequencing (**Figure 3.3.10**), the samples contained a variety of different species, suggestive of a richer biotic environment. Indeed, unlike with the DFU monocultures, supernatant screening from these samples did have a consistent downregulatory effect on the HIF-1α reporter (**Figure 3.3.8 – 3.3.9, 3.3.15**) suggesting it was a property of that community. We further characterised that the bioactive agent was consistent with a small molecule or peptide (**Figure 3.3.13-3.3.14**) and inhibited constitutive HIF-1α expression post-flash column purification (**Figure 3.3.14**). Metabolomic analysis confirmed that there were uniquely enriched metabolites present in two closely matched samples (**Figure 3.3.16**) providing a candidate list to narrow in on putative activators. Additionally, the data from the metabolomics regarding retention time of small molecules of interest will enable more accurate purification and isolation of the putative interactors with HPLC-based identification, using a similar workflow to our C18 flash column purification strategy.

It should be noted however, that in contrast with the refractive methods commented on earlier, this method of biodiscovery is more resource consuming than monoculture or mock community assisted discovery. We are taking a product-first approach to trying to decipher the interaction we are observing. This was due to the 16s rRNA sequencing results (**Figure 3.3.10-3.3.12**), which didn't provide a clearly upregulated abundant species and would require an in-depth cultureomic approach[362] to isolate single bacterial colonies and screen for activity against our HTS platform. While this is feasible, the crucial assumption is that it's one species producing the agent and

ignores the underlying collaborative biosynthetic environment[143,363] that could give rise to the effector. Our data is suggestive of a small molecule or peptide being a causative agent, but the work remaining in narrowing down the causative agent and confirming it has real anti-HIF activity is non-trivial. Based on prior efforts that identify small molecules from the microbiome have pursued those lines of investigation[190,192], this discovery project points to a program of work that consists of isolation of an active fraction via HPLC guided by the metabolomic results followed by independent confirmation of anti-HIF-1α functional downregulation by the agent and confirmation that it can replicate this activity with a synthetic analogue. Finally, it would be important physiologically to link the putative activity to a BGC or species. This is critical as we only detect the downregulation in a glycerol stock sample derived from a faecal sample that itself was not bioactive when culture enriched. Therefore, there remains a spectre of physiological relevance to the disease case over this project. As demonstrated by our and others interest in small molecule screening efforts, independent of a disease setting there is considerable value in defining small molecule inhibitors of HIF-1α, discussed elsewhere.

This putative detection of an IBD-associated population with HIF-1α downregulation is potentially impactful in understanding the complex host-microbial species dynamics that are present during IBD. HIF-1α is considered a protective factor to IBD disease progression, given its role in enhancing epithelial barrier function and promotion of cellular survival in hypoxic foci and basal hypoxia in the colonic epithelium[323]. This is borne out within *in vivo* models; whereby a decline in epithelial barrier function is rescued by prolyl hydroxylase inhibitor treatment[131] and HIF-1α knockouts in intestinal epithelial cells lead to more severe colitis[130]. In addition to its role in epithelial barrier homeostasis, HIF-1α is involved in Th17 and Treg balance through upregulation of RORγt expression, and HIF-1α deficient mouse models have decreased Th17 population[122]. This adds an extra layer of potential complexity to the *in vivo* role of HIF-1α in IBD pathogenesis. Classically, HIF-1α is considered pro-Th17 and anti-T_{reg}[122,355] however this has been challenged, with HIF-1α deficient T_{reg} cells being unable to mediate T-cell-regulated suppression of colitis[123]. Hence, these sets of experiments

begin to probe if there is an element of microbial-induced HIF-1α signalling and how it might interact with the microbiome and the immunological dysregulation of IBD.

Need for a functional *in vitro* AhR screening system for functional interrogation of microbial signalling

Using dFLASH-HIF to detect a putative bioactive small molecule from a patient IBD microbiome also provides more emphasis on adapting dFLASH toward AhR. AhR considered a protective factor and ligand-induced stimulation of AhR attenuating colitis and inflammation in murine models is well described[353,364-370]. While our initial version was not screen-ready (**Figure 3.3.17**), we were able to see consistent activity from two AhR ligands, indole and kynurenic acid. Both are produced or modified to more potent versions by commensal bacteria[371]. It's been previously shown that *Lactobacilli* can upregulate kynurenine from accelerated Trp metabolism which activates AhR and stimulates anti-inflammatory cytokine IL-22 independent of host Trp metabolism *in vivo*[352,368]. Cell-specific deletion of AhR in endothelial[372] and epithelial[373] cells results in dysregulated inflammatory responses, establishing AhR as a vital sensor for microbial and dietary ligands across the gut epithelial barrier to the blood. Additionally, AhR stimulates the production of IL-22 and the production of Th17 cells, a role that overlaps with reported HIF-1α activity[353,365]. While AhR has been extensively studied in murine models and supported, in some contexts, by human cell culture examples a persistent issue is many of these studies fail to appreciate the differences in the PAS-B ligand binding of rodent and murine AhR compared to human AhR (hAhR)[374]. Hence, the creation of dFLASH-AhR would enable interrogation of IBD-associated microbes and their products against hAhR in a high throughput setting in a similar process to what we have described above for HIF-1α.

Chapter 4. Final Discussion

This thesis encompasses the development and application of a novel genetic element (dFLASH) that can be adapted toward of range of signalling pathways. We ratified the activity of this reporter by using in several high throughput approaches targeted against the HIF pathway. We delineated two novel small molecule regulators of HIF-1α, an iron-chelating activator compound and an inhibitor that blocks HIF-1α transcription in a bimodal screen design. It covers a small molecule screen that resulted in detection of interfering compounds and how high content metrics can be leveraged with our screening approaches to eliminate interfering compounds for improved screen design. Finally, it covers an exploratory project that seeks to define interactions between the human microbiome and the HIF pathways using the established reporting techniques established in this thesis.

dFLASH and the pantheon of genetic reporting elements for HIF and hypoxia

dFLASH is not the first fluorescent reporting element for HIF signalling. There have been several previous fluorescent and luciferase-based genetic elements targeting HIF-1α activity. These elements have been deployed to target HIF-1α signalling in different cellular contexts, in drug discovery efforts and more recently have been leveraged to investigate non-canonical regulation of the HIF-1α pathway[45,185,186,375]. A common design for hypoxic or HIF sensors is the fusion of the ODD domain to a fluorescent protein, leading to its VHL-mediated degradation. This couples the stability of the fluorescent protein or luciferase with HIF-1α and its canonical regulatory pathway, as well as oxygen, iron, and 2-OG availability and limits off-target signalling[45,376-378] . Correspondingly, this has enabled investigations in tumour xerographs with luciferase variants[376,377] and in CRISPR screens with ODD-coupled fluorescent proteins[45,185,186].

While we have considered this approach, the core advantage of dFLASH is its ability to adapt its reporting capacity to different synthetic or endogenous pathways. Furthermore, coupling the fluorescent protein to the ODD will likely impacts the signal window, a key requirement for screening efforts. Instead, solution to detecting off-target signalling therefore, is in the dual fluorescent protein design, with the modulation

independent EGFP cassette acting as a biomarker for non-specific reporter activity. Indeed, we've demonstrated robust activation of dFLASH to a range of different pathways instead of over-specialisation for HIF-specific pathways (**Chapter 3.1**). Gal4RE-dFLASH can integrate with former approaches that utilise HRE-dependent expression of Gal4 binding proteins for signal amplification[377]. The fluorescent approach does come at the cost of signal sensitivity compared with luciferase approaches, such as in comparison with our adaption of dFLASH called NanoFIRE[379], which provides a much larger level of signal induction by swapping Tomato expression for nanoluciferase. This issue can be important in the case of minimisation, as scaling up to 384 or 1536 well plates with fluorescent reporters leads to a known decrease in sensitivity due to detection thresholds[293]. An addition drawback is that signal is heavily dependent on stability of the Tomato fluorophore post-signal induction, however prior work has shown stability of signal after periods of hypoxia followed by 4 hour recovery[197]. On the inverse however, luciferase screens are often end point assays, as opposed to fluorescent systems which allows for live cell imaging. This is more cost-effective at scale, at the expense of sensitivity, and facilitated our bimodal screening strategy for combined antagonist and agonist screening strategies.

In addition, there has been a lot of renewed interest in applying high content approaches, like what we have developed here, into CRISPR and drug screening approaches. This interest is facilitated by the ability to generate high complexity datasets at the level of primary screening. High complexity is defined as multiple population features, such as cell appearance, segmentation or sub selection of the population of interest and generation of multiple datapoints per analysed well for a more holistic overview of the sampled *in vitro* population instead of a singular datapoint[180]. As demonstrated in **Chapter 3.1** and **Chapter 3.2**, dFLASH enables a high complexity readout and compatibility to both cytometry and microscopy-based population segmentation.

Drug Discovery utilising dFLASH: Compound discovery and future directions

There have been multiple prior drug discovery efforts against HIF-1α that have discovered several regulators that target different points of the HIF-1α pathway. In

Chapter 3.1 we define two natural product derived compounds that regulated HIF-1α and how they interact with the HIF-1α pathway.

RQ200674 acts as a weak iron chelator, leading to HIF-1α stabilisation. Iron chelators are known to normoxically stabilise HIF-1α[259] however also have broader effects on other pathways, including the wider 2-OG dioxygenase family[380]. Targeting HIF-1α stabilisation with specific inhibitors of its regulatory pathway has been shown to be a successful therapeutic intervention for anaemia[86]. As iron chelators and 2-OG inhibitors drive HIF-stimulated wound healing[381], there has also been interest in applying these HIF regulators topically. Compared with other iron chelators, such as DP, **RQ200674** is comparatively weak and targeting **RQ200674's** pyridoindole motif as a structural scaffold also did not result in identification of other, stronger, activating compounds with a more selective mechanism of action (MOA). Furthermore, there are concerns with off-target effects with iron chelators in a clinical setting. Additionally, there are several PHD-specific inhibitors that interact with the 2-OG binding pocket on PHD2 and prevent 2-OG binding and HIF proline hydroxylation in a selective manner[90,158]. These compounds are in late-stage clinical trials[81,86,382], and unlike iron chelators offer a more specific mechanism of action. It should be noted however, they aren't side effect free and long-term risk factors still require further investigation[82]. Overall, **RQ200674** is a poor candidate for future drug development. It does however ratify that our dFLASH system can readily detect HIF-1α activators.

RQ500235 blocks HIF-1α transcription, leading to a decline in HIF-1α protein in the presence of DMOG. There are a range of previously reported HIF-1α inhibitors with different MOA. These include other transcriptional inhibitors[166,383], small molecules that block CBP/p300 recruitment[384] and direct inhibitors of HIF-1α:ARNT dimer formation[14,169]. The ability to detect a transcriptional inhibitor does provide confidence that our bimodal screening strategy and parameters with dFLASH resolves in on-target activity by identified inhibitors. However, the potential for deleterious side effects with **RQ500235** is high, given its MOA, which suggests it to be a poor candidate for further development.

The current gold standard for targeting the HIF pathway is the development of HIF-2α inhibitors that target the hydrophobic pocket and prevent dimerisation[17,18,160]. This has resulted in development of an FDA approved inhibitor for use in renal cell carcinomas resulting from von Hippel-Lindau Disease which leads to upregulated HIF signalling[162]. Both HIF-1α and HIF-2α have a hydrophobic PAS-B pocket[385]. HIF-1α's PAS-B pocket however has been shown to be druggable *in vitro*. Cardoso, et al. [13] targeted purified HIF-1α's PAS-B with 200 compounds, identifying several that could destabilise the HIF-1α:ARNT's protein-protein interaction. A similar strategy resulted in the identification of acriflavine which intercalates between HIFα and ARNT dimerisation through a β-sheet interaction[169]. Despite these prior attempts however, there is no clinically deployable inhibitor of HIF-1α. Many of the current commercially available inhibitors, such as acriflavine and YC-1 have deleterious side effects that have prevented clinical or, in certain contexts experimental, use, leaving open the door for a wider screening campaign than the pilot screens discussed here.

Drug Discovery utilising dFLASH: Merging of Target & Phenotypes

Chapter 3.1 and **Chapter 3.2** contain pilot screens that demonstrate dFLASH is applicable at scale, having screened 2407 compounds across both the Quinn and Bioaustralis libraries. These pilot screens demonstrate that the reporter outputs are sufficient to detect off-target effects and allow for isolation of positive and negative regulators of HIF-1α. Given in **Chapter 3.1** we demonstrated the cross-compatibility of dFLASH to PR and Gal4DBD fusion proteins, dFLASH can function as a broadly applicable general platform for drug discovery efforts. In **Chapter 3.2** however it is evident that our screening approaches can be improved.

Classic target-dependent drug discovery, such as the use of targeted genetic reporters, has been widely applied to targeting transcription factors, including HIF-1α[169,176,178,386-388]. A common criticism of target-dependent approaches however is that they have resulted in a high failure rate within the compound discovery to application rate[180,389]. As a result, high content or phenotypic approaches are increasingly being adopted as they target a rescue or reversion of a particular phenotype in a target agnostic fashion[390]. These approaches have been accelerated

with the increase in machine learning algorithms for identifying multiple cellular features at scale[180,278,390-392]. The primary issue with phenotypic screening is target deconvolution post-hit identification which can be an involved process[180]. Therefore, marrying target-based approaches with phenotypic screening approaches offers a more optimised approach. This is particularly important as at the end of a phenotypic screening campaign, it can be an uphill battle to then deconvolute the causative target.

In our initial application of dFLASH for HIF-1α drug discovery, we relied primarily on the output of the genetic reporter in a target-based approach (**Chapter 3.1, Chapter 3.2**). Integrating of nuclear shape with revaluating the Bioaustralis library data however (**Chapter 3.2**) pointed toward how phenotypic data can be integrated into the screening and decision-making pipeline with dFLASH and the HCS approach we've used. This makes it one of the highest-complexity approaches to HIF-1α drug discovery used to date.

There has been a prior published HCS phenotypic screen targeting markers of angiogenesis with immunofluorescence identified anti-HIF-1α compounds with subsequent target-based luciferase reporters[393]. Unlike this previous approach, dFLASH enables targeting of HIF-1α within the primary screen which leads us to propose that combinatorial or multiplexed screening with dFLASH would facilitate better outcomes than most strategies. Therefore, we suggest that dFLASH is a valid option for merging traditional target-based discovery with phenotypic screening approaches. As traditional primary screening usually relies on a single low complexity output, such as a single reporter readout from the bulk population[182], we've shown that dFLASH can provide a higher complexity, multi-reporter output coupled with assessments of cellular morphology and further segmentation of nuclei providing identification of individual cells.

Leveraging dFLASH for forward genetic screening:

We've demonstrated robust reporting to HIF-1α from dFLASH in a wider range of *in vitro* contexts than any of the prior HIF-1 reporters. We've developed techniques for high content protocols for dFLASH, demonstrated with our small molecule screening

efforts (**Chapters 3.1, 3.2**). Additionally, we are beginning to leverage the image-based approach for greater qualitative depth at a primary screening level (**Chapter 3.2**), although our current methods have room for increased refinement. This comes as a timely update to the pantheon of genetic HIF reporters as increasingly high content approaches are being looked to as a more informative method for forward genetic screening[189]. Feldman, et al. [241] demonstrated the utility of integrating high content imaging approaches with fluorescent outputs. They confirmed the known NF-κB translocation pathway through combining a translocation assay with an optical single-cell sequencing approach for barcode identification. They have further proposed integration of their methodology with genetic reporters[242], and as a result we propose dFLASH would be a good candidate for these imaged-based CRISPR approaches.

We've previously touched on the adaption of dFLASH-HIF toward CRISPR based approaches, including reporter response of CRISPR-knockdowns (**Chapter 3.1**) and the use of CRISPR knockouts of VHL for orthogonal screening applications (**Chapter 3.2**). This points to utility of dFLASH as a CRISPR screening platform. There have been CRISPR screens under hypoxia that have confirmed the canonical HIF-1α regulation pathway, unearthed novel HIF-1α regulators and begun to probe the HIF-1α-independent hypoxia signalling[45,185,186,394]. A competitive advantage for dFLASH over other fluorescent based-approaches to HIF-1α reporting is the inclusion of the downstream reporter cassette, providing a single-cell, transcriptional readout independent of the target pathway. As HIF responses can be cell-type dependent, optical imaging methods facilitate dissection of these pathways in complex cellular cultures and our work applying dFLASH to a high content setting, we propose dFLASH as a next-generation reporter for transcriptional pathway signalling given its integration with these approaches.

HIF and the microbiome: Therapeutic Opportunities

Investigating crosstalk between host signalling pathways and the microbiome is both interesting from understanding the pathophysiology of certain disease states such as IBD, discussed in **Chapter 3.3**, however also opens the door for therapeutic

exploitation. There are current clinical trials ongoing regarding faecal microbiome transplants within IBD patients[395]. These transplants, resulting in an exchange of the microbiome, is correlated with improved outcomes and patient quality of life. Many of the fundamentals in host-microbial signalling relationships point to a complex interaction between emergent community interactions and potential crosstalk between host signalling pathways and immune response that remain poorly delineated. The work in **Chapter 3.3** is exploratory in nature and is there to demonstrate that reporter assay development can be turned toward probing for these relationships.

Our results pointed to putative signalling between microbial communities and HIF-1α. Firstly, there have been prior reports regarding several species that were capable of cross-signalling to HIF-1α, most notably *Lactobacillus* and *P. aeruginosa* however HIF has also been suggested to be more broadly upregulated in various infections by different pathogens[339]. As there is great strain-level diversity, these data (**Chapter 3.3**) doesn't directly oppose or confirm these prior reports and proposed mechanisms and microbial crosstalk onto HIF-1α is likely a complex affair that can be mediated by physiological consequences, such as inflammatory hypoxia, instead of direct signalling between the microbe and the HIF-1α protein, which is what our refractive system was set up to investigate. We were unable to confirm any direct on-target reporting activity from monocultures in HEK293T cells and it was only in our most complex microbiome model, the IBD cultures, that we observed consistent reporter downregulation from a microbially-derived small molecule. Delineation of this effect may offer a novel insight into the underlying signalling mechanisms at play within an IBD context.

This investigation is also relevant to more than IBD and DFUs, the source for our microbial communities. Delineating interactions with the microbiome can also have value in understanding the role of HIF-1α signalling in the lung. Chronic infections can occur regularly in CF patients, where hypoxic microenvironments can form and dysbiosis of the microbiome can occur[396]. The CF transmembrane conductance regulator (CFTR) mutation causes mucosal build up which prevents mucosal clearance. This can cause a hypoxic environment within the mucosa due to reduced

O_2 diffusion and, given associated inflammation, an elevated O_2 consumption economy between the epithelial cells, neutrophils, and commensal bacteria[397]. These hypoxic microenvironments can cause a change in pulmonary pathogens, such as *P. aeruginosa*. Under anaerobic culture conditions, *P. aeruginosa* has been documented to form biofilms and upregulate quorum sensing factors that have been linked with repression of HIF[153] with culture-free supernatants. We saw that, in liquid BHI media and grown under anaerobic conditions, *P. aeruginosa* from DFUs did not active or inhibit dFLASH-HIF (**Chapter 3.3**), however our culture conditions were different from Legendre, et al. [153] which could affect biofilm formation. The detection of the downregulatory effect with the IBD cultures, however, does indicate that the possibility of a microbe-HIF repressive signalling axis that would exacerbate certain disease states.

Understanding these signalling events can lead to therapeutic opportunities. Because of the host-microbial signalling axis, manipulation of the microbiome is increasingly being looked at as a delivery vector for a variety of conditions[398,399]. This has been demonstrated with individual bacterial associations in the rescue a social disorder phenotype with addition of *L. reuteri* to a neurodevelopmental disorder model[400]. Synthetic circuits within microbial vectors are also becoming viable. For instance, engineered yeast strains expressing a signal-induced ATP-degrading enzyme to decrease extracellular ATP from commensal species, a proinflammatory signal, were shown to decrease symptoms of colitis in a TNBS murine model[401]. Use of microbial vectors in this setting have also been used to manipulate HIF-1α signalling in murine models. Sanmarco, et al. [402] utilised *E. coli* expressing lactate to drive expression of HIF-1α to attenuate an autoimmune phenotype. As a result, a comprehensive understanding of microbial population interactions with signalling pathways comes to the forefront for appropriate therapeutic intervention.

An additional layer of under-explored complexity lies in cell-specific HIF-1α and HIF-2α signalling differences within the gut. Within intestinal epithelial cells, HIF-1α is an established protective factor within colitis models[130,131,140]. In contrast, HIF-2α overexpression enhances colitis and HIF-2 knockouts in intestinal epithelial cells

attenuate symptoms[403]. This is of particular interest given that HIF-2α has a druggable ligand binding pocket[11,18,163]. We utilised our dFLASH-HIF HEK293T line as it does not report on HIF-2α, although we have engineered HIF-2α responsive dFLASH systems and shown function in HIF-1α and HIF-2α expressing cell types (**ref honours thesis, Chapter 3.1**). Therefore, future work can begin to look at probing if our identified activity was isoform-specific utilising our established synthetic toolbox.

Expansion of the synthetic toolbox: AhR and Beyond

High content, live cell approaches offered by dFLASH provide a versatile platform for high throughput screening, either drug screening or, given our preliminary work, genetic screening. Unlike traditional luciferase reporters, they can screen in a live cell, stain and reagent free environment which significantly reduces associated costs of high throughput screening campaigns. Another important facet of the dFLASH system that we cover as part of this thesis is the adaptability of the system to other targets, not just HIF-1α which is the target for most of this work. A sensible direction for future expansion of this system is to target the broader bHLH-PAS family. This is of particular interest as partial structures and *in silico* modelling of all the bHLH-PAS protein members show a conserved putative ligand binding pockets that suggest druggability[10]. Given the importance of these transcription factors in a variety of different niches and disease states[1,385,404], dFLASH provides an opportunity to generate high-throughput screening lines against these factors, particularly as outside HIF-1α and AhR, these have been no concerted efforts in targeting these family members with high throughput approaches.

In **Chapter 3.3** we show efforts to being to expand the series of dFLASH reporters toward other members of the bHLH-PAS family, having solved a backbone interference effect that held up development (**Chapter 3.1**). To do so we initially targeted AhR. The creation of an AhR system is particularly useful for probing disease-associated microbial interactions with the host through small molecules. AhR has several well-defined interactions with different microbial products[7] in its role as a xenobiotic responsive factor and exerts control over certain aspects of immune signalling that also intersect with HIF[355]. This also particularly pertinent as signalling

mechanisms between intestinal and inflammatory cells and microbial indole species is known to occur with many indole and tryptophan species shown to be ligands for AhR[260,352,366,372,405-409]. AhR signalling is known to play a role in maintenance of intestinal homeostasis but there are underappreciated differences between human AhR and murine AhR that result in different levels of activation that can have consequences when extrapolating murine signalling results to human disease[351]. AhR and HIF do have established cross-talk that can occur and both promote Th17 cell production which can be anti-inflammatory in the pathology of IBD[410]. Kim, et al. [411] utilised a high content screening approach against AhR by fluorescently tagging CYP1A1 endogenously, demonstrating this pathway is amenable to these approaches. However, their approach lacked the benefits of the stain-free, internally controlled approach of dFLASH. Therefore, generation of robust genetic reporters against these factors offers an opportunity to probe the wider bHLH-PAS family with forward genetic screening approaches and high throughput campaigns. In a broader sense however, this thesis demonstrates the utility of dFLASH to a range of applications and attempts to establish it as a general reporter platform that will facilitate targeting of different TF pathways by the wider scientific community.

Chapter 5: Appendix

Appendix for chapter 3.3:

Appendix Table 3.3.1. Bacterial species isolated from patient diabetic wounds and derived as monocultures for supernatant screening (Sourced from Dr. Nan Hao, Sherwin Lab).

Species	Origin	Growth Condition
Finegoldia magna	ATCC 29328	anaerobic, 37C, >3days
Anaerococcus vaginalis	Patient 1	anaerobic, 37C, >3days
Facklamia hominis	Patient 10	anaerobic, 37C, >3days
Finegoldia magna	Patient 10	anaerobic, 37C, >3days
Peptoniphilus harei	Patient 10	anaerobic, 37C, >3days
Finegoldia magna	Patient 12	anaerobic, 37C, >3days
Finegoldia magna	Patient 13	anaerobic, 37C, >3days
No Organism Identification Possible	Patient 13	anaerobic, 37C, >3days
Pseudomonas aeruginosa	Patient 13	aerobic, 37C, 1 day
Staphylococcus epidermidis	Patient 13	aerobic, 37C, O/N
Finegoldia magna	Patient 14	anaerobic, 37C, >3days
Peptoniphilus harei	Patient 14	anaerobic, 37C, >3days
Enterococcus faecalis	Patient 15	aerobic, 37C, O/N
Finegoldia magna	Patient 15	anaerobic, 37C, >3days
Enterococcus faecalis	Patient 2	aerobic, 37C, O/N
Finegoldia magna	Patient 2	anaerobic, 37C, >3days
Finegoldia magna	Patient 20	anaerobic, 37C, >3days
Anaerococcus murdochii	Patient 4	anaerobic, 37C, >3days
Anaerococcus vaginalis	Patient 4	anaerobic, 37C, >3days
Finegoldia magna	Patient 4	anaerobic, 37C, >3days
Morganella morganii	Patient 4	aerobic, 37C, O/N
Murdochiella asaccharolytica	Patient 4	anaerobic, 37C, >6days
Anaerococcus hydrogenalis	Patient 8	anaerobic, 37C, >3days
Finegoldia magna	Patient 8	anaerobic, 37C, >3days
Finegoldia magna	Patient 9	anaerobic, 37C, >3days
Peptoniphilus sp[2]	Patient 9	anaerobic, 37C, >4days
Anaerococcus vaginalis	Patient 1	anaerobic, 37C, >3days
Finegoldia magna	Patient 1	anaerobic, 37C, >3days
Staphylococcus aureus	Patient 1	aerobic, 37C, O/N
Peptoniphilus harei	Patient 10	anaerobic, 37C, >3days
Pseudomonas aeruginosa	Patient 13	aerobic, 37C, 1 day
Streptococcus agalactiae	Patient 1	aerobic, 37C, O/N
Enterobacter cloacae	Patient 1	aerobic, 37C, O/N

Dermabacter hominis	Patient 1	aerobic, 37C, 2 days
Peptoniphilus gorbachii	Patient 2	anaerobic, 37C, >3days
Enterococcus faecalis	Patient 2	aerobic, 37C, O/N
Klebsiella oxytoca	Patient 2	aerobic, 37C, O/N
Peptoniphilus grossensis	Patient 4	anaerobic, 37C, >5days
Anaerococcus murdochii	Patient 4	anaerobic, 37C, >3days
Morganella morganii	Patient 4	aerobic, 37C, O/N
Corynebacterium striatum	Patient 5	aerobic, 37C, O/N
Anaerococcus hydrogenalis	Patient 8	anaerobic, 37C, >3days
Enterobacter hormaechei	Patient 9	aerobic, 37C, O/N
Providencia rettgeri	Patient 9	aerobic, 37C, O/N
Staphylococcus simulans	Patient 10	aerobic, 37C, O/N
Staphylococcus epidermidis	Patient 10	aerobic, 37C, O/N
Staphylococcus caprae	Patient 11	aerobic, 37C, O/N
Proteus mirabilis	Patient 11	aerobic, 37C, O/N
Citrobacter freundii	Patient 12	aerobic, 37C, O/N
Escherichia coli	Patient 12	aerobic, 37C, O/N
Klebsiella aerogenes	Patient 12	aerobic, 37C, O/N
Staphylococcus lugdunensis	Patient 13	aerobic, 37C, O/N
Corynebacterium confusum	Patient 13	aerobic, 37C, 2 day
Staphylococcus aureus	Patient 1	aerobic, 37C, O/N
Peptoniphilus harei	Patient 10	anaerobic, 37C, >3days
Pseudomonas aeruginosa	Patient 13	aerobic, 37C, 1 day
Streptococcus agalactiae	Patient 1	aerobic, 37C, O/N
Enterobacter cloacae	Patient 1	aerobic, 37C, O/N
Dermabacter hominis	Patient 1	aerobic, 37C, 2 days
Peptoniphilus gorbachii	Patient 2	anaerobic, 37C, >3days
Enterococcus faecalis	Patient 2	aerobic, 37C, O/N
Klebsiella oxytoca	Patient2	aerobic, 37C, O/N
Peptoniphilus grossensis	Patient 4	anaerobic, 37C, >5days
Anaerococcus murdochii	Patient 4	anaerobic, 37C, >3days
Morganella morganii	Patient 4	aerobic, 37C, O/N
Corynebacterium striatum	Patient 5	aerobic, 37C, O/N
Anaerococcus hydrogenalis	Patient 8	anaerobic, 37C, >3days
Enterobacter hormaechei	Patient 9	aerobic, 37C, O/N
Providencia rettgeri	Patient 9	aerobic, 37C, O/N
Staphylococcus simulans	Patient 10	aerobic, 37C, O/N
Staphylococcus epidermidis	Patient 10	aerobic, 37C, O/N
Staphylococcus caprae	Patient 11	aerobic, 37C, O/N
Proteus mirabilis	Patient 11	aerobic, 37C, O/N
Citrobacter freundii	Patient 12	aerobic, 37C, O/N
Escherichia coli	Patient 12	aerobic, 37C, O/N
Klebsiella aerogenes	Patient 12	aerobic, 37C, O/N

Staphylococcus lugdunensis	Patient 13	aerobic, 37C, O/N
Corynebacterium confusum	Patient 13	aerobic, 37C, 2 day

Appendix Table 3.3.2. Patient-specific co-cultures used in **Figure 3.3.5**

Patient ID	**Sample ID**	**Species Name**
Patient 1	base (300ul) +	
	AH8003	*Streptococcus agalactiae*
	AH8004	*Enterobacter cloacae*
	AH8006	*Dermabacter hominis*
Patient 2	base (300ul) +	
	AH8003	*Streptococcus agalactiae*
	AH8010	*Enterococcus faecalis*
	AH8011	*Klebsiella oxytoca*
	AH8006	*Dermabacter hominis*
Patient 3	base (300ul) +	
	AH8014	*Peptoniphilus grossensis*
	AH8015	*Anaerococcus murdochii*
	AH8018	*Morganella morganii*
Patient 4	base (500ul) +	
	AH8019	*Corynebacterium striatum*
Patient 5	base (300ul) +	
	AH8024	*Enterobacter hormaechei*
	AH8025	*Providencia rettgeri*
Patient 6	base (300ul) +	
	AH8029	*Staphylococcus simulans*
	AH8030	*Staphylococcus epidermidis*
Patient 7	base (300ul) +	
	AH8024	*Enterobacter hormaechei*
	AH8032	*Staphylococcus caprae*
	AH8033	*Proteus mirabilis*
Patient 8	base (300ul) +	
	AH8035	*Citrobacter freundii*
	AH8036	*Escherichia coli*
	AH8037	*Klebsiella aerogenes*
Patient 9	base (300ul) +	
	AH8038	*Staphylococcus lugdunensis*
	AH8040	*Corynebacterium confusum*
	AH8030	*Staphylococcus epidermidis*
Patient 10	base (300ul) +	
	AH8010	*Enterococcus faecalis*
	AH8011	*Klebsiella oxytoca*

Patient 11	base (500ul) +	
	AH8032	*Staphylococcus caprae*
Patient 12	base (300ul) +	
	AH8024	*Enterobacter hormaechei*
	AH8033	*Proteus mirabilis*
	AH8006	*Dermabacter hominis*

Appendix Table 3.3.3. 10-species co-culture compositions used in **Figure 3.3.5E**		
Mixture 1	base (300ul) +	
	AH8003	*Streptococcus agalactiae*
	AH8004	*Enterobacter cloacae*
	AH8006	*Dermabacter hominis*
	AH8010	*Enterococcus faecalis*
	AH8011	*Klebsiella oxytoca*
Mixture 2	base (300ul) +	
	AH8006	*Dermabacter hominis*
	AH8014	*Peptoniphilus grossensis*
	AH8015	*Anaerococcus murdochii*
	AH8018	*Morganella morganii*
	AH8019	*Corynebacterium striatum*
Mixture 3	base (300ul) +	
	AH8024	*Enterobacter hormaechei*
	AH8025	*Providencia rettgeri*
	AH8029	*Staphylococcus simulans*
	AH8030	*Staphylococcus epidermidis*
	AH8032	*Staphylococcus caprae*
Mixture 4	base (300ul) +	
	AH8033	*Proteus mirabilis*
	AH8035	*Citrobacter freundii*
	AH8036	*Escherichia coli*
	AH8037	*Klebsiella aerogenes*
	AH8038	*Staphylococcus lugdunensis*
Mixture 5	base (300ul) +	
	AH8040	*Corynebacterium confusum*
	AH8030	*Staphylococcus epidermidis*
	AH8010	*Enterococcus faecalis*
	AH8011	*Klebsiella oxytoca*
	AH8032	*Staphylococcus caprae*
Mixture 6	base (300ul) +	
	AH8011	*Klebsiella oxytoca*
	AH8032	*Staphylococcus caprae*

	AH8024	*Enterobacter hormaechei*
	AH8033	*Proteus mirabilis*
	AH8006	*Dermabacter hominis*

Appendix Table 3.3.4 Enriched species by 16s rRNA sequencing in all glycerol stock derived pellets compared with bacterial pellets from raw samples

Enriched species identity	**Fold change**
Lactobacillus	13.95341
Lachnoclostridium	6.62169
Clostridiales Family XIII AD3011 group	5.674754
Escherichia-Shigella	2.497604
Bacteria	1.707914
Bifidobacterium	1.491163
Collinsella	1.483632
Coprococcus 1	1.405204
Peptostreptococcaceae	1.221784
Romboutsia	1.13088
Clostridium sensu stricto 1	1.129945
Bacteroides	1.124118
Peptoniphilus	1.084949

Appendix Table 3.3.5 Enriched species in 16-2 HAMS glycerol outgrowth (2nd fermentation) compared with raw sample outgrowth

Enriched species identity	Fold change
Clostridiales Family XIII AD3011 group	4.413697
Christensenellaceae R-7 group	3.668528
Ruminococcus 2	3.530958
Ruminococcus 1	3.492156
Streptococcus	3.42894
Blautia	2.66531
Peptostreptococcaceae	1.90371
Romboutsia	1.79231
Terrisporobacter	1.779717
Actinomyces	1.681408
Eubacterium] hallii group	1.643765
Turicibacter	1.24482
Ruminococcaceae UCG-004	1.18224
Dorea	1.110482
Subdoligranulum	1.107202
Collinsella	1.070584
Lachnospiraceae	1.03713

Appendix Table 3.3.6 Enriched species in 10-2 glycerol outgrowth (2nd fermentation, HAMS supplement) compared with raw sample outgrowth

Enriched species identity	Fold change
Escherichia-Shigella	129.221
Lactobacillus	17.15747
Enterococcus	1.138376

Chapter 6. References:

1 Bersten, D. C., Sullivan, A. E., Peet, D. J. & Whitelaw, M. L. bHLH-PAS proteins in cancer. *Nat Rev Cancer* **13**, 827-841 (2013). https://doi.org/10.1038/nrc3621

2 Moglich, A., Ayers, R. A. & Moffat, K. Structure and signaling mechanism of Per-ARNT-Sim domains. *Structure* **17**, 1282-1294 (2009). https://doi.org/10.1016/j.str.2009.08.011

3 Pongratz, I., Antonsson, C., Whitelaw, M. L. & Poellinger, L. Role of the PAS Domain in Regulation of Dimerization and DNA Binding Specificity of the Dioxin Receptor. *Molecular and Cellular Biology* **18** (1998).

4 Lindebro, M. C., Poellinger, L. & Whitelaw, M. Protein-protein interaction via PAS domains: role of the PAS domain in positive and negative regulation of the bHLH/PAS dioxin receptor-Arnt transcription factor complex. *The EMBO Journal* **14**, 3528-3539 (1995).

5 Whitelaw, M., Pongratz, I., Wilhelmsson, A., Gustafsson, J. A. & Poellinger, L. Ligand-dependent recruitment of the Arnt coregulator determines DNA recognition by the dioxin receptor. *Molecular and Cellular Biology* **13**, 2504-2514 (1993). https://doi.org/10.1128/mcb.13.4.2504

6 Henry, J. T. & Crosson, S. Ligand-binding PAS domains in a genomic, cellular, and structural context. *Annu Rev Microbiol* **65**, 261-286 (2011). https://doi.org/10.1146/annurev-micro-121809-151631

7 Hubbard, T. D., Murray, I. A. & Perdew, G. H. Indole and Tryptophan Metabolism: Endogenous and Dietary Routes to Ah Receptor Activation. *Drug Metab Dispos* **43**, 1522-1535 (2015). https://doi.org/10.1124/dmd.115.064246

8 Nebert, D. W. Aryl hydrocarbon receptor (AHR): "pioneer member" of the basic-helix/loop/helix per-Arnt-sim (bHLH/PAS) family of "sensors" of foreign and endogenous signals. *Prog Lipid Res* **67**, 38-57 (2017). https://doi.org/10.1016/j.plipres.2017.06.001

9 Gruszczyk, J. *et al.* Cryo-EM structure of the agonist-bound Hsp90-XAP2-AHR cytosolic complex. *Nature Communications* **13** (2022). https://doi.org/10.1038/s41467-022-34773-w

10 Wu, D., Su, X., Potluri, N., Kim, Y. & Rastinejad, F. NPAS1-ARNT and NPAS3-ARNT crystal structures implicate the bHLH-PAS family as multi-ligand binding transcription factors. *Elife* **5** (2016). https://doi.org/10.7554/eLife.18790

11 Wu, D., Potluri, N., Lu, J., Kim, Y. & Rastinejad, F. Structural integration in hypoxia-inducible factors. *Nature* **524**, 303-308 (2015). https://doi.org/10.1038/nature14883

12 Liang, J., Edelsbrunner, H. & Woodward, C. Anatomy of protein pockets and cavities: measurement of binding site geometry and implications for ligand design. *Protein Sci* **7**, 1884-1897 (1998). https://doi.org/10.1002/pro.5560070905

13 Cardoso, R. *et al.* Identification of Cys255 in HIF-1α as a novel site for development of covalent inhibitors of HIF-1α/ARNT PasB domain protein–protein interaction. *Protein Science* **21**, 1885-1896 (2012).

14 Miranda, E. *et al.* A cyclic peptide inhibitor of HIF-1 heterodimerization that inhibits hypoxia signaling in cancer cells. *J Am Chem Soc* **135**, 10418-10425 (2013). https://doi.org/10.1021/ja402993u

15 Guo, Y. *et al.* Regulating the ARNT/TACC3 axis: multiple approaches to manipulating protein/protein interactions with small molecules. *ACS Chem Biol* **8**, 626-635 (2013). https://doi.org/10.1021/cb300604u

16 Rogers, J. L. *et al.* Development of inhibitors of the PAS-B domain of the HIF-2alpha transcription factor. *J Med Chem* **56**, 1739-1747 (2013). https://doi.org/10.1021/jm301847z
17 Scheuermann, T. H. *et al.* Allosteric inhibition of hypoxia inducible factor-2 with small molecules. *Nat Chem Biol* **9**, 271-276 (2013). https://doi.org/10.1038/nchembio.1185
18 Scheuermann, T. H. *et al.* Isoform-Selective and Stereoselective Inhibition of Hypoxia Inducible Factor-2. *J Med Chem* **58**, 5930-5941 (2015). https://doi.org/10.1021/acs.jmedchem.5b00529
19 Diao, X. *et al.* Identification of oleoylethanolamide as an endogenous ligand for HIF-3alpha. *Nat Commun* **13**, 2529 (2022). https://doi.org/10.1038/s41467-022-30338-z
20 Semenza, G. L. HIF-1 mediates metabolic responses to intratumoral hypoxia and oncogenic mutations. *J Clin Invest* **123**, 3664-3671 (2013). https://doi.org/10.1172/JCI67230
21 Hu, C. J., Wang, L. Y., Chodosh, L. A., Keith, B. & Simon, M. C. Differential roles of hypoxia-inducible factor 1alpha (HIF-1alpha) and HIF-2alpha in hypoxic gene regulation. *Mol Cell Biol* **23**, 9361-9374 (2003). https://doi.org/10.1128/MCB.23.24.9361-9374.2003
22 Gruber, M. *et al.* Acute postnatal ablation of Hif-2alpha results in anemia. *Proc Natl Acad Sci U S A* **104**, 2301-2306 (2007). https://doi.org/10.1073/pnas.0608382104
23 Holmquist-Mengelbier, L. *et al.* Recruitment of HIF-1alpha and HIF-2alpha to common target genes is differentially regulated in neuroblastoma: HIF-2alpha promotes an aggressive phenotype. *Cancer Cell* **10**, 413-423 (2006). https://doi.org/10.1016/j.ccr.2006.08.026
24 Sowter, H. M., Raval, R. R., Moore, J., Ratcliffe, P. J. & Harris, A. L. Predominant Role of Hypoxia-Inducible Transcription Factor (Hif)-1 versus Hif-2 in Regulation of the Transcriptional Response to Hypoxia. *Cancer Research* **63**, 6130-6134 (2003).
25 Raval, R. R. *et al.* Contrasting properties of hypoxia-inducible factor 1 (HIF-1) and HIF-2 in von Hippel-Lindau-associated renal cell carcinoma. *Mol Cell Biol* **25**, 5675-5686 (2005). https://doi.org/10.1128/MCB.25.13.5675-5686.2005
26 Hu, C. J., Sataur, A., Wang, L., Chen, H. & Simon, M. C. The N-terminal transactivation domain confers target gene specificity of hypoxia-inducible factors HIF-1alpha and HIF-2alpha. *Mol Biol Cell* **18**, 4528-4542 (2007). https://doi.org/10.1091/mbc.e06-05-0419
27 Lau, K. W., Tian, Y. M., Raval, R. R., Ratcliffe, P. J. & Pugh, C. W. Target gene selectivity of hypoxia-inducible factor-alpha in renal cancer cells is conveyed by post-DNA-binding mechanisms. *Br J Cancer* **96**, 1284-1292 (2007). https://doi.org/10.1038/sj.bjc.6603675
28 Stiehl, D. P. *et al.* Non-canonical HIF-2alpha function drives autonomous breast cancer cell growth via an AREG-EGFR/ErbB4 autocrine loop. *Oncogene* **31**, 2283-2297 (2012). https://doi.org/10.1038/onc.2011.417
29 Schodel, J. *et al.* High-resolution genome-wide mapping of HIF-binding sites by ChIP-seq. *Blood* **117**, e207-217 (2011). https://doi.org/10.1182/blood-2010-10-314427
30 Smythies, J. A. *et al.* Inherent DNA-binding specificities of the HIF-1alpha and HIF-2alpha transcription factors in chromatin. *EMBO Rep* **20** (2019). https://doi.org/10.15252/embr.201846401

31 Mole, D. R. *et al.* Genome-wide association of hypoxia-inducible factor (HIF)-1alpha and HIF-2alpha DNA binding with expression profiling of hypoxia-inducible transcripts. *J Biol Chem* **284**, 16767-16775 (2009). https://doi.org/10.1074/jbc.M901790200
32 Bersten, D. *et al. Core and Flanking bHLH-PAS:DNA interactions mediate specificity and drive obesity* (Cold Spring Harbor Laboratory, 2022).
33 Keith, B., Johnson, R. S. & Simon, M. C. HIF1α and HIF2α: sibling rivalry in hypoxic tumor growth and progression. *Nat Rev Cancer* **12**, 9-22 (2012).
34 Hirsilä, M., Koivunen, P., Günzler, V., Kivirikko, K. I. & Myllyharju, J. Characterization of the Human Prolyl 4-Hydroxylases That Modify the Hypoxia-inducible Factor. *Journal of Biological Chemistry* **278**, 30772-30780 (2003). https://doi.org/10.1074/jbc.m304982200
35 Appelhoff, R. J. *et al.* Differential function of the prolyl hydroxylases PHD1, PHD2, and PHD3 in the regulation of hypoxia-inducible factor. *J Biol Chem* **279**, 38458-38465 (2004). https://doi.org/10.1074/jbc.M406026200
36 Lando, D. *et al.* FIH-1 is an asparaginyl hydroxylase enzyme that regulates the transcriptional activity of hypoxia-inducible factor. *Genes Dev* **16**, 1466-1471 (2002). https://doi.org/10.1101/gad.991402
37 Lando, D., Peet, D. J., Dean A. Whelan, Jeffery J. Gorman & Whitelaw, M. L. Asparagine Hydroxylation of the HIF Transactivation Domain: A Hypoxic Switch. *Science* **295** (2002).
38 Peyssonnaux, C., Nizet, V. & Johnson, R. S. Role of the hypoxia inducible factors HIF in iron metabolism. *Cell Cycle* **7**, 28-32 (2008). https://doi.org/10.4161/cc.7.1.5145
39 Koivunen, P. *et al.* Inhibition of hypoxia-inducible factor (HIF) hydroxylases by citric acid cycle intermediates: possible links between cell metabolism and stabilization of HIF. *J Biol Chem* **282**, 4524-4532 (2007). https://doi.org/10.1074/jbc.M610415200
40 Pollard, P. J. *et al.* Accumulation of Krebs cycle intermediates and over-expression of HIF1alpha in tumours which result from germline FH and SDH mutations. *Hum Mol Genet* **14**, 2231-2239 (2005). https://doi.org/10.1093/hmg/ddi227
41 Dang, L. *et al.* Cancer-associated IDH1 mutations produce 2-hydroxyglutarate. *Nature* **462**, 739-744 (2009). https://doi.org/10.1038/nature08617
42 Xu, W. *et al.* Oncometabolite 2-hydroxyglutarate is a competitive inhibitor of alpha-ketoglutarate-dependent dioxygenases. *Cancer Cell* **19**, 17-30 (2011). https://doi.org/10.1016/j.ccr.2010.12.014
43 Chowdhury, R. *et al.* The oncometabolite 2-hydroxyglutarate inhibits histone lysine demethylases. *EMBO Rep* **12**, 463-469 (2011). https://doi.org/10.1038/embor.2011.43
44 Koivunen, P. *et al.* Transformation by the (R)-enantiomer of 2-hydroxyglutarate linked to EGLN activation. *Nature* **483**, 484-488 (2012). https://doi.org/10.1038/nature10898
45 Burr, S. P. *et al.* Mitochondrial Protein Lipoylation and the 2-Oxoglutarate Dehydrogenase Complex Controls HIF1alpha Stability in Aerobic Conditions. *Cell Metab* **24**, 740-752 (2016). https://doi.org/10.1016/j.cmet.2016.09.015
46 Tyrakis, P. A. *et al.* S-2-hydroxyglutarate regulates CD8(+) T-lymphocyte fate. *Nature* **540**, 236-241 (2016). https://doi.org/10.1038/nature20165

47 Chandel, N. S. *et al.* Reactive oxygen species generated at mitochondrial complex III stabilize hypoxia-inducible factor-1alpha during hypoxia: a mechanism of O2 sensing. *J Biol Chem* **275**, 25130-25138 (2000). https://doi.org/10.1074/jbc.M001914200

48 Brune, B. & Zhou, J. Hypoxia-inducible factor-1alpha under the control of nitric oxide. *Methods Enzymol* **435**, 463-478 (2007). https://doi.org/10.1016/S0076-6879(07)35024-6

49 Kozlov, A. M., Lone, A., Betts, D. H. & Cumming, R. C. Lactate preconditioning promotes a HIF-1α-mediated metabolic shift from OXPHOS to glycolysis in normal human diploid fibroblasts. *Scientific Reports* **10** (2020). https://doi.org/10.1038/s41598-020-65193-9

50 Ali, M. A., Yasui, F., Matsugo, S. & Konishi, T. The lactate-dependent enhancement of hydroxyl radical generation by the Fenton reaction. *Free Radic Res* **32**, 429-438 (2000). https://doi.org/10.1080/10715760000300431

51 Dodd, K. M., Yang, J., Shen, M. H., Sampson, J. R. & Tee, A. R. mTORC1 drives HIF-1α and VEGF-A signalling via multiple mechanisms involving 4E-BP1, S6K1 and STAT3. *Oncogene* **34**, 2239-2250 (2015). https://doi.org/10.1038/onc.2014.164

52 Majumder, P. K. *et al.* mTOR inhibition reverses Akt-dependent prostate intraepithelial neoplasia through regulation of apoptotic and HIF-1-dependent pathways. *Nat Med* **10**, 594-601 (2004). https://doi.org/10.1038/nm1052

53 van Uden, P., Kenneth, N. S. & Rocha, S. Regulation of hypoxia-inducible factor-1alpha by NF-kappaB. *Biochem J* **412**, 477-484 (2008). https://doi.org/10.1042/BJ20080476

54 Gradin, K. *et al.* Functional Interference between Hypoxia and Dioxin Signal Transduction Pathways: Competition for Recruitment of the Arnt Transcription Factor. *Molecular and Cellular Biology* **16** (1996).

55 Liu, Y. V. *et al.* RACK1 competes with HSP90 for binding to HIF-1alpha and is required for O(2)-independent and HSP90 inhibitor-induced degradation of HIF-1alpha. *Mol Cell* **25**, 207-217 (2007). https://doi.org/10.1016/j.molcel.2007.01.001

56 Luo, W. *et al.* Hsp70 and CHIP selectively mediate ubiquitination and degradation of hypoxia-inducible factor (HIF)-1alpha but Not HIF-2alpha. *J Biol Chem* **285**, 3651-3663 (2010). https://doi.org/10.1074/jbc.M109.068577

57 Koh, M. Y., Lemos, R., Jr., Liu, X. & Powis, G. The hypoxia-associated factor switches cells from HIF-1alpha- to HIF-2alpha-dependent signaling promoting stem cell characteristics, aggressive tumor growth and invasion. *Cancer Res* **71**, 4015-4027 (2011). https://doi.org/10.1158/0008-5472.CAN-10-4142

58 Serocki, M. *et al.* miRNAs regulate the HIF switch during hypoxia: a novel therapeutic target. *Angiogenesis* **21**, 183-202 (2018). https://doi.org/10.1007/s10456-018-9600-2

59 Jaskiewicz, M., Moszynska, A., Gebert, M., Collawn, J. F. & Bartoszewski, R. EPAS1 resistance to miRNA-based regulation contributes to prolonged expression of HIF-2 during hypoxia in human endothelial cells. *Gene* **868**, 147376 (2023). https://doi.org/10.1016/j.gene.2023.147376

60 Bruning, U. *et al.* MicroRNA-155 promotes resolution of hypoxia-inducible factor 1alpha activity during prolonged hypoxia. *Mol Cell Biol* **31**, 4087-4096 (2011). https://doi.org/10.1128/MCB.01276-10

61 Vaupel, P., Mayer, A. & Höckel, M. Tumor hypoxia and malignant progression. *Methods Enzymol* **381**, 335-354 (2004). https://doi.org/10.1016/s0076-6879(04)81023-1
62 Semenza, G. L. Defining the role of hypoxia-inducible factor 1 in cancer biology and therapeutics. *Oncogene* **29**, 625-634 (2010). https://doi.org/10.1038/onc.2009.441
63 Yamamoto, Y. *et al.* Hypoxia-inducible factor 1alpha is closely linked to an aggressive phenotype in breast cancer. *Breast Cancer Res Treat* **110**, 465-475 (2008). https://doi.org/10.1007/s10549-007-9742-1
64 Carmeliet, P. *et al.* Role of HIF-1a in hypoxia mediated apoptosis, cell proliferationand tumour angiogenesis. (1998).
65 Ryan, H. E., Lo, J. & Johnson, R. S. HIF-1α is required for solid tumor formation and embryonic vascularization. *The EMBO Journal* **17** (1998).
66 Liao, D., Corle, C., Seagroves, T. N. & Johnson, R. S. Hypoxia-inducible factor-1alpha is a key regulator of metastasis in a transgenic model of cancer initiation and progression. *Cancer Res* **67**, 563-572 (2007). https://doi.org/10.1158/0008-5472.CAN-06-2701
67 Bellot, G. *et al.* Hypoxia-induced autophagy is mediated through hypoxia-inducible factor induction of BNIP3 and BNIP3L via their BH3 domains. *Mol Cell Biol* **29**, 2570-2581 (2009). https://doi.org/10.1128/MCB.00166-09
68 Sun, R. C. & Denko, N. C. Hypoxic regulation of glutamine metabolism through HIF1 and SIAH2 supports lipid synthesis that is necessary for tumor growth. *Cell Metab* **19**, 285-292 (2014). https://doi.org/10.1016/j.cmet.2013.11.022
69 Infantino, V., Santarsiero, A., Convertini, P., Todisco, S. & Iacobazzi, V. Cancer Cell Metabolism in Hypoxia: Role of HIF-1 as Key Regulator and Therapeutic Target. *Int J Mol Sci* **22** (2021). https://doi.org/10.3390/ijms22115703
70 Du, R. *et al.* HIF1alpha induces the recruitment of bone marrow-derived vascular modulatory cells to regulate tumor angiogenesis and invasion. *Cancer Cell* **13**, 206-220 (2008). https://doi.org/10.1016/j.ccr.2008.01.034
71 Carmeliet, P. & Jain, R. K. Principles and mechanisms of vessel normalization for cancer and other angiogenic diseases. *Nature Reviews Drug Discovery* **10**, 417-427 (2011). https://doi.org/10.1038/nrd3455
72 Chang, J. & Erler, J. Hypoxia-mediated metastasis. *Adv Exp Med Biol* **772**, 55-81 (2014). https://doi.org/10.1007/978-1-4614-5915-6_3
73 Wong, C. C. *et al.* Hypoxia-inducible factor 1 is a master regulator of breast cancer metastatic niche formation. *Proc Natl Acad Sci U S A* **108**, 16369-16374 (2011). https://doi.org/10.1073/pnas.1113483108
74 Chen, W. *et al.* Targeting renal cell carcinoma with a HIF-2 antagonist. *Nature* **539**, 112-117 (2016). https://doi.org/10.1038/nature19796
75 Toledo, R. A. *et al.* Hypoxia-Inducible Factor 2 Alpha (HIF2alpha) Inhibitors: Targeting Genetically Driven Tumor Hypoxia. *Endocr Rev* **44**, 312-322 (2023). https://doi.org/10.1210/endrev/bnac025
76 Semenza, G. L. Targeting HIF-1 for cancer therapy. *Nat Rev Cancer* **3**, 721-732 (2003). https://doi.org/10.1038/nrc1187
77 Briggs, K. J. *et al.* Paracrine Induction of HIF by Glutamate in Breast Cancer: EglN1 Senses Cysteine. *Cell* **166**, 126-139 (2016). https://doi.org/10.1016/j.cell.2016.05.042

78 Ricketts, C. J., Crooks, D. R. & Linehan, W. M. Targeting HIF2alpha in Clear-Cell Renal Cell Carcinoma. *Cancer Cell* **30**, 515-517 (2016). https://doi.org/10.1016/j.ccell.2016.09.016

79 Shinojima, T. *et al.* Renal cancer cells lacking hypoxia inducible factor (HIF)-1alpha expression maintain vascular endothelial growth factor expression through HIF-2alpha. *Carcinogenesis* **28**, 529-536 (2007). https://doi.org/10.1093/carcin/bgl143

80 Salama, R. *et al.* Heterogeneous Effects of Direct Hypoxia Pathway Activation in Kidney Cancer. *PLoS One* **10**, e0134645 (2015). https://doi.org/10.1371/journal.pone.0134645

81 Dhillon, S. Roxadustat: First Global Approval. *Drugs* **79**, 563-572 (2019). https://doi.org/10.1007/s40265-019-01077-1

82 Li, J., Haase, V. H. & Hao, C.-M. Updates on Hypoxia-Inducible Factor Prolyl Hydroxylase Inhibitors in the Treatment of Renal Anemia. *Kidney Diseases* **9**, 1-11 (2023). https://doi.org/10.1159/000527835

83 Nangaku, M. *et al.* Daprodustat Compared with Epoetin Beta Pegol for Anemia in Japanese Patients Not on Dialysis: A 52-Week Randomized Open-Label Phase 3 Trial. *Am J Nephrol* **52**, 26-35 (2021). https://doi.org/10.1159/000513103

84 Macdougall, I. C., Akizawa, T., Berns, J. S., Bernhardt, T. & Krueger, T. Effects of Molidustat in the Treatment of Anemia in CKD. *Clin J Am Soc Nephrol* **14**, 28-39 (2019). https://doi.org/10.2215/cjn.02510218

85 Akizawa, T. *et al.* A Placebo-Controlled, Randomized Trial of Enarodustat in Patients with Chronic Kidney Disease Followed by Long-Term Trial. *Am J Nephrol* **49**, 165-174 (2019). https://doi.org/10.1159/000496929

86 Chen, N. *et al.* Roxadustat Treatment for Anemia in Patients Undergoing Long-Term Dialysis. *N Engl J Med* **381**, 1011-1022 (2019). https://doi.org/10.1056/NEJMoa1901713

87 Chen, N. *et al.* Roxadustat for Anemia in Patients with Kidney Disease Not Receiving Dialysis. *N Engl J Med* **381**, 1001-1010 (2019). https://doi.org/10.1056/NEJMoa1813599

88 Chertow, G. M. *et al.* Vadadustat in Patients with Anemia and Non-Dialysis-Dependent CKD. *N Engl J Med* **384**, 1589-1600 (2021). https://doi.org/10.1056/NEJMoa2035938

89 Eckardt, K. U. *et al.* Safety and Efficacy of Vadadustat for Anemia in Patients Undergoing Dialysis. *N Engl J Med* **384**, 1601-1612 (2021). https://doi.org/10.1056/NEJMoa2025956

90 Yeh, T. L. *et al.* Molecular and cellular mechanisms of HIF prolyl hydroxylase inhibitors in clinical trials. *Chem Sci* **8**, 7651-7668 (2017). https://doi.org/10.1039/c7sc02103h

91 Cai, Z., Luo, W., Zhan, H. & Semenza, G. L. Hypoxia-inducible factor 1 is required for remote ischemic preconditioning of the heart. *Proc Natl Acad Sci U S A* **110**, 17462-17467 (2013). https://doi.org/10.1073/pnas.1317158110

92 Cai, Z. P., Parajuli, N., Zheng, X. & Becker, L. Remote ischemic preconditioning confers late protection against myocardial ischemia–reperfusion injury in mice by upregulating interleukin-10. *Basic Research in Cardiology* **107** (2012). https://doi.org/10.1007/s00395-012-0277-1

93 Olenchock, B. A. *et al.* EGLN1 Inhibition and Rerouting of alpha-Ketoglutarate Suffice for Remote Ischemic Protection. *Cell* **164**, 884-895 (2016). https://doi.org/10.1016/j.cell.2016.02.006
94 Vogler, M. *et al.* Pre- and post-conditional inhibition of prolyl-4-hydroxylase domain enzymes protects the heart from an ischemic insult. *Pflügers Archiv - European Journal of Physiology* **467**, 2141-2149 (2015). https://doi.org/10.1007/s00424-014-1667-z
95 Hong, W. X. *et al.* The Role of Hypoxia-Inducible Factor in Wound Healing. *Advances in Wound Care* **3**, 390-399 (2014). https://doi.org/10.1089/wound.2013.0520
96 Primer, K. R., Psaltis, P. J., Tan, J. T. M. & Bursill, C. A. The Role of High-Density Lipoproteins in Endothelial Cell Metabolism and Diabetes-Impaired Angiogenesis. *Int J Mol Sci* **21** (2020). https://doi.org/10.3390/ijms21103633
97 Mace, K. A., Yu, D. H., Paydar, K. Z., Boudreau, N. & Young, D. M. Sustained expression of Hif-1α in the diabetic environment promotes angiogenesis and cutaneous wound repair. *Wound Repair and Regeneration* **15**, 636-645 (2007). https://doi.org/10.1111/j.1524-475x.2007.00278.x
98 Botusan, I. R. *et al.* Stabilization of HIF-1alpha is critical to improve wound healing in diabetic mice. *Proc Natl Acad Sci U S A* **105**, 19426-19431 (2008). https://doi.org/10.1073/pnas.0805230105
99 Catrina, S.-B., Okamoto, K., Pereira, T., Brismar, K. & Poellinger, L. Hyperglycemia Regulates Hypoxia-Inducible Factor-1α Protein Stability and Function. *Diabetes* **53**, 3226-3232 (2004). https://doi.org/10.2337/diabetes.53.12.3226
100 Bento, C. F. *et al.* The chaperone-dependent ubiquitin ligase CHIP targets HIF-1alpha for degradation in the presence of methylglyoxal. *PLoS One* **5**, e15062 (2010). https://doi.org/10.1371/journal.pone.0015062
101 Thangarajah, H. *et al.* The molecular basis for impaired hypoxia-induced VEGF expression in diabetic tissues. *Proceedings of the National Academy of Sciences* **106**, 13505-13510 (2009). https://doi.org/10.1073/pnas.0906670106
102 Catrina, S. B. Impaired hypoxia-inducible factor (HIF) regulation by hyperglycemia. *J Mol Med (Berl)* **92**, 1025-1034 (2014). https://doi.org/10.1007/s00109-014-1166-x
103 Catrina, S.-B. & Zheng, X. Hypoxia and hypoxia-inducible factors in diabetes and its complications. *Diabetologia* **64**, 709-716 (2021). https://doi.org/10.1007/s00125-021-05380-z
104 Kalan, L. R. & Brennan, M. B. The role of the microbiome in nonhealing diabetic wounds. *Ann N Y Acad Sci* **1435**, 79-92 (2019). https://doi.org/10.1111/nyas.13926
105 Duscher, D. *et al.* Comparison of the Hydroxylase Inhibitor Dimethyloxalylglycine and the Iron Chelator Deferoxamine in Diabetic and Aged Wound Healing. *Plast Reconstr Surg* **139**, 695e-706e (2017). https://doi.org/10.1097/PRS.0000000000003072
106 Li, G. *et al.* A small molecule HIF-1alpha stabilizer that accelerates diabetic wound healing. *Nat Commun* **12**, 3363 (2021). https://doi.org/10.1038/s41467-021-23448-7
107 Taylor, C. T. & Colgan, S. P. Hypoxia and gastrointestinal disease. *J Mol Med (Berl)* **85**, 1295-1300 (2007). https://doi.org/10.1007/s00109-007-0277-z
108 Walaas, G. A. *et al.* Physiological hypoxia improves growth and functional differentiation of human intestinal epithelial organoids. *Frontiers in Immunology* **14** (2023). https://doi.org/10.3389/fimmu.2023.1095812

109 Synnestvedt, K. *et al.* Ecto-5'-nucleotidase (CD73) regulation by hypoxia-inducible factor-1 mediates permeability changes in intestinal epithelia. *Journal of Clinical Investigation* **110**, 993-1002 (2002). https://doi.org/10.1172/jci0215337
110 Kumar, T., Pandey, R. & Chauhan, N. S. Hypoxia Inducible Factor-1alpha: The Curator of Gut Homeostasis. *Front Cell Infect Microbiol* **10**, 227 (2020). https://doi.org/10.3389/fcimb.2020.00227
111 Saeedi, B. J. *et al.* HIF-dependent regulation of claudin-1 is central to intestinal epithelial tight junction integrity. *Mol Biol Cell* **26**, 2252-2262 (2015). https://doi.org/10.1091/mbc.E14-07-1194
112 Louis, N. A. *et al.* Selective induction of mucin-3 by hypoxia in intestinal epithelia. *J Cell Biochem* **99**, 1616-1627 (2006). https://doi.org/10.1002/jcb.20947
113 Furuta, G. T. *et al.* Hypoxia-Inducible Factor 1–Dependent Induction of Intestinal Trefoil Factor Protects Barrier Function during Hypoxia. *J Exp Med* **193** (2001).
114 Kelly, C. J. *et al.* Fundamental role for HIF-1alpha in constitutive expression of human beta defensin-1. *Mucosal Immunol* **6**, 1110-1118 (2013). https://doi.org/10.1038/mi.2013.6
115 Cramer, T. *et al.* HIF-1α Is Essential for Myeloid Cell-Mediated Inflammation. *Cell* **112**, 645-657 (2003). https://doi.org/10.1016/s0092-8674(03)00154-5
116 Peyssonnaux, C. *et al.* HIF-1alpha expression regulates the bactericidal capacity of phagocytes. *J Clin Invest* **115**, 1806-1815 (2005). https://doi.org/10.1172/JCI23865
117 O'Neill, L. A., Kishton, R. J. & Rathmell, J. A guide to immunometabolism for immunologists. *Nat Rev Immunol* **16**, 553-565 (2016). https://doi.org/10.1038/nri.2016.70
118 Tannahill, G. M. *et al.* Succinate is an inflammatory signal that induces IL-1beta through HIF-1alpha. *Nature* **496**, 238-242 (2013). https://doi.org/10.1038/nature11986
119 Atreya, I., Atreya, R. & Neurath, M. F. NF-kappaB in inflammatory bowel disease. *J Intern Med* **263**, 591-596 (2008). https://doi.org/10.1111/j.1365-2796.2008.01953.x
120 Culver, C. *et al.* Mechanism of hypoxia-induced NF-kappaB. *Mol Cell Biol* **30**, 4901-4921 (2010). https://doi.org/10.1128/MCB.00409-10
121 Bandarra, D., Biddlestone, J., Mudie, S., Muller, H. A. & Rocha, S. HIF-1alpha restricts NF-kappaB-dependent gene expression to control innate immunity signals. *Dis Model Mech* **8**, 169-181 (2015). https://doi.org/10.1242/dmm.017285
122 Dang, E. V. *et al.* Control of T(H)17/T(reg) balance by hypoxia-inducible factor 1. *Cell* **146**, 772-784 (2011). https://doi.org/10.1016/j.cell.2011.07.033
123 Clambey, E. T. *et al.* Hypoxia-inducible factor-1 alpha-dependent induction of FoxP3 drives regulatory T-cell abundance and function during inflammatory hypoxia of the mucosa. *Proc Natl Acad Sci U S A* **109**, E2784-2793 (2012). https://doi.org/10.1073/pnas.1202366109
124 Chan, M. C., Holt-Martyn, J. P., Schofield, C. J. & Ratcliffe, P. J. Pharmacological targeting of the HIF hydroxylases--A new field in medicine development. *Mol Aspects Med* **47-48**, 54-75 (2016). https://doi.org/10.1016/j.mam.2016.01.001
125 Colgan, S. P., Curtis, V. F. & Campbell, E. L. The inflammatory tissue microenvironment in IBD. *Inflamm Bowel Dis* **19**, 2238-2244 (2013). https://doi.org/10.1097/MIB.0b013e31828dcaaf

126 Groschwitz, K. R. & Hogan, S. P. Intestinal barrier function: molecular regulation and disease pathogenesis. *J Allergy Clin Immunol* **124**, 3-20; quiz 21-22 (2009). https://doi.org/10.1016/j.jaci.2009.05.038
127 Lanis, J. M., Kao, D. J., Alexeev, E. E. & Colgan, S. P. Tissue metabolism and the inflammatory bowel diseases. *J Mol Med (Berl)* **95**, 905-913 (2017). https://doi.org/10.1007/s00109-017-1544-2
128 Xavier, R. J. & Podolsky, D. K. Unravelling the pathogenesis of inflammatory bowel disease. *Nature* **448**, 427-434 (2007). https://doi.org/10.1038/nature06005
129 Giatromanolaki, A. *et al.* Hypoxia inducible factor 1α and 2α overexpression in inflammatory bowel disease. *J Clin Pathol* **56**, 209-213 (2003).
130 Karhausen, J. *et al.* Epithelial hypoxia-inducible factor-1 is protective in murine experimental colitis. *J Clin Invest* **114**, 1098-1106 (2004). https://doi.org/10.1172/JCI21086
131 Cummins, E. P. *et al.* The hydroxylase inhibitor dimethyloxalylglycine is protective in a murine model of colitis. *Gastroenterology* **134**, 156-165 (2008). https://doi.org/10.1053/j.gastro.2007.10.012
132 Keely, S. *et al.* Contribution of epithelial innate immunity to systemic protection afforded by prolyl hydroxylase inhibition in murine colitis. *Mucosal Immunol* **7**, 114-123 (2014). https://doi.org/10.1038/mi.2013.29
133 Marks, E. *et al.* Oral delivery of prolyl hydroxylase inhibitor: AKB-4924 promotes localized mucosal healing in a mouse model of colitis. *Inflamm Bowel Dis* **21**, 267-275 (2015). https://doi.org/10.1097/MIB.0000000000000277
134 Robinson, A. *et al.* Mucosal protection by hypoxia-inducible factor prolyl hydroxylase inhibition. *Gastroenterology* **134**, 145-155 (2008). https://doi.org/10.1053/j.gastro.2007.09.033
135 Bäcker, V., Cheung, F.-Y., Siveke, J. T., Fandrey, J. & Winning, S. Knockdown of myeloid cell hypoxia-inducible factor-1α ameliorates the acute pathology in DSS-induced colitis. *PLOS ONE* **12**, e0190074 (2017). https://doi.org/10.1371/journal.pone.0190074
136 Kerber, E. L. *et al.* The Importance of Hypoxia-Inducible Factors (HIF-1 and HIF-2) for the Pathophysiology of Inflammatory Bowel Disease. *International Journal of Molecular Sciences* **21**, 8551 (2020). https://doi.org/10.3390/ijms21228551
137 Dallas *et al.* The Microbiome and Butyrate Regulate Energy Metabolism and Autophagy in the Mammalian Colon. *Cell Metabolism* **13**, 517-526 (2011). https://doi.org/10.1016/j.cmet.2011.02.018
138 Kelly, C. J. *et al.* Crosstalk between Microbiota-Derived Short-Chain Fatty Acids and Intestinal Epithelial HIF Augments Tissue Barrier Function. *Cell Host Microbe* **17**, 662-671 (2015). https://doi.org/10.1016/j.chom.2015.03.005
139 Wang, R. X., Henen, M. A., Lee, J. S., Vögeli, B. & Colgan, S. P. Microbiota-derived butyrate is an endogenous HIF prolyl hydroxylase inhibitor. *Gut Microbes* **13**, 1938380 (2021). https://doi.org/10.1080/19490976.2021.1938380
140 Fachi, J. L. *et al.* Butyrate Protects Mice from Clostridium difficile-Induced Colitis through an HIF-1-Dependent Mechanism. *Cell Rep* **27**, 750-761 e757 (2019). https://doi.org/10.1016/j.celrep.2019.03.054
141 Chriett, S. *et al.* Prominent action of butyrate over beta-hydroxybutyrate as histone deacetylase inhibitor, transcriptional modulator and anti-inflammatory molecule. *Sci Rep* **9**, 742 (2019). https://doi.org/10.1038/s41598-018-36941-9

142 Chang, P. V., Hao, L., Offermanns, S. & Medzhitov, R. The microbial metabolite butyrate regulates intestinal macrophage function via histone deacetylase inhibition. *Proc Natl Acad Sci U S A* **111**, 2247-2252 (2014). https://doi.org/10.1073/pnas.1322269111
143 Gutierrez, N. & Garrido, D. Species Deletions from Microbiome Consortia Reveal Key Metabolic Interactions between Gut Microbes. *mSystems* **4** (2019). https://doi.org/10.1128/mSystems.00185-19
144 Lloyd-Price, J. *et al.* Multi-omics of the gut microbial ecosystem in inflammatory bowel diseases. *Nature* **569**, 655-662 (2019). https://doi.org/10.1038/s41586-019-1237-9
145 Vila, A. *et al.* Gut microbiota composition and functional changes in inflammatory bowel disease and irritable bowel syndrome. *Science Translational Medicine* **10** (2018).
146 Blouin, C. C., Page, E. L., Soucy, G. M. & Richard, D. E. Hypoxic gene activation by lipopolysaccharide in macrophages: implication of hypoxia-inducible factor 1alpha. *Blood* **103**, 1124-1130 (2004). https://doi.org/10.1182/blood-2003-07-2427
147 Frede, S., Stockmann, C., Freitag, P. & Fandrey, J. Bacterial lipopolysaccharide induces HIF-1 activation in human monocytes via p44/42 MAPK and NF-kappaB. *Biochem J* **396**, 517-527 (2006). https://doi.org/10.1042/BJ20051839
148 Taylor, C. T. & Scholz, C. C. The effect of HIF on metabolism and immunity. *Nat Rev Nephrol* **18**, 573-587 (2022). https://doi.org/10.1038/s41581-022-00587-8
149 Hartmann, H. *et al.* Hypoxia-independent activation of HIF-1 by enterobacteriaceae and their siderophores. *Gastroenterology* **134**, 756-767 (2008). https://doi.org/10.1053/j.gastro.2007.12.008
150 Fornelos, N. *et al.* Growth effects of N-acylethanolamines on gut bacteria reflect altered bacterial abundances in inflammatory bowel disease. *Nat Microbiol* **5**, 486-497 (2020). https://doi.org/10.1038/s41564-019-0655-7
151 Legendre, C. *et al.* Bile acids repress hypoxia-inducible factor 1 signaling and modulate the airway immune response. *Infect Immun* **82**, 3531-3541 (2014). https://doi.org/10.1128/IAI.00674-13
152 Phelan, J. P., Reen, F. J., Dunphy, N., O'Connor, R. & O'Gara, F. Bile acids destabilise HIF-1alpha and promote anti-tumour phenotypes in cancer cell models. *BMC Cancer* **16**, 476 (2016). https://doi.org/10.1186/s12885-016-2528-2
153 Legendre, C. *et al.* Pseudomonas aeruginosa Alkyl quinolones repress hypoxia-inducible factor 1 (HIF-1) signaling through HIF-1alpha degradation. *Infect Immun* **80**, 3985-3992 (2012). https://doi.org/10.1128/IAI.00554-12
154 Jaakkola, P. *et al.* Targeting of HIF-a to the von Hippel–Lindau Ubiquitylation Complex by O2-Regulated Prolyl Hydroxylation. *Science* **292** (2001).
155 Epstien, A. *et al.* C. elegans EGL-9 and Mammalian Homologs Define a Family of Dioxygenases that Regulate HIF by Prolyl Hydroxylation. *Cell* **107** (2001).
156 Chowdhury, R. *et al.* Structural basis for binding of hypoxia-inducible factor to the oxygen-sensing prolyl hydroxylases. *Structure* **17**, 981-989 (2009). https://doi.org/10.1016/j.str.2009.06.002
157 Chowdhury, R. *et al.* Structural basis for oxygen degradation domain selectivity of the HIF prolyl hydroxylases. *Nat Commun* **7**, 12673 (2016). https://doi.org/10.1038/ncomms12673

158 Figg, W. D. *et al.* Structural Basis of Prolyl Hydroxylase Domain Inhibition by Molidustat. *ChemMedChem* **16**, 2082-2088 (2021). https://doi.org/10.1002/cmdc.202100133
159 Rogers, J. L. *et al.* Development of Inhibitors of the PAS-B Domain of the HIF-2α Transcription Factor. *Journal of Medicinal Chemistry* **56**, 1739-1747 (2013). https://doi.org/10.1021/jm301847z
160 Scheuermann, T. H. *et al.* Artificial ligand binding within the HIF2alpha PAS-B domain of the HIF2 transcription factor. *Proc Natl Acad Sci U S A* **106**, 450-455 (2009). https://doi.org/10.1073/pnas.0808092106
161 Key, J., Scheuermann, T. H., Anderson, P. C., Dagget, V. & Gardner, K. H. Principles of Ligand Binding within a Completely Buried Cavity in HIF2r PAS-B. *J. Am. Chem. Soc* **131** (2009).
162 Jonasch, E. *et al.* Belzutifan for Renal Cell Carcinoma in von Hippel–Lindau Disease. *New England Journal of Medicine* **385**, 2036-2046 (2021). https://doi.org/10.1056/nejmoa2103425
163 Wu, D. *et al.* Bidirectional modulation of HIF-2 activity through chemical ligands. *Nat Chem Biol* **15**, 367-376 (2019). https://doi.org/10.1038/s41589-019-0234-5
164 Sun, H. L. *et al.* YC-1 inhibits HIF-1 expression in prostate cancer cells: contribution of Akt/NF-κB signaling to HIF-1α accumulation during hypoxia. *Oncogene* **26**, 3941-3951 (2007). https://doi.org/10.1038/sj.onc.1210169
165 Welsh, S., Williams, R., Kirkpatrick, L., Paine-Murrieta, G. & Powis, G. Antitumor activity and pharmacodynamic properties of PX-478, an inhibitor of hypoxia-inducible factor-1A. *Molecular Cancer Therapeutics* **3** (2004). https://doi.org/https://doi.org/10.1158/1535-7163.233.3.3
166 Koh, M. Y. *et al.* Molecular mechanisms for the activity of PX-478, an antitumor inhibitor of the hypoxia-inducible factor-1α. *Molecular Cancer Therapeutics* **7**, 90-100 (2008). https://doi.org/10.1158/1535-7163.mct-07-0463
167 Jacoby, J. J. *et al.* Treatment with HIF-1α Antagonist PX-478 Inhibits Progression and Spread of Orthotopic Human Small Cell Lung Cancer and Lung Adenocarcinoma in Mice. *Journal of Thoracic Oncology* **5**, 940-949 (2010). https://doi.org/10.1097/jto.0b013e3181dc211f
168 Tibes, R. *et al.* Results from a phase I, dose-escalation study of PX-478, an orally available inhibitor of HIF-1α. *Journal of Clinical Oncology* **28**, 3076-3076 (2010). https://doi.org/10.1200/jco.2010.28.15_suppl.3076
169 Lee, K. *et al.* Acriflavine inhibits HIF-1 dimerization, tumor growth, and vascularization. *Proc Natl Acad Sci U S A* **106**, 17910-17915 (2009). https://doi.org/10.1073/pnas.0909353106
170 Retraction for Lee et al., Acriflavine inhibits HIF-1 dimerization, tumor growth, and vascularization. *Proceedings of the National Academy of Sciences* **120** (2023). https://doi.org/10.1073/pnas.2305537120
171 Jeong, W. *et al.* Pilot trial of EZN-2968, an antisense oligonucleotide inhibitor of hypoxia-inducible factor-1 alpha (HIF-1α), in patients with refractory solid tumors. *Cancer Chemotherapy and Pharmacology* **73**, 343-348 (2014). https://doi.org/10.1007/s00280-013-2362-z
172 Wu, J. *et al.* Evaluation of a locked nucleic acid form of antisense oligo targeting HIF-1alpha in advanced hepatocellular carcinoma. *World J Clin Oncol* **10**, 149-160 (2019). https://doi.org/10.5306/wjco.v10.i3.149

173 Mistry, I. N. & Tavassoli, A. Reprogramming the Transcriptional Response to Hypoxia with a Chromosomally Encoded Cyclic Peptide HIF-1 Inhibitor. *ACS Synth Biol* **6**, 518-527 (2017). https://doi.org/10.1021/acssynbio.6b00219
174 Li Petri, G., Di Martino, S. & De Rosa, M. Peptidomimetics: An Overview of Recent Medicinal Chemistry Efforts toward the Discovery of Novel Small Molecule Inhibitors. *Journal of Medicinal Chemistry* **65**, 7438-7475 (2022). https://doi.org/10.1021/acs.jmedchem.2c00123
175 Narita, T. *et al.* Identification of a novel small molecule HIF-1alpha translation inhibitor. *Clin Cancer Res* **15**, 6128-6136 (2009). https://doi.org/10.1158/1078-0432.CCR-08-3180
176 Xia, M. *et al.* Identification of small molecule compounds that inhibit the HIF-1 signaling pathway. *Mol Cancer* **8**, 117 (2009). https://doi.org/10.1186/1476-4598-8-117
177 Razorenova, O. V., Ivanov, A. V., Budanov, A. V. & Chumakov, P. M. Virus-based reporter systems for monitoring transcriptional activity of hypoxia-inducible factor 1. *Gene* **350**, 89-98 (2005). https://doi.org/10.1016/j.gene.2005.02.006
178 Rapisarda, A. *et al.* Identification of Small Molecule Inhibitors of Hypoxia-inducible Factor 1 Transcriptional Activation Pathway. *Cancer Res* **62** (2002).
179 Korn, K. & Krausz, E. Cell-based high-content screening of small-molecule libraries. *Curr Opin Chem Biol* **11**, 503-510 (2007). https://doi.org/10.1016/j.cbpa.2007.08.030
180 Lin, S., Schorpp, K., Rothenaigner, I. & Hadian, K. Image-based high-content screening in drug discovery. *Drug Discov Today* **25**, 1348-1361 (2020). https://doi.org/10.1016/j.drudis.2020.06.001
181 Auld, D. S., Thorne, N., Nguyen, D.-T. & Inglese, J. A Specific Mechanism for Nonspecific Activation in Reporter-Gene Assays. *ACS Chem Biol* **3** (2008). https://doi.org/10.1021/cb8000793
182 Beitz, A. M., Oakes, C. G. & Galloway, K. E. Synthetic gene circuits as tools for drug discovery. *Trends Biotechnol* **40**, 210-225 (2022). https://doi.org/10.1016/j.tibtech.2021.06.007
183 Adamson, B. *et al.* A Multiplexed Single-Cell CRISPR Screening Platform Enables Systematic Dissection of the Unfolded Protein Response. *Cell* **167**, 1867-1882 e1821 (2016). https://doi.org/10.1016/j.cell.2016.11.048
184 Ortmann, B. M. & Nathan, J. A. Genetic approaches to understand cellular responses to oxygen availability. *The FEBS Journal* (2021). https://doi.org/10.1111/febs.16072
185 Ortmann, B. M. *et al.* The HIF complex recruits the histone methyltransferase SET1B to activate specific hypoxia-inducible genes. *Nature Genetics* **53**, 1022-1035 (2021). https://doi.org/10.1038/s41588-021-00887-y
186 Miles, A. L., Burr, S. P., Grice, G. L. & Nathan, J. A. The vacuolar-ATPase complex and assembly factors, TMEM199 and CCDC115, control HIF1α prolyl hydroxylation by regulating cellular iron levels. *eLife* **6** (2017). https://doi.org/10.7554/elife.22693
187 Nunez, J. K. *et al.* Genome-wide programmable transcriptional memory by CRISPR-based epigenome editing. *Cell* **184**, 2503-2519 e2517 (2021). https://doi.org/10.1016/j.cell.2021.03.025
188 Tycko, J. *et al.* Mitigation of off-target toxicity in CRISPR-Cas9 screens for essential non-coding elements. *Nat Commun* **10**, 4063 (2019). https://doi.org/10.1038/s41467-019-11955-7

189 Bock, C. *et al.* High-content CRISPR screening. *Nature Reviews Methods Primers* **2** (2022). https://doi.org/10.1038/s43586-021-00093-4
190 Chen, H. *et al.* Highly multiplexed bioactivity screening reveals human and microbiota metabolome-GPCRome interactions. *Cell* (2023). https://doi.org/10.1016/j.cell.2023.05.024
191 Cao, Y. *et al.* Commensal microbiota from patients with inflammatory bowel disease produce genotoxic metabolites. *Science* **378**, eabm3233 (2022). https://doi.org/10.1126/science.abm3233
192 Chen, H. *et al.* A Forward Chemical Genetic Screen Reveals Gut Microbiota Metabolites That Modulate Host Physiology. *Cell* **177**, 1217-1231 e1218 (2019). https://doi.org/10.1016/j.cell.2019.03.036
193 Schneider, C. A., Rasband, W. S. & Eliceiri, K. W. NIH Image to ImageJ: 25 years of image analysis. *Nat Methods* **9**, 671-675 (2012). https://doi.org/10.1038/nmeth.2089
194 Zhang, J.-H., Chung, T. & Oldenburg, K. A Simple Statistical Parameter for Use in Evaluation and Validation of High Throughput Screening Assays. *Journal of Biomolecular Screening* **4** (1999).
195 Birmingham, A. *et al.* Statistical methods for analysis of high-throughput RNA interference screens. *Nature Methods* **6**, 569-575 (2009). https://doi.org/10.1038/nmeth.1351
196 Benjamini, Y. & Hochberg, Y. Controlling the False Discovery Rate: A Practical and Powerful Approach to Multiple Testing. *Journal of the Royal Statistical Society: Series B (Methodological)* **57**, 289-300 (1995). https://doi.org/https://doi.org/10.1111/j.2517-6161.1995.tb02031.x
197 Allen, T. *Cell based drug screening systems for the bHLH-PAS transcription factors* Degree of Bachelor of Science (Honours) thesis, University of Adelaide, (2018).
198 Taylor, S. L. *et al.* The cystic fibrosis gut as a potential source of multidrug resistant pathogens. *Journal of Cystic Fibrosis* **20**, 413-420 (2021). https://doi.org/10.1016/j.jcf.2020.11.009
199 Taylor, S. L. *et al.* Long-Term Azithromycin Reduces Haemophilus influenzae and Increases Antibiotic Resistance in Severe Asthma. *Am J Respir Crit Care Med* **200**, 309-317 (2019). https://doi.org/10.1164/rccm.201809-1739OC
200 Becton, Dickenson & Company. (Ashland, OR, 2021).
201 Wickham, H. in *Elegant Graphics for Data Analysis* VIII, 213 (Springer New York, NY, 2009).
202 Lee, T. I. & Young, R. A. Transcriptional regulation and its misregulation in disease. *Cell* **152**, 1237-1251 (2013). https://doi.org/10.1016/j.cell.2013.02.014
203 Darnell, J. E., Jr. Transcription factors as targets for cancer therapy. *Nat Rev Cancer* **2**, 740-749 (2002). https://doi.org/10.1038/nrc906
204 Sahu, B. *et al.* Sequence determinants of human gene regulatory elements. *Nat Genet* **54**, 283-294 (2022). https://doi.org/10.1038/s41588-021-01009-4
205 Tycko, J. *et al.* High-Throughput Discovery and Characterization of Human Transcriptional Effectors. *Cell* **183**, 2020-2035 e2016 (2020). https://doi.org/10.1016/j.cell.2020.11.024
206 DelRosso, N. *et al.* Large-scale mapping and mutagenesis of human transcriptional effector domains. *Nature* (2023). https://doi.org/10.1038/s41586-023-05906-y

207 Tan, X., Letendre, J. H., Collins, J. J. & Wong, W. W. Synthetic biology in the clinic: engineering vaccines, diagnostics, and therapeutics. *Cell* **184**, 881-898 (2021). https://doi.org/10.1016/j.cell.2021.01.017
208 Choe, J. H. *et al.* SynNotch-CAR T cells overcome challenges of specificity, heterogeneity, and persistence in treating glioblastoma. *Science Translational Medicine* **13** (2021).
209 Allen, G. M. *et al.* Synthetic cytokine circuits that drive T cells into immune-excluded tumors. *Science* **378**, 1186-+ (2022). https://doi.org/ARTN eaba1624 10.1126/science.aba1624
210 Hernandez-Lopez, R. A. *et al.* T cell circuits that sense antigen density with an ultrasensitive threshold. *Science* **371**, 1166-+ (2021). https://doi.org/10.1126/science.abc1855
211 Roybal, K. T. *et al.* Engineering T Cells with Customized Therapeutic Response Programs Using Synthetic Notch Receptors. *Cell* **167**, 419-+ (2016). https://doi.org/10.1016/j.cell.2016.09.011
212 Hasle, N. *et al.* High-throughput, microscope-based sorting to dissect cellular heterogeneity. *Mol Syst Biol* **16**, e9442 (2020). https://doi.org/10.15252/msb.20209442
213 Tchasovnikarova, I. A., Marr, S. K., Damle, M. & Kingston, R. E. TRACE generates fluorescent human reporter cell lines to characterize epigenetic pathways. *Mol Cell* (2021). https://doi.org/10.1016/j.molcel.2021.11.035
214 Singhal, R. & Shah, Y. M. Oxygen battle in the gut: Hypoxia and hypoxia-inducible factors in metabolic and inflammatory responses in the intestine. *J Biol Chem* **295**, 10493-10505 (2020). https://doi.org/10.1074/jbc.REV120.011188
215 Wegiel, B., Vuerich, M., Daneshmandi, S. & Seth, P. Metabolic Switch in the Tumor Microenvironment Determines Immune Responses to Anti-cancer Therapy. *Front Oncol* **8**, 284 (2018). https://doi.org/10.3389/fonc.2018.00284
216 Triner, D. & Shah, Y. M. Hypoxia-inducible factors: a central link between inflammation and cancer. *J Clin Invest* **126**, 3689-3698 (2016). https://doi.org/10.1172/JCI84430
217 Tian, Y.-M. *et al.* Differential Sensitivity of Hypoxia Inducible Factor Hydroxylation Sites to Hypoxia and Hydroxylase Inhibitors. *Journal of Biological Chemistry* **286**, 13041-13051 (2011). https://doi.org/10.1074/jbc.m110.211110
218 Villemure, J. F., Savard, N. & Belmaaza, A. Promoter suppression in cultured mammalian cells can be blocked by the chicken beta-globin chromatin insulator 5'HS4 and matrix/scaffold attachment regions. *J Mol Biol* **312**, 963-974 (2001). https://doi.org/10.1006/jmbi.2001.5015
219 Emerman, M. & Temin, H. Comparison of promoter suppression in avian and murine retrovirus vectors. *Nucleic Acids Res* **14** (1986).
220 O'Connell, R. W. *et al. Ultra-high throughput mapping of genetic design space* (Cold Spring Harbor Laboratory, 2023).
221 Vora, S. *et al.* Rational design of a compact CRISPR-Cas9 activator for AAV-mediated delivery. *bioRxiv*, 298620 (2018). https://doi.org/10.1101/298620
222 Lydon, J. P. *et al.* Mice lacking progesterone receptor exhibit pleiotropic reproductive abnormalities. *Genes & Development* **9**, 2266-2278 (1995). https://doi.org/10.1101/gad.9.18.2266

223 Dinh, D. T. *et al.* Tissue-specific progesterone receptor-chromatin binding and the regulation of progesterone-dependent gene expression. *Scientific Reports* **9** (2019). https://doi.org/10.1038/s41598-019-48333-8
224 Grimm, S. L., Hartig, S. M. & Edwards, D. P. Progesterone Receptor Signaling Mechanisms. *J Mol Biol* **428**, 3831-3849 (2016). https://doi.org/10.1016/j.jmb.2016.06.020
225 Giannoukos, G., Szapary, D., Smith, C. L., Meeker, J. E. & Simons, S. S., Jr. New antiprogestins with partial agonist activity: potential selective progesterone receptor modulators (SPRMs) and probes for receptor- and coregulator-induced changes in progesterone receptor induction properties. *Mol Endocrinol* **15**, 255-270 (2001). https://doi.org/10.1210/mend.15.2.0596
226 Kampmann, M. CRISPRi and CRISPRa Screens in Mammalian Cells for Precision Biology and Medicine. *ACS Chem Biol* **13**, 406-416 (2018). https://doi.org/10.1021/acschembio.7b00657
227 Masoud, G. N. & Li, W. HIF-1alpha pathway: role, regulation and intervention for cancer therapy. *Acta Pharm Sin B* **5**, 378-389 (2015). https://doi.org/10.1016/j.apsb.2015.05.007
228 Semenza, G. L. Pharmacologic Targeting of Hypoxia-Inducible Factors. *Annual Review of Pharmacology and Toxicology* **59**, 379-403 (2019). https://doi.org/10.1146/annurev-pharmtox-010818-021637
229 Bracken, C. P. *et al.* Cell-specific regulation of hypoxia-inducible factor (HIF)-1alpha and HIF-2alpha stabilization and transactivation in a graded oxygen environment. *J Biol Chem* **281**, 22575-22585 (2006). https://doi.org/10.1074/jbc.M600288200
230 Ran, F. A. *et al.* Genome engineering using the CRISPR-Cas9 system. *Nature Protocols* **8**, 2281-2308 (2013). https://doi.org/10.1038/nprot.2013.143
231 Huang, L. *et al.* Inhibitory action of Celastrol on hypoxia-mediated angiogenesis and metastasis via the HIF-1α pathway. *International Journal of Molecular Medicine* **27** (2011). https://doi.org/10.3892/ijmm.2011.600
232 Ma, J. *et al.* Celastrol inhibits the HIF-1α pathway by inhibition of mTOR/p70S6K/eIF4E and ERK1/2 phosphorylation in human hepatoma cells. *Oncology Reports* **32**, 235-242 (2014). https://doi.org/10.3892/or.2014.3211
233 Shang, F.-F. *et al.* Design, synthesis of novel celastrol derivatives and study on their antitumor growth through HIF-1α pathway. *European Journal of Medicinal Chemistry* **220**, 113474 (2021). https://doi.org/10.1016/j.ejmech.2021.113474
234 Srinivasan, B., Johnson, T. E. & Xing, C. Chalcone-based inhibitors against hypoxia-inducible factor 1—Structure activity relationship studies. *Bioorganic & Medicinal Chemistry Letters* **21**, 555-557 (2011). https://doi.org/10.1016/j.bmcl.2010.10.063
235 Wan, C. *et al.* Genome-scale CRISPR-Cas9 screen of Wnt/β-catenin signaling identifies therapeutic targets for colorectal cancer. *Science Advances* **7**, eabf2567 (2021). https://doi.org/10.1126/sciadv.abf2567
236 Semesta, K. M., Tian, R., Kampmann, M., Von Zastrow, M. & Tsvetanova, N. G. A high-throughput CRISPR interference screen for dissecting functional regulators of GPCR/cAMP signaling. *PLOS Genetics* **16**, e1009103 (2020). https://doi.org/10.1371/journal.pgen.1009103

237 Adamson, B. *et al.* A Multiplexed Single-Cell CRISPR Screening Platform Enables Systematic Dissection of the Unfolded Protein Response. *Cell* **167**, 1867-1882.e1821 (2016). https://doi.org/10.1016/j.cell.2016.11.048
238 Potting, C. *et al.* Genome-wide CRISPR screen for PARKIN regulators reveals transcriptional repression as a determinant of mitophagy. *Proc Natl Acad Sci U S A* **115**, E180-E189 (2018). https://doi.org/10.1073/pnas.1711023115
239 Ilegems, E. *et al.* HIF-1a inhibitor PX-478 preserves pancreatic Beta cell function in diabetes. *Science Translational Medicine* **14** (2022).
240 Yin, J.-A. *et al.* Robust and Versatile Arrayed Libraries for Human Genome-Wide CRISPR Activation, Deletion and Silencing. *bioRxiv*, 2022.2005.2025.493370 (2023). https://doi.org/10.1101/2022.05.25.493370
241 Feldman, D. *et al.* Optical Pooled Screens in Human Cells. *Cell* **179**, 787-799.e717 (2019). https://doi.org/10.1016/j.cell.2019.09.016
242 Feldman, D. *et al.* Pooled genetic perturbation screens with image-based phenotypes. *Nat Protoc* **17**, 476-512 (2022). https://doi.org/10.1038/s41596-021-00653-8
243 Yan, X. *et al.* High-content imaging-based pooled CRISPR screens in mammalian cells. *Journal of Cell Biology* **220** (2021). https://doi.org/10.1083/jcb.202008158
244 Nandagopal, N. *et al.* Dynamic Ligand Discrimination in the Notch Signaling Pathway. *Cell* **172**, 869-880.e819 (2018). https://doi.org/10.1016/j.cell.2018.01.002
245 Agarwal, V. *et al.* Massively parallel characterization of transcriptional regulatory elements in three diverse human cell types. *bioRxiv* (2023). https://doi.org/10.1101/2023.03.05.531189
246 Gordon, M. G. *et al.* lentiMPRA and MPRAflow for high-throughput functional characterization of gene regulatory elements. *Nat Protoc* **15**, 2387-2412 (2020). https://doi.org/10.1038/s41596-020-0333-5
247 Bersten, D. C. *et al.* Inducible and reversible lentiviral and Recombination Mediated Cassette Exchange (RMCE) systems for controlling gene expression. *PLoS One* **10**, e0116373 (2015). https://doi.org/10.1371/journal.pone.0116373
248 Dinh, T. *et al.* OR08-1 Context-Specific Chromatin Binding Properties of Progesterone Receptor and Consequential Effects on Gene Expression in Mouse Reproductive Tissues. *J Endocr Soc* **3** (2019).
249 Singhal, H. *et al.* Genomic agonism and phenotypic antagonism between estrogen and progesterone receptors in breast cancer. *Sci Adv* **2**, e1501924 (2016). https://doi.org/10.1126/sciadv.1501924
250 Chen, D.-Y. *et al.* Ankyrin Repeat Proteins of Orf Virus Influence the Cellular Hypoxia Response Pathway. *Journal of Virology* **91**, JVI.01430-01416 (2017). https://doi.org/10.1128/jvi.01430-16
251 Dehairs, J., Talebi, A., Cherifi, Y. & Swinnen, J. V. CRISP-ID: decoding CRISPR mediated indels by Sanger sequencing. *Sci Rep* **6**, 28973 (2016). https://doi.org/10.1038/srep28973
252 Sanson, K. R. *et al.* Optimized libraries for CRISPR-Cas9 genetic screens with multiple modalities. *Nat Commun* **9**, 5416 (2018). https://doi.org/10.1038/s41467-018-07901-8
253 Ritz, C., Baty, F., Streibig, J. C. & Gerhard, D. Dose-Response Analysis Using R. *PLOS ONE* **10**, e0146021 (2016). https://doi.org/10.1371/journal.pone.0146021

254 Wong, F. C. *et al.* Antioxidant, Metal Chelating, Anti-glucosidase Activities and Phytochemical Analysis of Selected Tropical Medicinal Plants. *Iran J Pharm Res* **13**, 1409-1415 (2014).
255 Curtin, J. A., Dane, A. P., Swanson, A., Alexander, I. E. & Ginn, S. L. Bidirectional promoter interference between two widely used internal heterologous promoters in a late-generation lentiviral construct. *Gene Ther* **15**, 384-390 (2008). https://doi.org/10.1038/sj.gt.3303105
256 Emerman, M. & Temin, H. Genes with promoters in retrovirus vectors can be independently suppressed by an epigenetic mechanism. *Cell* **39**, 459-467 (1984). https://doi.org/https://doi.org/10.1016/0092-8674(84)90453-7.
257 Sulser, P. *et al.* HIF hydroxylase inhibitors decrease cellular oxygen consumption depending on their selectivity. *FASEB J* **34**, 2344-2358 (2020). https://doi.org/10.1096/fj.201902240R
258 Wilkins, S. E., Abboud, M. I., Hancock, R. L. & Schofield, C. J. Targeting Protein-Protein Interactions in the HIF System. *ChemMedChem* **11**, 773-786 (2016). https://doi.org/10.1002/cmdc.201600012
259 Roatsch, M. *et al.* The Clinically Used Iron Chelator Deferasirox Is an Inhibitor of Epigenetic JumonjiC Domain-Containing Histone Demethylases. *ACS Chem Biol* **14**, 1737-1750 (2019). https://doi.org/10.1021/acschembio.9b00289
260 Diani-Moore, S. *et al.* Discovery and biological characterization of 1-(1H-indol-3-yl)-9H-pyrido[3,4-b]indole as an aryl hydrocarbon receptor activator generated by photoactivation of tryptophan by sunlight. *Chem Biol Interact* **193**, 119-128 (2011). https://doi.org/10.1016/j.cbi.2011.05.010
261 Gasparova, Z., Stara, V. & Stolc, S. Effect of antioxidants on functional recovery after in vitro-induced ischemia and long-term potentiation recorded in the pyramidal layer of the CA1 area of rat hippocampus. *General physiology and biophysics* **33**, 43-52 (2014). https://doi.org/10.4149/gpb_2013062
262 Stempel, E. & Gaich, T. Cyclohepta[b]indoles: A Privileged Structure Motif in Natural Products and Drug Design. *Accounts of Chemical Research* **49**, 2390-2402 (2016). https://doi.org/10.1021/acs.accounts.6b00265
263 Jiang, Y. *et al.* Temporal regulation of HIF-1 and NF-κB in hypoxic hepatocarcinoma cells. *Oncotarget* **6**, 9409-9419 (2015). https://doi.org/10.18632/oncotarget.3352
264 Nagle, D. G. & Zhou, Y. D. Marine Natural Products as Inhibitors of Hypoxic Signaling in Tumors. *Phytochem Rev* **8**, 415-429 (2009). https://doi.org/10.1007/s11101-009-9120-1
265 Liu, Y. *et al.* Methylalpinumisoflavone inhibits hypoxia-inducible factor-1 (HIF-1) activation by simultaneously targeting multiple pathways. *J Biol Chem* **284**, 5859-5868 (2009). https://doi.org/10.1074/jbc.M806744200
266 Mao, S. C. *et al.* Lipophilic 2,5-Disubstituted Pyrroles from the Marine Sponge Mycale sp. Inhibit Mitochondrial Respiration and HIF-1 Activation. *J. Nat. Prod.*, 1927-1936 (2009).
267 Zhou, Y.-D. *et al.* Hypoxia-Inducible Factor-1 Activation by (−)-Epicatechin Gallate: Potential Adverse Effects of Cancer Chemoprevention with High-Dose Green Tea Extracts. *Journal of Natural Products* **67**, 2063-2069 (2004). https://doi.org/10.1021/np040140c

268 Harvey, A. L., Edrada-Ebel, R. & Quinn, R. J. The re-emergence of natural products for drug discovery in the genomics era. *Nat Rev Drug Discov* **14**, 111-129 (2015). https://doi.org/10.1038/nrd4510
269 Cheng, J. *et al.* 2-Oxonanonoidal Antibiotic Actinolactomycin Inhibits Cancer Progression by Suppressing HIF-1alpha. *Cells* **8** (2019). https://doi.org/10.3390/cells8050439
270 Piorecka, K., Kurjata, J. & Stanczyk, W. A. Acriflavine, an Acridine Derivative for Biomedical Application: Current State of the Art. *J Med Chem* **65**, 11415-11432 (2022). https://doi.org/10.1021/acs.jmedchem.2c00573
271 Beutler, J. A. in *Current Protocols in Pharmacology* (2009).
272 Zheng, X. *et al.* Biosynthesis of the pyrrolidine protein synthesis inhibitor anisomycin involves novel gene ensemble and cryptic biosynthetic steps. *Proceedings of the National Academy of Sciences* **114**, 4135-4140 (2017). https://doi.org/10.1073/pnas.1701361114
273 Fredrick, K. & Noller, H. F. Catalysis of Ribosomal Translocation by Sparsomycin. *Science* **300** (2003).
274 Ledger, P. W. & Tanzer, M. L. Monensin — a perturbant of cellular physiology. *Trends in Biochemical Sciences* **9**, 313-314 (1894).
275 Klejborowska, G. *et al.* Antiproliferative activity of ester derivatives of monensin A at the C-1 and C-26 positions. *Chemical Biology & Drug Design* **94**, 1859-1864 (2019). https://doi.org/10.1111/cbdd.13581
276 Niu, C. *et al.* Toxic effects of the Emamectin Benzoate exposure on cultured human bronchial epithelial (16HBE) cells. *Environ Pollut* **257**, 113618 (2020). https://doi.org/10.1016/j.envpol.2019.113618
277 Baader, E., Tschank, G., Baringhaus, K. H., Burghard, H. & GÜNzler, V. Inhibition of prolyl 4-hydroxylase by oxalyl amino acid derivatives in vitro, in isolated microsomes and in embryonic chicken tissues. *Biochemical journal* **300**, 525-530 (1994). https://doi.org/10.1042/bj3000525
278 Moen, E. *et al.* Deep learning for cellular image analysis. *Nat Methods* **16**, 1233-1246 (2019). https://doi.org/10.1038/s41592-019-0403-1
279 Rohban, M. H. *et al.* Systematic morphological profiling of human gene and allele function via Cell Painting. *Elife* **6** (2017). https://doi.org/10.7554/eLife.24060
280 Heckenbach, I. *et al.* Nuclear morphology is a deep learning biomarker of cellular senescence. *Nature Aging* **2**, 742-755 (2022). https://doi.org/10.1038/s43587-022-00263-3
281 Tamashunas, A. C. *et al.* High-throughput gene screen reveals modulators of nuclear shape. *Molecular Biology of the Cell* **31**, 1392-1402 (2020). https://doi.org/10.1091/mbc.e19-09-0520
282 Filippi-Chiela, E. C. *et al.* Nuclear Morphometric Analysis (NMA): Screening of Senescence, Apoptosis and Nuclear Irregularities. *PLoS ONE* **7**, e42522 (2012). https://doi.org/10.1371/journal.pone.0042522
283 Buchser, W. *et al. Assay Development Guidelines for Image-Based High Content Screening, High Content Analysis and High Content Imaging*. (Eli Lilly & Company and the National Center for Advancing Translational Sciences, 2012).
284 Lever, J., Krzywinski, M. & Altman, N. Principal component analysis. *Nature Methods* **14**, 641-642 (2017). https://doi.org/10.1038/nmeth.4346

285 Thorne, N., Auld, D. S. & Inglese, J. Apparent activity in high-throughput screening: origins of compound-dependent assay interference. *Curr Opin Chem Biol* **14**, 315-324 (2010). https://doi.org/10.1016/j.cbpa.2010.03.020
286 Inglese, J., Shamu, C. E. & Guy, R. K. Reporting data from high-throughput screening of small-molecule libraries. *Nature Chemical Biology* **3**, 438-441 (2007). https://doi.org/10.1038/nchembio0807-438
287 Paltoglou, S. M. & Roberts, B. J. Role of the von Hippel-Lindau tumour suppressor protein in the regulation of HIF-1alpha and its oxygen-regulated transactivation domains at high cell density. *Oncogene* **24**, 3830-3835 (2005). https://doi.org/10.1038/sj.onc.1208531
288 Cummins, E. P. *et al.* Prolyl hydroxylase-1 negatively regulates IkappaB kinase-beta, giving insight into hypoxia-induced NFkappaB activity. *Proc Natl Acad Sci U S A* **103**, 18154-18159 (2006). https://doi.org/10.1073/pnas.0602235103
289 Cheng, K. C.-C. *et al.* Actinoramide A Identified as a Potent Antimalarial from Titration-Based Screening of Marine Natural Product Extracts. *Journal of Natural Products* **78**, 2411-2422 (2015). https://doi.org/10.1021/acs.jnatprod.5b00489
290 Chen, S. Screening-Based Chemical Approaches to Unravel Stem Cell Biology. *Stem Cell Reports* **11**, 1312-1323 (2018). https://doi.org/10.1016/j.stemcr.2018.11.012
291 Cook, E., Hermes, J., Li, J. & Tudor, M. 179-195 (Springer New York, 2018).
292 Korostylev, A. *et al.* A high-content small molecule screen identifies novel inducers of definitive endoderm. *Mol Metab* **6**, 640-650 (2017). https://doi.org/10.1016/j.molmet.2017.04.009
293 Wolff, M., Wiedenmann, J., Nienhaus, G. U., Valler, M. & Heilker, R. Novel fluorescent proteins for high-content screening. *Drug Discov Today* **11**, 1054-1060 (2006). https://doi.org/10.1016/j.drudis.2006.09.005
294 Maria, S. S., Vidal, B. d. C. & Mello, M. L. S. Image analysis of DNA fragmentation and loss in V79 cells under apoptosis. *Genetics and Molecular Biology* **23** (2000).
295 Imbalzano, A. N., Imbalzano, K. M. & Nickerson, J. A. BRG1, a SWI/SNF chromatin remodeling enzyme ATPase, is required for maintenance of nuclear shape and integrity. *Commun Integr Biol* **6**, e25153 (2013). https://doi.org/10.4161/cib.25153
296 Imbalzano, K. M. *et al.* Nuclear shape changes are induced by knockdown of the SWI/SNF ATPase BRG1 and are independent of cytoskeletal connections. *PLoS One* **8**, e55628 (2013). https://doi.org/10.1371/journal.pone.0055628
297 Tran, K. D. *et al.* Hypoxic response is driven by the BAF form of SWI/SNF (*preprint*). *bioRxiv* (2022). https://doi.org/10.1101/2022.02.16.480689
298 Sena, J. A., Wang, L. & Hu, C. J. BRG1 and BRM chromatin-remodeling complexes regulate the hypoxia response by acting as coactivators for a subset of hypoxia-inducible transcription factor target genes. *Mol Cell Biol* **33**, 3849-3863 (2013). https://doi.org/10.1128/MCB.00731-13
299 Chen, B. *et al.* Small molecule-mediated disruption of Wnt-dependent signaling in tissue regeneration and cancer. *Nat Chem Biol* **5**, 100-107 (2009). https://doi.org/10.1038/nchembio.137
300 Kang, J. *et al.* Improving drug discovery with high-content phenotypic screens by systematic selection of reporter cell lines. *Nature Biotechnology* **34**, 70-77 (2016). https://doi.org/10.1038/nbt.3419

301 Bagheri, N., Carpenter, A. E., Lundberg, E., Plant, A. L. & Horwitz, R. The new era of quantitative cell imaging-challenges and opportunities. *Mol Cell* **82**, 241-247 (2022). https://doi.org/10.1016/j.molcel.2021.12.024
302 Ziegler, S., Sievers, S. & Waldmann, H. Morphological profiling of small molecules. *Cell Chem Biol* **28**, 300-319 (2021). https://doi.org/10.1016/j.chembiol.2021.02.012
303 Chan, C. K., Hadjitheodorou, A., Tsai, T. Y. C. & Theriot, J. A. Quantitative comparison of principal component analysis and unsupervised deep learning using variational autoencoders for shape analysis of motile cells. *bioRxiv* (2020). https://doi.org/10.1101/2020.06.26.174474
304 Pincus, Z. & Theriot, J. A. Comparison of quantitative methods for cell-shape analysis. *J Microsc* **227**, 140-156 (2007). https://doi.org/10.1111/j.1365-2818.2007.01799.x
305 Ruan, X. & Murphy, R. F. Evaluation of methods for generative modeling of cell and nuclear shape. *Bioinformatics* **35**, 2475-2485 (2019). https://doi.org/10.1093/bioinformatics/bty983
306 Giuliani, A. The application of principal component analysis to drug discovery and biomedical data. *Drug Discov Today* **22**, 1069-1076 (2017). https://doi.org/10.1016/j.drudis.2017.01.005
307 Chevrette, M. G. *et al.* Microbiome composition modulates secondary metabolism in a multispecies bacterial community. *Proc Natl Acad Sci U S A* **119**, e2212930119 (2022). https://doi.org/10.1073/pnas.2212930119
308 Giri, R. *et al.* Secreted NF-κB suppressive microbial metabolites modulate gut inflammation. *Cell Reports* **39**, 110646 (2022). https://doi.org/10.1016/j.celrep.2022.110646
309 Shine, E. E. & Crawford, J. M. Molecules from the Microbiome. *Annu Rev Biochem* **90**, 789-815 (2021). https://doi.org/10.1146/annurev-biochem-080320-115307
310 Sugimoto, Y. *et al.* A metagenomic strategy for harnessing the chemical repertoire of the human microbiome. *Science* **366** (2019). https://doi.org/10.1126/science.aax9176
311 Patel, J. R., Oh, J., Wang, S., Crawford, J. M. & Isaacs, F. J. Cross-kingdom expression of synthetic genetic elements promotes discovery of metabolites in the human microbiome. *Cell* **185**, 1487-1505 e1414 (2022). https://doi.org/10.1016/j.cell.2022.03.008
312 Lozano, G. L. *et al.* Introducing THOR, a Model Microbiome for Genetic Dissection of Community Behavior. *mBio* **10** (2019). https://doi.org/10.1128/mBio.02846-18
313 Turnbaugh, P. J. *et al.* The human microbiome project. *Nature* **449**, 804-810 (2007). https://doi.org/10.1038/nature06244
314 Cohen, L. J. *et al.* Functional metagenomic discovery of bacterial effectors in the human microbiome and isolation of commendamide, a GPCR G2A/132 agonist. *Proc Natl Acad Sci U S A* **112**, E4825-4834 (2015). https://doi.org/10.1073/pnas.1508737112
315 Colosimo, D. A. *et al.* Mapping Interactions of Microbial Metabolites with Human G-Protein-Coupled Receptors. *Cell Host Microbe* **26**, 273-282 e277 (2019). https://doi.org/10.1016/j.chom.2019.07.002
316 Guo, C. J. *et al.* Discovery of Reactive Microbiota-Derived Metabolites that Inhibit Host Proteases. *Cell* **168**, 517-526 e518 (2017). https://doi.org/10.1016/j.cell.2016.12.021

317 Donia, M. S. *et al.* A systematic analysis of biosynthetic gene clusters in the human microbiome reveals a common family of antibiotics. *Cell* **158**, 1402-1414 (2014). https://doi.org/10.1016/j.cell.2014.08.032
318 Zhang, Y. *et al.* Discovery of bioactive microbial gene products in inflammatory bowel disease. *Nature* (2022). https://doi.org/10.1038/s41586-022-04648-7
319 Wu, G., Zhao, N., Zhang, C., Lam, Y. Y. & Zhao, L. Guild-based analysis for understanding gut microbiome in human health and diseases. *Genome Med* **13**, 22 (2021). https://doi.org/10.1186/s13073-021-00840-y
320 Lerman, O. Z., Galiano, R. D., Armour, M., Levine, J. P. & Gurtner, G. C. Cellular Dysfunction in the Diabetic Fibroblast. *The American Journal of Pathology* **162**, 303-312 (2003). https://doi.org/10.1016/s0002-9440(10)63821-7
321 Imhann, F. *et al.* Interplay of host genetics and gut microbiota underlying the onset and clinical presentation of inflammatory bowel disease. *Gut* **67**, 108-119 (2018). https://doi.org/10.1136/gutjnl-2016-312135
322 Schirmer, M. *et al.* Compositional and Temporal Changes in the Gut Microbiome of Pediatric Ulcerative Colitis Patients Are Linked to Disease Course. *Cell Host Microbe* **24**, 600-610 e604 (2018). https://doi.org/10.1016/j.chom.2018.09.009
323 Glover, L. E. & Colgan, S. P. Hypoxia and metabolic factors that influence inflammatory bowel disease pathogenesis. *Gastroenterology* **140**, 1748-1755 (2011). https://doi.org/10.1053/j.gastro.2011.01.056
324 Masterson, J. C. *et al.* Epithelial HIF-1alpha/claudin-1 axis regulates barrier dysfunction in eosinophilic esophagitis. *J Clin Invest* **129**, 3224-3235 (2019). https://doi.org/10.1172/JCI126744
325 Hernandez, C. *et al.* Induction of trefoil factor (TFF)1, TFF2 and TFF3 by hypoxia is mediated by hypoxia inducible factor-1: implications for gastric mucosal healing. *Br J Pharmacol* **156**, 262-272 (2009). https://doi.org/10.1111/j.1476-5381.2008.00044.x
326 Britton, G. J. *et al.* Microbiotas from Humans with Inflammatory Bowel Disease Alter the Balance of Gut Th17 and RORgammat(+) Regulatory T Cells and Exacerbate Colitis in Mice. *Immunity* **50**, 212-224 e214 (2019). https://doi.org/10.1016/j.immuni.2018.12.015
327 Dehne, N. & Brune, B. HIF-1 in the inflammatory microenvironment. *Exp Cell Res* **315**, 1791-1797 (2009). https://doi.org/10.1016/j.yexcr.2009.03.019
328 Citron, D. M., Goldstein, E. J., Merriam, C. V., Lipsky, B. A. & Abramson, M. A. Bacteriology of moderate-to-severe diabetic foot infections and in vitro activity of antimicrobial agents. *J Clin Microbiol* **45**, 2819-2828 (2007). https://doi.org/10.1128/JCM.00551-07
329 Dowdell, A. S. *et al.* Essential role for epithelial HIF-mediated xenophagy in control of Salmonella infection and dissemination. *Cell Reports* **40**, 111409 (2022). https://doi.org/10.1016/j.celrep.2022.111409
330 Weiss, A. S. *et al.* In vitro interaction network of a synthetic gut bacterial community. *The ISME Journal* **16**, 1095-1109 (2022). https://doi.org/10.1038/s41396-021-01153-z
331 Stubbendieck, R. M., Vargas-Bautista, C. & Straight, P. D. Bacterial Communities: Interactions to Scale. *Front Microbiol* **7**, 1234 (2016). https://doi.org/10.3389/fmicb.2016.01234
332 Oh, Y. T. *et al.* Lipopolysaccharide induces hypoxia-inducible factor-1 alpha mRNA expression and activation via NADPH oxidase and Sp1-dependent pathway in BV2

murine microglial cells. *Neurosci Lett* **431**, 155-160 (2008). https://doi.org/10.1016/j.neulet.2007.11.033

333 Sherwood, R. & Walsham, N. Fecal calprotectin in inflammatory bowel disease. *Clinical and Experimental Gastroenterology*, 21 (2016). https://doi.org/10.2147/ceg.s51902

334 Pascal, V. *et al.* A microbial signature for Crohn's disease. *Gut* **66**, 813-822 (2017). https://doi.org/10.1136/gutjnl-2016-313235

335 McOrist, A. L. *et al.* Fecal butyrate levels vary widely among individuals but are usually increased by a diet high in resistant starch. *J Nutr* **141**, 883-889 (2011). https://doi.org/10.3945/jn.110.128504

336 Nayfach, S., Shi, Z. J., Seshadri, R., Pollard, K. S. & Kyrpides, N. C. New insights from uncultivated genomes of the global human gut microbiome. *Nature* **568**, 505-510 (2019). https://doi.org/10.1038/s41586-019-1058-x

337 Renwick, S. *et al.* Culturing Human Gut Microbiomes in the Laboratory. *Annu Rev Microbiol* **75**, 49-69 (2021). https://doi.org/10.1146/annurev-micro-031021-084116

338 Esfandiary, A. *et al.* Lactobacilli Modulate Hypoxia-Inducible Factor (HIF)-1 Regulatory Pathway in Triple Negative Breast Cancer Cell Line. *Cell J* **18**, 237-244 (2016). https://doi.org/10.22074/cellj.2016.4319

339 Werth, N. *et al.* Activation of hypoxia inducible factor 1 is a general phenomenon in infections with human pathogens. *PLoS One* **5**, e11576 (2010). https://doi.org/10.1371/journal.pone.0011576

340 Buszewski, B. & Noga, S. Hydrophilic interaction liquid chromatography (HILIC)--a powerful separation technique. *Anal Bioanal Chem* **402**, 231-247 (2012). https://doi.org/10.1007/s00216-011-5308-5

341 Canene-Adams, K. Reverse-phase HPLC analysis and purification of small molecules. *Methods Enzymol* **533**, 291-301 (2013). https://doi.org/10.1016/B978-0-12-420067-8.00023-4

342 Wishart, D. S. *et al.* HMDB 5.0: the Human Metabolome Database for 2022. *Nucleic Acids Res* **50**, D622-d631 (2022). https://doi.org/10.1093/nar/gkab1062

343 Sanada, S. *et al.* Intestinal microbial metabolite stercobilin involvement in the chronic inflammation of ob/ob mice. *Sci Rep* **10**, 6479 (2020). https://doi.org/10.1038/s41598-020-63627-y

344 Kibrick, A. C. & Milhorat, A. T. Glycylprolylhydroxyproline: Methods for its quantitative determination in urine and blood serum. *Biochemical Medicine* **4**, 79-88 (1970). https://doi.org/https://doi.org/10.1016/0006-2944(70)90085-2

345 Rosen, M. D. *et al.* Benzimidazole-2-pyrazole HIF Prolyl 4-Hydroxylase Inhibitors as Oral Erythropoietin Secretagogues. *ACS Med Chem Lett* **1**, 526-529 (2010). https://doi.org/10.1021/ml100198y

346 Won, M. S. *et al.* A novel benzimidazole analogue inhibits the hypoxia-inducible factor (HIF)-1 pathway. *Biochem Biophys Res Commun* **385**, 16-21 (2009). https://doi.org/10.1016/j.bbrc.2009.05.022

347 Chen, J. *et al.* Benzimidazole analogs as potent hypoxia inducible factor inhibitors: synthesis, biological evaluation, and profiling drug-like properties. *Anticancer Res* **34**, 3891-3904 (2014).

348 Bansal, Y. & Silakari, O. The therapeutic journey of benzimidazoles: a review. *Bioorg Med Chem* **20**, 6208-6236 (2012). https://doi.org/10.1016/j.bmc.2012.09.013

349 Zhan, P., Li, D., Li, J., Chen, X. & Liu, X. Benzimidazole Heterocycle as a Privileged Scaffold in Antiviral Agents. *Mini-Reviews in Organic Chemistry* **9**, 397-410 (2012). https://doi.org/10.2174/157019312804699456
350 Borthwick, A. D. 2,5-Diketopiperazines: synthesis, reactions, medicinal chemistry, and bioactive natural products. *Chem Rev* **112**, 3641-3716 (2012). https://doi.org/10.1021/cr200398y
351 Hubbard, T. D. *et al.* Adaptation of the human aryl hydrocarbon receptor to sense microbiota-derived indoles. *Sci Rep* **5**, 12689 (2015). https://doi.org/10.1038/srep12689
352 Zelante, T. *et al.* Tryptophan catabolites from microbiota engage aryl hydrocarbon receptor and balance mucosal reactivity via interleukin-22. *Immunity* **39**, 372-385 (2013). https://doi.org/10.1016/j.immuni.2013.08.003
353 Monteleone, I. *et al.* Aryl hydrocarbon receptor-induced signals up-regulate IL-22 production and inhibit inflammation in the gastrointestinal tract. *Gastroenterology* **141**, 237-248, 248 e231 (2011). https://doi.org/10.1053/j.gastro.2011.04.007
354 Qiu, J. *et al.* The aryl hydrocarbon receptor regulates gut immunity through modulation of innate lymphoid cells. *Immunity* **36**, 92-104 (2012). https://doi.org/10.1016/j.immuni.2011.11.011
355 Button, E. L., Bersten, D. C. & Whitelaw, M. L. HIF has Biff - Crosstalk between HIF1a and the family of bHLH/PAS proteins. *Exp Cell Res* **356**, 141-145 (2017). https://doi.org/10.1016/j.yexcr.2017.03.055
356 Berghard, A., Gradin, K., Pongratz, I., Whitelaw, M. L. & Poellinger, L. Cross-Coupling of Signal Transduction Pathways: the Dioxin Receptor Mediates Induction of Cytochrome P-450IA1 Expression via a Protein Kinase C-Dependent Mechanism. *Molecular and Cellular Biology* **13**, 677-689 (1993).
357 Patel, N. J. *et al.* Recognition of intestinal epithelial HIF-1alpha activation by Pseudomonas aeruginosa. *Am J Physiol Gastrointest Liver Physiol* **292**, G134-142 (2007). https://doi.org/10.1152/ajpgi.00276.2006
358 Hemmerling, F. & Piel, J. Strategies to access biosynthetic novelty in bacterial genomes for drug discovery. *Nat Rev Drug Discov* **21**, 359-378 (2022). https://doi.org/10.1038/s41573-022-00414-6
359 Gavriilidou, A. *et al.* Compendium of specialized metabolite biosynthetic diversity encoded in bacterial genomes. *Nat Microbiol* **7**, 726-735 (2022). https://doi.org/10.1038/s41564-022-01110-2
360 Cimermancic, P. *et al.* Insights into secondary metabolism from a global analysis of prokaryotic biosynthetic gene clusters. *Cell* **158**, 412-421 (2014). https://doi.org/10.1016/j.cell.2014.06.034
361 Raymond, F. *et al.* Culture-enriched human gut microbiomes reveal core and accessory resistance genes. *Microbiome* **7**, 56 (2019). https://doi.org/10.1186/s40168-019-0669-7
362 Lagier, J. C. *et al.* Culture of previously uncultured members of the human gut microbiota by culturomics. *Nat Microbiol* **1**, 16203 (2016). https://doi.org/10.1038/nmicrobiol.2016.203
363 Caballero, S. *et al.* Cooperating Commensals Restore Colonization Resistance to Vancomycin-Resistant Enterococcus faecium. *Cell Host & Microbe* **21**, 592-602.e594 (2017). https://doi.org/10.1016/j.chom.2017.04.002

364 Benson, J. M. & Shepherd, D. M. Aryl hydrocarbon receptor activation by TCDD reduces inflammation associated with Crohn's disease. *Toxicol Sci* **120**, 68-78 (2011). https://doi.org/10.1093/toxsci/kfq360
365 Lamas, B. *et al.* CARD9 impacts colitis by altering gut microbiota metabolism of tryptophan into aryl hydrocarbon receptor ligands. *Nat Med* **22**, 598-605 (2016). https://doi.org/10.1038/nm.4102
366 Lv, Q. *et al.* Norisoboldine, a natural AhR agonist, promotes Treg differentiation and attenuates colitis via targeting glycolysis and subsequent NAD(+)/SIRT1/SUV39H1/H3K9me3 signaling pathway. *Cell Death Dis* **9**, 258 (2018). https://doi.org/10.1038/s41419-018-0297-3
367 Singh, N. P. *et al.* Activation of aryl hydrocarbon receptor (AhR) leads to reciprocal epigenetic regulation of FoxP3 and IL-17 expression and amelioration of experimental colitis. *PLoS One* **6**, e23522 (2011). https://doi.org/10.1371/journal.pone.0023522
368 Takamura, T. *et al.* Lactobacillus bulgaricus OLL1181 activates the aryl hydrocarbon receptor pathway and inhibits colitis. *Immunol Cell Biol* **89**, 817-822 (2011). https://doi.org/10.1038/icb.2010.165
369 Wang, Q. *et al.* Aryl hydrocarbon receptor inhibits inflammation in DSSinduced colitis via the MK2/pMK2/TTP pathway. *Int J Mol Med* **41**, 868-876 (2018). https://doi.org/10.3892/ijmm.2017.3262
370 Schiering, C. *et al.* Feedback control of AHR signalling regulates intestinal immunity. *Nature* **542**, 242-245 (2017). https://doi.org/10.1038/nature21080
371 Lavelle, A. & Sokol, H. Gut microbiota-derived metabolites as key actors in inflammatory bowel disease. *Nat Rev Gastroenterol Hepatol* (2020). https://doi.org/10.1038/s41575-019-0258-z
372 Wiggins, B. G. *et al.* Endothelial sensing of AHR ligands regulates intestinal homeostasis. *Nature* (2023). https://doi.org/10.1038/s41586-023-06508-4
373 Metidji, A. *et al.* The Environmental Sensor AHR Protects from Inflammatory Damage by Maintaining Intestinal Stem Cell Homeostasis and Barrier Integrity. *Immunity* **49**, 353-362 e355 (2018). https://doi.org/10.1016/j.immuni.2018.07.010
374 Murray, I. A. *et al.* Evidence for ligand-mediated selective modulation of aryl hydrocarbon receptor activity. *Mol Pharmacol* **77**, 247-254 (2010). https://doi.org/10.1124/mol.109.061788
375 Burr, S. P. *et al.* Mitochondrial Protein Lipoylation and the 2-Oxoglutarate Dehydrogenase Complex Controls HIF1α Stability in Aerobic Conditions. *Cell Metabolism* **24**, 740-752 (2016). https://doi.org/10.1016/j.cmet.2016.09.015
376 Harada, H. *et al.* The combination of hypoxia-response enhancers and an oxygen-dependent proteolytic motif enables real-time imaging of absolute HIF-1 activity in tumor xenografts. *Biochem Biophys Res Commun* **360**, 791-796 (2007). https://doi.org/10.1016/j.bbrc.2007.06.149
377 Fomicheva, E. V. *et al.* Double Oxygen–sensing Vector System for Robust Hypoxia/Ischemia-regulated Gene Induction in Cardiac Muscle In Vitro and In Vivo. *Molecular Therapy* **16**, 1594-1601 (2008). https://doi.org/10.1038/mt.2008.136
378 Erapaneedi, R., Belousov, V. V., Schafers, M. & Kiefer, F. A novel family of fluorescent hypoxia sensors reveal strong heterogeneity in tumor hypoxia at the cellular level. *EMBO J* **35**, 102-113 (2016). https://doi.org/10.15252/embj.201592775

379 Roennfeldt, A. E. *et al.* NanoFIRE: A NanoLuciferase and Fluorescent Integrated Reporter Element for Robust and Sensitive Investigation of HIF and Other Signalling Pathways. *Biomolecules* **13** (2023). https://doi.org/10.3390/biom13101545
380 Hewitson, K. S. & Schofield, C. J. The HIF pathway as a therapeutic target. *Drug Discov Today* **9**, 704-711 (2004). https://doi.org/10.1016/S1359-6446(04)03202-7
381 Botusan, I. R. *et al.* Stabilization of HIF-1α is critical to improve wound healing in diabetic mice. *Proceedings of the National Academy of Sciences* **105**, 19426-19431 (2008). https://doi.org/10.1073/pnas.0805230105
382 Zhu, X., Jiang, L., Wei, X., Long, M. & Du, Y. Roxadustat: Not just for anemia. *Front Pharmacol* **13**, 971795 (2022). https://doi.org/10.3389/fphar.2022.971795
383 Greenberger, L. M. *et al.* A RNA antagonist of hypoxia-inducible factor-1α, EZN-2968, inhibits tumor cell growth. *Molecular Cancer Therapeutics* **7**, 3598-3608 (2008). https://doi.org/10.1158/1535-7163.mct-08-0510
384 Shirakawa, K. *et al.* Salicylate, diflunisal and their metabolites inhibit CBP/p300 and exhibit anticancer activity. *Elife* **5** (2016). https://doi.org/10.7554/eLife.11156
385 Wu, D. & Rastinejad, F. Structural characterization of mammalian bHLH-PAS transcription factors. *Curr Opin Struct Biol* **43**, 1-9 (2017). https://doi.org/10.1016/j.sbi.2016.09.011
386 Zhang, H. *et al.* Digoxin and other cardiac glycosides inhibit HIF-1alpha synthesis and block tumor growth. *Proc Natl Acad Sci U S A* **105**, 19579-19586 (2008). https://doi.org/10.1073/pnas.0809763105
387 Jones, D. T. & Harris, A. L. Identification of novel small-molecule inhibitors of hypoxia-inducible factor-1 transactivation and DNA binding. *Mol Cancer Ther* **5**, 2193-2202 (2006). https://doi.org/10.1158/1535-7163.MCT-05-0443
388 Kong, D. *et al.* Echinomycin, a small-molecule inhibitor of hypoxia-inducible factor-1 DNA-binding activity. *Cancer Res* **65**, 9047-9055 (2005). https://doi.org/10.1158/0008-5472.CAN-05-1235
389 Waring, M. J. *et al.* An analysis of the attrition of drug candidates from four major pharmaceutical companies. *Nature Reviews Drug Discovery* **14**, 475-486 (2015). https://doi.org/10.1038/nrd4609
390 Krentzel, D., Shorte, S. L. & Zimmer, C. Deep learning in image-based phenotypic drug discovery. *Trends Cell Biol* **33**, 538-554 (2023). https://doi.org/10.1016/j.tcb.2022.11.011
391 Durr, O. *et al.* Robust hit identification by quality assurance and multivariate data analysis of a high-content, cell-based assay. *J Biomol Screen* **12**, 1042-1049 (2007). https://doi.org/10.1177/1087057107309036
392 Piccinini, F. *et al.* Advanced Cell Classifier: User-Friendly Machine-Learning-Based Software for Discovering Phenotypes in High-Content Imaging Data. *Cell Syst* **4**, 651-655 e655 (2017). https://doi.org/10.1016/j.cels.2017.05.012
393 Li, S. *et al.* Identification of Angiogenesis Inhibitors Using a Co-culture Cell Model in a High-Content and High-Throughput Screening Platform. *SLAS Technology* **23**, 217-225 (2018). https://doi.org/10.1177/2472630317729792
394 Jain, I. H. *et al.* Genetic Screen for Cell Fitness in High or Low Oxygen Highlights Mitochondrial and Lipid Metabolism. *Cell* **181**, 716-727.e711 (2020). https://doi.org/10.1016/j.cell.2020.03.029

395 Paramsothy, S. *et al.* Multidonor intensive faecal microbiota transplantation for active ulcerative colitis: a randomised placebo-controlled trial. *The Lancet* **389**, 1218-1228 (2017). https://doi.org/10.1016/s0140-6736(17)30182-4
396 Natalini, J. G., Singh, S. & Segal, L. N. The dynamic lung microbiome in health and disease. *Nature Reviews Microbiology* **21**, 222-235 (2023). https://doi.org/10.1038/s41579-022-00821-x
397 Schaible, B., Schaffer, K. & Taylor, C. T. Hypoxia, innate immunity and infection in the lung. *Respiratory Physiology & Neurobiology* **174**, 235-243 (2010). https://doi.org/10.1016/j.resp.2010.08.006
398 Canale, F. P. *et al.* Metabolic modulation of tumours with engineered bacteria for immunotherapy. *Nature* **598**, 662-666 (2021). https://doi.org/10.1038/s41586-021-04003-2
399 Puurunen, M. K. *et al.* Safety and pharmacodynamics of an engineered E. coli Nissle for the treatment of phenylketonuria: a first-in-human phase 1/2a study. *Nature Metabolism* **3**, 1125-1132 (2021). https://doi.org/10.1038/s42255-021-00430-7
400 Buffington, S. A. *et al.* Dissecting the contribution of host genetics and the microbiome in complex behaviors. *Cell* **184**, 1740-1756.e1716 (2021). https://doi.org/10.1016/j.cell.2021.02.009
401 Scott, B. M. *et al.* Self-tunable engineered yeast probiotics for the treatment of inflammatory bowel disease. *Nature Medicine* **27**, 1212-1222 (2021). https://doi.org/10.1038/s41591-021-01390-x
402 Sanmarco, L. M. *et al.* Lactate limits CNS autoimmunity by stabilizing HIF-1α in dendritic cells. *Nature* **620**, 881-889 (2023). https://doi.org/10.1038/s41586-023-06409-6
403 Xue, X. *et al.* Endothelial PAS domain protein 1 activates the inflammatory response in the intestinal epithelium to promote colitis in mice. *Gastroenterology* **145**, 831-841 (2013). https://doi.org/10.1053/j.gastro.2013.07.010
404 Fribourgh, J. L. & Partch, C. L. Assembly and function of bHLH-PAS complexes. *Proc Natl Acad Sci U S A* **114**, 5330-5332 (2017). https://doi.org/10.1073/pnas.1705408114
405 Denison, M. S. & Faber, S. C. And Now for Something Completely Different: Diversity in Ligand-Dependent Activation of Ah Receptor Responses. *Curr Opin Toxicol* **2**, 124-131 (2017). https://doi.org/10.1016/j.cotox.2017.01.006
406 Denison, M. S., Soshilov, A. A., He, G., DeGroot, D. E. & Zhao, B. Exactly the same but different: promiscuity and diversity in the molecular mechanisms of action of the aryl hydrocarbon (dioxin) receptor. *Toxicol Sci* **124**, 1-22 (2011). https://doi.org/10.1093/toxsci/kfr218
407 Iyer, S. S. *et al.* Dietary and Microbial Oxazoles Induce Intestinal Inflammation by Modulating Aryl Hydrocarbon Receptor Responses. *Cell* **173**, 1123-1134 e1111 (2018). https://doi.org/10.1016/j.cell.2018.04.037
408 Jin, U. H. *et al.* Microbiome-derived tryptophan metabolites and their aryl hydrocarbon receptor-dependent agonist and antagonist activities. *Mol Pharmacol* **85**, 777-788 (2014). https://doi.org/10.1124/mol.113.091165
409 Murray, I. A. & Perdew, G. H. Ligand activation of the Ah receptor contributes to gastrointestinal homeostasis. *Curr Opin Toxicol* **2**, 15-23 (2017). https://doi.org/10.1016/j.cotox.2017.01.003

410 Zenewicz, L. A. *et al.* Innate and Adaptive Interleukin-22 Protects Mice from Inflammatory Bowel Disease. *Immunity* **29**, 947-957 (2008). https://doi.org/10.1016/j.immuni.2008.11.003

411 Kim, J. W. *et al.* Live-cell screening platform using human-induced pluripotent stem cells expressing fluorescence-tagged cytochrome P450 1A1. *The FASEB Journal* **34**, 9141-9155 (2020). https://doi.org/10.1096/fj.201903110r